

1999

NRL Review

Naval Research Laboratory
Washington, DC 20375-5320

Cover: Highlights from NRL's 75th Anniversary celebration, June 15-19, 1998.

In June 1991, NRL held its first Science-as-Art Competition. This competition was held to honor Dr. Herbert Friedman, Chief Scientist Emeritus of the E.O. Hulbert Center for Space Research, on his 75th birthday. Dr. Friedman has long been known for his appreciation of the arts as well as his scientific contributions. As part of the NRL 75th Anniversary celebrations, the Science-As-Art competition was again held. Artwork on the cover and the divider pages of this 1999 *NRL Review* displays some of the winners of the Special 75th Anniversary Science-as-Art Competition.

This 1999 *NRL Review* introduces you to the Naval Research Laboratory—the Navy's Corporate Laboratory—and focuses on research highlights from fiscal year 1998. In addition, it presents the special honors awarded to NRL employees and describes programs available to NRL and non-NRL employees. As you read the *NRL Review*, you will become even more aware that the Naval Research Laboratory comprises a dynamic team of scientists, engineers, and support personnel working together to promote programs that will continue to foster discoveries and scientific advances for the Navy of the future.

General information on the research described in this *NRL Review* can be obtained from the Public Affairs Office, Code 1230, (202) 767-2541. Information concerning Technology Transfer is available from Dr. Richard Rein, head of the Technology Transfer Office, Code 1004, (202) 767-7230. Sources of information on the various educational programs at NRL are listed in the chapter entitled "Programs for Professional Development."

For additional information about NRL, the *Fact Book* lists the organization, key personnel, and major facilities for each division. It contains information about Laboratory funding, programs, and field sites. The *Fact Book* can be obtained from the Technical Information Division, Publications Branch, Code 5230, (202) 767-2782.

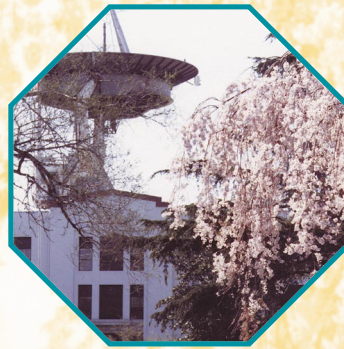
Quick Reference Telephone Numbers

	NRL Washington	NRL- SSC	NRL- Monterey	NRL CBD
Hotline	(202) 767-6543	(228) 688-5001	(831) 656-4721	(202) 767-6543
Personnel Locator	(202) 767-3200	(228) 688-3390	(831) 656-4731	(410) 257-4000
DSN	297- or 754-	485	878	—
Direct-in-Dialing	767- or 404-	688	656	257
Public Affairs	(202) 767-2541	(228) 688-5328	(831) 656-4708	—

Additional telephone numbers are listed on page 227.

1999

NRL Review



Mission

To conduct a broadly based multidisciplinary program of scientific research and advanced technological development directed toward maritime applications of new and improved materials, techniques, equipment, systems, and ocean, atmospheric, and space sciences and related technologies.

The Naval Research Laboratory provides

- primary in-house research for the physical, engineering, space, and environmental sciences;
- broadly based exploratory and advanced development programs in response to identified and anticipated Navy needs;
- broad multidisciplinary support to the Naval Warfare Centers; and
- space and space systems technology development and support.

In This Review

VIEW FROM THE TOP

View from the Top—CAPT Bruce W. Buckley, USN, and Dr. Timothy Coffey

75th ANNIVERSARY CELEBRATION

THE NAVAL RESEARCH LABORATORY

- 3 NRL—Our Heritage
- 4 1998 in Review
- 7 NRL Today
- 24 Looking Ahead
- 29 “Our People Make the Difference—featuring ...”

FEATURED RESEARCH

- 35 Array-Based Biosensor for Multianalyte Sensing
J.P. Golden, C.A. Rowe, M.J. Feldstein, S.B. Scruggs, L.M. Tender, and F.S. Ligler
- 43 The North Pacific Experiment (NORPEX-98)
R.H. Langland, R. Gelaro, G.D. Rohaly, and T.E. Rosmond
- 55 Thirty Years of NRL Research in Functional Ceramics: From Failure Analysis to Novel Ceramic Devices
D. Lewis III, C. Kim, C.C.M. Wu, T.L. Jessen, M.T. Chase, and M. Kahn

ACOUSTICS

- 71 A Search Algorithm for Resonance Anomalies (SARA)
S.A. Chin-Bing, D.B. King, R.A. Zingarelli, and A. Warn Varnas
- 72 Sound Propagation Through a Sand-Water Interface
H.J. Simpson and B.H. Houston
- 75 Estimation of Seabed Properties from Chirp Sonar Data
A. Turgut, S.N. Wolf, and M. Orr

CHEMICAL/BIOCHEMICAL RESEARCH

- 81 Flight Test Data from the Sodium Sulfur Battery Cell Space Experiment
J.C. Garner
- 84 Structure/Property Relationships and Applications of Low Dielectric Cyanurate Resins
L.J. Buckley and A.W. Snow
- 86 New Materials for Heavy Metal Removal Applications
M. Pazirandeh and J.M. Mauro
- 87 Carbon Nanotubes: Experiments Catch Up with Theory
C.T. White and J.W. Mintmire

ELECTRONICS AND ELECTROMAGNETICS

- 93 Automatic Radar Periscope Detection and Discrimination
D.W. Baden, R.S. DeCampo, G. Herman, and D.W. Kerr
- 94 Development Testing of AN/SPQ-9B Radar Preproduction Model
D.J. Cardiel, L.M. Schaus, and L.M. Leibowitz

- 96 A Method for Determining the Angle of Arrival (AOA) of Impinging Radio Waves in the Presence of Mutlipath
J.H. Frankovich and A.Y. Tse
- 99 The Microelectronics and Photonics Test Bed Experiment
A.B. Campbell, III and S. Buchner
- 100 Fabrication of a Fast Turn-off Transistor by Wafer Bonding
K.D. Hobart, F.J. Kub, G. Dolny, M. Zafrani, and J.M. Neilson
- 102 Low-Power, High-Speed InAs-Based High Electron Mobility Transistors
J.B. Boos, B.R. Bennett, W. Kruppa, D. Park, and M.J. Yang
-

ENERGETIC PARTICLES, PLASMAS, AND BEAMS

- 107 EX 252 IR Seduction Decoy
W. Humphries and M.A. Snapp
- 109 The Path to Record Kilovolt X-Ray Emission
J. Davis, J.P. Apruzese, K.G. Whitney, J.W. Thornhill, and R.W. Clark
- 112 The Behavior of Deuterium at Extreme Pressures
A.N. Mostovych
-

INFORMATION TECHNOLOGY AND COMMUNICATION

- 117 Gaiter: A Locomotion Control for Distributed Simulation
J.N. Templeman, L.E. Sibert, P.S. Denbrook, R.C Page, and J.A. McCune
- 119 Triangulation Range—Imaging Using Correlation Codes
F. Pipitone and R. Hartley
- 120 Automating CIC Communications for Reduced Manning
A. Schmidt-Nielsen, L.B Achille, and K.G. Schulze
-

MATERIALS SCIENCE AND TECHNOLOGY

- 125 Protein Crystal Growth Cessation and Reinitiation
M.A. Perozzo and J.H. Konnert
- 127 Novel Aerogel Materials
D.R. Rolison and C.I. Merzbacher
- 128 A New Way to Measure Spin Polarization
R.J. Soulen, Jr., M.S. Osofsky, B. Nadgorny, and J. Byers
- 130 Computational Screening of Candidate Thermoelectric Materials
D.J. Singh
- 132 Disorder-Induced Colossal Magnetoresistance
R. Stroud, V. Browning, J. Byers, V. Harris, and W. Fuller-Mora
-

OCEAN AND ATMOSPHERIC SCIENCE AND TECHNOLOGY

- 137 POAM III Monitors the Polar Stratosphere
J.S. Hornstein, R.M. Bevilacqua, R.L. Lucke, E.P. Shettle, M. Daehler, K.W. Hoppel, G. Nedoluha, D.T. Chen, D.R. Korwan, M.D. Fromm, and J.D. Lumpe
- 141 Nuclear Contamination Studies in the Russian Arctic
D.R. Johnson, S.E. King, M. Krosshavn, and T.A. McClimans
- 143 The Dynamics of Unusual Coastal Wave Clouds
S.D. Burk and T. Haack

- 145 Baroclinic Oscillations on the Louisiana Continental Shelf During Hurricane Andrew
T.R. Keen and S.E. Allen
- 148 High-Resolution Observations of Foreshore Morphodynamics
K.T. Holland and J. Puleo
-

OPTICAL SCIENCE

- 153 Confined Photons in Semiconductor Microcavities
T.L. Reinecke, P.A. Knipp, M. Bayer, and A. Forchel
- 155 Optical Detection of Defects Below the Surface of Nontransparent Materials
M. Bashkansky, M.D. Duncan, and J.F. Reintjes
- 156 Dark HORSE (Hyperspectral Overhead Reconnaissance—Surveillance Experiment)
J.V. Michalowicz and F. Bucholtz
- 159 The NRL Infrared Range Facility
K.A. Snail and R.G. Priest
-

REMOTE SENSING

- 163 Multifrequency Polarimetric SAR Images of Gulf Stream Features from Space
S.R. Chubb, T.F. Donato, F. Askari, A.L. Cooper, and S.A. Mango
- 164 Autonomous Survey System
B.S. Bourgeois and A.B. Martinez
-

SIMULATION, COMPUTING, AND MODELING

- 169 Ground Truth Reference System
A.C. Hosmer
- 170 Master Stability Functions for Synchronizing Systems
L.M. Pecora and T.L. Carroll
- 174 Reduced Manning—Its Impact on Damage Control
P.A. Tatem and F.W. Williams
- 175 Transition to Detonation in Turbulent Flames
A.M. Khokhlov and E.S. Oran
- 177 Atmospheric RF Propagation Effects on Tracking, Navigation, and Communication Links
J. Choi and M. Regan
-

SPACE RESEARCH AND SATELLITE TECHNOLOGY

- 183 Ionospheric Forecasting with Dynamic GPS Assimilation
M.J. Keskinen
- 186 Far-Infrared Spectroscopy of Colliding Galaxies
J. Fischer and M. Luhman
- 188 Modelling Radiation Effects on Spacecraft: CREME96
A.J. Tylka
- 190 Interim Control Module (ICM)
A.B. Jacoby
- 192 First U.S. Flight Hall Thruster Electric Propulsion System
P.R. Lynn, Jr. and M.F. Osborn II

SPECIAL AWARDS AND RECOGNITION

- 197 Special Awards and Recognition
- 209 Alan Berman Research Publication and Edison Patent Awards

PROGRAMS FOR PROFESSIONAL DEVELOPMENT

- 217 Programs for NRL Employees—Graduate Programs; Continuing Education; Technology Transfer; Technology Base; Professional Development; Equal Employment Opportunity (EEO) Programs; and Other Activities
- 221 Programs for Non-NRL Employees—Recent Ph.D., Faculty Member, and College Graduate Programs; Professional Appointments; Student Programs; and High School Programs

GENERAL INFORMATION

- 225 Technical Output
- 226 Technology Transfer at NRL
- 227 Key Personnel
- 228 Employment Opportunities for Entry-Level and Experienced Personnel
- 229 Location of NRL in the Capital Area
- 230 Contributions by Divisions, Laboratories, and Departments
- 233 Subject Index
- 236 Author Index



First United States reconnaissance satellite system, the Galactic Radiation and Background (GRAB) satellite system

While attending NRL's week-long Diamond Jubilee Celebration in Washington, D.C., Mr. Keith Hall, Director, National Reconnaissance Office, and RADM Lowell E. Jacoby, USN, Director of Naval Intelligence, announced the declassification of the first United States reconnaissance satellite system, the Galactic Radiation and Background (GRAB) satellite system. GRAB was proposed, developed, built, and operated by the Naval Research Laboratory.

View from the Top



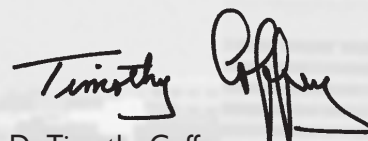
Dr. Timothy Coffey
Director of Research

This year's Review is published in the afterglow of a highly successful 75th anniversary celebration. The celebration was an experience which money could not buy. It provided us an opportunity to recognize, in some cases for the last time, the great past employees of this great Laboratory. It gave us an opportunity to showcase our accomplishments to the public and to ourselves. The event helped reinforce the strong institutional pride that we all feel about NRL. The process of identifying the 75 innovations that were recognized during the celebration demonstrated how important it is for us to have unambiguous documentation of our contributions. While only 75 innovations were highlighted, the process of identifying these 75 made it clear that there are thousands of contributions from NRL that have been enabling in so many different ways.

The 75th anniversary program was a very challenging undertaking. It demonstrated once again what has been a characteristic of NRL over the years, namely, that the Lab, when challenged, will put forth whatever effort is required to overcome that challenge. Another thing that struck me as I worked through the details of the 75th anniversary program was how much has changed, yet how little has changed. In this regard, we need to keep things in perspective. We certainly are in a period of rapid and sometimes alarming change. On the other hand, NRL's history is full of such change, and adapting to and sometimes guiding that change is probably what has kept the Laboratory's intellectual vitality high.

"The next 75 years will see NRL accomplishments as important and as enabling as those of the past 75 years."

The 75th anniversary gave me the opportunity to look back on the great achievers who made NRL what it is. I concluded that they had several attributes in common. Among them were that they were scientifically or technically very strong. They were able to recognize an important idea, and they often ran with an idea that emerged outside of their own discipline. They tended to regularly exceed their authority, and they were willing to accept the risks associated with the above. The next 75 years will see NRL accomplishments as important and as enabling as those of the past 75 years. I suspect that the attributes described above will also prevail in those great achievements yet to come.


Dr. Timothy Coffey

This has been a fabulous year in celebration of 75 years of pioneering contributions to the Navy, the Department of Defense, and indeed to the national and international body of science and technology. Contributions like the discovery of the underlying principles of the high frequency radio wave skip distance effect; the invention and early development of radar in this country; the concept and early design of the nuclear powered submarine; the world's third satellite to orbit, Vanguard; this country's first reconnaissance satellite, GRAB; the discovery of powerful rare earth magnets; the invention and early prototypes for the Global Positioning System; and many, many more.

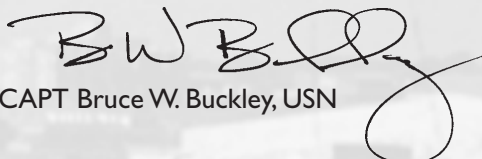


CAPT Bruce W. Buckley, USN
Commanding Officer

I just spent two days at a symposium of aerospace executives. Presidents and CEOs of major aerospace corporations were discussing the theme of "Formulas for Success." Each had their own formulation. Predictably, many of the key elements of each formula were common to most—people, processes, customer satisfaction, and partnering. I have often characterized the formula that has evolved at NRL over the years in similar terms. Give the right people the right processes and immerse them in the right environment and the result can't help but be success. In our case, the obtaining and renewing of the right people began with the very first pioneers of the laboratory—Page, Taylor, Hulburt, and others. These greats attracted and retained others to perpetuate the greatness. The responsibility to do the same now rests with you. Our processes have evolved into a very decentralized set of processes that give the Divisions and Branches a great deal of authority and autonomy in the pursuit of their technical program within the broad guidelines set by the senior leadership. And the right environment could be described as the coexistence of very basic to very applied research and the maintenance of a broad multidisciplinary technical program and expertise. Perhaps most important to the success over many years has been the authority of the Commanding Officer and Director of Research to direct all aspects of the constant adjustments required in people, processes, and environment.

No matter how you describe the details of the formula, it seems clear to me from the long list of achievements we celebrated this past year, that the Naval Research Laboratory has struck upon the right formula for success. It has been my pleasure and honor to represent you these past three and a half years, I wish you all the very best for your continued success, and I look forward to coming back at the Centennial to witness the celebration of many more significant contributions to the Navy and Marine Corps.

"Give the right people the right processes and immerse them in the right environment and the result can't help but be success."


CAPT Bruce W. Buckley, USN



75th Anniversary Celebration

June 15-19, 1998

A week of Celebration to commemorate our Diamond Jubilee was held at the Naval Research Laboratory during June 15-19, 1998. Each day brought a special focus to these celebrations:

Monday, June 15	Science-as-Art Awards
Tuesday, June 16	Focus on Materials
Wednesday, June 17	Focus on Space
Thursday, June 18	Focus on Naval Systems

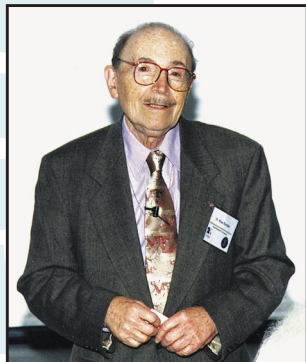


The celebrations culminated in a series of special events on Friday, June 19. The day began with a Forum at the Laboratory that featured presentations by distinguished guests from government, private industry, and academia. Friday evening celebrations moved to the National Museum of American History in Washington, D.C. There, at the Forum on Innovation, 75 NRL developments that reflect the breadth and sustained impact of the Laboratory's programs were formally recognized. These included some of NRL's most important contributions to science, technology, national security, and society. The evening concluded with a reception in the Palm Court at the museum during which today's employees shared experiences with those who had come before, those who had relentlessly paved the way for the great Laboratory of today. Together we celebrated our glorious past and shared our vision and plans for the future.

Focus on Materials

Tuesday, June 16, 1998

Symposium Speakers



Dr. Elias Burnstein

Dr. Charles H. Townes, Professor, University of California at Berkeley, Nobel Prize 1964
“The Past and Prospects”

Dr. Philip H. Abelson, Editor, Science magazine
“Early History of the Nuclear Submarine”

Dr. William D. Phillips, National Institute of Standards and Technology, Nobel Prize 1997
“Almost Absolute Zero: The Story of Laser Cooling and Trapping”

Dr. Elias Burnstein, Mary Amanda Wood Professor of Physics, Emeritus, University of Pennsylvania

“Semiconductors: The Continuing Story at NRL”

Dr. Jerome Karle, NRL, Nobel Prize 1985
“Fifty-four Years with NRL and Science, Respite, Adspice, Prospice”



Dr. Charles Townes



Dr. William Phillips



Mr. Alex Scott, Managing Director of TMS, presents Dr. Bhatka Rath with the Minerals, Metals, and Materials Society (TMS) Award.

Dr. Michael DeHaemer, Managing Director of ASM International, presents Dr. Bhatka Rath with a plaque in recognition of NRL's long-standing contributions in the field of Materials Science and Engineering.



Dr. Bhatka Rath presents Dr. Jerome Karle with a watercolor portrait for his 80th birthday.



Drs. Isabella and Jerome Karle arriving at the Materials symposium.



Albert Einstein makes a special appearance on Materials Day.

Focus on Space

Wednesday, June 17, 1998

Symposium Speakers

Milton W. Rosen, NRL (retired)
"The Vanguard Story"

Dr. Herbert Friedman, NRL
"The Earth in Space"

Roger Easton, NRL (retired)
"Why GPS Would Not Sell"

Mr. Keith Hall, Director, National
Reconnaissance Office
Declassification Announcement

RADM Lowell E. Jacoby, Director,
Naval Intelligence, Comments

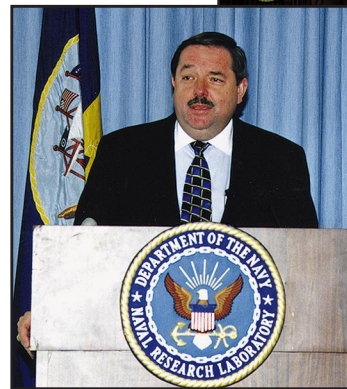
Mr. Peter Wilhelm, NRL
"Space Technology"



Mr. Milton Rosen and Mr. Roger Easton



RADM Lowell Jacoby



Mr. Keith Hall



Unveiling of the GRAB satellite, which was declassified to coincide with the 75th anniversary celebration.



Former NRL Director of Research, Dr. Oscar Marzke (center) is welcomed by CAPT Buckley and accompanied by Ms. Denise Quinn.



GRAB satellite pioneers with CAPT Buckley and Dr. Coffey.



Mr. Peter Wilhelm officially debriefs the GRAB pioneers on the previously classified satellite program.



Principals of Space symposium.

75th Anniversary Events

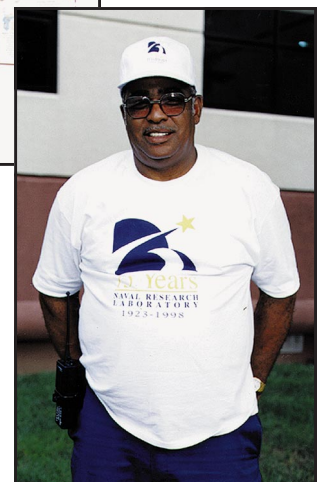
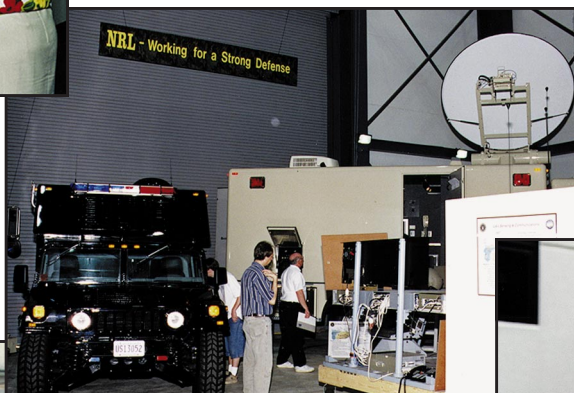
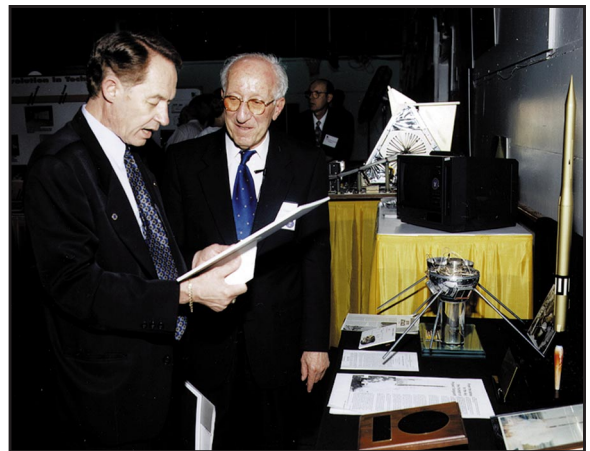
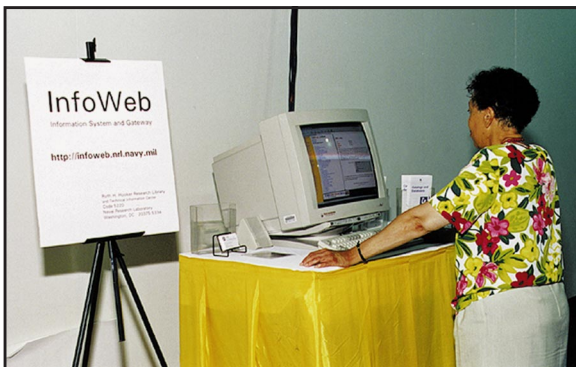
NRL recognizes 75 years of progress through research—for the Navy and the Nation

This was truly a “Class Act” in celebration of the Navy’s Corporate Laboratory, and we are looking forward to continuing the long history of contributions to the Navy and Marine Corps, National Defense, and the world of science.

— CAPT Bruce Buckley and Dr. Timothy Coffey

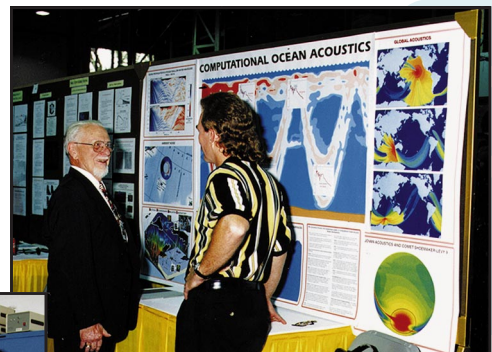


An NRL P-3 flies by Building 43 on the actual day of NRL's 75th anniversary, July 2, 1998.



75th Anniversary Events

Poster Sessions and Tours



75th Anniversary

Focus on Naval Systems

Thursday, June 18, 1998

Symposium Speakers

Professor James Brittain, Professor Emeritus,
Georgia Institute of Technology
"Back to the Future (1923-1961)"

Dr. Gary Weir, Navy Historical Center
"Back to the Future (1962-1998)"

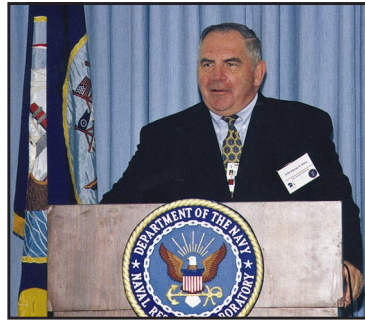
ADM Stanley R. Arthur (Ret), VP for Naval
Systems, Lockheed-Martin

"The Past 35 Years of Naval Systems"

VADM Arthur K. Cebrowski, Director, Space,
Information Warfare and C2 (N-6)

"The Next 35 Years of Naval Systems"

Mr. Bran Ferren, Walt Disney Imagineering
"The Next 75 Years"



ADM Stanley Arthur



VADM Arthur Cebrowski



Mr. Bran Ferren



Professor James Brittain



Dr. Gary Weir



Principals and symposium guest speakers.

Dr. John Montgomery,
Superintendent of the
Tactical Electronic
Warfare Division,
hosted Thursday's
symposium on Naval
Systems.



CAPT Buckley and Dr. Montgomery chat with
Ms. Katie Ratigan and ADM Arthur while other
guests continue to arrive.



A Hum-V on display outside Building 210, Tactical
Electronic Warfare Division, during the afternoon
tours.

Forum

Friday, June 19, 1998



Senator John W. Warner

Forum Speakers

The Honorable Jerry Hultin
Under Secretary of the Navy
The Honorable John W. Warner
U.S. Senator, Virginia
RADM Paul Gaffney
Chief of Naval Research
Mr. Peter Teets

President and COO, Lockheed-Martin
Dr. John Deutch
Institute Professor, Massachusetts
Institute of Technology



The Honorable Jerry Hultin



Dr. John Deutch



RADM Paul Gaffney, Chief of Naval Research, greets The Honorable Jerry Hultin, Under Secretary of the Navy.



Mr. Peter Teets



Dr. Herbert Gursky of the Space Science Division and Dr. David Nagel of the Condensed Matter and Radiation Sciences Division exchange thoughts during the celebration.



CAPT Buckley and Dr. Coffey escort Senator John Warner from the Forum, which was held in Building 226 on Friday morning.



Ms. Sarah Crozier, Mr. Richard Bussey, and Ms. Shannan Hammonds were three of the many individuals who helped to ensure the week-long events went smoothly.

FORUM

Innovation Awards Ceremony and Reception

Friday evening, June 19, 1998



CAPT Buckley honors Dr. Isabella Karle with NRL's Lifetime Achievement Award.



Dr. Coffey, Director of Research, presents the 75 Awards for Innovation.



CAPT Buckley presents Mr. Peter Wilhelm with NRL's Lifetime Achievement Award.



Mrs. Louise McDonald and Ms. Denise Quinn, principal coordinators for the 75th anniversary events, prepare the stage for the evening program.



Innovators were asked to stand and be recognized.



NRL's past and present VIPs, employees, and guests gather to recognize the honorees of the 75th Innovations and Lifetime Achievement Awards.



Dr. Jerome Karle and his daughter, Dr. Jean Karle share a moment beside the innovation award plaque.

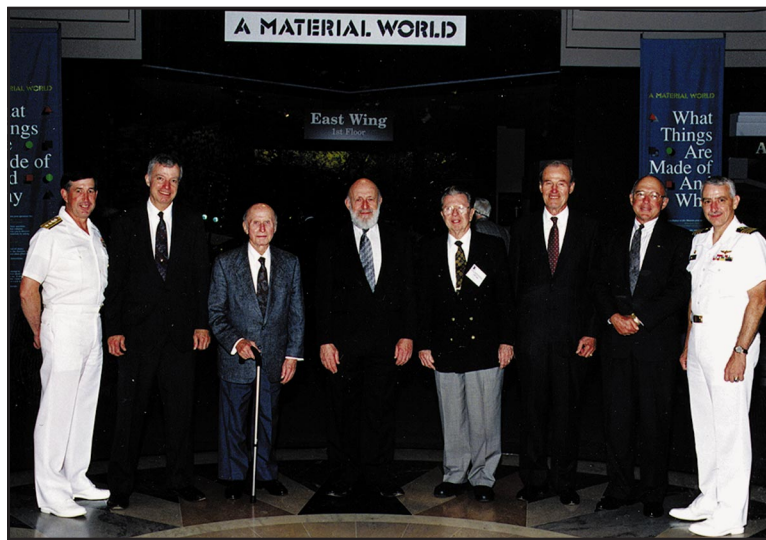
at the National Museum of American History



Afterwards, attendees enjoy a lavish reception.



Hostesses for the evening event were (top) Ms. Agnes Green, Ms. Joanne Kemper; (bottom) Ms. Carol Jarboe, Ms. Michelle Harris, Ms. Robin Williams, and Ms. Shannan Hammonds.



Former and present Commanding Officers and Directors of Research (from left to right): RADM Paul G. Gaffney II, USN (1991-1994); Dr. Timothy Coffey (present DOR); Dr. Oscar T. Marzke (DOR, 1956-1957); Dr. Alan Berman (DOR, 1967-1982); CAPT Earle W. Sapp, USN (1970-1973); CAPT John T. Geary, USN (1973-1976); CAPT William G. Clautice, USN (1987-1989); and CAPT Bruce W. Buckley, USN (1996 to present).

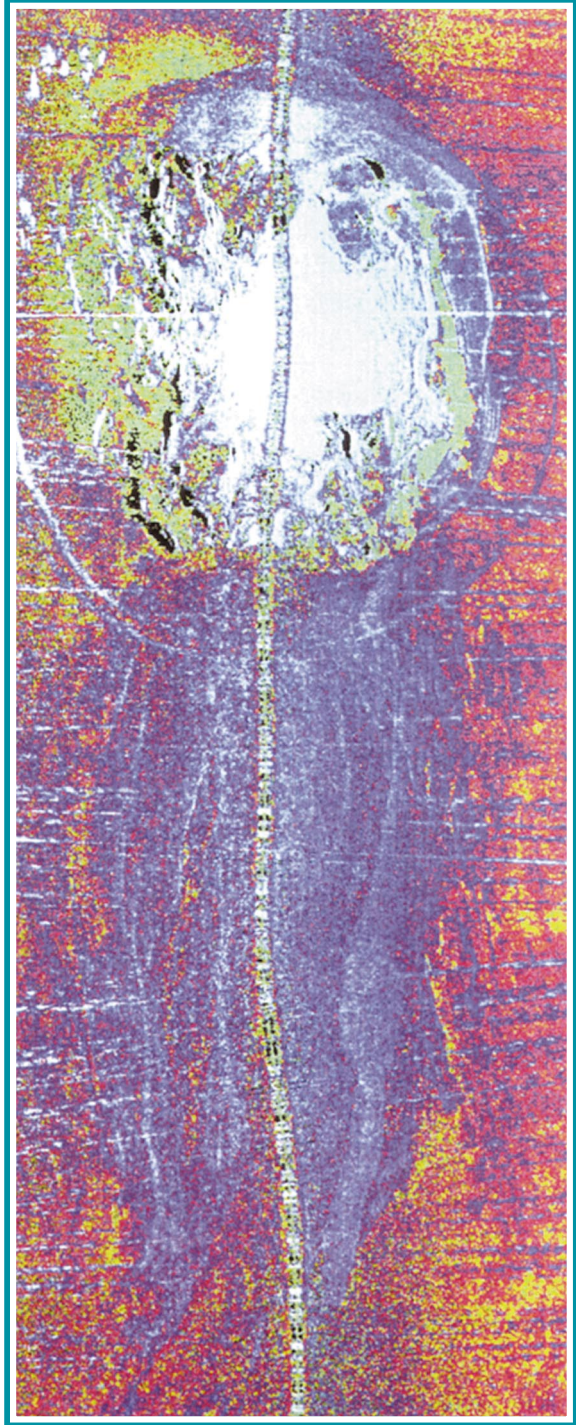


Dr. Thomas Schriempf, Dr. Graham Hubler, Dr. Donald Gubser, Dr. Alexander Ehrlich, Ms. Dorothy Hubler, and Ms. Virginia Gubser enjoy the reception immediately following the awards ceremony.



Reception in the Palm Court of the National Museum of American History following the Forum on Innovation.

OVERVIEW



A Seafloor Mud Volcano Illuminated in Ultrasound
Science-as-Art contest – Honorable Mention
Submitted by: Warren Wood, Peter Vogt, and Rick Hagen

Sidescan “sonograph” of an active mud volcano discovered by NRL in 1989 at 72°N in 1250-m water depth on the continental margin northwest of Norway. The towfish was “flown” 40 m above the seafloor. Pixels have been color-coded according to the relative intensity of acoustic backscatter from the seafloor. The image comprises a single NW (top) - SW (bottom) oriented data swath about 1 km wide and 2.5 km long. The track of the towfish on the seafloor is shown by the vertical stripe down the image. The white and light blue tints represent the area of strongest acoustic backscatter in the central part of the mud volcano. The thin rim encircling the mud volcano is a fault along which the mud volcano is subsiding relative to surrounding sediments. Small black spots, the weakest backscatter, are probably acoustic shadows and craters on the outer parts of this cookie-shaped structure on the seafloor. The blue “beard” extending down from the mud volcano edifice is caused by sediment flows that have emanated from the mud volcano and traveled several kilometers down the regional slope. Numerous intermittent horizontal lines in the image are “biologic noise,” the sounds of minke whales spotted around the research vessel at the same time.

This is the only way we have to map a mud volcano in detail and to study what is happening on its surface. When displayed in different colors and shades of gray, the sonograph tells scientists what is going on, where the hydrate is, where the craters and mounds are, where the surrounding moat is, and the location of its circular fault. None of these details were known prior to this sonar imaging and display.

3	NRL—Our Heritage
4	1998 in Review
7	NRL Today
24	Looking Ahead
29	Featuring ... People Who Make a Difference

NRL — Our Heritage

Today, when government and science seem inextricably linked, when virtually no one questions the dependence of national defense on the excellence of national technical capabilities, it is noteworthy that in-house defense research is relatively new in our Nation's history. The Naval Research Laboratory (NRL), the first modern research institution created within the United States Navy, began operations in 1923.

Thomas Edison's Vision: The first step came in May 1915, a time when Americans were deeply worried about the great European war. Thomas Edison, when asked by a *New York Times* correspondent to comment on the conflict, argued that the Nation should look to science. "The Government," he proposed in a published interview, "should maintain a great research laboratory...In this could be developed...all the technique of military and naval progression without any vast expense." Secretary of the Navy Josephus Daniels seized the opportunity created by Edison's public comments to enlist Edison's support. He agreed to serve as the head of a new body of civilian experts—the Naval Consulting Board—to advise the Navy on science and technology. The Board's most ambitious plan was the creation of a modern research facility for the Navy. Congress allocated \$1.5 million for the institution in 1916, but wartime delays and disagreements within the Naval Consulting Board postponed construction until 1920.

The Laboratory's two original divisions—Radio and Sound—pioneered in the fields of high-frequency radio and underwater sound propagation. They produced communications equipment, direction-finding devices, sonar sets, and perhaps most significant of all, the first practical radar equipment built in this country. They also performed basic research, participating, for example, in the discovery and early exploration of the ionosphere. Moreover, the Laboratory was able to work gradually toward its goal of becoming a broadly based research facility. By the beginning of World War II, five new divisions had been added: Physical Optics, Chemistry, Metallurgy, Mechanics and Electricity, and Internal Communications.

The War Years and Growth: Total employment at the Laboratory jumped from 396 in 1941 to 4400 in 1946, expenditures from \$1.7 million to \$13.7 million, the number of buildings from 23 to 67, and the number of projects from 200 to about 900. During WWII, scientific activities necessarily were concentrated almost entirely on applied research. New electronics equipment—radio, radar, sonar—was developed. Countermeasures were devised. New lubricants were produced, as were antifouling paints, luminous identification tapes, and a sea marker to help save survivors of disasters at sea. A thermal diffusion process was conceived and used to supply some of the ^{235}U isotope needed for one of the first atomic bombs. Also, many new devices that developed from booming wartime industry were type tested and then certified as reliable for the Fleet.

NRL Reorganizes for Peace: Because of the major scientific accomplishments of the war years, the United States emerged into the postwar era determined to consolidate its wartime gains in science and technology and to preserve the working relationship between its armed forces and the scientific community. While the Navy was establishing its Office of Naval Research (ONR) as a liaison with and supporter of basic and applied scientific research, it was also encouraging NRL to broaden its scope and become, in effect, its corporate research laboratory. There was a transfer of NRL to the administrative oversight of ONR and a parallel shift of the Laboratory's research emphasis to one of long-range basic and applied investigation in a broad range of the physical sciences.

However, rapid expansion during the war had left NRL improperly structured to address long-term Navy requirements. One major task—neither easily nor rapidly accomplished—was that of reshaping and coordinating research. This was achieved by transforming a group of largely autonomous scientific divisions into a unified institution with a clear mission and a fully coordinated research program. The first attempt at reorganization vested power in an executive committee composed of all the division superintendents. This committee was impracticably large, so in 1949, a civilian director of research was

named and given full authority over the program. Positions for associate directors were added in 1954.

The Breadth of NRL: During the years since the war, the areas of study at the Laboratory have included basic research concerning the Navy's environments of Earth, sea, sky, and space. Investigations have ranged widely—from monitoring the Sun's behavior to analyzing marine atmospheric conditions to measuring parameters of the deep oceans. Detection and communication capabilities have benefitted by research that has exploited new portions of the electromagnetic spectrum, extended ranges to outer space, and provided a means of transferring information reliably and securely, even through massive jamming. Submarine habitability, lubricants, shipbuilding materials, fire fighting, and the study of sound in the sea have remained steadfast concerns, to which have been added recent explorations within the fields of virtual reality, superconductivity, and biomolecular science and engineering.

The Laboratory has pioneered naval research into space from atmospheric probes with captured V-2 rockets through direction of the *Vanguard* project—

America's first satellite program—to involvement in such projects as the Navy's Global Positioning System. Today NRL is the Navy's lead laboratory in space systems research, fire research, tactical electronic warfare, microelectronic devices, and artificial intelligence.

The consolidation in 1992 of NRL and the Naval Oceanographic and Atmospheric Research Laboratory, with centers at Bay St. Louis, Mississippi, and Monterey, California, added critical new strengths to the Laboratory. NRL now is additionally the lead Navy center for research in ocean and atmospheric sciences, with special strengths in physical oceanography, marine geosciences, ocean acoustics, marine meteorology, and remote oceanic and atmospheric sensing. The expanded Laboratory is focusing its research efforts on new Navy strategic interests and needs in the post-Cold War world. Although not abandoning its interests in blue-water operations and research, the Navy is also focusing on defending American interests in the world's littoral regions. NRL scientists and engineers are working to give the Navy the special knowledge and capabilities it needs to operate in these waters.

1998 in Review

NRL celebrated its diamond jubilee this year, with a week of special speakers, "Science as Art" and research poster exhibits, and the presentation of 75 Science Innovation Awards for outstanding contributions by NRL scientists and engineers to national security and the advancement of knowledge. As part of the celebrations, the NRL-conceived and built Galactic Radiation and Background (GRAB) satellite was declassified. GRAB, which became operational in July 1960, was the first United States' reconnaissance satellite. One of GRAB's early achievements was detection of a Soviet radar that supported a capability to destroy ballistic missiles.

This year was also the anniversary of the NRL-built Vanguard I satellite. Vanguard I is the world's longest surviving manmade satellite, having been launched from Cape Canaveral, Florida, on March 17, 1958. Vanguard I, the world's first solar-powered satellite, was the second artificial satellite placed in orbit by the United States. The satellite has made more than 158,000 revolutions of the Earth and has travelled more than 4.59 billion nautical miles.

In a year that marked the celebration of NRL historic firsts in space science and technology, Laboratory scientists continued to make significant advances in space research. NRL's Polar Ozone and Aerosol Monitor III (POAM III) instrument was launched, as a continuation of efforts to monitor the polar stratosphere. The POAM III will provide valuable information on the way Earth's ozone layer is responding to decreased abundances of chlorine in the atmosphere as a result of restrictions in CFC emissions. Such restrictions were mandated in the international Montreal Protocol. The POAM collects detailed stratospheric information by scanning through the stratosphere at sunrise and sunset. Information collected includes details on the abundance of aerosol particles, ozone, and other atmospheric constituents at a vertical resolution of 1 kilometer.

The Naval Research Laboratory is developing the Navy Earth Map Observer (NEMO) imaging satellite program in partnership with the Space Technology Development Corporation of Arlington, Virginia. The program will demonstrate and refine a new imaging



First United States' reconnaissance satellite system, the Galactic Radiation and Background (GRAB) satellite system. GRAB was proposed, developed, built, and operated by NRL.

technology from space called Hyperspectral Imaging that will augment and enhance traditional remote sensing techniques. The images will assist future efforts in defining and modeling the global littoral ocean. The images are also useful in commercial efforts to assess geology, agriculture, and the natural environment.

In other space research, scientists from NRL and Rice University announced the existence of new, undiscovered classes of transient astrophysical sources. Using the currently accepted blast-wave model for gamma-ray bursts, the NRL scientists interpreted and modeled prompt and delayed afterglow data from gamma-ray bursts at many different wavelengths. Their work suggests that new types of cosmic flashes with specific flaring behaviors should exist.

NRL researchers, in conjunction with colleagues from the University of Alaska and the Air Force Research Laboratory, have made aircraft observations of newly discovered phenomena that occur in the stratosphere and mesosphere above thunderstorms. The phenomena, classified as Red Sprites, Blue Jets, and Elves, appear as luminous flashes at various altitudes. They are produced through electron impact excitation of the ambient atmosphere. The most dramatic of the three, Red Sprites, can reach from near the cloud tops to the bottom of the ionosphere. NRL scientists are preparing instruments that will collect photometric and spectroscopic data in the near ultraviolet that will aid in furthering understanding of the electron energetics in these phenomena.

In the area of materials science, NRL successfully tested a high-temperature superconducting electromagnet producing a magnet field of 7.25 Tesla. The magnet broke a previous world record announced by Japan in October 1997. It will be used by NRL for solid state physics research and the development of Navy applications of high-temperature superconductivity.

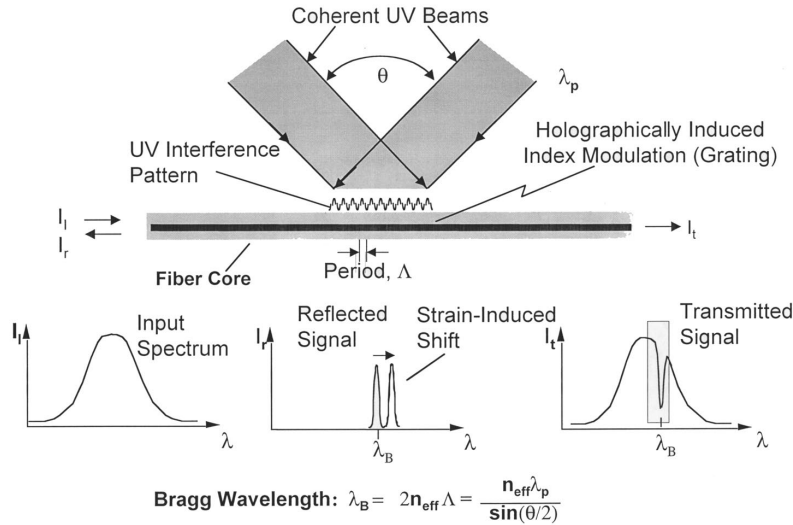
In optical sciences, researchers have developed several new types of semiconductor lasers that emit light in the mid-wave infrared spectral region. The new lasers are suitable for both military and civilian applications, including chemical sensing, protection against heat-seeking missiles, laser surgery, laser radar, and infrared (IR) scene projection. This year also saw the opening of NRL's new Infrared Range Facility. The IR Facility is a tri-service facility designed to simulate the IR environment from sea level to altitudes of 30,000 feet. Its primary mission is to assist low observable (LO) engineers in the development of new IR LO technologies.

Finally, NRL marine scientists continued their efforts in studying hydrates and methane seepage on the continental margin and volcanism in the oceanic rift valleys. A joint international expedition, featuring NRL, German, Norwegian, and Russian ocean scientists, spent five weeks on the Russian oceanographic vessel, the S.S. *Keldysh*. The cruise was to the Greenland-Norwegian Sea continental margin and the Knipovich Ridge Valley, a northern extension of the mid-Atlantic rift zone. The expedition was a follow-up to the 1996 cruise of the S.S. *Professor Logachev* to the same area. On this year's cruise, the Russian deep diving submersibles, the MIRS, were used to carry out ocean bottom studies.

Technology Transfer: During 1998, NRL's Technology Transfer Office continued its successful pattern of facilitating the implementation of NRL technology by the commercial sector by means of Cooperative Research and Development Agreements (CRADAs) and licensing of NRL patents.

NRL established a CRADA with SpecTran Specialty Optics Corporation to implement NRL's patented process for writing Fiber Bragg gratings on optical fibers on the fiber draw tower. This cost-saving processing method will allow SpecTran to manufacture fibers and Fiber Bragg grating arrays for a variety of sensors.

Different configurations of NRL's patented Fiber Bragg grating sensors are being investigated for oil and marine exploration with Schlumberger Technology Corporation and Optical Products, Inc. Schlumberger has licensed NRL's interferometric



NRL's Fiber Bragg grating technology has generated widespread interest in the commercial sector. Applications include exploration for oil and gas reserves, seismic surveys, and strain gauges for structures such as bridges and roads. Schlumberger Technology Corporation and Cidra Corporation have both licensed the technology.

receiver system and, in conjunction with NRL, is developing sensor arrays for land and offshore oil exploration. With Optical Products, NRL is developing towed array sensor systems for seismic applications.

The Condensed Matter & Radiation Sciences Division is using its unique radiation testing capabilities to examine solar cells and other electronic devices under the scope of CRADAs with several organizations, including the University of Houston Space Vacuum Epitaxy Center and Essential Research, Inc.

Under the scope of a CRADA with Envirionics, Inc., NRL's Chemistry Division is assessing the range of performance of its ozone concentration detector. This patented technology allows the detection and measurement of atmospheric ozone at levels as low as five parts per billion. Envirionics plans to market a low-cost, hand-held detector under license from the Navy.

NRL has licensed its hyperspectral imaging system to Space Technology Development Corporation (STDC). STDC is working with NRL on a Dual-use Applications Program (DUAP) to compress and analyze satellite hyperspectral imaging data for commercial

applications, including agriculture, mineralogy, and resource management. (See http://www.acq.osd.mil/ousda/press/fy97_dual-use_slides/sld003.htm for more information.)

The Physical Acoustics Branch of the Acoustics Division is applying its unique near-field acoustic holography (NAH) measurement and analysis methods to the characterization of acoustic noise sources in aerospace structures. This is in collaboration with NASA and several companies, including Automated Analysis Corporation and the Cessna Aircraft Company.

A number of successful CRADAs have been extended to continue development of the research ideas. These include a CRADA with Shipley Company to develop novel liquid crystal displays based on the technology Shipley has licensed from NRL. Different liquid crystal display approaches are also under investigation with SpatiaLight, Inc.

Additionally, NRL has extended its CRADA with Clark-MXR, Inc., to continue investigating its patented high-power amplifiers for use in pulsed mode-locked fiber lasers.

NRL Today

ORGANIZATION AND ADMINISTRATION

The Naval Research Laboratory is a field command under the Chief of Naval Research, who reports to the Secretary of the Navy via the Assistant Secretary of the Navy for Research, Development and Acquisition.

Heading the Laboratory with joint responsibilities are CAPT Bruce W. Buckley, USN, Commanding Officer, and Dr. Timothy Coffey, Director of Research. Line authority passes from the Commanding Officer and the Director of Research to three Associate Directors of Research, a Director of the Naval Center for Space Technology, and an Associate Director for Business Operations. Research is performed in the following areas:

- Systems
- Materials Science and Component Technology
- Ocean and Atmospheric Science and Technology
- Naval Center for Space Technology.

NRL operates as a Navy Working Capital Fund (NWCF). All costs, including overhead, are charged to various research projects. Funding in FY 98 came from the Chief of Naval Research, the Naval Sys-

tems Commands, and other Navy sources; government agencies, such as the U.S. Air Force, Advanced Research Projects Agency, the Department of Energy, and the National Aeronautics and Space Administration; and several nongovernment activities.

PERSONNEL DEVELOPMENT

At the end of FY 98, NRL employed 3359 persons—51 officers, 137 enlisted, and 3171 civilians. In the research staff, there are 869 employees with doctorate degrees, 428 with masters degrees, and 630 with bachelors degrees. The support staff assists the research staff by providing administrative, computer-aided design, machining, fabrication, electronic construction, publication, personnel development, information retrieval, large mainframe computer support, and contracting and supply management services.

Opportunities for higher education and other professional training for NRL employees are available through several programs offered by the Employee Development Branch. These programs provide for graduate work leading to advanced degrees, advanced training, college course work, short courses, continuing education, and career counseling. Graduate students, in certain cases, may use their NRL research for thesis material.



NRL main site, located off Interstate 295 in S.W. Washington, D.C., as viewed from the Potomac River.

For non-NRL employees, several postdoctoral research programs exist. There are also agreements with several universities for student opportunities under the Student Career Experience Program (formerly known as Cooperative Education), as well as summer and part-time employment programs. Summer and interchange programs for college faculty members, professional consultants, and employees of other government agencies are also available.

NRL has active chapters of Women in Science and Engineering, Sigma Xi, Toastmasters International, Federally Employed Women, and the Federal Executive and Professional Association. Three computer clubs meet regularly—NRL Microcomputer User's Group, NeXT, and Sun NRL Users Group. An amateur radio club, a drama group (the Showboaters), and several sports clubs are also active. NRL has a Recreation Club that provides basketball and softball leagues and swim, sauna, whirlpool bath, gymnasium, and weight-room facilities. The Recreation Club also offers classes in martial arts, aerobics, swimming, and water walking.

The Community Outreach Program traditionally has used its extensive resources to foster programs that provide benefits to students and other community citizens. Volunteer employees assist with and judge science fairs, give lectures, and serve as tutors, mentors, coaches, and classroom resource teachers. The program also sponsors African American History Month art and essay contests for local schools, student tours of NRL, a student Toastmasters Youth Leadership Program, an annual holiday party for neighborhood children in December, an equipment/computer transfer program that provides surplus equipment to partnership schools, a book donation program for both students and teachers, and an annual math-science award for high school students. Through the Community Outreach Program, NRL has active partnerships with four District of Columbia, three Aberdeen, Maryland, and three Calvert County, Maryland, public schools.

NRL has an active, growing Credit Union. Since its creation in 1946, NRL Federal Credit Union (NRL FCU) has grown to serve more than 22,000 members and has assets of \$190 million. NRL FCU is a leader in providing innovative financial services such as a dynamic home page and Online Access (Internet home banking) with bill payer. Focusing on the credit union philosophy of *People Helping People*, NRL FCU offers a wide array of no-fee services plus financial education and assistance. NRL FCU is a full service financial institution providing various mortgage programs and creative lending services.

Public transportation to NRL is provided by Metrobus. Metrorail service is three miles away.

For more information, see the *NRL Review* chapter entitled, "Programs for Professional Development."

SCIENTIFIC FACILITIES

In addition to its Washington, D.C., campus of about 130 acres and 102 main buildings, NRL maintains 14 other research sites, including a vessel for fire research and a Flight Support Detachment. The many diverse scientific and technological research and support facilities are described in the following paragraphs.

RESEARCH FACILITIES

Radar

NRL has gained worldwide renown as the "birthplace of radar" and, for a half-century, has maintained its reputation as a leading center for radar-related research and development. An impressive array of facilities managed by NRL's Radar Division continues to contribute to this reputation.

In connection with airborne radar, the division uses a Radar Imaging Facility, employing an inverse synthetic aperture radar (ISAR) deployed either in the air, on the ground, or aboard ship for radar-imaging data collection. There is a space-time adaptive processing (STAP) array and associated processors for the airborne early warning (AEW) area. In connection with ship-based radar, the division operates



View of a portion of the bayfront at the Chesapeake Bay Detachment showing long-range air-search radars on top of the building and the SPQ-9B development facility in the radome and shelter to the right on the ground. The site provides an overwater environment for testing new techniques for fleet radar systems.

a multiuser, high-resolution 3-D visual and audio environment that projects computer-generated images onto three walls and the floor to create an immersive, large-scale, shared virtual environment.

The NEWAVE facility has been developed as a multiscreen distributed simulation laboratory and viewport. Powered by SGI and Pentium workstations and linked to the NRL parallel computing facilities with ATM/SONET networking, the facility is capable of handling high-performance computing, graphics, and distributed simulation.

Optical Sciences

The Optical Sciences Division has a broad program of basic and applied research in optics and electro-optics. Areas of concentration include fiber optics, integrated optical devices, signal processing, optical information processing, fiber-optic and infrared sensors, laser development, surveillance, and reconnaissance.

The division occupies some of the most modern optical facilities in the country. This includes an Ultralow-loss, Fiber-Optic Waveguide Facility using high-temperature infrared glass technology. There is also a Focal-Plane Evaluation Facility to measure the optical and electrical characteristics of infrared focal-plane arrays being developed for advanced Navy sensors. The IR Missile-Seeker Evaluation Facility performs open-loop measurements of the susceptibilities of IR tracking sensors to optical countermeasures. The Large-Optic, High-Precision Tracker system is used for atmospheric transmission and target signature measurements.

There are several fiber-optic sensor facilities with fiber splicers, an acoustic test cell, a three-axis magnetic sensor test cell, equipment for evaluating optical fiber coatings, and various computers for concept analysis. The Digital Processing Facility is used to collect, process, analyze, and manipulate infrared data and imagery from several sources. The Emission Measurements Facility performs measurements of directional hemispherical reflectance. An extensive set of laboratories exist to develop and test new laser and nonlinear frequency conversion concepts and to evaluate nondestructive test and evaluation techniques.

The newest facility is the Infrared Test Chamber, or IR Range, which is an ultradry test chamber used to measure the IR signatures of new surface treatments, scale models, and components used for observables control on ships, aircraft, and missiles.

Electronic Warfare

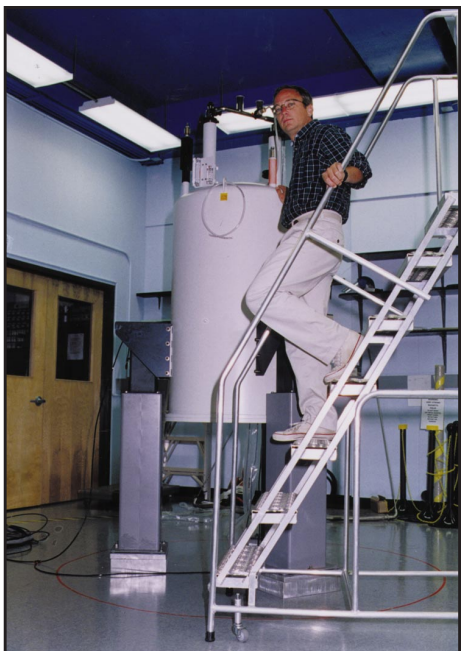
The scope of the Tactical Electronic Warfare (TEW) Division's program for electronic warfare (EW) research and development covers the entire electromagnetic spectrum. The program examines basic technology research and advanced developments and their applicability to producing EW products. The range of ongoing activities includes components, techniques, and subsystems development as well as system conceptualization, design, and effectiveness evaluation. The focus of the research activities extends across the entire breadth of the battlespace. These activities emphasize providing the methods and means to counter enemy hostile actions—from the beginning, when enemy forces are being mobilized for an attack, through to the final stages of the engagement. In conducting this program, the TEW Division has an extensive array of special research and development laboratories, anechoic chambers, and modern computer systems for modeling and simulation work. Dedicated field sites and an NP-3D EW flying laboratory allow for the conduct of field experiments and operational trials. This assembly of scientists, engineers, and specialized facilities also facilitates the innovative use of all organic defensive and offensive EW resources now available to the Fleet.

Laboratory for Structure of Matter

This laboratory investigates the atomic arrangements in materials to improve them or facilitate the development of new substances. Various diffraction methodologies are used to make these investigations. Subjects of interest include the structural and functional aspects of energy conversion, ion transport, device materials, and physiologically active substances such as drugs, antibiotics, and antiviral agents. Theoretical chemistry calculations are used to complement the structural research. A real-time graphics system aids in modeling and molecular dynamics studies.

Chemistry

NRL has been a major center for chemical research in support of naval operational requirements since the late 1920s. The Chemistry Division continues this tradition with a broad spectrum of basic and applied research programs focusing on controlled energy release (fuels, fire, combustion, countermea-



A new high-field, self-shielded 500 MHz nuclear magnetic resonance (NMR) spectroscopy system comes online in the Chemistry Division. Dr. Ken McGrath makes final adjustments to the magnet component of the new instrumentation. NMR provides an unparalleled ability to nondestructively probe the smallest internal structures of materials.

sure decoys, explosives), surface chemistry (corrosion, adhesion, tribology, adsorbents, film growth/etch), advanced materials (high-strength/low-weight structures, drag reduction, damping, polymers, thin films), and advanced detection techniques (environment, chemical/biological, surveillance). Facilities for research include a wide range of modern photon/electron, magnetic- and ion-based spectroscopic/microscopic techniques for bulk and surface analysis; nanometer-scale fabrication and characterization; multiple facilities for materials synthesis and physical/chemical characterization; an 11,400 ft³ fire-research chamber (Fire I); and the 475-ft ex-USS *Shadwell* (LSD-15) advanced fire-research ship.

The new Environmental Quality Sciences Section has a mission that includes characterization of chemically polluted environments, remediation technologies and evaluations, pollution-prevention strategies for Fleet and shore-side operations, environmental security, and disposal of chemical-warfare agents. Facilities in support of this research are laboratories for molecular biology, microbiology, biodegradation assessment, environmental biosensors, and geochemistry. In addition, a mesocosm facility has

been established to bridge between laboratory and field work, with controlled scale-up of environmental systems.

Materials Science and Technology

NRL has capabilities for X-ray and electron-diffraction analyses and for electron and Auger spectroscopy. Scanning, transmission, and combined scanning-transmission electron microscopes are used to study surface and/or internal microstructures. The division has a secondary ion mass spectrometer for surface analysis that significantly extends the diagnostic capability of the technique. A high-resolution, reverse-geometry mass spectrometer is used to probe reactions between ions and molecules. The Laboratory has a fully equipped fatigue and fracture laboratory, a modern vacuum arc-melting furnace for reactive metals, an ultrasonic gas-atomization system for making metal powders, and hot isostatic press facilities. The Laboratory's cryogenic facilities include dilution refrigerators and superconducting magnetic sensors for measuring ultrasmall magnetic fields. Also available are two molecular beam epitaxy devices for growing thin films.

Laboratory for Computational Physics and Fluid Dynamics

The Laboratory for Computational Physics and Fluid Dynamics is in round-the-clock production for computational studies in the fields of compressible and incompressible fluid dynamics, reactive flows, fluid-structure interaction (including submarine, ship, and aerospace applications), atmospheric and solar magnetoplasma dynamics, application of parallel processing to large-scale problems such as unstructured grid generation for complex flows, target tracking and correlations for battle management, and other disciplines of continuum and quantum computational physics. The facility is used to develop and maintain state-of-the-art analytical and computational capabilities in fluid dynamics and related fields of physics, to establish in-house expertise in parallel processing and on-line graphical rendering for large-scale scientific computing, to perform analyses and computational experiments on specific relevant problems, and to transfer this technology to new and ongoing projects through cooperative programs.

The Parallel High Performance Computer/Graphics Facility is a heterogeneous high-performance computer system composed of a number of autonomous computers with a composite peak speed

equivalent to about 15 Cray 90 processors. The system is coupled directly to the advanced video recording center described below. The main computational engine comprises three Intel iPSC/860 Touchstone Gamma parallel supercomputers supported by the hardware and software environment necessary to develop, debug, and benchmark parallel simulations. With multi-Mflop processors as building blocks, the Intel iPSC/860 is a MIMD-distributed memory machine configured as a hypercube. These three machines comprise a block of 224 parallel nodes with a peak computational speed of 18 Gflops with a cross-connected disk farm file system and network connections.

The facility's disk farm also supports three IBM RS/6000 and three DEC AXP high-capacity compute-server computers, providing the facility with medium-to-large-scale memory and computational power enabling heterogeneous simulations with a significant scalar component, algorithm development, and diagnostic and postprocessing for large simulations. Special software allows simultaneous use of these computers on a single problem. Access to various other HPC capabilities around the United States is accomplished through this system by using the new DoD high-bandwidth communication networks. A six-processor, 5-Gbyte SGI Onyx provides the division with state-of-the-art high-performance visualization.

A high-quality video studio has been created around a Sony D2 digital recording system, with a coupled Lyon-Lamb animation controller and a large memory Silicon Graphics ONYX workstation. Through the network, other graphics stations, including the extensive resources of NRL's Visualization Laboratory, can create and record high-quality graphical images of simulation data for analysis and presentation by using digital recording techniques.

Condensed Matter and Radiation Sciences

The Condensed Matter and Radiation Sciences Division is the primary Navy center studying the effects of radiation on materials, electronic equipment, satellites, etc., and the production of thin films on diverse objects. The facilities for production and employment of photons, ions, and hypervelocity projectiles available to the division include:

High-Power Microwave (HPM) Facility: The large anechoic chamber (4.9 m × 4.9 m × 9.8 m) can be used at frequencies ranging from 0.5 to 94 GHz. Effects, susceptibility, and survivability of systems are the major research areas of interest.

Trace Element Accelerator Mass Spectrometry (TEAMS) – 3 MV Tandem Pelletron Accelerator Facility: Used for standard materials analysis such as Rutherford backscattering, for MeV-energy ion implantation and, new in 1998, for accelerator mass spectrometry (AMS). AMS measures trace elements in parallel with 3-D imaging at 10- μ m lateral resolution (0.01 μ m in depth) to 10-ppt sensitivity, and isotopes for sample dating and forensics.

Laser Facilities: Pulses of up to several joules are available from one system, while time resolutions down to 30 femtoseconds are produced by another. Synchronized Q-switched oscillators are configured for pump-probe experiments.

Thin-Film Preparation Facilities: The division has several major capabilities for preparation of thin films of advanced materials, such as high-temperature superconductors and active dielectrics. These include ion-assisted evaporation (which produces dense, adherent films), various dc plasma sources (which can etch as well as deposit films), and pulsed laser deposition (for production of chemically complex films).



View of high-energy segment of the Condensed Matter and Radiation Sciences Division Trace Element Accelerator Mass Spectrometry (TEAMS) facility showing the ± 100 kV, 30° electrostatic analyzer (silver dome on right) and the 33-ton Enge split-pole magnetic spectrograph with 1.5-m-long focal plane (blue magnet on left).

X-ray Facility: Laboratory X-ray sources, monochromators, detectors, and related equipment are available for X-ray energies from 0.7 to 25 keV and dose rates up to 10^5 rads/s.

Synchrotron Radiation Facility: Intense, monochromatic X-ray photon beams tunable from 10 eV to 12 keV are available from the three beam lines developed by NRL at the National Synchrotron Light Source at the Brookhaven National Laboratory. Environmental target chambers can span a pressure range from 10^{-12} to 10^5 atm and temperatures from 10 to 1500 K.

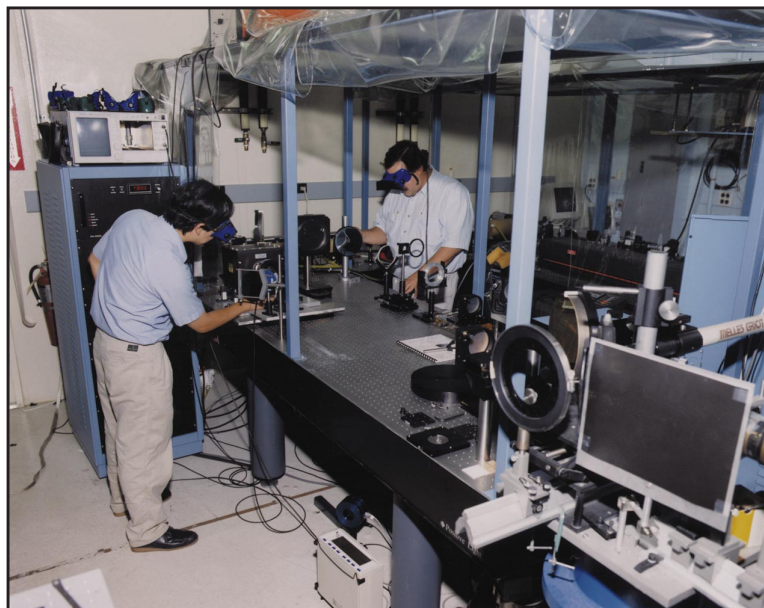
Ion Implantation Facility: The facility consists of a 200-keV ion implanter with specialized ultra-high vacuum chambers and associated in situ specimen analysis instrumentation.

3-MeV Tandem Van de Graaff: This facility is used to study charged-particle radiation damage effects such as occur in space, to provide high-sensitivity analysis of materials, and to perform MeV energy implants in materials.

Plasma Physics

The Plasma Physics Division is the major center for in-house Navy and DoD plasma physics research. The division conducts a broad experimental and theoretical program in basic and applied research in plasma physics, which includes laboratory and space

plasmas, pulsed-power sources, plasma discharges, intense electron and ion beams and photon sources, atomic physics, laser physics, advanced spectral diagnostics, plasma processing, nonlinear dynamics and chaos, and numerical simulations. The facilities include an extremely high-power laser—Pharos III—for the laboratory simulation of space plasmas and nuclear weapons effects studies and a short pulse, high-intensity Table-Top Terawatt (T^3) laser to study intense laser-plasma, laser-electron beam, and laser-matter interactions. The division also has an 11 m^3 space chamber capable of reproducing the near-Earth space plasma environment and a Large Area Plasma Processing System (LAPPS) facility to study material modification such as surface polymerization or ion implantation. The division has developed a variety of pulsed-power sources to generate intense electron and ion beams, powerful discharges, and various types of radiation. The largest of these pulsers—GAMBLE II—is used to study the production of megampere electron and ion beams and to produce very hot, high-density plasmas. Other generators are used to produce particle beams that are injected into magnetic fields and/or cavities to generate intense microwave pulses (e.g., the Relativistic Klystron Amplifier (RKA), in the 1 to 10 GHz regime). A large array of high-frequency microwave sources (35 to 120 GHz) are available to conduct research on microwave processing of advanced ceramic materials.



The NRL Table-Top-Terawatt (T^3) Laser Facility. The T^3 laser currently operates at 0.4 ps, 2.5 TW, and $5 \times 10^{18}\text{ W/cm}^2$ and provides a facility to conduct research in intense laser-plasma interactions, intense laser-electron beam interactions, and intense laser-matter interactions.

A major 3 kJ KrF laser facility opened in June 1995. This facility is being initiated to provide intense radiation for studying inertial confinement fusion target heating at short wavelengths (0.25 microns) and high-pressure physics.

Electronics Science and Technology

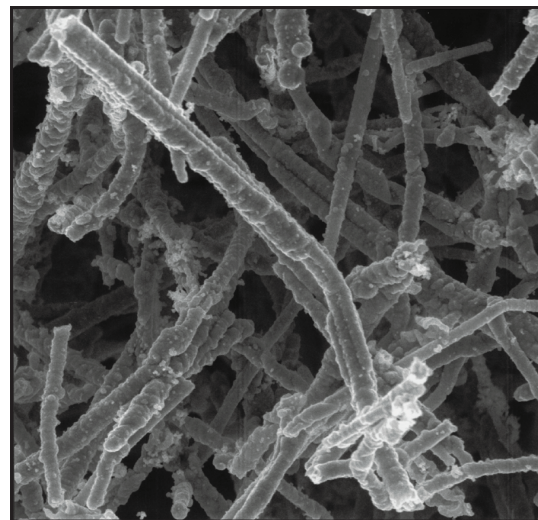
In addition to specific equipment and facilities to support individual science and technology programs, NRL operates the Nanoelectronics Processing Facility (NPF), the Penthouse Processing Facility (PPF), the Laboratory for Advanced Material Synthesis (LAMS), and the EPICENTER. The NPF's mission is to provide service to both NRL and external organizations requiring micro- and nanofabrication processing support. Lithography is a particular strength of the NPF, with definition of feature sizes down to 150 Å possible with an e-beam nanowriter. The NPF can supply items ranging from individual discrete structures and devices to circuits with very-large-scale integration complexity. The PPF is dedicated to processing III-V semiconductor devices and circuits in addition to serving the hands-on fabrication needs of individual NRL scientists. The PPF uses a single-pass air-ventilation system to minimize human risk to potentially hazardous III-V semiconductor processes and associated chemicals, thereby further meeting existing safety standards. The LAMS fabricates thin epitaxial layers of semiconductors that are used in fundamental and applied studies of new materials and novel device concepts for use in, for example, high-temperature or high-power device structures. The LAMS uses organometallic vapor phase epitaxy to synthesize a wide range of thin films such as InSb, InGaP, InP, and GaN. The EPICENTER (a joint activity of the Electronics Science and Technology, Materials Science and Technology, and Chemistry Divisions) is dedicated to the production of multilayer microstructures using in situ surface analytical techniques in either of two ultrahigh vacuum, molecular-beam-epitaxy growth chambers—one for III-V semiconductors and the other for magnetic materials and II-VI semiconductors.

Bio/Molecular Science and Engineering

The Center for Bio/Molecular Science and Engineering conducts research and development using biotechnological approaches to solve problems for the Navy, DoD, and the nation at large. Problems currently being addressed include advanced material development (for electronic, biomedical, and struc-

tural applications), environmental quality (including pollution cleanup and control), and biological warfare defense. The approach to these problems involves long-term research focused on the study of complex materials systems, coupled with integrated exploratory and advanced development programs. The staff of the center is an interdisciplinary team that performs basic and applied research and development in areas that require expertise in bio- and surface chemistry, biophysics, genetic engineering, cell biology, advanced organic synthesis, solid-state and theoretical physics, and electronics and materials engineering. In addition, the center has many collaborations throughout the Laboratory, at universities, and in industry to ensure that a broad base of the required expertise and critical evaluations are part of the research and development programs. Highlights of the program include the manipulation of biologically derived structures on the nanometer scale, the development of ferroelectric liquid crystal systems with microsecond response times, discovery of an advanced resist system for high-speed, high-density integrated circuits, the patterning of neuronal cells to form neural networks, and the development of biosensors for environmental monitoring.

Since October 1994, the center has occupied newly renovated laboratories and offices in Building 30. These modern facilities, designed to be used into the next century, include general laboratories for research in chemistry, biochemistry, molecular biology, and physics. Specialized areas include a 600-ft² Class 1000 clean room; an advanced Electron Microscope facility; and a Scanning Probe Microscope labora-



Novel biomaterial derived from self-assembled lipid tubules.

tory. Instrument rooms in the new building provide access to a variety of spectrophotometers (IR, GC-MS, NMR, and UV-Vis) and other equipment used in biochemical or physical analyses of biomaterials. Additional laboratories accommodate an X-ray diffraction instrument, a liquid crystal fabrication facility, and equipment for advanced electronics and biosensor programs.

Acoustics

The Acoustics Division has three integrated acoustic pool facilities, including one with a sandy bottom, that support research in submarine target characteristics for ASW, submarine acoustic design and quieting, sensors for hull-mounted sonars, and structural acoustics for mine countermeasures and torpedo quieting. Scaled submarine targets, real mine structures, sensors mounted on hull simulators, underwater buried objects, and actual torpedoes can all be examined with advanced nearfield holographic and scanning 3-D laser vibrometer systems to measure and visualize the sound fields near a structure, the vibrations of the structure itself, the resulting farfield sound fields, and the physics of the sound-structure-fluid interactions.

The division operates several acoustic projectors and receive arrays for the generation and collection of experimental data. Source projectors include five towed XF4 flextensional transducers, two moored organ-pipe projectors, and a battery-operated arbitrary waveform projector system. Receive systems include a moored, 32-element (up to 50 kHz) vertical array with an RF telemetry system, a 64-element (25 Hz to 2 kHz) towed oil-filled seismic-type array, and a 64-element (25 Hz to 2 kHz) array that can either be deployed along the ocean bottom or moored vertically. The 64-element arrays use direct-link cabling to a 256-channel (expendable to 1024 channel), 50 kHz bandwidth data acquisition and processing system with a 330 Gbyte recording system. The division also has unique, self-recording digital acquisition buoy systems (DABS) that are used to obtain multichannel (up to 128) acoustic data in the 10 Hz to 5 kHz regime. These systems provide up to 250 Gbytes of data on a single 15-in. reel of 1-in. tape. The division has recently developed the Satellite-Linked Vertical Line Array (SLVA) system to collect acoustic and oceanographic data and transmit selected data to a remote shore station in real time. The buoy has a local-area network and computers on board to control the collection, preprocessing, and transmission of data. The multichannel data are sent via



NRL's Satellite-Linked Vertical Line Array (SVLA) buoy during a recent ocean deployment. Data from an array of hydrophones are collected and stored within the buoy and simultaneously transmitted to both ships in the vicinity and distant shore stations using RF and satellite communications.

high-speed satellite channel at speeds in excess of 1 Mbit/s, using commercial K_u -band satellites.

The division conducts underwater acoustic communications research using digital, acoustic modems capable of receiving and processing signals from 8 channels at various carrier frequencies and with various bit rates.

The division operates high-frequency (up to 600 kHz) acoustic measurement systems to obtain scattering, target strength, and propagation data using bottom-moored instrumentation towers and a high-speed, remotely operated vehicle. These data are used to simulate the performance of weapons and mine countermeasure sonars (including advanced synthetic aperture sonars) in shallow and very shallow water environments.

The Tactical Oceanography Simulation Laboratory (TOSL) is a modeling and simulation architecture consisting of a set of tools for ingesting and processing climatological and real-time environmental data and applying energy propagation models to those data to determine acoustic and nonacoustic propagation loss. TOSL also contains tools to provide physical performance modeling using the available environmental data. TOSL is coupled with a storage repository of environmental data and a wide-area network (WAN), which allow full participation in a

distributed simulation environment. TOSL features a high-performance computational capability to provide real or near-real-time calculations in support of training, war games, operations rehearsal, and other distributed simulation functions.

Remote Sensing

The Remote Sensing Division conducts a program of basic research, science, and applications to develop new concepts for sensors and imaging systems for objects and targets on Earth, in the near-Earth environment, and in deep space. The research, both theoretical and experimental, leads to discovering and understanding the basic physical principles and mechanisms that give rise to background environmental emissions and targets of interest and to absorption and emission mechanisms of the intervening medium. Accomplishing this research requires the development of sensor systems' technology. The developmental effort includes active and passive sensor systems used for the study and analysis of the physical characteristics of phenomena that evolve from naturally occurring background radiation, such as that caused by the Earth's atmosphere and oceans and man-made or induced phenomena, such as ship/submarine hydrodynamic effects. The research includes theory, laboratory, and field experiments leading to ground-based, airborne, or space systems for use in remote sensing, astrometry, astrophysics, surveillance, nonacoustic ASW, meteorological/oceanographic support systems for the operational Navy, and the environmental/global climate change initiatives. Special emphasis is given to developing space-based platforms and exploiting existing space systems.

The Navy Prototype Optical Interferometer (NPOI), a major facility of the Remote Sensing Division, is actually two collocated instruments for making high-angular-resolution optical measurements of stars. Light from widely separated individual siderostats is combined simultaneously to synthesize the angular resolution of a telescope tens to hundreds of meters in diameter. Four siderostats are placed in an array with extremely accurate metrology to enable very-high-precision measurements of stellar positions (wide-angle astrometry). These measurements are used by the U.S. Naval Observatory to refine the celestial reference frame, determine Earth rotation parameters, and thus satisfy Navy requirements for precise time and navigation data. They also provide determinations of basic astrophysical parameters, such as stellar masses and diameters. Additional relocatable siderostats can be placed out

to distances of 250 m from the array center and used to construct very-high-resolution images of stars. These images provide fundamental astrophysical information on stellar structure and activity. When complete, the NPOI will be the most advanced high-resolution imaging optical interferometer in the world.

Oceanography

The Oceanography Division is the major center for in-house Navy research and development in oceanography. It is known nationally and internationally for its unique combination of theoretical, numerical, experimental, and remote sensing approaches to oceanographic problems. The division numerically models the ocean and coastal areas of the world. This modeling is conducted on the Navy's and DoD's most powerful vector and parallel-processing machines. To study the results of this intense modeling effort, the division operates a number of highly sophisticated graphic systems to visualize ocean and coastal dynamic processes. The seagoing experimental programs of the division range worldwide. Unique measurement systems include towed sensor and advanced microstructure profiler systems for studying micro- and fine-scale ocean structures; an integrated absorption cavity, optical profiler system, and towed optical hyperspectral towed array for studying ocean optical characteristics; and self-contained bottom-mounted upward-looking acoustic Doppler current profilers for measuring ocean variability. In the laboratory, the division operates an environmental scanning electron microscope and a laser confocal scanning microscope for detailed studies of biocorrosion in naval materials. The division's remote sensing capabilities include the ability to analyze and process multi/hyper-spectral, IR, SAR, and other satellite data sources. The division is a national leader in the development and analysis of Sea WiFS data for oceanographic processes and naval application in littoral areas.

Marine Geosciences

The Marine Geosciences Division is the major center for in-house naval research and development in marine geology, geophysics, geoacoustics, and geotechnology. It is also the Navy's lead activity for mapping, charting, and geodesy research and development. The division has acquired unique instrumentation suites for studies of the seafloor and subseafloor. These include sidescan sonar systems; a deep-towed, low-frequency acoustic-reflection system; a parametric acoustic-swath subbottom-mapping system;



The Marine Geosciences Division's JEM-3010 scanning and transmission electron microscope (STEM) provides images of hydrated samples sealed within a carbon windowed chamber at close to atmospheric pressures. STEM's main advantage is its higher voltage, which provides greater resolution, greater ability to view thicker samples, less electron beam damage to sensitive organic samples, and enhanced analytical performance.

remotely operated vehicles; and electromagnetic mapping sensors. These systems allow studies ranging from sediment classification to mapping of inclusions and changes in the seafloor subbottom structure. The division deploys ocean bottom and subbottom seismometer systems for use in studies ranging from tectonic noise to whale migration. Specialized seafloor probes allow measurement of the water pressure in sediment pores, electrical conductivity, and acoustic compression and shear wave velocity and attenuation. Laboratory equipment includes two transmission electron microscopes (100 and 300 kV) with environmental cells to carry out sediment-fabric and sediment-pollutant adsorption studies.

The Moving-Map Composer Facility, a collection of computers and work stations with associated graphics manipulation software, is used to design mission-specific map coverages for tactical fighter pilots and to compress map information onto a CD-ROM for Navy and Marine Corps aircraft digital moving maps. The division also operates the NRL Magnetic Observatory at SSC. This facility includes two specially built wooden buildings with minimal ferrous content and arrays of magnetometers that extend radially from the building. The Magnetic Observatory measures the Earth's ambient magnetic field, its changes, and other magnetic phenomena. The observatory is part of a worldwide observing system.

Marine Meteorology

The Marine Meteorology Division is located in Monterey, California. NRL-Monterey (NRL-MRY) is the only Navy facility with a mission to serve the Navy's needs for basic research in atmospheric sciences and its need for the development of meteorological analysis and prediction products to support

global and tactical operations. The division is dedicated to advancing fundamental scientific understanding of the atmosphere, to applying scientific discoveries in the development of innovative objective weather prediction systems, and to developing ways to provide atmospheric data input to the tactical decision maker.

NRL-MRY is collocated with Fleet Numerical Meteorology and Oceanography Center (FNMOC), the Navy's operational center of expertise in numerical weather prediction. This provides NRL-MRY efficient access to a variety of classified and unclassified computer resources, databases, and numerical prediction systems. Large supercomputer mainframes and databases at FNMOC are used along with local NRL-MRY resources to develop and transition operational analysis and prediction systems, and to provide on-site and remote access to the model output data for continued research purposes. NRL-MRY is also networked to the DoD High Performance Computing Centers, which support research in atmospheric process studies and coupled air-ocean model development. In addition, interfaces to the Defense Research and Engineering Network have also been established.

Locally, to support research and development needs, NRL-MRY has recently established the Bergen Data Center. This Center includes a 24TB capacity data center with a hierarchical storage management capability to provide archival and easy retrieval of research data sets. The John B. Hovermale Visualization Laboratory provides state-of-the-art capability for data visualization, which aids the interpretation of both observational and modeled data and the development of weather briefing tools. High-performance graphics workstations, network file-servers, and tactical applications systems are used to conduct numerical weather prediction experiments, process

and analyze satellite data, perform simulation studies, and provide demonstrations of tactical weather products. State-of-the-art satellite receiving and processing systems allow local collection of real-time geostationary data globally, from four different satellites, for applications research in support of the Navy and Joint Typhoon Warning Center operations. This capability has allowed NRL-MRY to take the lead in developing meteorological applications of satellite data for the NSDS-E (Navy Satellite Display System-Enhanced), which is currently being installed at the Navy's regional meteorological/oceanographic (METOC) centers.

Space Science

The Space Science Division conducts and supports a number of space experiments in the areas of upper atmospheric, solar, and astronomical research aboard NASA, DoD, and other government-agency space platforms. Division scientists are involved in major research thrusts that include remote sensing of the upper and middle atmospheres, studies of the solar atmosphere, and astronomical radiation ranging from the ultraviolet through cosmic rays. In support of this work, the division maintains facilities to design, construct, assemble, and calibrate space experiments. A network of computers, workstations, image-processing hardware, and special processors is used to analyze and interpret space data. The division's space science data acquisition and analysis efforts include: mission operations and data analyses of the Oriented Scintillation Spectrometer Experiment (OSSE) for NASA's Compton Observatory; observation of the Sun's interaction with the Earth's upper atmosphere through the Solar Ultraviolet Spectral Irradiance Monitor (SUSIM) experiment in support of NASA's Upper Atmosphere Research Satellite (UARS); observation and analysis of solar flares using the Bragg Crystal Spectrometer (BCS) on the Japanese Yohkoh space mission; and observation and analysis of the evolution and structure of the solar corona from the disk to 0.14 AU. This latter effort involves acquiring and analyzing data from the Large-Angle Spectrometric Coronagraph (LASCO) and Extreme Ultraviolet Imaging Telescope (EIT) on the Solar Heliospheric Observatory satellite. In each of these missions, NRL maintains a complete database of spacecraft observations and control over acquisition of data from new observations. These data are available to qualified investigators at DoD and civilian

agencies. In addition, the division has a sounding rocket program that affords the possibility of obtaining specific data of high interest and of testing new instrument concepts. These include the general area of high-resolution solar and stellar spectroscopy, extreme ultraviolet imagery of the Sun, and high-resolution, ultraviolet spectral-imaging of the Sun.

In addition, selected celestial and atmospheric targets in the ultraviolet and X-ray bands are observed by three Advanced Research and Global Observation Satellite (ARGOS) experiments—Global Imaging of the Ionosphere (GIMI), High-Resolution Airglow and Auroral Spectroscopy (HIRAAS), and Unconventional Stellar Aspect (USA). ARGOS is scheduled to be launched in early 1999. As part of this program, NRL is establishing collaborative programs to make use of ARGOS data to validate various upper atmosphere models.

Optical calibration facilities, including clean rooms, are maintained to support these activities. These calibration facilities are routinely used by outside groups to support their own calibration requirements.

Space Technology

In its role as a center of excellence for space systems research, the Naval Center for Space Technology (NCST) designs, builds, analyzes, tests, and operates spacecraft as well as identifies and conducts promising research to improve spacecraft and their support systems. NCST facilities that support this work include large and small anechoic radio frequency chambers, clean rooms, shock and vibration facilities, an acoustic reverberation chamber, large and small thermal/vacuum test chambers, a control system interaction laboratory, satellite command and control ground stations, a fuels test facility, and modal analysis test facilities. Also, the Center maintains and operates a number of electrical and electronic development laboratories and fabrication facilities for radio frequency equipment, spacecraft power systems, telemetry, and command and control systems, and includes an electromagnetic interference-electromagnetic compatibility test chamber. NCST has a facility for long-term testing of satellite clock time/frequency standards under thermal/vacuum conditions linked to the Naval Observatory; a 5-m optical bench laser laboratory; and an electro-optical communication research laboratory to conduct research in support of the development of space systems.

RESEARCH SUPPORT FACILITIES

Technical Information Services

The Ruth H. Hooker Research Library carries out a comprehensive program of scientific information services to support the research of NRL-DC employees, on-site contractors, and ONR Headquarters staff. The Library maintains a 50,000-volume research collection of technical books and scholarly monographs; a scientific journal collection containing approximately 1,000 current subscriptions, with extensive back files maintained as bound volumes or on microfilm; and a research reports collection of more than one million items stored in paper, microform, and digital format. Services include the circulation of library materials, interlibrary loan, literature searches, and a full range of reference and information services covering both open-literature and classified information sources.

The Library is in the forefront in implementing digital services to enable researchers to meet their information needs 24 hours a day, 7 days a week, from work, at home, or while on travel. Through the InfoWeb Information System and Gateway [<http://infoweb.nrl.navy.mil>], NRL users in Washington, DC, Bay St. Louis, Mississippi, Monterey, California, and at ONR Headquarters in Arlington, Virginia, have a single point of entry to hundreds of locally stored and distributed databases and publications. Some important examples of InfoWeb resources are: the STILAS Web-based catalog with hyperlinks to thousands of reports the Library has digitized; OCLC First Search for searching INSPEC and 50 other databases; the ISI "Web of Science" Science Citation Index Expanded, covering the years 1973 to present; the subscription module for the Contents-to-Go journal

alerting service; and TORPEDO Ultra, for browsing and searching some 250 locally archived journals, thousands of research reports, and NRL publications including press releases, journal articles, and conference papers. InfoWeb also links users to another 300 journals available from publisher Web sites under license agreements implemented by the Library.

The Library has entered into a collaborative relationship with publishers and with other libraries to increase the range of digital resources it can make available. For example, it is currently assisting the American Institute of Physics in expanding the digital contents of its Web-based Online Journal Service under a Cooperative Research and Development Agreement (CRADA). In 1997, the Library formed the National Research Library Alliance with the libraries of the National Institute of Standards and Technology, NASA Goddard Space Flight Center, and the National Science Foundation. In 1998, it became an associate member of the New Mexico Library Alliance, strengthening its relationships with both Los Alamos National Laboratory and the Air Force (Phillips) Research Laboratory. In 1998, it also became part of the collaborative Digital Library Initiative at the University of Illinois at Urbana-Champaign. The NRL Library joins with other Navy libraries to license databases and electronic publications through the Consortium of Navy Libraries.

Publication services include writing, editing, composition, publications consultation and production, and printing management. Quick turnaround black and white as well as color copying services are provided. The primary focus is on using computer-assisted publishing technology to produce scientific and technical information containing complex artwork, equations, and tabular material.



The Publications Branch of the Technical Information Division has a Xerox DocuColor 40, a digital color production system that provides high volume, print-on-demand, and fast turnaround color copying at a speed of 40 copies per minute.

The research conducted at NRL requires a diversity of graphic support from the Systems/Photographic Branch. This support includes technical and scientific illustrations, computer graphics, design services, photographic composites, calligraphy, display panels, sign making, and framing. Photographic services include still-camera coverage for data documentation both at NRL and in the field. Photographic images can also be captured with state-of-the-art digital cameras. A photographic laboratory offers custom processing and printing of black and white and color films. Quick-service color prints are also available. Video services include producing video reports of scientific and technical programs. A video studio and editing facility with high-quality Beta Cam and digital video editing equipment are available to support video production. The NRL Exhibits Program develops and produces displays, audiovisual material, and multimedia programs for presentation at technical meetings, conferences, and symposia. The Multimedia Center has the capability of authoring/producing multimedia programs. The Center uses two complete multimedia systems with Macromedia Director and Adobe Photoshop and a digital video editing system, the AVID Media Composer 1000. The Visual Design/Imaging Center offers high-quality output from computer-generated files in EPS, Postscript, PICT, TIFF, Photoshop, and PowerPoint. Photographic-quality color prints and viewgraphs are available from Kodak dye-sublimation printers. High-resolution scanning to a Macintosh or PC disk is available. The Novajet Pro 600c printer offers excep-



The Multimedia Center has the capability of authoring/producing multimedia programs. The Center uses two complete multimedia systems with Macromedia Director and Adobe Photoshop and a digital video editing system, the AVID Media Composer 1000.

tional color print quality up to 600 dpi. It produces large-format posters and signs up to 60 inches wide.

The Administrative Services Branch is responsible for collecting and preserving the documents that comprise NRL's corporate memory. Archival documents include personal papers and correspondence, laboratory notebooks, and work project files—documents that are appraised for their historical or informational value and considered to be permanently valuable. The branch provides records management services, training, and support for the maintenance of active records, including electronic records and e-mail, as an important information resource. The Administrative Services Branch is also responsible for NRL's postal mail services, NRL's Forms and Reports management programs (including electronic forms), coordination of NRL's parking facilities, and scheduling of NRL auditoriums.

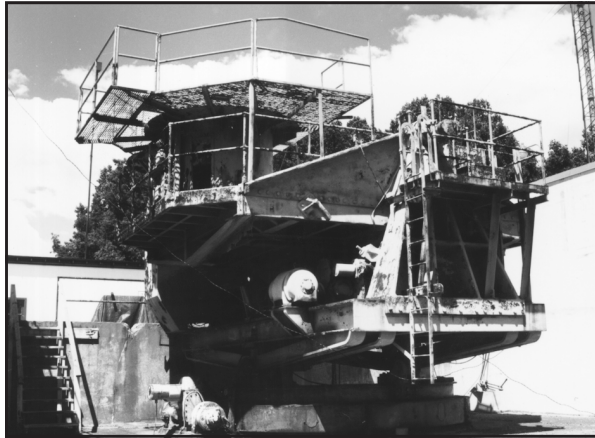
Center for Computational Science

The Center for Computational Science (CCS) conducts research and development to further the advancement of computing and communications systems to solve Navy problems. Promising technologies are transitioned to production systems. The CCS develops and maintains a leading-edge information infrastructure that provides support for NRL, Navy, and DoD research. The CCS participates as a Distributed Center in the DoD High Performance Computing Modernization Program with three massively parallel High Performance Computing (HPC) systems: a 128-processor SGI/Cray Origin2000, a 64-processor HP/Convex Exemplar SPP-2000, and a 148-processor Sun HPC Ultra. File services and archival storage are provided by robotic storage systems running the Multiresident Andrew File System (MRAFS) for both NRL and HPC applications.

The CCS pioneered and maintains the Washington area ATDnet experimental ATM network and is a partner in the MONET research effort. MONET is a leading-edge, all-optical, transparent network being deployed within ATDnet as a part of the DARPA/HPCC Next Generation Internet initiative.

The CCS collaborates with industry and DoD in the development of leading-edge progressive motion imagery for broadcast and network dissemination of all-digital HDTV signals at 720-p and 1080-p.

Additional CCS computational facilities are provided for general NRL use. These include the Scientific Visualization Laboratory (Viz Lab), which functions as an information center, a video production unit, and a training center for the latest tools in scientific visualization and visual supercomputing.



The ship-motion simulator, located on the shoreline of the Chesapeake Bay at NRL's Chesapeake Bay Detachment, allows radar, satellite communications, and line-of-sight RF communications systems to be tested before shipboard installation or in lieu of actual at-sea testing.

degrees (5 degrees to stern and 5 degrees to bow). Periods along both axes, pitch and roll, are variable—from a slow 32-s to a brisk 4-s rate. Variable azimuth motion can also be added to the pitch and roll action. Synchronized positioning information ($\times 1$ and $\times 36$) is available for each of the three axes of the SMS.

Because of its location high above the western shore of the Chesapeake Bay, unique experiments can be performed in conjunction with the Tilghman Island site, 16 km across the bay from CBD. Some of these experiments include low clutter and generally low-background radar measurements. By using CBD's support vessels, experiments are performed that involve dispensing chaff over water and radar target characterizations of aircraft and ships. Basic research is also conducted in radar antenna properties, testing of radar remote-sensing concepts, use of radar to sense ocean waves, and laser propagation. CBD also hosts facilities of the Navy Technology Center for Safety and Survivability, which conducts fire research on simulated carrier, surface, and submarine platforms.

Marine Corrosion Test Facility

Located on Fleming Key at Key West, Florida, this facility offers an ocean-air environment and clear, unpolluted, flowing seawater for studies of environmental effects on materials. Equipment is available for experiments involving weathering, general corrosion, fouling, and electrochemical phenomena as well as coatings, cathodic protection devices, and other means to combat environmental degradation.

Stennis Space Center (NRL-SSC)

NRL-SSC, a tenant activity at NASA's Stennis Space Center, is located in the southwest corner of Mississippi, about 50 miles northeast of New Orleans, Louisiana, and 20 miles from the Mississippi Gulf Coast. The Center encompasses more than 200 square miles of land area, including a perimeter buffer zone to insulate surrounding civilian communities from the noise of rocket-engine testing by NASA. Other Navy tenants at SSC include the Commander, Naval Meteorology and Oceanography Command and the Naval Oceanographic Office, who are major operational users of the oceanographic and atmospheric research and development performed by NRL. The Naval Oceanographic Office provides access for NRL researchers to one of the Navy's largest supercomputers. This unique concentration of operational and research oceanographers makes SSC the center of naval oceanography and the largest such grouping in the Western world.

NRL-SSC provides administrative and business operations for entities of the Acoustics and Marine Geosciences Division and the Oceanography Division. NRL-SSC occupies more than 200,000 square feet of research, computation, laboratory, administrative, and warehouse space. Facilities include the new microscopy center, a visualization laboratory, numerous large antennas to receive available oceanographic and meteorological satellite data, the Magnetic Observatory—part of a worldwide observing system, the Pattern Analysis Laboratory, a Map Data Formatting Facility, and numerous laboratories for acoustic and oceanographic computation, instrumentation, analysis, and testing. Special areas are available for constructing, staging, refurbishing, and storing sea-going equipment.

Marine Meteorology Division (NRL-MRY)

NRL's Marine Meteorology Division (NRL-MRY) is located in Monterey, California, on the grounds of the Naval Postgraduate School (NPS) Annex, which is about a mile from the NPS main campus. As a tenant activity of the Naval Support Activity, Monterey Bay, the NRL facility is collocated with the Navy's operational Fleet Numerical Meteorology and Oceanography Center (FNMOC) and with a NOAA National Weather Service Forecast Office (NWSFO). The NPS Annex campus, which covers approximately 5 acres, comprises four primary buildings—one occupied exclusively by NOAA, one that houses the FNMOC supercomputer/operational facility, and two large

buildings containing office space, computer laboratories, and conference facilities that are shared by FNMOC and NRL-MRY personnel. The site also provides warehouse space and recreational facilities. NRL-MRY occupies approximately 30,000 square feet in shared buildings. This includes not only office space, but also a small library, the John B. Hovermale Visualization Laboratory, the Bergen Data Center, the Geostationary Satellite Processing Facility, and space for the hardware supporting the Tactical Environmental Support System (TESS), the Tactical Atmospheric Modeling System/Real-Time (TAMS/RT), and the Master Environmental Laboratory.

NRL-MRY is dedicated to advancing fundamental scientific understanding of the atmosphere, including the air-sea interface, and to applying those scientific discoveries in the development of innovative objective weather prediction systems. FNMOC is the Navy's primary facility for the production and distribution of numerical weather prediction products in support of Navy operations around the globe, as well as to other defense-related activities. Thus, Fleet Numerical is the primary customer for the numerical weather prediction systems that are developed by NRL-MRY. This collocation of the scientific developer with the operational customer offers advantages for the successful implementation of new systems and system upgrades, and for the rapid infusion of new research results from the community at large. NRL-MRY has efficient access to FNMOC's large classified vector supercomputer and other systems. This allows advanced development to take place using the real-time on-site global atmospheric and oceanographic databases. Collocation also offers the opportunity for FNMOC scientists to team with NRL-MRY scientists during the transition and implementation process, and NRL-MRY scientists remain readily available for consultation on any future problems that arise.

NRL-MRY benefits from the opportunities provided by NPS for continuing education and for performing collaborative research with the Department of Meteorology and others. The NWSFO has also proven to be a valuable partner for both NRL-MRY

and FNMOC. Data and products are exchanged, and valuable feedback is provided about the performance and utility of the numerical models and satellite-based products developed at NRL-MRY.

Midway Research Center

The Midway Research Center (MRC) is located on a 158-acre site in Stafford County, Virginia. Located adjacent to the Quantico Marine Corps' Combat Development Command, the MRC has 10,000 square feet of operations and administration area and three precision 18.5-m-diameter parabolic antennas housed in 100-ft radomes. The MRC, under the auspices of the Naval Center for Space Technology, provides NRL with state-of-the-art facilities dedicated solely to space-related applications in naval communications, navigation, and basic research.

Other Sites

Some field sites have been chosen primarily because they provide favorable conditions to operate specific antennas and electronic subsystems and are close to NRL's main site. Pomonkey, Maryland, a field site south of NRL, has a free-space antenna range to develop and test a variety of antennas. The antenna model measurement range in Brandywine, Maryland, has a 4.6-m diameter turntable in the center of a 305-m-diameter ground plane for conducting measurements on scale-model shipboard and other antenna designs. A site on the cliffs overlooking the Chesapeake Bay provides an over-the-water range of approximately 10 miles to Tilghman Island.

Research Platforms

Mobile research platforms contribute greatly to NRL's research. These include six P-3 Orion turboprop aircraft and one ship, the ex-USS *Shadwell* (LSD-15), berthed in Mobile Bay, Alabama. The ex-*Shadwell* is used for research on fire-suppression techniques on-board ship.

Looking Ahead

To provide preeminent research for tomorrow's Navy, NRL must maintain and upgrade its scientific and technological equipment to keep it at the forefront of modern research facilities. The physical plant to house this equipment must also be state of the art. NRL has embarked on a Corporate Facilities Plan to accomplish these goals. This plan and future facility plans are described below.

THE CORPORATE FACILITIES INVESTMENT PLAN (CFIP)

The CFIP is a financial spending plan to provide modern research facilities at NRL by the year 2000. The plan calls for both Congressional and Laboratory investment and is updated and altered as changes occur in scientific emphasis and Congressional attitude. During the past five years, Congressionally approved military construction (MILCON) funds were used to construct the new Electro-Optics Laboratory and a high-bay facility for the Naval Center for Space Technology. MILCON funds were approved in the FY 97 Congressional budget for the construction of an Ocean Acoustics Research Laboratory building at NRL-SSC. Future MILCON funds have also been requested for the construction of a Nano Science Research building at NRL-DC.

To complement these efforts, overhead funds have been used to renovate and upgrade laboratory and support areas in several existing buildings. Modern laboratory facilities have recently been provided for the Center for Bio/Molecular Science and Engineering, the Materials Science and Technology Division, the Remote Sensing Division, and the Acoustics Division. Work that is currently in progress will provide new facilities for the Information Technology Division and the Radar Division.

In parallel with efforts to upgrade laboratory buildings to the most modern standards, those buildings that were built during World War II and do not lend themselves to renovation are being demolished. This will provide space for the construction of future MILCON buildings, and it will also reduce the Laboratory's overhead costs.

Information Technology

The Information Technology Division's Center for Computational Science (CCS) operates three scalable, massively parallel Global Shared Memory (GSM) computer systems. A 128-processor SGI/Cray

Origin2000 and 64-processor HP/Convex Exemplar SPP-2000 have cache-coherent Non-Uniform Memory Access (ccNUMA) architectures. A 148-processor Sun HPC Ultra distributed system has 96 processors that operate symmetrically in a Cache-Only Memory Access (COMA) architecture. These systems comprise the Distributed Center (DC) at NRL whose hardware is funded by the DoD High Performance Computing Modernization Program (HPCMP). The systems are used in the innovative exploration and evaluation of MPP technology for the solution of significant militarily relevant problems relating to computational and information science. The systems allow for leading-edge research in support of heterogeneous parallel processing applications by the Navy and DoD science and technology communities.

Chemistry

Nanostructured materials promise both challenges to current models of materials performance and opportunities for new technological solutions to Navy problems. A new laboratory building is planned to provide the carefully controlled environment (temperature, vibration, magnetic, electrical, humidity) necessary to work with atomic scale precision (0.1 nm).

Plasma Physics

The Plasma Physics Division has set up a Large Area Plasma Processing System (LAPPS) facility to investigate a new technique to produce plasmas for plasma processing. Applications include production of large-area flat-screen displays or elements for phased arrays or materials modification such as surface polymerization or ion implantation. The system is based on low-energy electron beam ionization of a background gas to produce the desired plasma. The system may have advantages over existing techniques for production of large-area (square meter) plasmas, efficiency of plasma production, and control of reactive species.

Electronics Science and Technology

Important division emphasis is focused on the continual upgrading of the Nanoelectronics Processing Facility (NPF) and the Penthouse Processing Facility (PPF) and expanding activities in the nanoelectronics, heterostructures, and vacuum elec-

issues of acoustic and shock-wave propagation, mine burial, and mine countermeasures.

Vacuum Ultraviolet Space Instrument Test Facility

The Space Science Division facilities include an ultraclean solar instrument test facility in Building A-13 on the main NRL campus. The new facility is designed to satisfy the rigorous contamination requirements of state-of-the-art solar spaceflight instruments. The facility has a 400-ft² Class 10 clean room and a large Solar Coronagraph Optical Test Chamber (SCOTCH). This completely dry-pumped, 550-ft³ vacuum chamber is maintained at synchrotron levels of cleanliness. Solar instrumentation up to 1 m in diameter and 5 m in length can be physically accommodated in the chamber. The instrument's optical performance is probed and calibrated with a variety of visible and XUV sources mounted on the chamber's 11-m beamline. The optical testing and characterization of the Large-Angle Spectrometric Coronagraph (LASCO) instrument for the European Space Agency's Solar Heliospheric Observatory satellite were conducted in this chamber. Coronagraph stray-light characterization was carried out by mounting a set of baffles in the main beamline, illuminating the instrument with a simulated solar beam, and measuring the residual radiation. A stray light background measurement of 10^{-12} was successfully measured in the LASCO C3 channel. Coronagraph calibration was carried out by installing back-illuminated calibrated opals in front of the instrument entrance aperture. Instrument polarization properties were analyzed by using a variety of polarizers installed in a wheel located between the opal and the instrument. The wheel was remotely controlled from outside the chamber. Instrument Mueller matrices were verified with a 12-in. diameter, two-plate partial polarizer. Calibration and focus of XUV solar instrumentation are accomplished by exposing the instrument to an XUV windowless collimator at the end of the tank. The facility also has a small thermal bake/vacuum test chamber used for vacuum conditioning and thermal testing of spaceflight components and subassemblies. Both the SCOTCH and the small test chamber are instrumented with temperature-controlled quartz-crystal monitors and residual gas analyzers for real-time, quantitative measurements of volatile contamination.

REHABILITATION OF SCIENTIFIC FACILITIES

Specialized facilities are being installed or upgraded in several of the research and support divisions.

Flight Support Detachment

NRL's Flight Support Detachment (FSD) has continued to improve both capabilities and diversity among its aircraft platforms. Aircraft 153442 continues to undergo extensive modifications with Lockheed Martin to install a "rotodome" antenna and full AEW radar system. These modifications will support the Navy's Theater Air Defense programs, while providing a testbed for advanced EW radar research. Additionally, all aircraft have completed extensive bomb-bay design improvements that will allow the aircraft to carry more diverse scientific payloads. Aircraft 158227's communications capabilities were significantly upgraded with a state-of-the-art satellite telephone; aircraft 154589 is next in line to receive this INMARSAT system. These upgrades and modifications will ensure that NRL will have the finest airborne research capabilities well into the next century.

Information Technology

The Information Technology Division continues to transition stable technology from high-performance network testbed activities into the NRL local area network. This effort includes deployment of ATM technology at stream rates of 622 Mbps (OC12c) and 2.5 Gbps (OC48) across the enterprise. The current computing architectures, the SGI/Cray Origin2000, the HP/Convex Exemplar SPP-2000, and the Sun Ultra, are continuously undergoing upgrade and evaluation of both hardware and software. The two CM-500e systems were retired at the end of FY 98. The NRL CCS works closely with the DoD HPC community and the HPC vendors to provide insight, balance, and value-added capabilities within the MPP testbed infrastructure.

Materials Science and Technology

Renovation is in progress for Building 3, which is composed of two of the original five buildings at

NRL, to contain modern laboratories for studies of thin-film deposition and characterization, superconducting materials, magnetic materials, and other materials science projects. The new space will feature the most modern molecular beam epitaxy and other materials synthesis and processing equipment, an up-to-date fatigue and fracture laboratory, and state-of-the-art diagnostic equipment, including electron microscopes, spectrometers, and electron and X-ray diffraction equipment. The renovated building will also contain office and laboratory space for approximately 70 technical personnel.

Plasma Physics

A state-of-the-art short-pulse (0.4 ps), high-intensity Table-Top Terawatt (T³) laser currently operates at 2.5 TW and 5×10^{18} W/cm² for a variety of physics studies. The T³ laser will be upgraded to boost its power to 25 TW and intensities to $>10^{19}$ W/cm². This will provide a facility to do fundamental physics experiments in intense laser-plasma interactions, intense laser-electron beam interactions, and intense laser-matter interactions.

The division is adding a 15-kW average power, 83 GHz gyrotron to its facility for research on high-frequency microwave processing of materials. The Russian-made gyrotron produces a focused, high-intensity millimeter-wave beam ($10^3 - 10^5$ W/cm²) that has unique capabilities for rapid, selective heating of a wide range of nonmetallic materials. The new gyrotron-based system will be used to investigate the

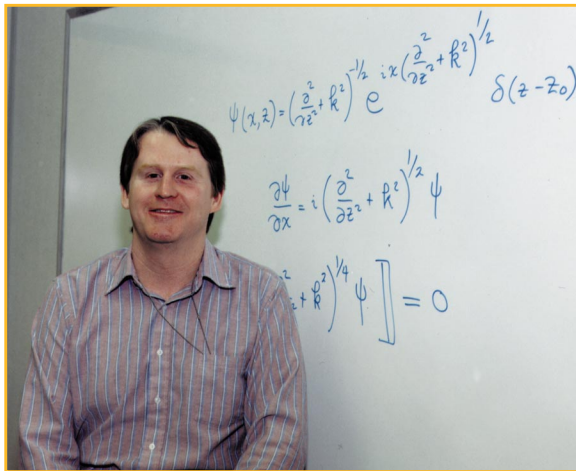
application of such beams to important areas of material processing, including coating of materials, soldering and brazing, and treatment of ceramics, semiconductors, and polymers.

Electronics Science and Technology

The Electronics Science and Technology Division continues to upgrade and expand its capability in nanofabrication science. Facilities will be enhanced with the addition of two new laboratories and a vacuum processing chamber for the existing EPICENTER. The first new laboratory is the Laboratory for Proximal Probe Nanofabrication, which will use proximal probes to explore the limits of nanolithography. The second is the Laboratory for Advanced Materials Processing, which will explore the chemistry and physics of the process, such as dry etching and contact formation that are routinely used in the formation of modern devices. It will also be used to develop new processing techniques that can be used in nanoscale fabrication. Both of these new facilities are expected to be operational by the end of 1998. The vacuum processing chamber will enable the vapor phase etching of materials for both epitaxial regrowth and fundamental surface science studies done in the EPICENTER. It will result in the realization of new device structures, e.g., lattice matched heteroepitaxial surface passivation for detector and laser structures, and the development of new surface treatment techniques for material modification.

★ “Our People Make the Difference—featuring ...”

The preceding pages dramatically illustrate the range of research capabilities that have been and are being developed to provide the Naval Research Laboratory with the world-class facilities for which we are known. However, these inanimate objects, however expensive and complex, are of no value without the highly motivated people who work here. It is these people who make the Laboratory the great institution that it is, who provide the ideas and sustained efforts to make these great research capabilities “come to life.” In this section, we highlight some of these special people.



Dr. Michael D. Collins

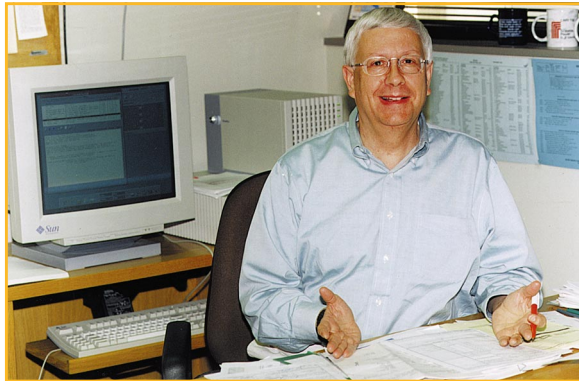
Dr. Michael D. Collins is a mathematician in the Acoustics Division. His interests include wave propagation and inverse problems. Ocean acoustic modeling is a complex problem due to large propagation distances, spatial and temporal variations in sound speed, scattering from rough surfaces and ice cover, and interaction with sediments that may support shear waves, interface waves, and two types of compressional waves. Inverse problems include estimating the parameters of the ocean and sediments as well as determining the locations of sources. These problems are complicated by interference from ambient noise and uncertainties in environmental and system parameters. The Acoustics Division has recently been involved in acoustic modeling associated with monitoring global warming, enforcing the Comprehensive Test Ban Treaty, and the impact of Comet Shoemaker-Levy 9 with Jupiter. “Many careers at NRL begin with a decision between academia, industry, and government. I made my choice and have stuck with it. I’ve never regretted it because I’m not aware of a better place to do research.”

Mr. Steven D. Harrison was appointed Director of the Research & Development Services Division in May 1996. His division is responsible for the physical plant of the Naval Research Laboratory including its field sites. The NRL physical plant consists of approximately 530 acres, with more than 100 buildings totalling over 3 million square feet. “I am proud to lead the effort in providing facilities support to the NRL research community. Providing the physical plant support to the NRL community is anything but mundane, the Lab’s unique requirements provide many interesting challenges. Over the years, NRL has provided me the opportunity to achieve many personal goals. The achievement of these goals could not have been accomplished without the hard work, dedication, and support of the employees of the Research & Development Services Division. It’s a consolidated team effort that keeps the NRL physical plant operational.”



Mr. Steven D. Harrison

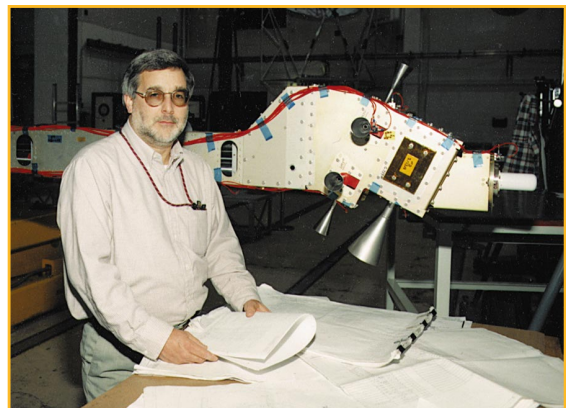
Dr. Harley E. Hurlburt has performed ocean modeling research for the U.S. Navy since 1975, first as an NRL contractor in Washington, D.C., then since 1977 for the Naval Ocean Research and Development Activity, which became part of the Naval Oceanographic and Atmospheric Research Laboratory and finally in 1992, NRL-Stennis. Dr. Hurlburt leads a research team on eddy-resolving global and basin-scale ocean modeling and prediction, an area of research made feasible in the 1990s



Dr. Harley E. Hurlburt

by technological advances in high performance computing (HPC), satellite oceanography and meteorology, and data communication. “I like the impetus to research that comes from working in a mission-oriented research environment where basic research is valued, and the years since NOARL merged with NRL have been the best. It is a privilege to work with the research team we have at NRL. The research team, the facilities, the support from management and staff, the exceptional DoD High Performance Computing resources, the access to data, and the emphasis on research and understanding, rather than engineering approaches, all act to create an outstanding environment for research productivity and the opportunity to tackle grand challenge research problems.”

Mr. Allyn Jacoby serves on the staff of the Naval Center for Space Technology’s (NCST) Spacecraft Engineering Department Mechanical Design group. In his previous assignment, he was responsible for significant portions of the mechanical design efforts on the Shuttle/Titan Launch Dispenser and numerous auxiliary experiments and payload missions. Recently, Mr. Jacoby was selected as the Program Manager to lead the NRL team for the design, development, manufacturing, testing, integration, and launch of the Interim Control Module (ICM). Representing a key assembly of NASA’s International Space Station (ISS), the ICM will provide critical reboost and attitude control of the ISS and will represent the first dedicated application of the Shuttle for the launch of a primary NRL-built payload. “As with previous programs in which I have participated, the ICM program receives the combined and dedicated resources of a tried and proven team of engineers, scientists, and support personnel who offer years of experience. It is truly an honor to lead the ICM team on a program that receives such high national interest, with technology challenges and mission demands not previously encountered. Our greatest strength is our people and their willingness to respond to each and every problem we encounter. Members of our team span more than 30 years of sustained program success and have established a strong foundation for all future programs. NCST’s strength is to leverage this resource and provide the opportunity to participate in programs where leading edge technologies and advanced concepts and applications are required.”



Mr. Allyn Jacoby

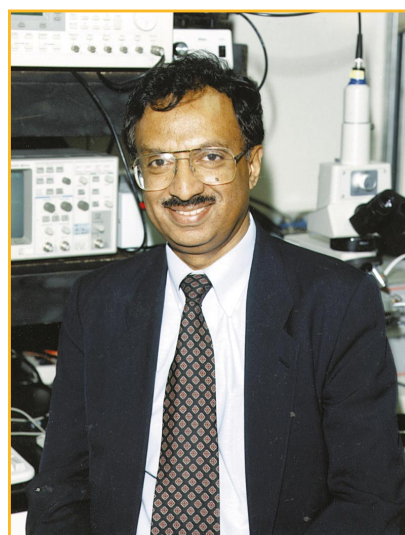


Ms. Kathy Parrish

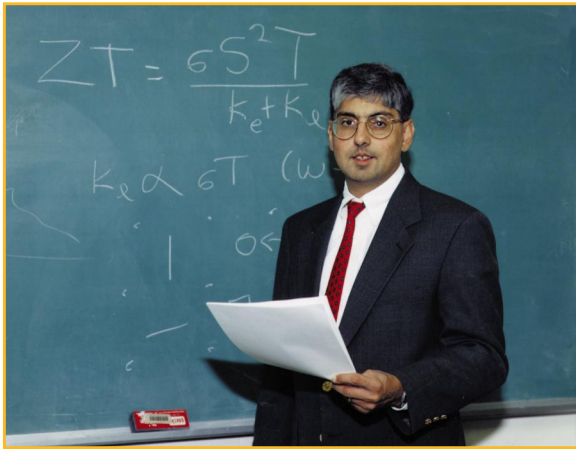
Ms. Kathy Parrish is Acting Head of the Publications Branch, Technical Information Division. The branch transforms the experimental research and investigations of the Laboratory's scientists and engineers into books, technical and nontechnical reports, brochures, portfolios, and folders. Kathy credits the Publications and Photography teams in TID with having significantly improved the image of NRL through the publications it produces. Many of the Laboratory's brochures and books have won prestigious awards in national and international competitions. Ms. Parrish came to NRL in 1966 and worked in the Sound Division at the Chesapeake Bay Annex until 1970, when she joined the Oceanography Division. Her "first career" was as a marine biologist. She raised marine crustaceans and mollusks in closed-culture aquarium systems and used these organisms in bioassay studies of creosote and copper-chromium-arsenic compounds. Following a major Laboratory reorganization in 1983, Ms. Parrish began her "second career" in the Technical Information Division as a writer/editor, where she now supervises a staff of technical writers and graphics personnel. "I feel very fortunate in having had the opportunity to work at such a pres-

tigious institution in both sides of the house—in a scientific division and in a service division. It's helped me see the complete picture. My work in TID as a publisher has been very rewarding. Here, we can carry a project from its inception as an idea, to its birth as a handsome publication. Now there's an exciting career! My Dad, who worked with Jerome and Isabella Karle and Herbert Friedman, told me NRL was a great place to work. I'm glad I took him up on his suggestion. I came to NRL and have never looked back."

Dr. Ranganathan Shashidhar is Head of the Laboratory for Molecularly Engineered Materials and Surfaces in the Center for Bio/Molecular Science and Engineering. Coming to NRL as an internationally renowned scientist in the field of liquid crystals, he initiated both basic research and applied science programs aimed at the development of advanced liquid crystal materials, displays, and devices for numerous Navy applications. Electro-optical materials for high-resolution displays, pyroelectric liquid crystals for uncooled IR sensors, conducting polymers for plastic and flexible displays, and photo-alignment monolayers for liquid crystal alignment are areas that have put NRL in the forefront of research in liquid crystal technology. "When I joined NRL, I realized how fortunate I was to be working in a Laboratory that has a wealth of scientific expertise in so many areas of physical sciences and has the state-of-the-art facilities to conduct any kind of experimental work imaginable. I was also thrilled at the prospect of working with the highly multidisciplinary group of scientists at the Center. Understanding the fundamental principles of self-assembly of molecules at different length scales and harnessing them is becoming a reality for me."

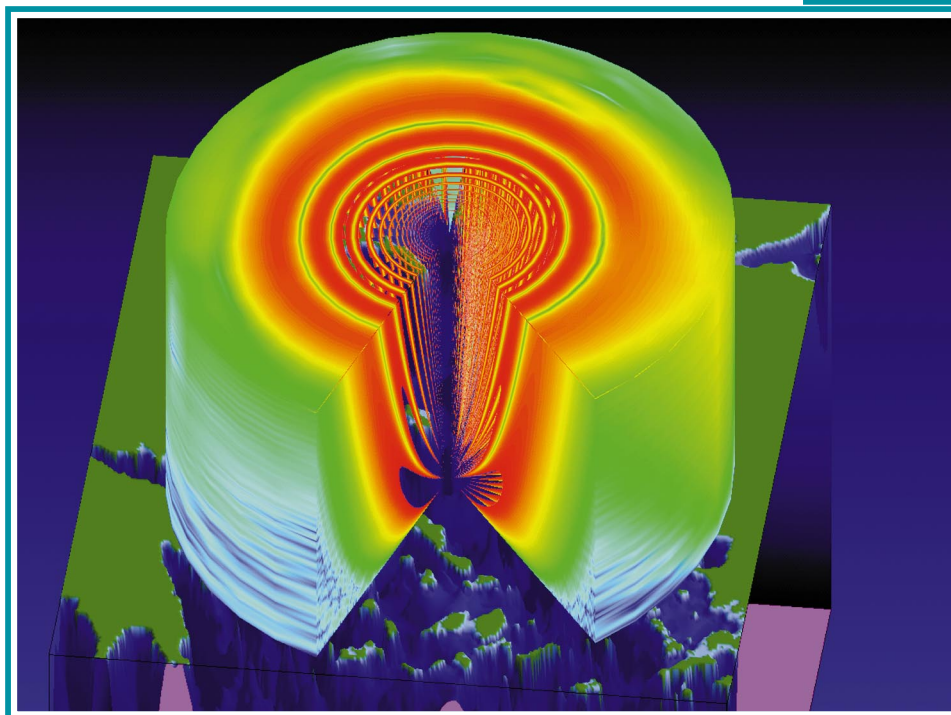


Dr. Ranganathan Shashidhar



Dr. David Singh

Dr. David Singh is a research physicist in the Complex Systems Theory Branch, Condensed Matter and Radiation Sciences Division. Scientists in the branch develop and use computational and theoretical approaches to search for new enhanced materials for Navy systems. Dr. Singh uses density functional theory, implemented on high performance computers, to investigate new advanced materials of Navy interest. He is the author of more than 150 publications and is a fellow of the American Physical Society. “Materials research is becoming less and less a “needle in hay stack” endeavour and more and more a synergy between synthesis, characterization, and theory. The glue that binds these elements is computational work. The importance of this was recognized by the award of the 1998 Nobel Prize in Chemistry to Walter Kohn for developing density functional theory. Key ingredients in that glue, which NRL maintains, are excellent scientists, interactive working environments, and access to state-of-the-art computer hardware. NRL is a world-leading laboratory in this field, and I am honored to be here.”



The Keyhole
Science-as-Art contest – Second Place winner
Submitted by: Susan Starke and Richard Owens

By using software developed for NRL-Stennis' Tactical Oceanography Simulation Laboratory (TOSL), this image depicts transmission loss using the Radio Physical Optics model in the Aegean Sea. The bathymetric data shown have one-minute resolution and were acquired through the Tactical Oceanography Wide Area Network. The transmission loss is shown as a cut-out view of a series of 36 radials, with their tops and outer sides connected. Coloration is done via a rainbow type of colorbar, with values outside of the minimum and maximum rendered transparently, which explains the somewhat hollow region in the center of the radials.

- 35 Array-Based Biosensor for Multianalyte Sensing
J.P. Golden, C.A. Rowe, M.J. Feldstein, S.B. Scruggs, L.M. Tender, and F.S. Ligler
- 43 The North Pacific Experiment (NORPEX-98)
R.H. Langland, R. Gelaro, G.D. Rohaly, and T.E. Rosmond
- 55 Thirty Years of NRL Research in Functional Ceramics: From Failure Analysis to Novel Ceramic Devices
D. Lewis III, C. Kim, C.C.M. Wu, T.L. Jessen, M. Kahn, and M.T. Chase

Array-Based Biosensor for Multianalyte Sensing

J.P. Golden, C.A. Rowe, M.J. Feldstein, S.B. Scruggs, L.M. Tender, and F.S. Ligler
Center for Bio/Molecular Science and Engineering

Our laboratory is developing a multianalyte sensor for detecting biological agents and clinical analytes that is portable, inexpensive, and easy to use. To achieve these goals, we use a cooled charge-coupled device, a diode laser, and disposable waveguides. We have fabricated a prototype biosensor that fits into a compact case and can be controlled by a portable computer. Standard microscope slides are used as waveguides and are precoated with arrays of immobilized antibodies. Fluorescence immunoassays have been performed on up to six samples at a time. Samples have been analyzed for as many as four different analytes simultaneously. Limits of detection in the 1-10 ng/ml range have been achieved in 10-minute assays. Results from recent field trials have shown sensitivities approaching or equivalent to analysis by the enzyme-linked immunosorbent assay (ELISA), considered the gold standard. Moreover, initial studies indicate that assays can be run on samples such as whole blood, plasma, urine, saliva, and nasal secretions.

INTRODUCTION

During Operation Desert Storm, our troops came under the direct threat of biological warfare attack. In fact, Iraq subsequently admitted to making anthrax, botulinum toxin, and aflatoxin, all of which are deadly biowarfare agents. Battlefield scenarios could involve exposure to such agents from demolition of secret biowarfare agent manufacturing plants as well as direct attack. Since the presence of such agents is imperceptible, a method for rapid detection would clearly benefit military operations and possibly avoid troop anxiety due to uncertainty. Recent transgressions against civilian populations, as in the Tokyo subway attack, also demonstrate the need for a portable, sensitive detection system capable of identifying biowarfare agents.

Presently, the industry standard for identification and quantitation of biological agents centers around the enzyme-linked immunosorbent assay (ELISA). Unfortunately, the ELISA is not easily portable and can take 1 to 12 hours to produce the results. In response to the unmet need for a portable, rapid detection system, our laboratory in the Center for Bio/Molecular Science and Engineering has developed biosensors capable of detecting the presence of bacteria, viruses, toxins, or biowarfare simulants with sensitivities approaching those of the ELISA.¹⁻³

We have further advanced this work by developing the array-based biosensor that can test for the presence of several of these analytes simultaneously in a single milliliter sample.^{4,6} The array biosensor consists of the detection system in a single carry-on case and a personal computer for system control and storing assay results. It has recently been taken to field trials, where in a blind test, we were able to detect and identify three different agents/simulants in a 10-minute assay with sensitivities similar to the standard ELISA method.

BACKGROUND

A biosensor is a device that uses selective biological molecules as the recognition component. The recognition component of the array biosensor is the antibody, a naturally occurring protein in mammals that is part of the immune system. The immune system manufactures antibodies to bind with their antigen, substances that are foreign to the body and tagged for removal. The array-based biosensor uses antibodies to bind their antigens, in this case the analyte, to the surface of an optical waveguide and then uses fluorescence to indicate its presence. Fluorophores are excited by a certain wavelength of light and emit a longer wavelength of light, fluorescence, that can be optically detected.

In a typical assay, the recognition antibodies (capture antibodies) are chemically immobilized in discrete locations on the surface of a standard glass microscope slide. The sample to be analyzed is flowed over the surface, and the analyte, such as a toxin or bacteria, is “captured” by the immobilized antibody. A second antibody with a fluorophore attached is introduced and binds to the captured analyte, forming an antibody/analyte/antibody “sandwich” on the surface (Fig. 1). This sandwich can then be illuminated with laser light and the resulting fluorescence indicates the presence of the analyte.

A specially designed detection system was developed to provide evanescent wave excitation of the fluorophores at the surface of a microscope slide and efficient collection of the fluorescence emission (Figs. 2 and 3). In this system, a laser beam is expanded and launched into the edge of the microscope slide, filling the entire width of the slide. The laser light traveling down the length of the slide has associated with it a surface wave, or evanescent wave, that extends a few hundred nanometers out from the surface of the waveguide. Since the antibody/analyte sandwich is bound to the waveguide surface, it is effectively within the evanescent wave field and can be readily excited. Not only does using the evanescent wave provide a confined excitation zone for the fluorophores bound to the surface, it also greatly reduces the undesired background signal due to scattered excitation light compared to other excitation methods.

The fluorescence from the antibody/analyte complex is imaged onto a cooled charge-coupled device

(CCD) imaging array. Optical filters reject scattered laser light and a 2-dimensional graded index (GRIN) lens array focuses the fluorescent image onto the CCD. The short focal length of the GRIN lens array allows for a very compact fluorescent array imaging system.⁷ This is an important factor in making the final device small and portable. The CCD captures an image of the patterned fluorescent array that is used to determine the location and intensity of the individual fluorescent array elements. Since the pattern of the array elements is known, the analyte can be identified by examining the position of array elements that light up. The positions of the fluorescent spots indicate the presence and identity of specific agents. The intensity of the fluorescence indicates the relative concentration of the agent.

ASSAY PREPARATION

The capture antibody is chemically immobilized on the surface of the microscope slide waveguide by an avidin-biotin bridge. To immobilize the antibody on the slide, the glass surface is cleaned and treated with a silane and a heterobifunctional crosslinker.⁶ Avidin is then attached to the crosslinker, forming a covalent link between the avidin and the glass surface. The capture antibody is labeled with biotin, which binds to the avidin on the surface. The affinity of the avidin/biotin interaction is the strongest known non-covalent interaction between protein and ligand.⁸ After the slides are prepared with the avidin, any biotin-labeled capture antibody can be immobilized in any location on the slide surface.

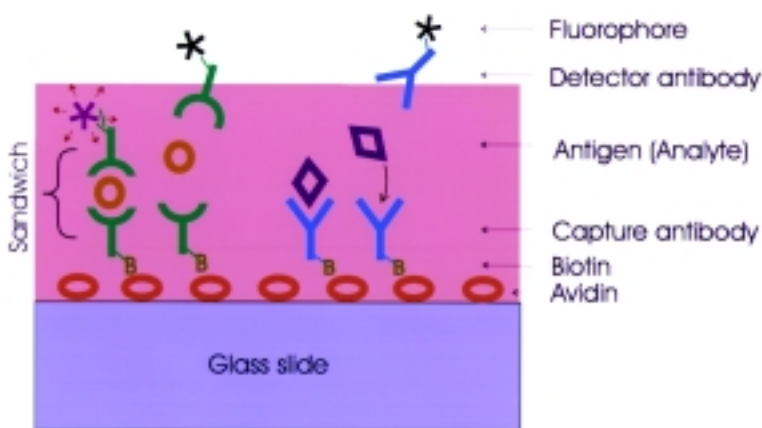


FIGURE 1 Antibody/analyte binding. Analyte binds to the immobilized capture antibody. A second, fluorescently labeled “detection” antibody binds to the analyte, forming an antibody/analyte/antibody complex, or “sandwich.” The pink area represents the effective penetration depth of the evanescent wave.

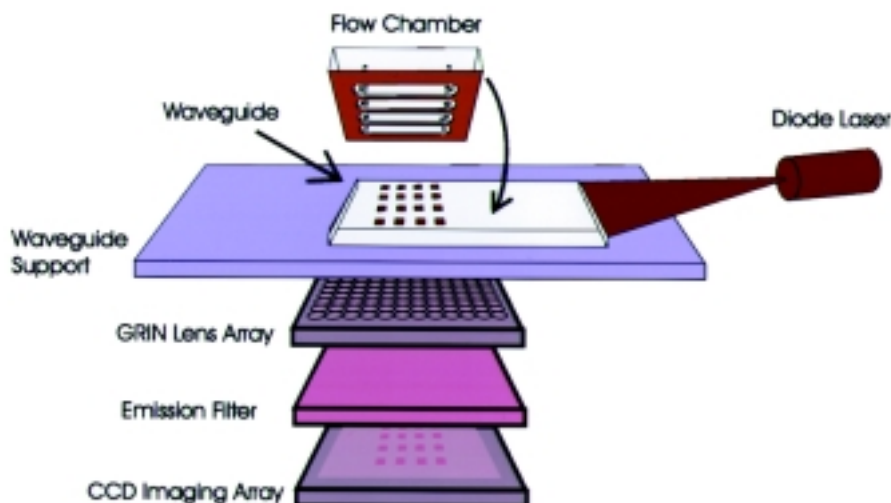


FIGURE 2
 Sensor design schematic. A patterned glass slide is placed on the support and evanescently illuminated by 635-nm light from a diode laser. The fluorescent sandwich immunoassay patterns are focused onto a scientific-grade CCD through a GRIN lens array. Optical filters transmit the fluorescence and absorb the unwanted laser light.

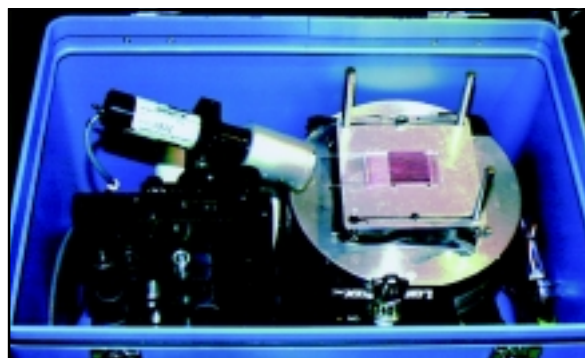


FIGURE 3
 The array biosensor.

Flow chambers for immobilizing the antibody and performing the assays are molded out of polydimethylsiloxane (PDMS). Capture antibodies are patterned on the sensor surface by placing a PDMS flow chamber with vertically oriented channels onto the avidin-coated slide (Fig. 4(a)). Biotin-labeled capture antibodies for different analytes, represented by the letters A through E, are flowed into each chamber and allowed to bind to the surface via an avidin-biotin bridge. This procedure produces six vertical stripes of capture antibody on the slide. The slides are now ready to perform assays, and can be stored for future use. For performing the assays, a different PDMS flow chamber is placed on the patterned slide. This flow chamber has horizontally oriented channels (Fig. 4(b)). Each of the horizontal channels can

test a different sample, or can be used as redundant tests for the same sample. Since all of the vertical stripes appear in each of the horizontal channels, each channel can assay for all of the analytes.

Samples are assayed using the sandwich immunoassay format (Fig. 1). After flowing the sample through the horizontal channels, fluorescent antibody is flowed into the same channels and allowed to bind to the captured analyte. Antibody/analyte binding occurs only in the vertical stripe that is coated with the appropriate antibody, yielding an array of assays in each channel. Since the location and order of vertical stripes are already known, this information can be used to identify what was in the sample. An image of the entire multianalyte array is captured and stored. We developed image analysis software that

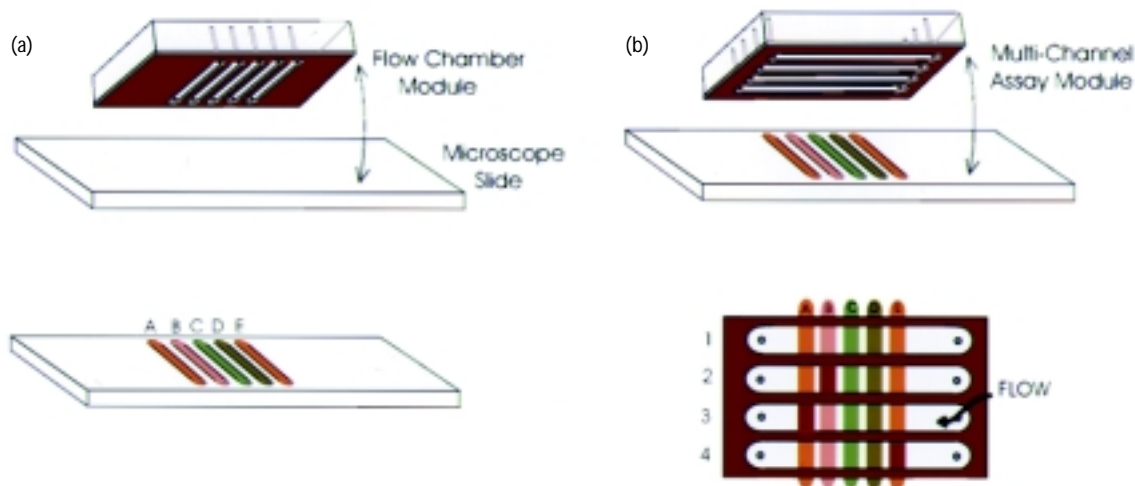


FIGURE 4
(a) Physically isolated patterning of capture antibodies; (b) analysis of samples.

automatically determines the fluorescent signal from each element in the array and displays the results on the computer screen. The entire assay, from sample injection to signal determination, takes approximately 10 minutes.

DEMONSTRATION ASSAYS

- **Blind Testing**—Blind tests were performed at the Naval Medical Research Center (Bethesda, Maryland) to demonstrate the ability of the array biosensor to detect and distinguish between different *classes* of analytes (bacterial, viral, protein). Three well-characterized analytes were used in this study: *Bacillus globigii* (BG), a nonpathogenic, gram-positive, sporulating soil bacterium; MS2, a small, nonpathogenic RNA virus that infects only certain bacteria; and staphylococcal enterotoxin B (SEB), a common cause of food poisoning.

To prepare for the blind testing trials, we patterned 126 slides with the capture antibodies and stored them for convenient retrieval at the test site. Capture antibodies that specifically bind SEB were immobilized in columns 1 and 2, antibodies against MS2 in columns 3 and 4, and antibodies recognizing BG in columns 5 and 6 (Fig. 5). Channel 1 (row 1) was used as a positive control to ensure the efficacy of patterning, good quality of detector agents, and reliability of the imaging apparatus. Each unknown sample was introduced to channels 2-5 simultaneously for analysis. Each of the channels 3 through 5 provided for detection of one analyte, while channel 2 provided detection capability for all three analytes. Figure 5(a) shows which elements should light up in

the case of a positive for each of the analytes examined.

In the blind field trials, analyte concentrations both above and below the limits of detection of the array biosensor were tested, along with samples with no analyte present (blank samples). Of the 60 samples analyzed that contained analyte at or above the limit of detection, 58 were correctly identified at the time of analysis (59 excluding operator error). The limits of detection for each agent were similar or identical to those obtained with ELISA testing performed on the same samples. Images of samples containing SEB, MS2, and BG are shown in Fig. 5(b,c, and d), respectively.

- **Simultaneous Assays**—The blind tests described above demonstrate the ability of the array biosensor to analyze a single sample for the presence of multiple analytes. However, our biosensor can be used to analyze several samples simultaneously for the presence of multiple analytes and can detect mixtures (Fig. 6). This capability is especially important in situations (such as a site inspection or an emergency response following a biological incident) in which large numbers of samples must be analyzed and the presence of a combination of agents is suspected.

- **Detection in Complex Samples**—Often in situations outside the laboratory, it is desirable to detect the analyte in complex samples without a sample preprocessing step. For example, clinical applications require the assays to be performed in whole blood, saliva, or urine. For many other types of biosensors, data document interference of such complex samples with subsequent measurements. Assays for detecting

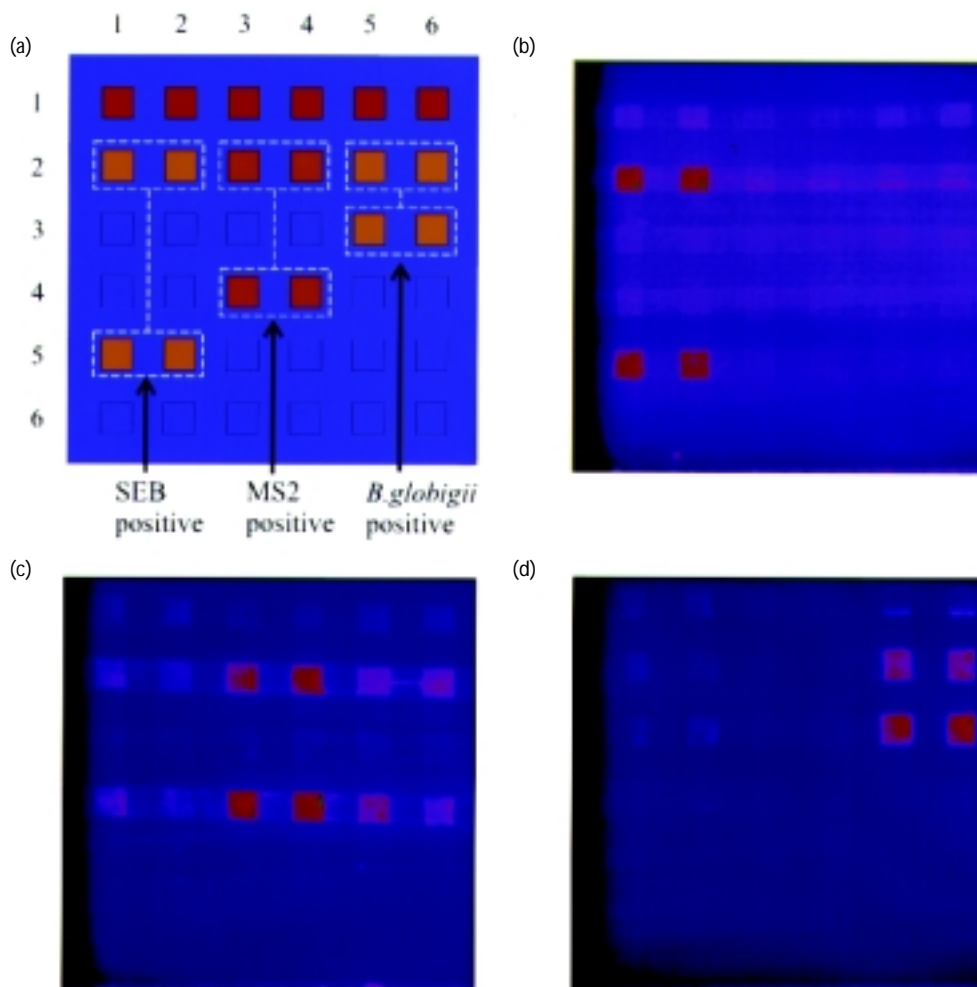


FIGURE 5 Fluorescent patterns of unknown samples from blind field trials: (a) idealized fluorescent patterns for positive detection of each analyte; fluorescent patterns from actual samples are shown in (b) (SEB), (c) (MS2), and (d) (*B. globigii*).

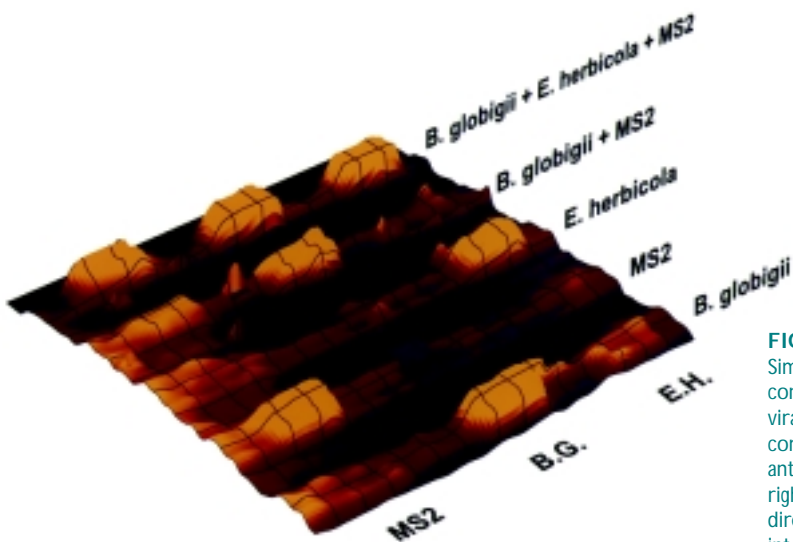


FIGURE 6 Simultaneous detection of mixed analytes. Samples containing bacterial (*B. globigii*, *Erwinia herbicola*) and viral (MS2) analytes were analyzed either alone or in combination, as indicated on upper right. Capture antibodies were immobilized as indicated on lower right. A mixture of fluorescent detector antibodies directed against all three analytes was used to interrogate the array. Yellow peaks indicate positive detection.

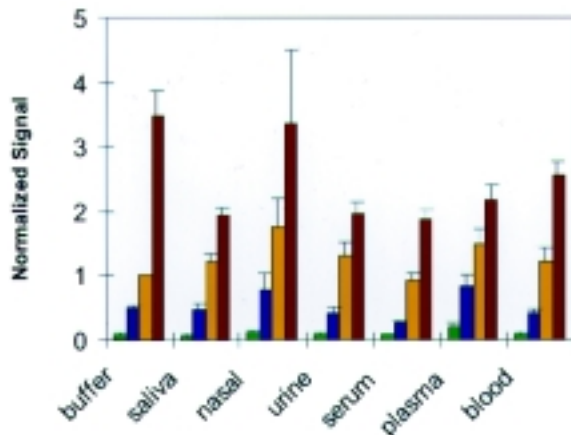


FIGURE 7
F1 antigen spiked into buffer and physiological fluids. Shown are fluorescent signals for unspiked samples (green) and samples spiked with 25 ng/ml (blue), 125 ng/ml (yellow), and 625 ng/ml (red). These latter concentrations are commonly found in samples from patients with plague, and are used for diagnosis.

proteins and toxins were performed using the array biosensor to determine the effect of the sample matrix on the resulting signal levels. As an example, the assay for F1 protective antigen, a component of *Yersinia pestis* (causative agent for plague), was performed in different fluids often used in clinical testing. Signals were obtained for each fluid matrix and normalized to the signal generated by a standard concentration of the F1 protective antigen in laboratory buffer. Results, shown in Fig. 7, indicate little effect of sample matrix on assay response.

CONCLUSIONS

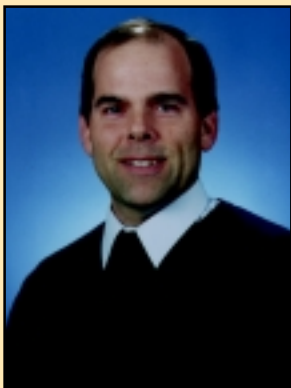
The array-based biosensor is a sensitive, rapid multianalyte detection system, with detection limits similar to those of the standard ELISA. The GRIN lens imaging array confers a compact optical design, making the detection system amenable to portability. With the present optical resolution, 20 to 30 different analytes could potentially be assayed simultaneously in one channel. Multiple samples can be interrogated simultaneously. Automated fluidics and an imbedded computer are being added to enable autonomous, remote sensing.

[Sponsored by DoD and ONR]

REFERENCES

- ¹F.S. Ligler, J.P. Golden, L.C. Shriver-Lake, R.A. Ogert, D. Wijesuria, and G.P. Anderson, "Fiber Optic Biosensor for the Detection of Hazardous Materials," *Immunometh.* **3**, 1-6 (1993).
- ²G.P. Anderson, J.P. Golden, L.K. Cao, D. Wijesuria, L.C. Shriver-Lake, and F.S. Ligler, "Development of an Evanescent Wave Fiber Optic Biosensor," *IEEE Eng. Med. Biol.* **13**, 358-363 (1994).
- ³J.P. Golden, E.W. Saaski, L.C. Shriver-Lake, G. Anderson, and F.S. Ligler, "A Portable Multichannel Fiber Optic Biosensor for Field Detection," *Opt. Eng.* **36**(4), 1008-1013 (1997).
- ⁴R.M. Wadkins, J.P. Golden, L.M. Pritsiolas, and F.S. Ligler, "Detection of Multiple Toxic Agents Using a Planar Array Immunosensor," *Biosens. Bioelectron.* **13**(3-4), 407-415 (1998).
- ⁵R.M. Wadkins, J.P. Golden, and F.S. Ligler "Patterned Planar Array Immunosensor for Multianalyte Detection," *J. Biomed. Opt.* **2**(1), 74-79 (1997).
- ⁶C.A. Rowe, S.B. Scruggs, M.J. Feldstein, J.P. Golden, and F.S. Ligler, "An Array Immunosensor for Simultaneous Detection of Clinical Analytes," *Anal. Chem.* **71**, 433-439 (1999).
- ⁷J.P. Golden, "Chemical Sensor Using Two-Dimensional Lens Array," U.S. Patent 5,827,748, Oct. 27, 1998.
- ⁸N.M. Green, "Avidin. 1. The Use of [¹⁴C]biotin for Kinetic Studies and for Assay," *Biochem. J.* **89**, 585-591 (1963). ★

THE AUTHORS



JOEL P. GOLDEN received his B.S. degree in electrical engineering from the University of Maryland in 1984 at which time he came to the Naval Research Laboratory. He received his M.S. in electrical engineering from the Johns Hopkins University in 1992, specializing in hologram creation and durability. He came to the Center for Bio/Molecular Science and Engineering in 1989. During this time he has worked on developing evanescent wave biosensors, most notably the fiber-optic biosensor and the array-based biosensor.



CHRIS A. ROWE received her A.B. degree in biology from Dartmouth College in 1984. After receiving an M.S. degree in pomology at Cornell University in 1986, she received her Ph.D. in biology at the Johns Hopkins University in 1995, specializing in protein biochemistry. She joined the Center for Bio/Molecular Science and Engineering in 1995 as a postdoctoral fellow and continues her work with the biosensor team as a full-time employee. Dr. Rowe has concentrated on detection of analytes in clinical fluids and is currently interested in sensing methods for detecting “families” of agents.



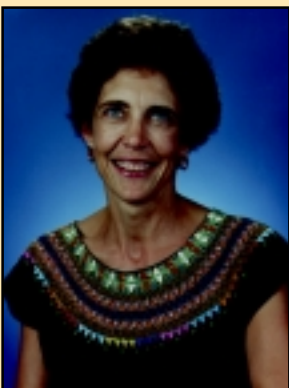
MARK J. FELDSTEIN is currently a National Research Council Postdoctoral Associate in the Center for Bio/Molecular Science and Engineering at the Naval Research Laboratory. He has earned a B.S. in chemistry and a B.A. in philosophy from The George Washington University and an M.S. in chemistry from the University of Chicago as well as a Ph.D. in physical chemistry from the University of Pennsylvania. Dr. Feldstein’s research focuses primarily on the design and development of optical, fluidic, and image analysis elements of biosensor systems.



STEPHANIE B. SCRUGGS is a graduate of Virginia Polytechnic and State University with a master's degree in chemical engineering. During her stay at NRL as a GEO-CENTERS contractor, she worked on prototyping the array biosensor. She has now taken a position at Independent Project Analysis (IPA) in Reston, Virginia.



LEONARD M. TENDER is currently a senior scientist in the Center for Bio/Molecular Science and Engineering at the Naval Research Laboratory. He earned a B.S. in chemistry from the Massachusetts Institute of Technology and a Ph.D. in analytical chemistry from the University of North Carolina. Prior to joining NRL, he completed postdoctoral fellowships at Stanford and the University of California Berkeley, and was a research professor at the University of New Mexico. His primary interests include fundamental research in new methods of biosensing.



FRANCES S. LIGLER is currently head of the Biosensors and Biomaterials Laboratory in the Center for Bio/Molecular Science and Engineering at the Naval Research Laboratory and a DoD Senior Scientist. She earned a D.Phil. from Oxford University, Oxford, England, and completed Postdoctoral Fellowships at University of Texas Health Science Centers at San Antonio (biochemistry) and Dallas (immunology). After 5 years in academic research, she spent 5 years in industry (DuPont) and then joined NRL in 1985. Dr. Ligler has published more than 150 patents and full-length articles in scientific journals. She is the winner of the National Drug Control Policy Technology Transfer Award, the Chemical Society Hillebrand Award, Navy Merit Award, three NRL Edison Awards for Patent of the Year, the Furman University Bell Tower Award, and the Women in Science and Engineering (WISE) Outstanding Achievement in Science Award. She co-chairs several sensor meetings for the Society for Photooptical Instrumentation Engineers and was the elected chair of the 1994 Gordon Research Conference on Bio/Analytical Sensors. She serves on the editorial boards of Journal of Biomedical Optics, Biomolecular Engineering, and Applied Biochemistry & Biotechnology, and on the Board of Trustees of Furman University.

The North Pacific Experiment (NORPEX-98)

R.H. Langland, R. Gelaro, G.D. Rohaly, and T.E. Rosmond
Marine Meteorology Division

An interagency atmospheric field program, the North Pacific Experiment (NORPEX-98), occurred between January 16 and February 27, 1998, involving the Naval Research Laboratory (Marine Meteorology Division, Monterey, California), the National Oceanic and Atmospheric Administration (NOAA), the U.S. Air Force, and scientists from several U.S. universities. The observations collected in NORPEX-98 include approximately 700 targeted tropospheric soundings from global positioning system (GPS) dropsondes deployed by reconnaissance aircraft, and high-resolution wind observations derived from geostationary satellites. The goals of NORPEX-98 are twofold: to test and evaluate strategies for objectively targeting observations to improve numerical weather forecasts, and to understand the structure and dynamics of fast-growing errors that frequently occur in model representations of the atmosphere.

INTRODUCTION

Numerical weather prediction is a method to forecast the future state of the atmosphere from a defined or analyzed state (initial condition) using dynamical and physical relations integrated forward in time by computer models. In a chaotic system such as the atmosphere, the problem of predictability on time scales of a few days or less centers on the effects of the inevitable inaccuracies and uncertainties that exist in the initial conditions provided to numerical forecast models.

A significant problem in operational weather prediction is the forecasting of synoptic-scale (1000-2000 km horizontal wavelength) midlatitude weather systems. These are the typical eastward-moving high pressure centers (anticyclones) and low pressure centers (cyclones) that create much of the potentially damaging winter weather (cold air outbreaks, frontal passages, heavy precipitation, flooding, and high winds) in the latitude band from 25° to 65°.

Although the basic large-scale structure of these weather systems can generally be well-predicted, forecast errors often occur that limit our ability to accurately predict the timing, intensity, and other aspects of relevant weather (such as precipitation amounts), even on time scales of three days or less. To a large

extent, these short-range forecast errors are attributable to rapid growth of errors that originate in critical upstream areas of strong dynamical “sensitivity,” where observational data are lacking or are not adequate to provide accurate initial conditions for the forecast model.

TARGETED OBSERVATIONS

Recently, the concept of “targeting” special atmospheric observations to particular areas has been proposed as a method to improve forecast model initial conditions and thereby reduce fast-growing errors that degrade the quality of weather forecasts in various situations. For instance, to improve the forecast of a winter storm expected over the central United States three days from now, it is possible to identify, in advance, a dynamically sensitive “target” region (perhaps over the eastern Pacific ocean) where additional atmospheric observations are likely to provide the most value in terms of improving a forecast of this storm relative to observations that might be added in other locations. (A “target area” is defined as a dynamically sensitive region in which the assimilation of additional high-quality atmospheric observations is likely to produce the greatest improvement in forecast skill of a weather event over a specified

verification area.) Target area locations are dependent on atmospheric flow conditions and are therefore subject to continuous change.

Targeted observations are not intended to reduce the *largest* initial condition (analysis) error, but rather are intended to reduce the growing component of initial condition error that is most relevant to the forecast of a particular weather feature. The targeted error comprises a small fraction of total analysis error considered in a global sense, and generally has small magnitude, but can amplify substantially as the forecast evolves over several days.

Objective, model-based techniques (including the singular vector method described below) have been developed to estimate locations of atmospheric sensitivity in advance, with sufficient time to deploy observational resources, such as reconnaissance aircraft, to obtain atmospheric data in target areas. The following procedure was used by NRL scientists for targeting observations in real time during NORPEX-98.

- identify forecast problem (storm or weather feature) of interest from conventional numerical forecast;
- define forecast verification area (the fixed region 30-60°N, 100-130°W was used in NORPEX-98);
- use singular vectors (or other method) a priori to identify target area;
- deploy observational resources to target area; and
- assimilate special observations into forecast model initial conditions.

SINGULAR VECTORS

The leading singular vectors (SVs) of the model forecast trajectory define the structures that grow most rapidly with respect to a chosen metric (norm), and provide the basis for targeting special observations in a real-time operational context (as in NORPEX-98). The SVs provided for targeted observing in NORPEX-98 use an energy metric¹ and are calculated with the adjoint system² of the Navy Operational Global Atmospheric Prediction System (NOGAPS). The SV method provides a first-order (tangent linear) approximation to the growth of typical errors found in nonlinear model forecasts over intervals as long as three to four days.

Singular vectors form a set of orthogonal (3-dimensional) basis functions ordered by amplification rate, so that there are as many SVs as there are degrees of freedom in the numerical model ($O \sim 10^6$). Typically, however, only the leading few (5-20), most-

rapidly growing SVs are calculated for targeting or diagnostic applications. The leading SVs can be thought of as the perturbation configurations (of temperature, wind, and pressure) that will grow most rapidly when added to the background atmospheric state trajectory over a specified interval. In a predictability context, the leading SVs are significant because the relatively small fraction of analysis error that projects onto these few most unstable structures often explains a large fraction of the forecast error that may be corrected through improvements to the initial conditions.³

Target regions for special observations are defined by the extrema of the leading SVs. During NORPEX-98, singular vectors were calculated once daily at 00 UTC using the time configuration shown in Fig. 1. Targeting guidance was configured specifically to improve 2-day forecasts within the verification region 30-60°N, 100-130°W (the western U.S. and Canada). This was accomplished by imposing a constraint on the SV calculation that limited perturbation growth to this region at the verification time, while placing no formal restriction on the upstream locations of the targets.

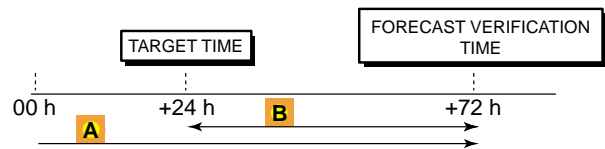


FIGURE 1 Temporal configuration for targeted observing in NORPEX-98. **A** is a nonlinear forecast trajectory used for calculating singular vectors optimized for the 48-h interval **B**. Target area guidance from **B** is made available at +12 h (or earlier), allowing deployment of observational resources (reconnaissance aircraft) to the target area at time +24 h. The targeted observations are assimilated at +24 h to improve the 48-h forecast verifying at +72 h.

NORPEX-98 OBSERVATIONS

Reconnaissance Aircraft

In NORPEX-98, targeted observations were provided by reconnaissance aircraft (NOAA Gulfstream-IV (G-IV) and several U.S. Air Force C-130s) equipped with global positioning system (GPS) dropsondes. Targeted observing missions were performed on 26 days between January 16 and February 27, 1998, from bases in Honolulu and Anchorage. On several occasions, two or three aircraft were used for targeting surveys on the same day. Missions were typically 8-10 hours in duration and deployed 15-20 dropsondes. Upstream survey missions were performed for nearly

every Pacific storm reaching the U.S. West Coast during the field program.

Half of the NORPEX-98 flights were tasked by the Naval Research Laboratory and half by the National Centers for Environmental Prediction (NCEP), testing different strategies for identification of target areas. Figure 2 shows the flight tracks of all 38 NORPEX-98 targeted observing missions. In addition to surveys of specific “target” areas, many of these flights also provide in situ observations of upper-level jet stream structure, baroclinic zones, low-pressure centers, and cloud features, which document atmospheric structure over the eastern North Pacific basin during the strong El Niño event of January and February 1998.

GPS dropsondes provide high-quality vertical profiles of temperature, wind, humidity, and pressure from near flight level (typically 30-40,000 ft) to the sea surface. During NORPEX-98, nearly 700 dropsondes were deployed, with all data transmitted via satellite in real time for assimilation by operational forecast centers worldwide. Figure 3 shows an example of a temperature and humidity profile from a dropsonde deployed by the NOAA G-IV on a flight north of Hawaii on January 22, 1998 (flight tracks and target areas for January 22 appear in Fig. 6).

Dropsonde observations provide data with high vertical resolution but are limited to areas that can be reached by reconnaissance aircraft. During NORPEX-98, there were many occasions when surveys of identified target areas were not possible due to distance

from the bases in Hawaii and Alaska. There were also numerous instances when only partial surveys of target areas could be obtained.

Despite these logistical limitations, the assimilation of targeted dropsonde data obtained in NORPEX-98 produces a 9.6 % mean improvement in the skill of 2-day forecasts verifying over the western U.S., compared to control forecasts that contain no dropsonde data or geostationary satellite wind observations over the North Pacific. The mean error statistic considers forecasts started from all 26 days on which targeted dropsondes were deployed. All dropsonde deployments are centered on 00 UTC. Forecasts use NOGAPS at T79L18 resolution. Verification is based on analyses with all satellite wind data. The measure of forecast error is an “error energy norm” based on temperature, wind, and pressure, with units of $J\ kg^{-1}$. Reference 1 provides details. Errors are reduced by as much as 35 % in individual forecast cases. However, these positive impacts are reduced significantly in many cases when skill is measured against forecasts that contain wind data from geostationary satellites (see below). The skill of 2-day forecasts is a basic measure of success or failure, since these are explicitly the forecasts that the targeted dropsondes were designed to improve in NORPEX-98.

The effect of the targeted dropsonde data on 2-day forecast skill is shown in scatter plot form in Fig. 4. A range of impacts is seen, with some of the largest control errors reduced by as much as 35% when observations were obtained in the most dynamically

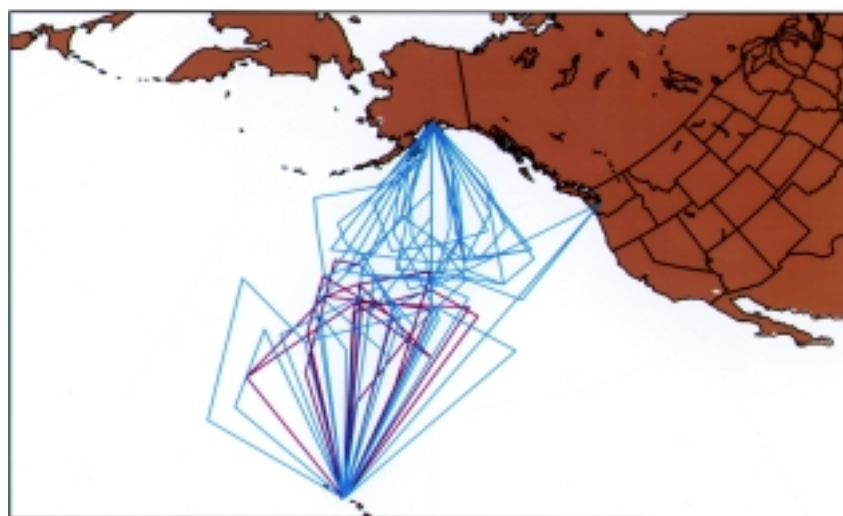


FIGURE 2
Flight tracks of NORPEX-98 targeted observing missions (red-NOAA G-IV, 8 flights; blue-USAF C-130s, 30 flights). Aircraft bases are Elmendorf Air Force Base (AFB), Anchorage, AK; Hickam AFB, Honolulu, HI; and McChord AFB, Tacoma, WA. Flight days are January 16, 17, 18, 19, 20, 21, 22, 23, 25, 27, 29, 30, 31, February 1, 2, 4, 5, 7, 9, 11, 15, 18, 20, 22, 26, 27 (1998).

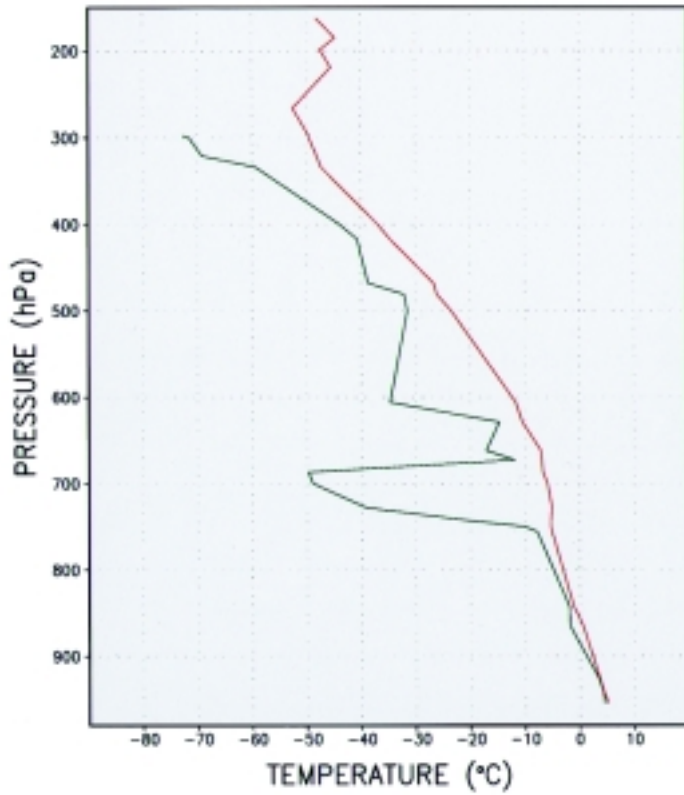


FIGURE 3
Profiles of temperature (K-red) and dewpoint temperature (K-green) from a GPS dropsonde deployed by the NOAA G-IV at 41.9°N, 160.2°W, at 00 UTC 22 January 1998.

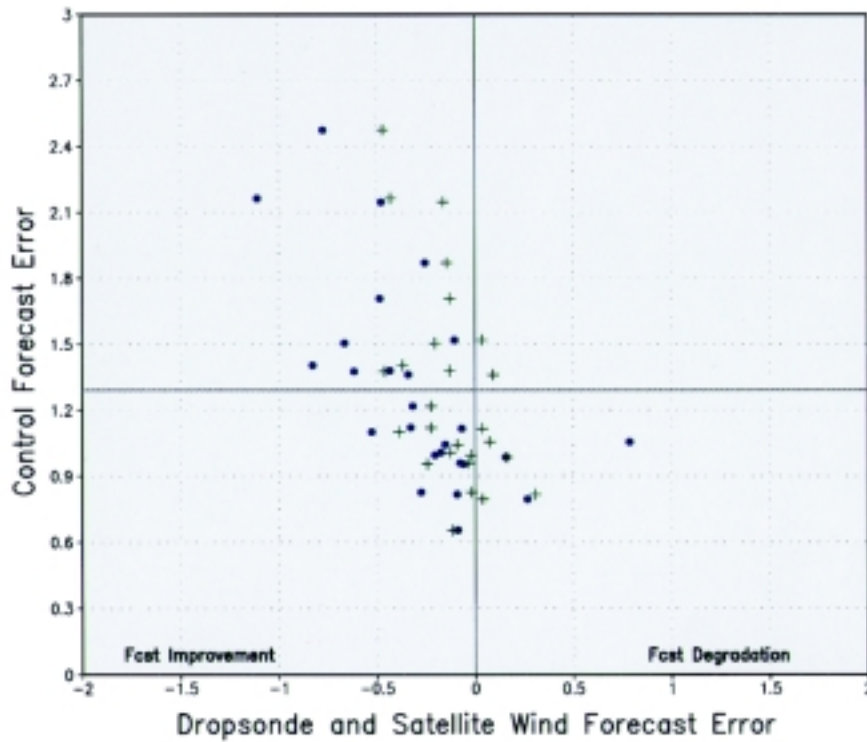


FIGURE 4
Forecast error statistics for 2-day NOGAPS forecasts evaluated in the region 30-60°N, 100-130°W. Twenty-six cases are shown, corresponding to days on which targeted dropsondes were deployed during NORPEX-98. Green + symbols indicate forecasts in which dropsonde observations (but no satellite data) were assimilated. Blue • symbols indicate forecasts in which satellite wind data (but no dropsonde data) were assimilated. The horizontal line at 1.29 J kg⁻¹ is the mean control error.

sensitive regions. The largest improvements in forecast skill are generally obtained for those forecasts that have largest errors in the control forecast. Smaller improvements are obtained when control errors are smaller, or when logistics prevented the reconnaissance aircraft from providing observations in the appropriate target areas. In a limited number of cases, forecast skill is degraded by addition of dropsonde data (points to the right of the vertical line in Fig. 4). This can occur when, for various reasons, the data assimilation procedure (which is a statistically based process) makes changes to the initial conditions that actually increase the error slightly in these sensitive locations. This problem can occur with dropsondes as well as other types of observations, and is a subject of current research in the Marine Meteorology Division.

Geostationary Satellite Winds

A large amount of tropospheric wind data over the North Pacific basin were provided every day, at 6-hour intervals during NORPEX-98 by the GOES-9 and GMS-5 geostationary satellites. These wind data, derived by tracking features in infrared, visible, and water vapor imagery,⁴ are perhaps the most com-

prehensive, regular source of atmospheric observations over oceanic regions equatorward of 60° latitude. The Marine Meteorology Division was the first agency to develop and test methods for operational assimilation of wind data from geostationary satellites, for both tropical⁵ and extratropical applications.

Although not specifically “targeted,” the satellite wind data often provide good observational coverage in dynamically sensitive regions, and their assimilation is thereby able to correct many fast-growing forecast errors. The main limitation of these data occurs in areas with cirrus cloud cover, which blocks observation of the mid and lower troposphere (Fig. 5).

The assimilation of geostationary satellite wind data during NORPEX-98 provides a 21% mean improvement in the skill of 2-day forecasts verifying over the western U.S. In comparison to the dropsonde observations, the satellite wind data produce a somewhat greater variation (both larger improvements and larger degradations), as shown in Fig. 4. For the 26 cases shown, all forecasts with control errors greater than the mean value were improved by assimilation of the satellite wind data. For individual forecast cases, satellite wind data can reduce forecast error by as much as 60%.

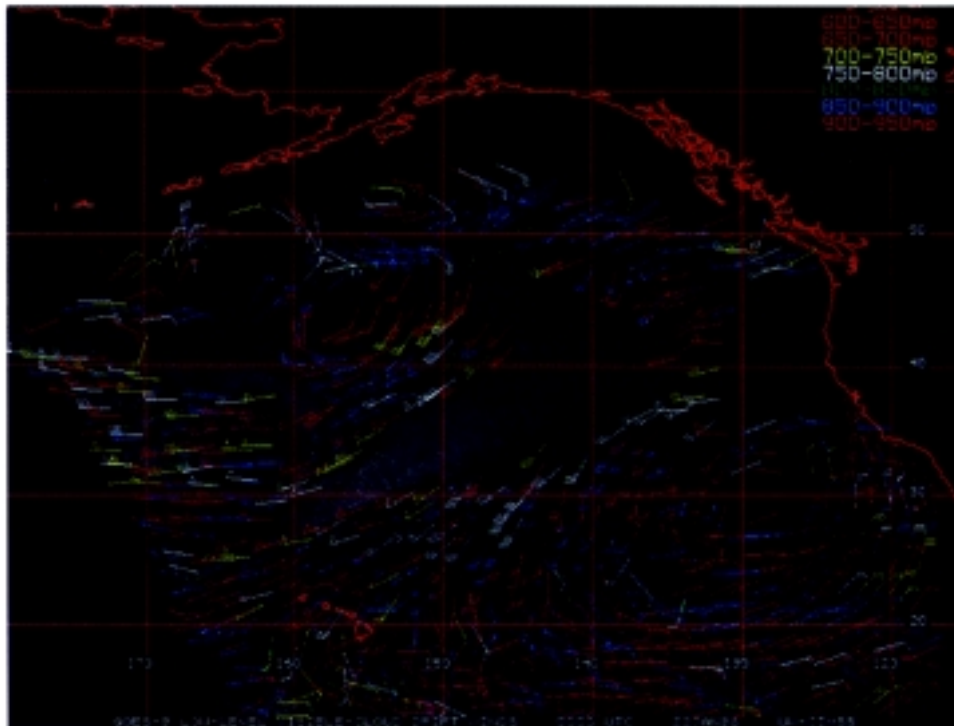


FIGURE 5
Wind vectors derived from GOES-9 visible imagery at 00 UTC, 22 January 1998. Color indicates pressure level of wind observation (650-950 mb), coverage at higher levels not shown. Figure provided by Christopher Velden, Cooperative Institute for Meteorological Satellite Studies, University of Wisconsin-Madison.

Several factors explain the highly beneficial effects of the satellite wind observations. These include the large area over which observations are provided (the entire North Pacific basin), and the assimilation of the wind data into the forecast model every 6 hours, rather than once per day or once every other day as in the case of the targeted dropsonde data.

JANUARY 22-24, 1998

The case of January 22, 1998 is an example of how targeted observations can improve the 2-day forecast of a major Pacific storm system. Two reconnaissance flights were flown using the NOAA G-IV from Honolulu and an Air Force C-130 from Anchorage. A total of 37 dropsondes were deployed. The SV target region includes two areas of strong sensitivity, one northwest of Hawaii, and the other in the eastern Gulf of Alaska (Fig. 6). The 700-mb level (roughly 10,000 ft) is shown because it is typically a level of maximum sensitivity to initial temperature error in midlatitude winter storm developments. Singular vector 4 (the SV with the fourth largest amplification rate) is shown because it is the structure that, in this case, carries the largest projection of forecast error (diagnosed a posteriori).

Target regions with fast-growing forecast errors are often in baroclinic zones (regions of strong horizontal temperature gradients). These are locations where errors can grow rapidly, because small inaccuracies in model initial conditions can directly influence baroclinic instability, which is the primary dynamical mechanism for midlatitude storm development based on the conversion of available potential energy (contained in meridional thermal gradients) into kinetic energy.

As seen in Fig. 6, SV 4 has large amplitude in areas with strong temperature gradients. Note that the SVs are eigenvectors, so additional scaling is required to obtain amplitudes consistent with those of standard meteorological fields. The other leading SVs (1-3, 5,6) have somewhat different structure but are also concentrated in these same baroclinic zones. They define a basically similar target area. In this particular case, the region of strong SV amplitude extended too far west for a complete survey by the Hawaii-based NOAA G-IV. Despite this limitation, the dropsonde coverage on January 22 is considered among the best for all cases during NORPEX-98, and produced a forecast improvement of 33% in terms of a reduction in 2-day forecast error over the region 30-60°N, 100-130°W.

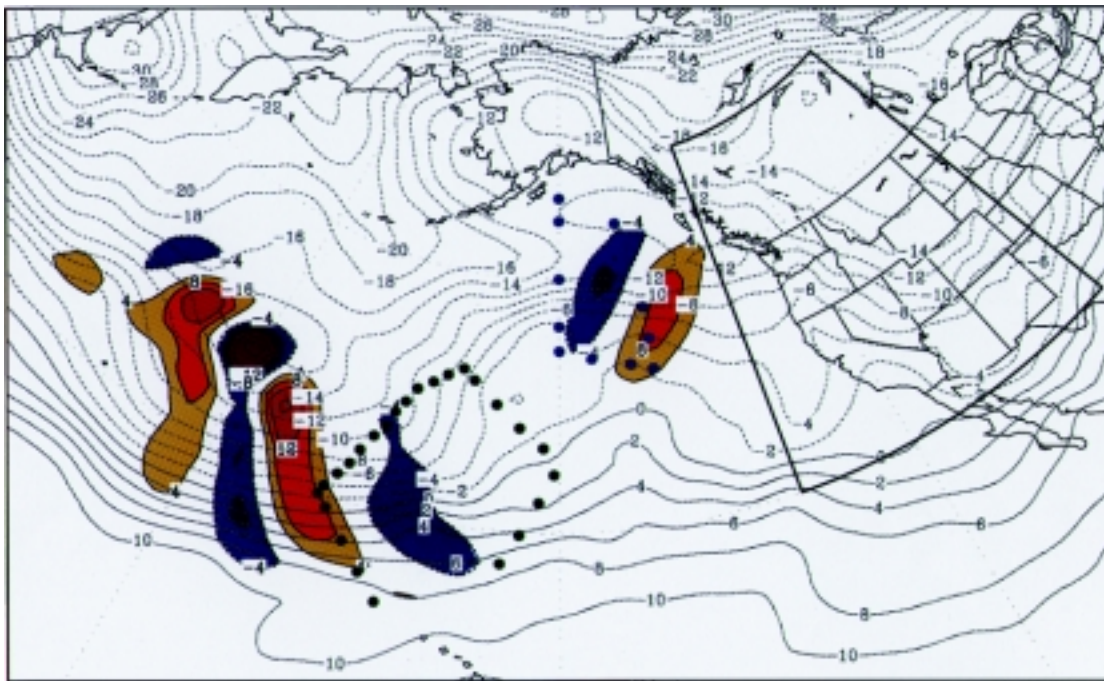


FIGURE 6
 The SV 4 target structure in terms of 700-mb temperature (shaded, contour interval = 4 °C) at 00 UTC 22 January 1998. Isotherms of analyzed 700-mb temperature are shown as gray lines with a contour interval of 2 K. Solid dots indicate positions of dropsondes deployed by the NOAA G-IV (green) and USAF C-130 (blue) during the interval from 19 UTC 21 January-04 UTC 22 January 1998. Assimilation of dropsonde data produces maximum changes to the initial temperature field of 1-5 °C (not shown). The NORPEX-98 forecast verification area is 30-60°N, 100-130°W.

By comparison, wind data over the entire north Pacific, provided by geostationary satellites, produced a 45% reduction in this same measure of forecast error. This is only slightly greater than that provided by the 37 targeted dropsondes. When both types of observations are assimilated, a 56% error reduction is achieved, suggesting that in this case the dropsonde data were able to correct initial condition error in locations where satellite wind data were inadequate. This is an example of how targeted in situ observations can be used to achieve a complimentary “mix” with data from other observing systems.

Figure 7 shows the change in 2-day forecast error, quantified in terms of height of the 500-mb pressure surface. The 500-mb level is representative of conditions in the midtroposphere. The largest corrections to 500-mb height error are found in a zone extending from Washington and Oregon to the southwest over the eastern Pacific. The maximum correction, on the Oregon coastline, is collocated with a strong landfalling cold front with heavy precipitation. This is the forecast feature that was “targeted” for improvement. The addition of dropsonde and satellite wind data provides a substantial improvement in the 2-day prediction of this heavy rain event on the West Coast (not shown).

It can be noted that the evolution of SV 4 (Fig. 8) has large amplitude in the area of maximum forecast error correction along the Oregon coastline (Fig. 7). This suggests that the evolution of forecast error (at least in early stages) can be strongly linked to atmospheric structures described by leading singular vectors, even though these SVs are computed a priori, without knowledge of the subsequent forecast error. This link between dynamics and error growth is the basis for targeting observations using the singular vector approach.

Figure 9 summarizes the amount of 2-day forecast error that projects onto the 20 fastest-growing singular vectors in this case. For each SV, four vertical bars correspond to errors contained in, respectively, the control forecast (no dropsonde or satellite wind data), the dropsonde forecast (control plus dropsonde data), the satellite wind forecast (control plus satellite wind data), and the dropsonde+satellite forecast (control plus dropsonde and satellite wind data).

In many instances, the most rapidly growing structure (SV 1) accounts for a larger fraction of forecast error than other SVs. This is not always the case, however, and in the present example the largest amount of forecast error projects onto SV 4. When combined, the leading six SVs explain a substantial amount of the total forecast error, even though these

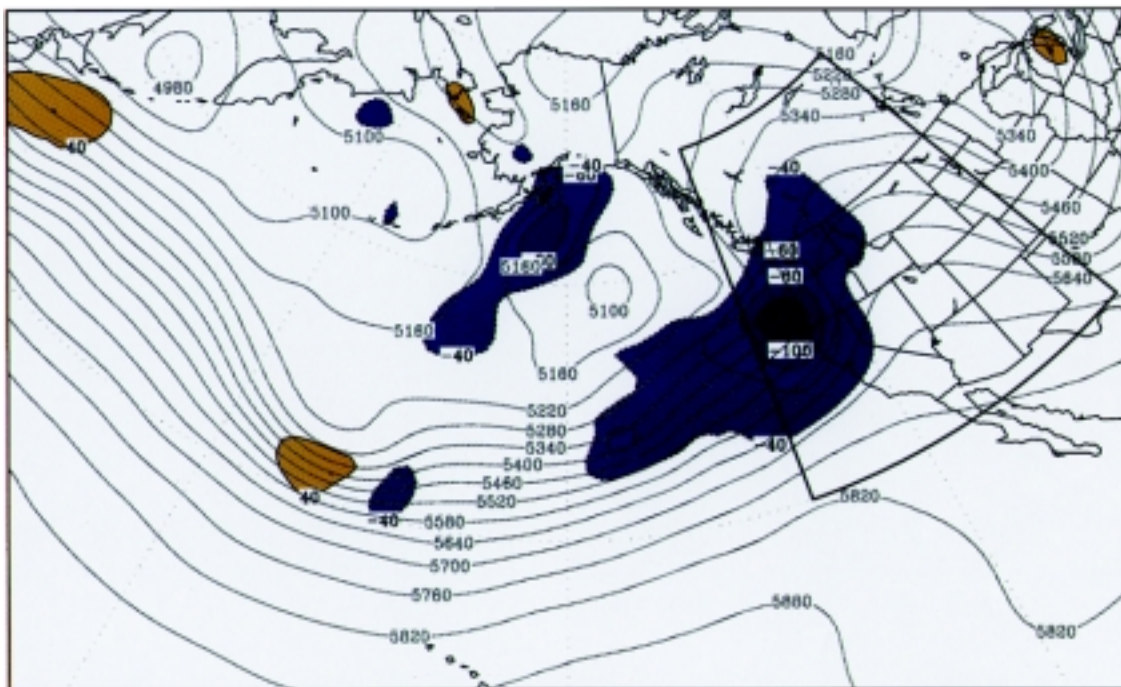


FIGURE 7
Change in 48-h forecast 500-mb height error (shaded, contour interval = 20 m) at 00 UTC January 24, 1998, due to assimilation of targeted dropsonde and satellite wind observations at 00 UTC 22 January 1998. Negative (positive) values indicate reduced (increased) forecast error. Isopleths of analyzed 500-mb height are shown as gray lines with a contour interval of 60 m.

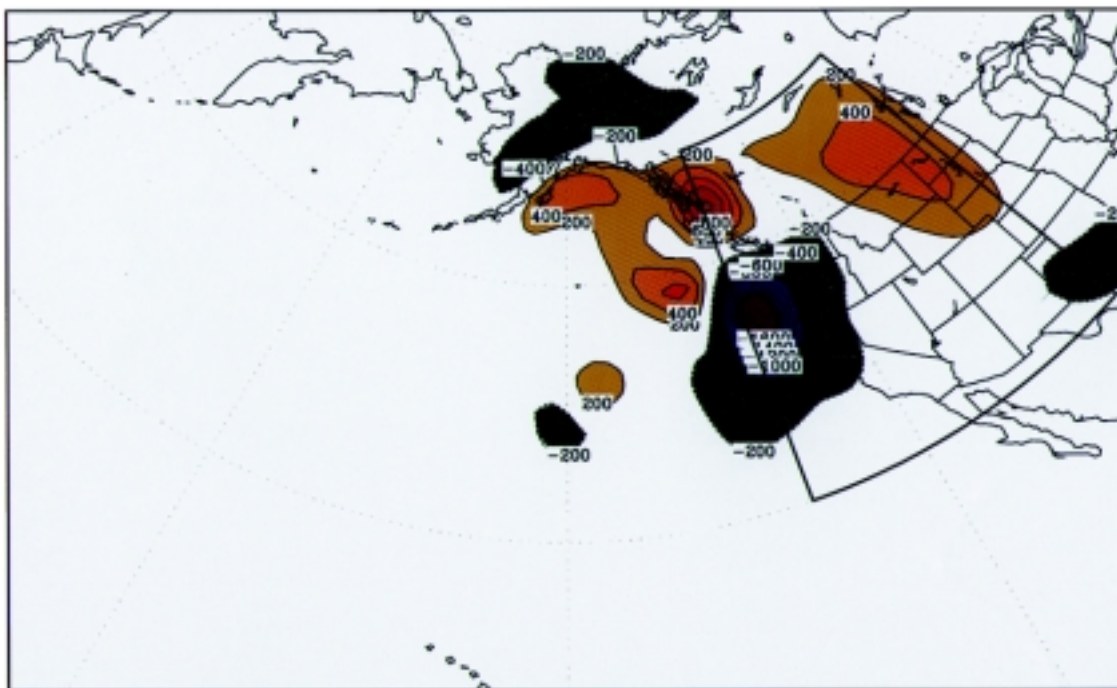


FIGURE 8
Evolution of the SV 4 target structure in terms of 500-mb height (shaded, contour interval = 200 m) at the verification time 00 UTC 24 January 1998.

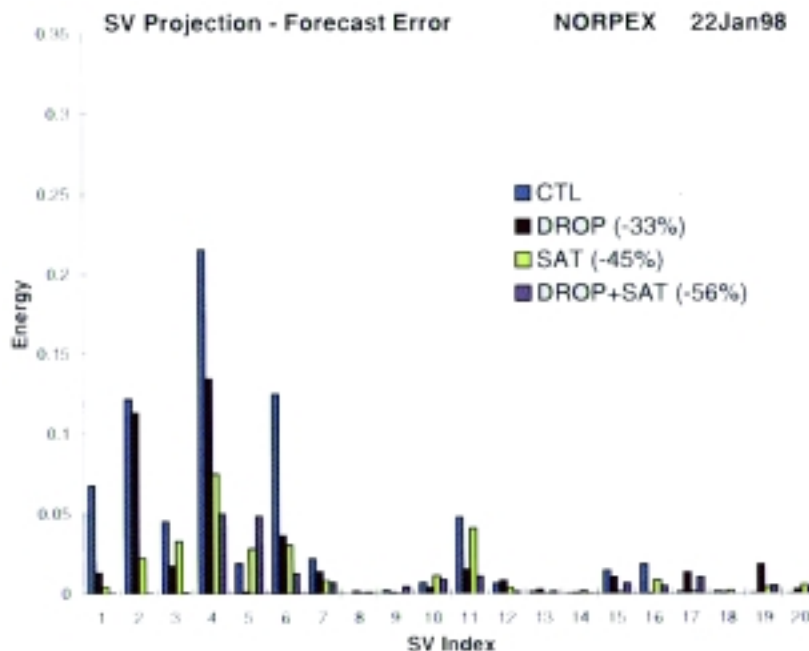


FIGURE 9
Projection of 48-h forecast error (energy-weighted, units = $J kg^{-1}$) onto the 20 leading singular vectors whose growth is optimized at 00 UTC 24 January 1998 in the area 30-60°N, 100-130°W. Experiments are described in the text.

few structures represent a very small part of the model dynamical space.

Forecasts that incorporate the dropsonde and satellite wind data reduce the total error in the control forecast, as described earlier, and this is accomplished primarily by the reduction of error projecting on the leading singular vectors. In particular, Fig. 9 shows that the dropsonde data reduce a significant amount of error on SVs 1, 4, and 6, while the satellite wind data reduce error on SVs 1, 2, 4, and 6. From a targeted observing perspective, these results are encouraging. They suggest that selective improvements to forecast model initial conditions in the small subspace of the leading singular vectors can be used to make significant reductions in short-range forecast error.

SUMMARY

Targeted dropsonde profiles and satellite wind data collected in the NORPEX-98 field program are providing insight to questions of atmospheric predictability and error growth. These data provide unprecedented observational coverage of winter season atmospheric conditions over the North Pacific basin, including documentation of storm development and cyclone life cycles during an extreme El Niño event. Improved model analyses and forecasts, which incorporated NORPEX-98 observations, allowed operational forecasters to provide more accurate warnings of precipitation, winds, waves, and other severe weather during the series of strong El Niño-driven storms on the Pacific coast during January and February 1998.

Predictability studies using NORPEX-98 data demonstrate that the early stages of error growth in forecasts of synoptic-scale weather systems can be described in terms of a relatively small number of unstable phase space directions, which can be approximated by the leading singular vectors of the forecast trajectory. These results support the concept that fast-growing forecast errors often originate in the middle and low troposphere, rather than in the level of the upper-level jet stream. Therefore, it is important for observational systems, whether in-situ or remote, to provide observing capability in regions below 500 mb. Limited amounts of observations are available from commercial aircraft, ships, polar-orbiting satellites, and other sources, but these often are not adequate to eliminate fast-growing forecast errors that frequently occur over the Pacific basin.

The results of NORPEX-98 show that reconnaissance aircraft can be used to deploy targeted dropsondes and improve short-range weather forecasts. However, it is not always logistically feasible to obtain adequate surveys of the appropriate target area, and this can often limit the probability that the dropsonde data that are obtained will have a positive impact on forecast skill. Perhaps more importantly, it has been found that observational data from geostationary satellites already provide considerable value over the North Pacific basin. For this reason, it will be increasingly difficult to demonstrate additional improvements in forecast skill through the deployment of in situ resources such as reconnaissance aircraft.

Future work will center on the improvement of adjoint-based targeting procedures and methods for assimilation of targeted observations. In the Marine Meteorology Division of NRL, studies of predictability and error growth are ongoing for both winter storm and hurricane forecasting problems.

ACKNOWLEDGMENTS

The targeted observing dropsonde deployment missions in NORPEX-98 were accomplished by personnel of the U.S. Air Force 53rd Weather Reconnaissance Squadron, Keesler Air Force Base, Mississippi, and the NOAA Aircraft Operations Center, MacDill Air Force Base, Florida. Many persons contributed to the NORPEX-98 effort; among them we especially thank Jon Talbot, Sean White, Mel Shapiro, Nick Bond, Zoltan Toth, Chris Velden, and Paul Hirschberg.

[Sponsored by ONR]

REFERENCES

- ¹T.N. Palmer, R. Gelaro, J. Barkmeijer, and R. Buizza, "Singular Vectors, Metrics and Adaptive Observations," *J. Atmos. Sci.* **55**, 633-653 (1998).
- ²T.E. Rosmond, "A Technical Description of the NRL Adjoint Modeling System," NRL/MR/7532/97/7230, Naval Research Laboratory, Monterey, CA 93943-5502 (1997).
- ³R. Gelaro, R. Buizza, T.N. Palmer, and E. Klinker, "Sensitivity Analysis of Forecast Errors and the Construction of Optimal Perturbations Using Singular Vectors," *J. Atmos. Sci.* **55**, 1012-1037 (1998).
- ⁴S.J. Nieman, W.P. Menzel, C.M. Hayden, D. Gray, S. Wanzong, C.S. Velden, and J. Daniels, "Fully Automated Cloud Drift Winds in NESIDS Operations," *Bull. Amer. Meteor. Soc.* **78**, 1121-1134 (1997).
- ⁵J.S. Goerss, C.S. Velden, and J.D. Hawkins, "The Impact of Multispectral GOES-8 Wind Information on Atlantic Tropical Cyclone Track Forecasts in 1995. Part II: NOGAPS Forecasts," *Mon. Wea. Rev.* **126**, 1219-1227. ★

THE AUTHORS



ROLF H. LANGLAND received a B.A. degree in physical geography from the University of Georgia at Athens in 1978, an M.S. degree in meteorology from the University of Wisconsin at Madison in 1984, and a Ph.D. in meteorology from the Naval Postgraduate School, Monterey, in 1996. His dissertation work involved the use of adjoint numerical methods in diagnostic studies of extratropical cyclones. Dr. Langland joined the Naval Environmental Prediction Research Facility (later to become the NRL-Monterey Marine Meteorology Division) in 1985, and his recent work has emphasized applications of adjoint methods with global and regional atmospheric forecast models. In addition to his participation in NORPEX-98, Dr. Langland was a flight scientist on several targeted observing missions in 1997 during the Fronts and Atlantic Storm Track Experiment (FASTEX) based in Shannon, Ireland, and is a member of the FASTEX Scientific Steering Committee.



RONALD GELARO received B.S., M.S., and Ph.D. degrees in meteorology from the Pennsylvania State University in 1980, 1983, and 1989, respectively. Dr. Gelaro joined the Naval Environmental Prediction Research Facility (later to become the NRL-Monterey Marine Meteorology Division) in 1985, where he began working on problems in model initialization, error growth, and tropical-extratropical interactions. He was a visiting scientist at the European Centre for Medium-range Weather Forecasts (ECMWF) from 1994-95, performing research in atmospheric predictability using adjoint methods and participating in the development of the ECMWF ensemble prediction system. He established and is the principal investigator of NRL's research program in atmospheric predictability. In addition to his participation in NORPEX, Dr. Gelaro served as a flight scientist on targeted observing missions during the 1997 Fronts and Atlantic Storm Track Experiment (FASTEX) based in Shannon, Ireland.



GREGORY D. ROHALY received a B.S. degree in meteorology from Millersville University near Lancaster, Pennsylvania, in 1988 and an M.S. degree in meteorology from The Florida State University at Tallahassee in 1991. Mr. Rohaly joined the Naval Research Laboratory's Marine Meteorology Division in 1994. His recent work includes the use of adjoint-based adaptive observation strategies for extratropical and tropical cyclones, development of a diabatic initialization procedure for the Navy's global model, and identification of the causes of errors in the Navy global operational modeling system. Mr. Rohaly is currently focused on furthering the development of the Navy's global model physics and using remotely sensed observations to facilitate improved atmospheric analyses.



THOMAS E. ROSMOND received B.S. and M.S. degrees in oceanography from the University of Washington in 1966 and 1968, respectively, and a Ph.D. degree in atmospheric sciences from the University of Washington in 1972. He spent 18 months at California State University, Fresno, on the geography department faculty, and then joined the Naval Environmental Prediction Research Facility (NEPRF) in Monterey, California, in 1974. In 1976 he became the head of a newly formed NEPRF Numerical Modeling Department, a position he held until 1990. During this time he directed the development of the Naval Operational Global Atmospheric Prediction System (NOGAPS), which is the primary numerical weather prediction model supplying environmental weather support for DoD operations worldwide. In recent years he has continued NOGAPS model development, and has also worked on adjoint and singular vector model development in support of atmospheric predictability research projects such as FASTEX and NORPEX-98.

Thirty Years of NRL Research in Functional Ceramics: From Failure Analysis to Novel Ceramic Devices

D. Lewis III, C. Kim, C.C.M. Wu, and T.L. Jessen
Materials Science and Technology Division

M. Kahn and M.T. Chase
Potomac Research International

NRL scientists have been active in the area of functional ceramics and ceramics devices for approximately 30 years—beginning with failure analysis for Navy sonar ceramics and ceramic capacitors, and evolving into development of test methodology for ceramics and new ceramic materials for the Navy. Subsequent efforts focused on development of novel functional ceramic devices. The scope of these recent efforts, which initially included only sonar devices, has expanded greatly. One recent project here developed sonar hydrophones using multilayer capacitor technology to produce piezoelectric ceramics with arrays of ordered voids. The development of these devices led to the successful testing and transition of towed array hydrophones of increased performance and *greatly* decreased size and cost. Current projects in this area include composite ceramic/polymer hydrophones for low-cost, large-scale, flank-mounted sonar arrays (to replace towed arrays), novel high-authority actuators (high force *and* high displacement output), and high-voltage, high-current capacitors and inductors for modular power supplies. The actuators are intended for applications such as active vibration control in machinery and control surface actuation in helicopters and aircraft. The capacitors and inductors are intended for use in the compact, high-power modular power supplies being developed under the Navy's Power Electronic Building Block (PEBB) program. Future plans in this research area include development of techniques for production of integrated power electronic devices using solid free-form fabrication methods.

HISTORICAL BACKGROUND

NRL scientists have been active in the area of functional ceramics and functional ceramics device for approximately 30 years. Functional ceramics is here defined as ceramic materials used in applications where the most critical properties are those other than the mechanical properties, i.e., strength, stiffness, resistance to fracture. This includes materials optimized for such properties as optical, tribological, electromagnetic, electrical, electromechanical, thermal, and chemical. This has long been a logical area for research and development programs for a Navy laboratory such as NRL. The Navy has used and continues to use functional ceramics and functional ceramic devices in a number of application areas. These include, among others, electronics (packaging, substrates, passive devices such as capacitors); radar;

optical and IR sensors and windows; bearings and seals; and sonar devices. The last began as 'Sound Navigation And Ranging,' but this technology area now includes a wide array of related electromechanical transduction devices and applications.

This last application (sonar and related devices) is one that is unique to the Navy (within DoD), and in which the Navy is the recognized technical leader. Not only is this a Navy-specific technical area, but it also is one in which the Navy makes a very large and continuing investment in material and device development, acquisition, and maintenance. There are literally millions of electromechanical transducers in use currently on Navy systems. In this area of sonar and related devices, the civilian market is relatively small, confined primarily to depth gauges, fish finders, and medical ultrasound. In many of the other areas listed, on the contrary, there are significant programs in

other portions of DoD, as well as commercial efforts to supply the necessary materials and technologies. Thus requirements for specific DoD support in the technology areas are not nearly as critical as they are for the transducer area.

FAILURE ANALYSIS STUDIES, INTRINSIC PROPERTIES, AND ECONOMICS

Some of the earliest work in the field of functional ceramics at NRL involved failure analysis for sonar ceramics and ceramic capacitors used in Navy systems, i.e., determining the strength and fracture toughness of the materials in the devices noted and the nature of the critical defects, which limited the design strength of the materials in the devices.¹⁻³ Capacitors and sonar components can fail during assembly or in service from a variety of defects. Identification and elimination of these defects is critical to device and system performance.

One significant point here relates to the intrinsic properties of some functional ceramic materials. The ceramic components used in capacitors and sonar ceramics are typically produced of perovskite materials such as BaTiO_3 or $\text{Pb}_{1-x}\text{Zr}_x\text{TiO}_3$ solid solutions. These materials are selected primarily on the basis of electromechanical performance parameters, such as permittivity, electromechanical coupling coefficients, and Curie temperature. Unfortunately, the same physics that produces the desirable electromechanical properties in these materials also produces low resistance to fracture. These materials are thus readily subject to failure from mechanical stresses, requiring careful material preparation and clever device designs. The two materials cited above have approximately the resistance to fracture as window glass.

It is also significant that failures of relatively inexpensive functional ceramic materials and devices can be quite expensive in toto. Failure of a single ceramic capacitor in an intercontinental ballistic missile guidance system can result in failure of the missile to reach its target. Failure of sonar transducers in a destroyer bow dome can result in the need for a ship to be placed in dry dock for repairs, with the crew paid to take extended shore leave; in a combat situation, such failure could result in loss of the ship and its crew. For these reasons, a significant effort at NRL went into developing the scientific basis and techniques for failure analysis in ceramics and into corollary programs, including test methodology and techniques for improving the critical properties of functional ceramics.

TEST METHODOLOGY FOR FUNCTIONAL CERAMICS

The program at NRL thus naturally evolved into development of test methodology for ceramics, including measuring the resistance to fracture (fracture toughness, fracture energy) of ceramic materials. Some tests were adapted from those developed for metals, but others were developed at NRL to meet the unique requirements of ceramics.² These NRL-developed test methodologies were applied successfully to a wide range of functional ceramics and specimen sizes. The applied moment double cantilever beam (DCB) test, originally designed for samples approximately $1 \times 12 \times 50$ mm, was successfully adapted for test specimens cut from ceramic multi-layer capacitors with *maximum* specimen sizes of $2 \times 5 \times 7$ mm. In addition to measurement of fracture toughness, improved techniques for measurement of the tensile strength of ceramics were developed, again specialized for functional ceramics (high hardness, high stiffness, low fracture toughness). Improved data analysis techniques were also developed for processing the strength data, using property distribution functions and parameter determination methods appropriate to functional ceramics. These techniques were needed because the low fracture toughness of the functional ceramics results in very large scatter in measured strengths and related design difficulties. Accurate characterization of the statistical distribution of mechanical properties is critical for successful use of load-bearing functional ceramic materials.

NEW FUNCTIONAL CERAMIC MATERIALS AND THE SHIFT TO DEVICES

The program also subsequently explored development of new functional ceramic materials for the Navy with better properties and improved processes for producing these materials. Previous efforts on failure analysis identified processing problems as causing unanticipated mechanical failure of ceramic sonar devices. These programs on failure analysis and processing produced substantial understanding of the materials issues involved and some gains in performance, but these gains were limited by intrinsic material property considerations.

One program, which anticipated the current Office of Naval Research/Defense Advanced Research Projects Agency (ONR/DARPA) single-crystal piezoelectric effort, investigated SbSI in various forms as a hydrophone material. It was found that single-crystal

devices of SbSI exhibited very high sensitivity as hydrophones but were severely limited by poor mechanical properties. The same material, in polycrystalline form, had acceptable mechanical properties but marginally better piezoelectric properties. A compromise, which produced good piezoelectric properties *and* acceptable mechanical properties, was to fabricate an aligned polycrystalline body with crystallographically aligned grains.⁴ Novel processing techniques were developed to make this possible. However, subsequent geopolitical developments and changes in the operational theaters for the Navy made this an unlikely choice for hydrophones. The material, SbSI, has a Curie temperature of approximately 35 °C, restricting its use to areas where the water temperature is less than 20-25 °C. SbSI hydrophones would work fine in the North Atlantic or Arctic Oceans against Soviet submarines, but not very well in the Persian Gulf in more temperate waters.

Following the research and development efforts described above, it became clear that few advances were to be made in the sonar and transducer areas, or in other areas, through development or improvement of functional ceramic *materials*. Subsequent

efforts focused on development of novel functional ceramic *devices*, e.g., using state-of-the-art functional ceramic materials in novel ways or in novel device configurations to improve performance. This, until very recently, has been the focus of nearly all the work in functional ceramic materials at NRL.

PZT WITH ORDERED VOIDS FOR TOWED ARRAY HYDROPHONES

One of the recent projects in this area entailed development of sonar hydrophones using modified multilayer capacitor technology to produce piezoelectric (PZT) ceramics with arrays of ordered voids. This project exploited scientific understanding, developed at NRL, Penn State University, and in Japan, of the fundamental properties that limited the performance of bulk, monolithic PZT materials as hydrostatic transducers. The inclusion of an array of ordered voids in a bulk PZT material changed the material from an isotropic one with near-zero hydrostatic response to an anisotropic one in which the hydrostatic response approached the excellent uniaxial response of the material.⁵ Figure 1 shows an example of the ordered

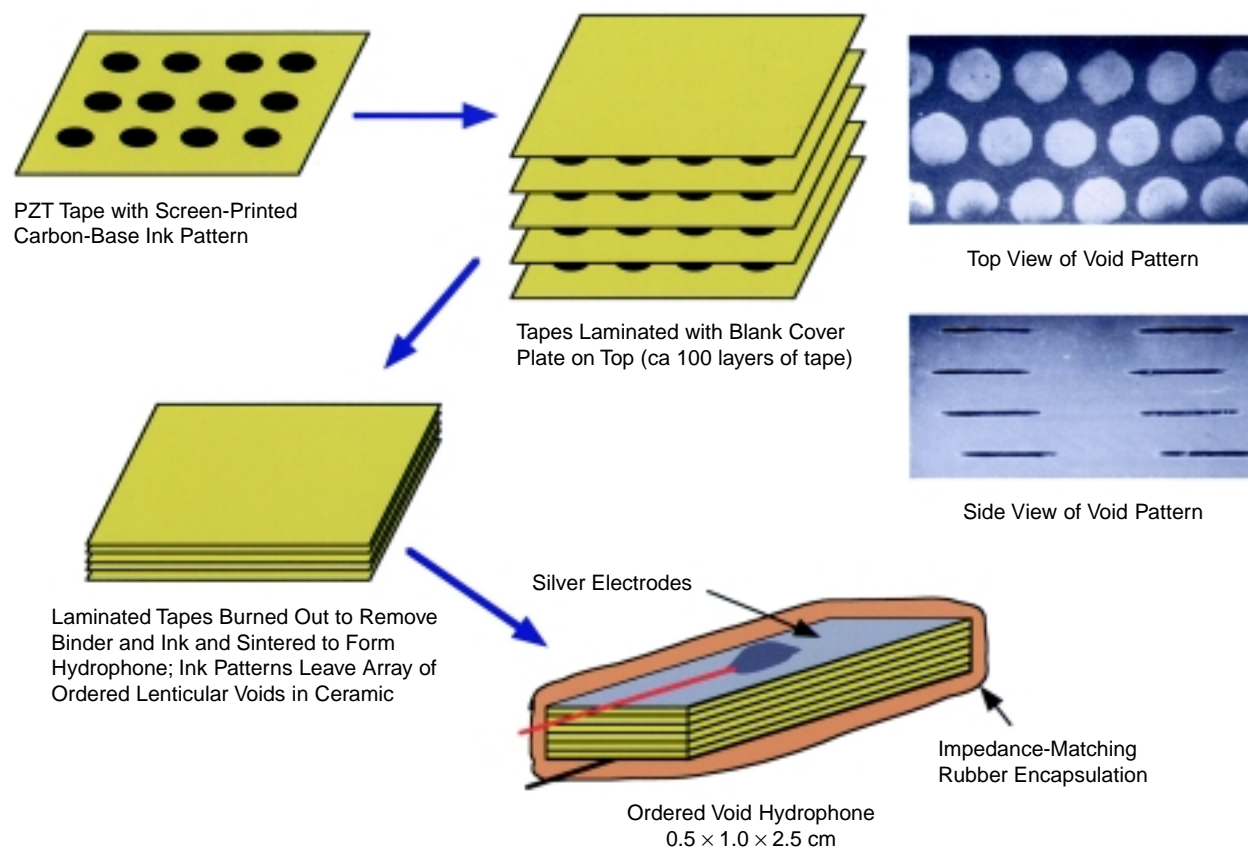


FIGURE 1 PZT with ordered voids for towed array hydrophones; 100x reduction in size and cost vs current technology.

void materials. In addition to the excellent performance, this approach led to a *two order of magnitude* reduction in the size and *cost* of hydrophone transducers for towed arrays. These devices have passed two sets of sea trials (built into towed arrays), and efforts are underway to provide large-scale manufacturing capabilities for these new towed array hydrophones. Similar technologies have also been applied at NRL to electronic packaging with locally tailored dielectric properties and built-in cooling passages.⁶

COMPOSITE HYDROPHONES AND SPIOFFS

Other projects at this time explored different approaches to achieve higher performance through device configurations to increase the output or sensitivity, or other schemes to obtain anisotropic performance from isotropic piezoelectrics. One innovative approach here used doping of PZT to increase the local conductivity and achieve differential poling of a monolithic PZT device.⁷ In this approach, a portion of the device was poled by an applied electric field

(made active electromechanically) while the remainder was not. This permitted fabrication of mechanically reliable monolithic bending transducers that would provide relatively large deflection outputs. The concept is shown schematically in Fig. 2(a). Most piezoelectric actuators and transducers produce relatively small output displacements (although large forces). This flexural transducer would replace conventional ones made by bonding two differentially poled segments with an electrode layer and other complicated designs, as shown in Fig. 2(b). Such laminated transducers historically have suffered from performance-limiting failures in the joints between the ceramic layers and the metallic electrode interlayer. The NRL design eliminates this weakness in this particular transducer configuration, albeit at some sacrifice in potential performance.

NRL efforts at this time included the production of modified “1-3” composite ceramic/polymer piezoelectric transducers for both sensors and projectors. The notation indicates that the active elements (PZT) are continuous in *one* dimension, and the passive matrix material is continuous in *three* dimensions. The NRL designs sought to eliminate lateral effects

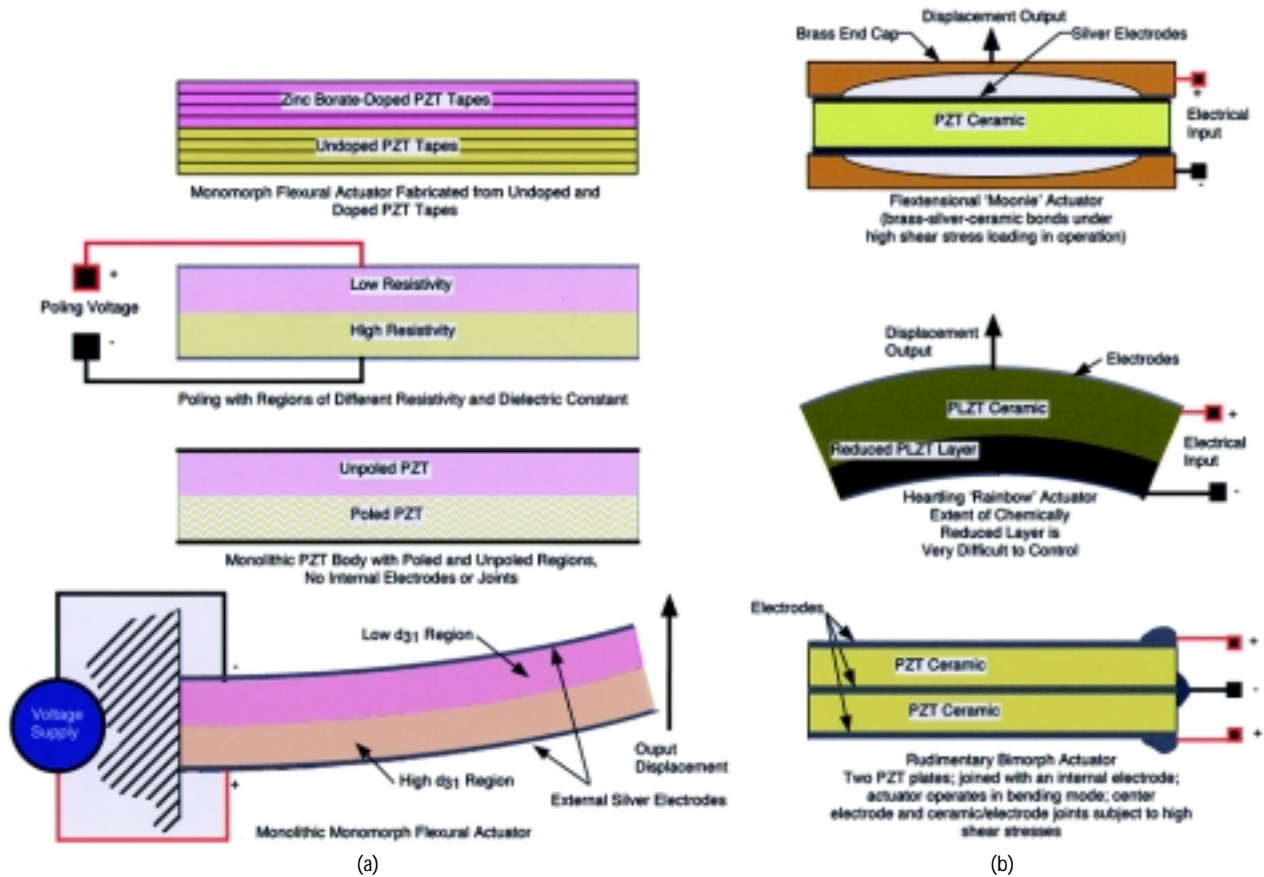


FIGURE 2 Flexural monomorph actuator (a) fabrication and operation—no internal electrodes or stressed metal-ceramic joints; (b) conventional high displacement actuators—complicated construction, internal electrodes, highly stressed joints.

through inclusion of low-modulus and high-modulus lossy polymers separating rod-like PZT transducer elements. The modified designs, using two types of polymers, called 1-1-3 composites with the active material and a soft polymer filler continuous in one dimension, and a rigid polymer matrix continuous in three dimensions (Fig. 3).⁸⁻⁹ Techniques were developed at NRL for production and automated assembly of the necessary components to reduce the cost of the composite transducers to those of conventional transducers.¹⁰ These cost-reduction efforts were moderately successful, and the transducers produced showed performance far superior to that of conventional transducers.

Unfortunately, changes in DoD acquisition philosophy precluded their insertion into Navy systems, because of virtually flat DoD budgets that required new systems to be cheaper than present ones. It was clear that, barring some dramatic technology breakthroughs, the composite hydrophones would never be cheap enough to permit their use, particularly with some of the newer uses envisaged. One of these would require *large* numbers of piezoelectric transducers, mounting them in flank arrays on the hulls of surface ships and submarines, to replace towed arrays. The shift to littoral (shallow-water) theaters for Navy operations made use of existing towed arrays problematical. Sharp turns, coral reefs, and shallow

waters, typical of littoral conditions, are not practical for deep-water towed arrays.

LOW-COST PIEZOELECTRIC TRANSDUCERS FOR LARGE ARRAYS

Two types of composite piezoelectric transducers were explored for large, low-cost arrays. The first built on earlier Japanese and NRL/Orlando work and explored 0-3 composite transducers, basically rubbery polymers filled with particles of piezoelectric material. Work in this area showed that durable, low-cost hydrophones for large hull-mounted arrays could be produced. However, intrinsic limitations of this approach precluded meeting performance requirements for such hydrophones. The extremely low cost of the materials was therefore of no benefit. As a result, extensive efforts went into modifications of the original 0-3 composite materials to enhance their performance. The results, first from an NRL 6.1 program and now from a follow-on 6.2 program, are basically 1-3 composite transducers made by a small modification of 0-3 composite processing. The modifications involve greatly increasing the size of the piezoelectric ceramic granules in the polymer to more than that of the polymer layer. With the addition of cover plates, the resulting assemblies function as 1-3 composite transducers, but with far lower fabrication

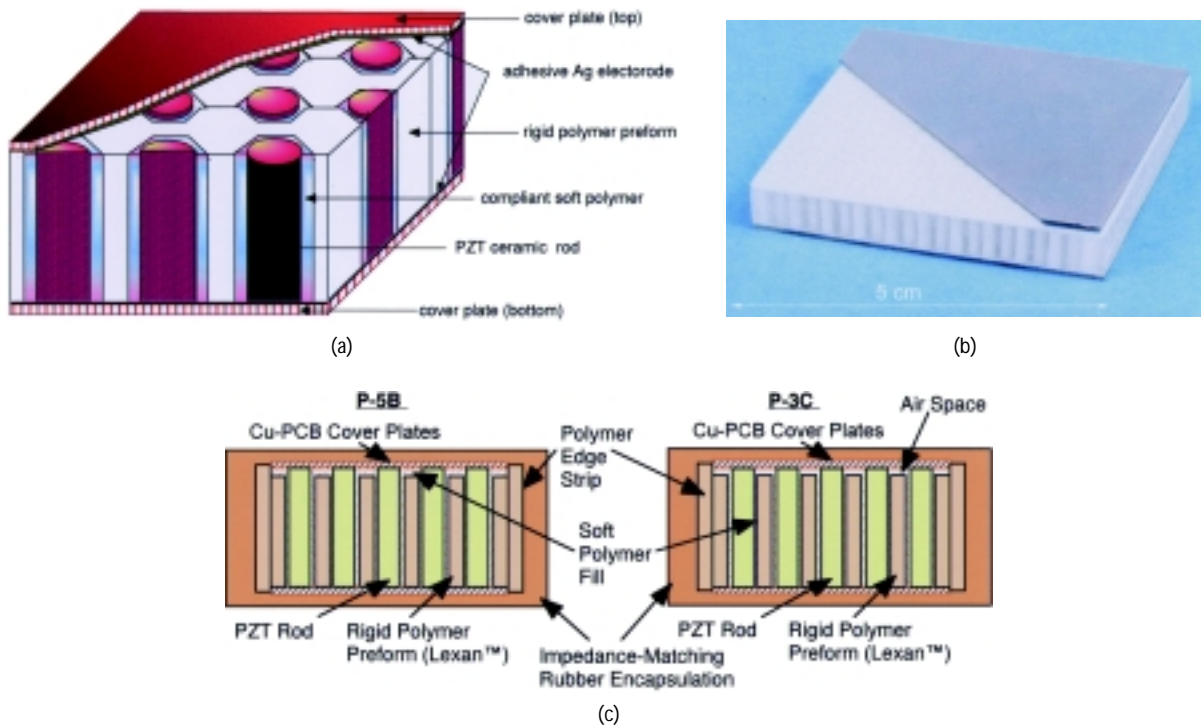


FIGURE 3 1-1-3 modified 1-3 composite transducers for hydrophones and projectors: (a) schematic; (b) example; (c) configurations to maximize hydrostatic response; P-3C has 2-3 times hydrostatic response of other configurations.

cost. The devices and their fabrication steps, shown in Fig. 4, are termed Piezogran™ transducers. These transducers are still relatively low in cost and weight and now have performance comparable to current discrete hydrophones. These devices also have performance nearly comparable to that of far more expensive 1-3 composite transducers made by an injection molding process developed under ONR and DARPA funding at a small company (MSI). As such, they are a possible candidate for use in large flank-mounted sonar arrays, especially if the MSI materials prove too costly, even in large-scale production, for such applications.

OTHER CURRENT PROGRAMS IN FUNCTIONAL CERAMICS

Current projects in this area include novel high-authority actuators (high force *and* high displacement output) and high-voltage, high-current capacitors and inductors for modular power supplies. The high-authority actuators were developed to meet DARPA requirements for high torque or force and large displacement piezoelectric for use in active vibration

control and control surface actuation in helicopters and aircraft, and as active, vibration isolation machinery mounts. The high displacements are not typical of piezoelectrics, which generally produce large forces, but displacements measured only in micrometers. Some actuators, imaginatively called moonies, rainbows, or cymbals, use mechanical amplification to achieve higher displacements (Fig. 2(b)), but sacrifice force output and device stiffness to obtain higher displacements and entail complex structures and numerous joints that add cost and diminish reliability.

NRL scientists have developed and patented two high-authority actuator designs that eliminate many of the problems of the other approaches to high-authority actuators. The first, a unique concept using the shear mode of actuation (termed d_{15}) in the piezoelectric jargon, provides a direct *torsional* output.¹¹⁻¹² Such an output is ideal for driving a control surface on a helicopter or aircraft or for twisting a helicopter rotor blade. Nearly all other piezoelectric actuators have *linear* outputs, which require inefficient mechanical devices to convert linear to rotary motion. This device (Fig. 5) is constructed of a number of tubular PZT segments bonded together with

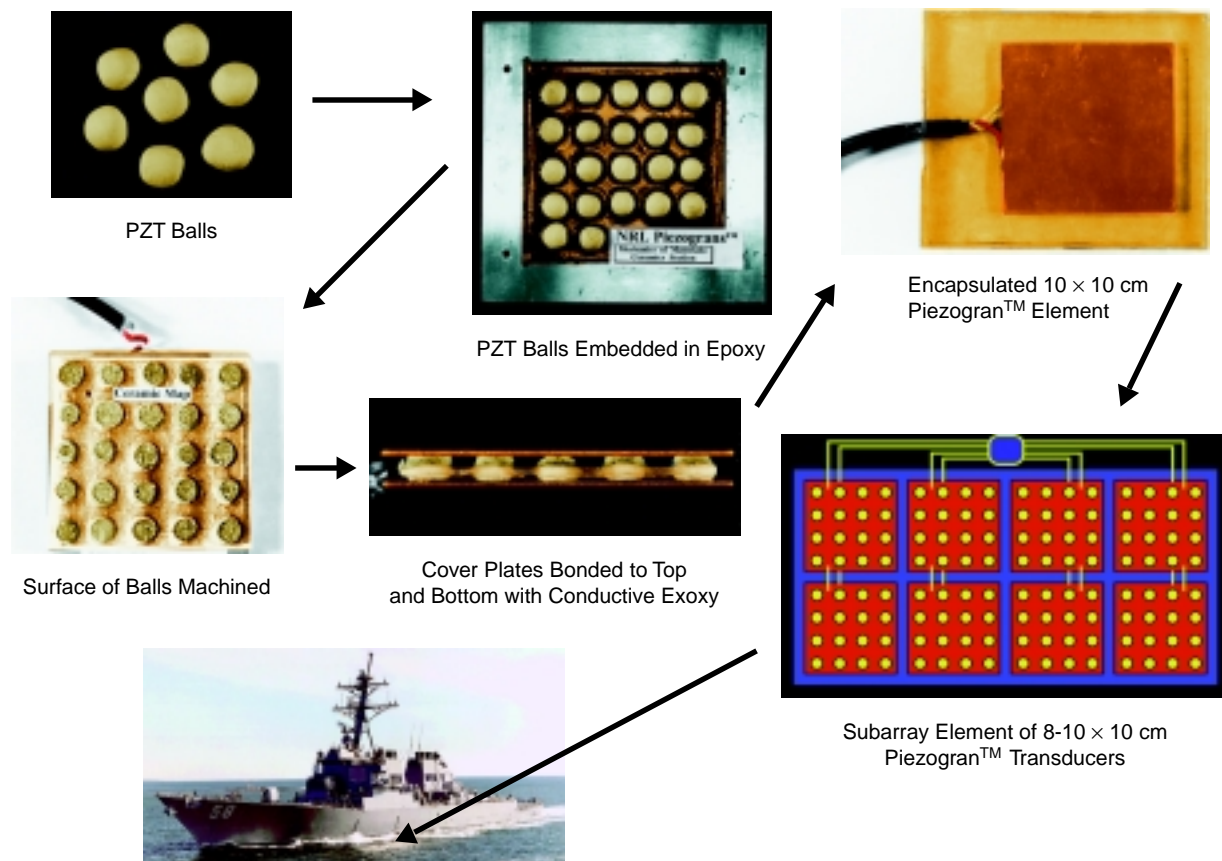


FIGURE 4 Piezogran™ transducers for flank-mounted arrays—simple, low-cost fabrication of flank-mounted wide aperture sonar arrays.

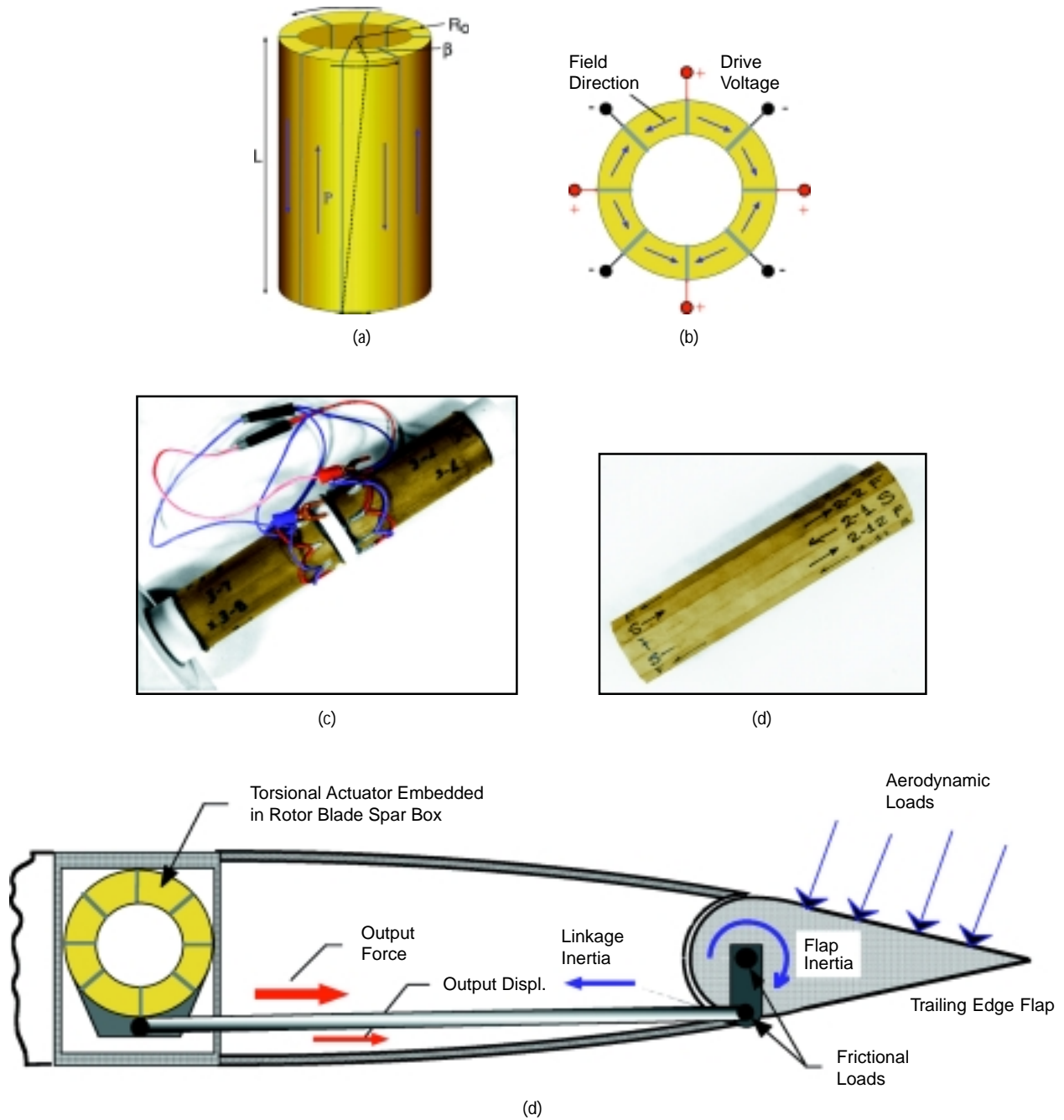


FIGURE 5 High-authority torsional actuator: (a) segments shear and assembly twists—torque proportional to cross-sectional area; angle of twist proportional to $1/d$ of assembly; (b) dual, circular cross-section torsional actuator assembly tested—approx. 2.5-cm diameter and 20-cm length; joints of high-strength conductive epoxy stronger than ceramic segments; (c) polygonal (12-sided) assembly—comparable performance and stresses, much easier fabrication; (d) torsional actuator in helicopter rotor spar box to drive trailing edge flap—large actuator length gives large angular displacement.

intervening electrodes. When a voltage is applied to these electrodes, each segment attempts to shear in its major plane, and the whole assembly twists about its long axis. The torque output of this device is proportional to its cross-sectional area, and the rotational angle to its aspect ratio (length/diameter). These torsional actuators can be tailored to specific requirements for torque and displacement simply by changing their dimensions. The geometry of this actuator is ideal for some cases where the shape of the actuator uses the space available efficiently, e.g., a helicopter rotor spar.

A last application of the torsional actuator being explored is as a drive for a piezoelectric motor, with the actuator operating at resonance. In this mode, the actuator is extremely efficient, with very high output, as shown in Fig. 6. Here, the torsional actuator would be used to drive a rotary inchworm mechanism, providing the piezoelectric equivalent of a stepper motor. The piezoelectric motor should be capable of fairly high rotation speed, e.g., tens of degrees per second, and extremely high torque, as the inchworm mechanism locks in place mechanically when the motor is not operating. Linear piezoelectric inchworm devices have been built, but this is the first with a direct rotational output, and on which patent applications have been filed.

The other high-authority actuator being developed at NRL is a novel solid state, telescoping *linear* actuator. This actuator, also developed under DARPA sponsorship for applications such as helicopter rotor control, has a variety of other potential applications. The geometry of this device is not as well suited to the helicopter application as the torsional actuator (cf. Fig. 7), but its geometry is better suited for active vibration control of machinery. The actuator, placed

between machinery and supports, is driven by a control system to null out the motions of the machinery. The telescoping actuator, as shown in Fig. 7, is basically a folded stack actuator. The force output of the device is proportional to the cross-section of the smallest tubular segment and the displacement output to the combined length of the tubular segments. Thus, it is possible to make a relatively compact device (in terms of height) with large force and displacement output. The same displacement output in a stack actuator would require an unreasonably long and impractical stack, with many weak joints. The telescoping actuator can be fabricated from individual tubes, with a small number of bonded joints or in a single monolithic form, using solid free-form techniques, with no joints (Fig. 7(d)). It is also possible to produce such devices in a wide range of sizes and force/displacement capabilities and as arrays, especially using novel fabrication techniques such as the various solid free-form processes.

A sidelight of the NRL work on high-authority actuators has been the development of a number of novel processing and fabrication technologies. This is not normally part of a materials research program, but it has become far more important here when actual devices are being produced. An example of this is the development of a continuous poling process to permit the poling (making piezoelectric ceramics active as transducers) of the unusual component shapes of the parts of the torsional and telescoping actuators. Here conventional poling would require voltages on the order of hundreds of kilovolts and would be totally impractical. The continuous poling system developed (Fig. 8) produces the same resultant properties as conventional poling and handles exotic component shapes without difficulty.¹³

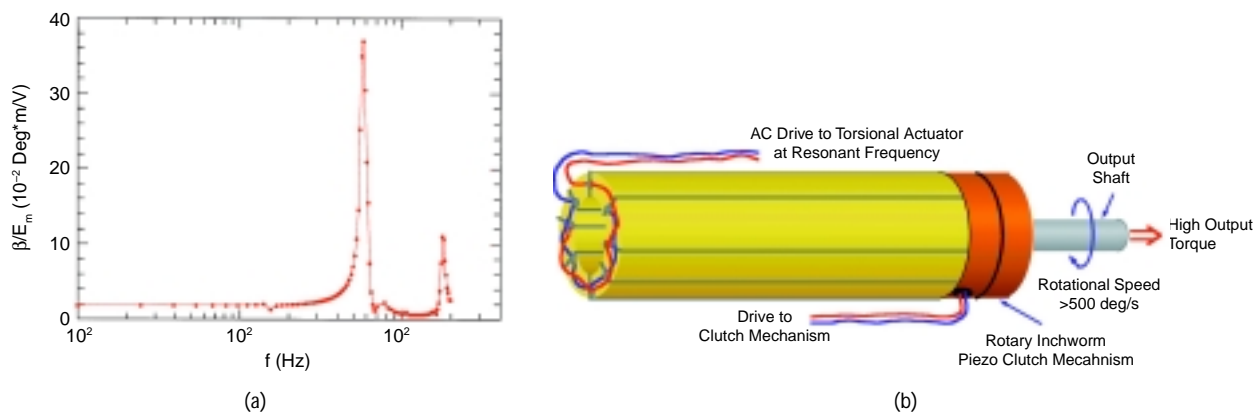


FIGURE 6 Torsional actuator in rotary inchworm piezomotor application: (a) output at resonance, ca. 20 times that off-resonance, provides efficient use in inchworm piezomotor application; field of 105 V/mm gives speed of 550 deg/s for piezomotor; (b) piezomotor with rotary inchworm clutch; very high torque and moderate rotational speeds, very high efficiency with coupled inductors for energy.

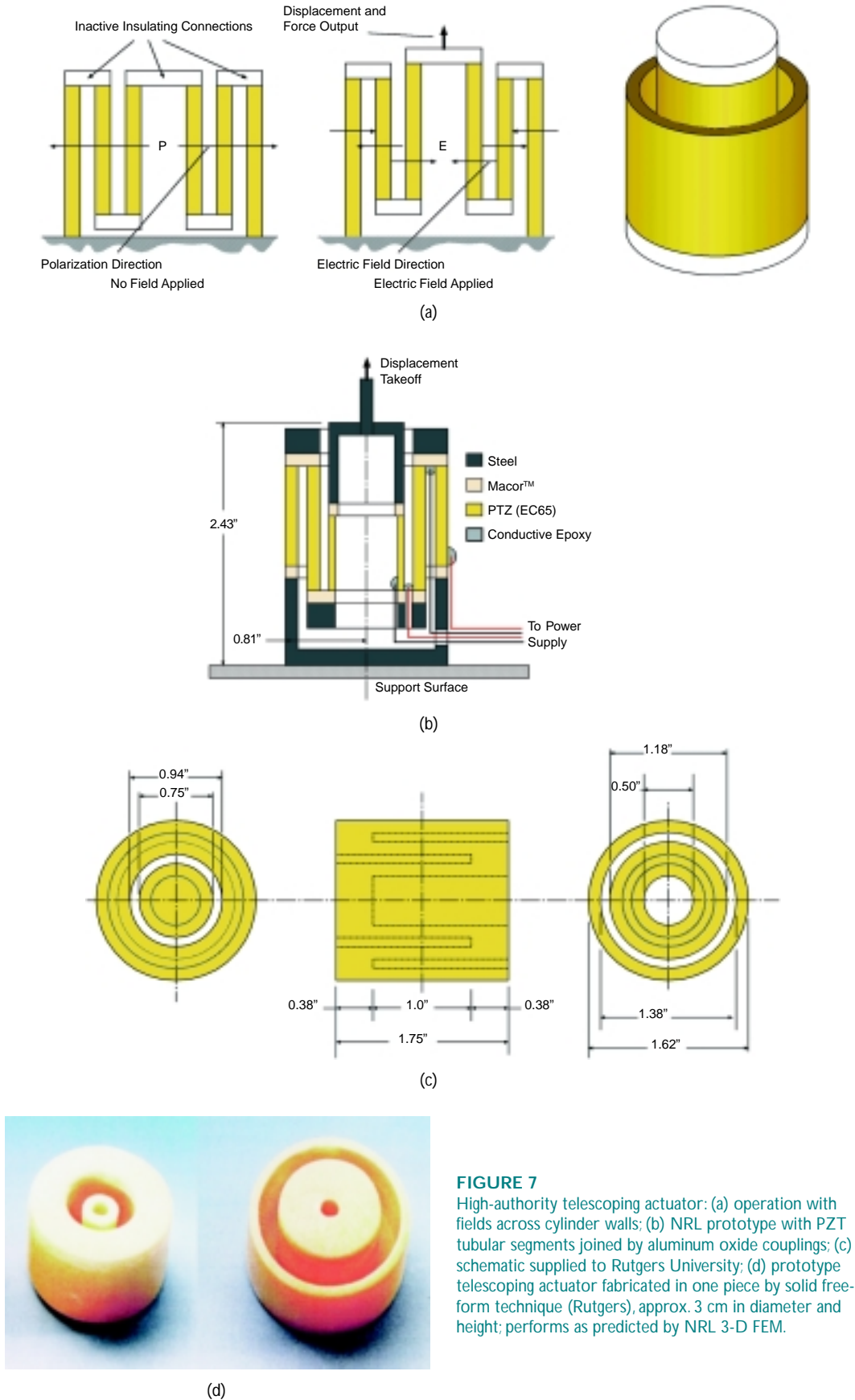


FIGURE 7 High-authority telescoping actuator: (a) operation with fields across cylinder walls; (b) NRL prototype with PZT tubular segments joined by aluminum oxide couplings; (c) schematic supplied to Rutgers University; (d) prototype telescoping actuator fabricated in one piece by solid free-form technique (Rutgers), approx. 3 cm in diameter and height; performs as predicted by NRL 3-D FEM.

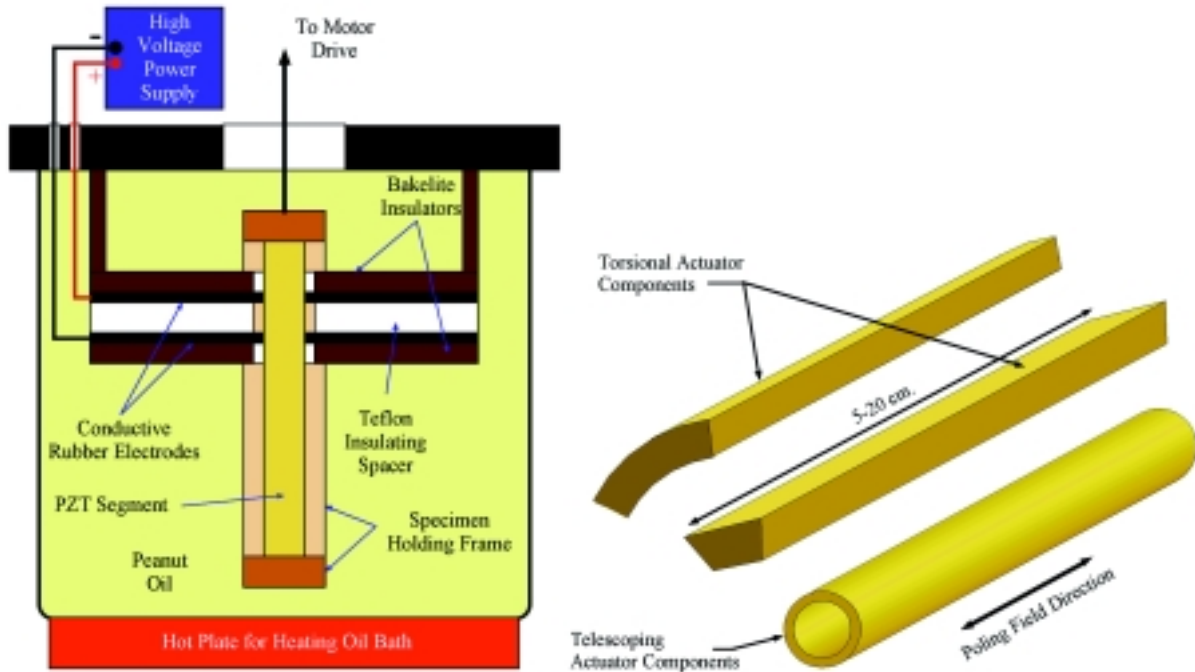


FIGURE 8 Continuous poling technology for high-authority actuator components—piezoelectric ceramic segments drawn through electrodes, 2-5 kV/mm field between electrodes (2-5 kV/mm), in 120-350 °C oil bath to pole unusual shapes as shown.

Another recent project at NRL in functional ceramics has resulted from Navy work on compact, high-power modular power supplies under the PEBB program. This program seeks to construct compact (shoebox-size) AC/DC power supplies, configured via software, that can produce nearly any output voltage, current, or waveform from a standard input bus voltage. The use of these modular power supplies would greatly reduce the power supply inventory required on Navy ships. Research effort have greatly reduced the size of the active elements involved (high-current, high-voltage switching transistors), but the passive elements, capacitors and inductors, for buffering the input bus and filtering the output waveform, remain the critical problem. Currently, the passive elements occupy two refrigerator-size cabinets, rather than the two-thirds of the shoebox they are intended to occupy.

NRL scientists have been investigating novel dielectric materials for production of greatly improved output filter capacitors to address this problem. The approach at NRL has been to use the existing science and technology base for PZT materials (from the transducer work) to produce dielectric materials with improved properties. The critical properties here include not only dielectric constant, but sensitivity of dielectric constant and loss tangent to electric field

and temperature. The NRL work, which has been funded out of NRL core 6.1 funds, has been quite successful to-date, and prototype capacitors with excellent properties have been produced. Current efforts include further material modifications for even better electrical performance and studies on processing techniques for producing high-quality raw materials and capacitor components from these raw materials. Other efforts, supported by NRL and ONR 6.2 funds, are directed at production of sufficient quantities of materials and capacitors to satisfy the requirements for a PEBB power module for a demonstration in an actual device. In addition there is also a smaller, parallel effort at NRL to develop better (i.e., much smaller) inductors through production of improved ferrites, also funded by NRL 6.1 funds.

Future plans in this research area include development of techniques for production of integrated power electronic devices using both conventional and solid free-form fabrication methods. It is expected that this NRL effort will become part of a power electronic thrust at NRL to support future Navy work in this area. One of the goals here is to provide a capability for direct production of components with integrated active and passive devices in thermal management packaging. It is felt that work in the technical areas described here will continue to evolve and ex-

pand into new technical areas, materials, and devices for Navy systems. This is a consequence of the shift in costs of Naval systems to electronics and embedded functional devices, coupled with the expected large increases in the uses of such electronics and functional devices in Naval systems associated with the need for reduced manning and operational and maintenance costs.

At this point, the functional ceramics research efforts at NRL have come almost full circle, beginning with capacitors and failure analysis of functional ceramics, and now back again with capacitors, although the size of the capacitors has changed dramatically. This is after a long detour through piezoelectric sensor and actuator development. The remainder of the journey may be completed with the possible addition of a DARPA-funded program on single-crystal piezoelectrics, in which NRL scientists will have the primary task of mechanical testing, failure analysis, and fractography on the single-crystal piezoelectric materials, thus bringing the program back where it began some 30 years ago.

[Sponsored by DARPA]

REFERENCES

¹ S.W. Freiman, D.R. Mulville, and P.W. Mast, "Crack Propagation Studies in Brittle Materials," NRL Report 7575 (July 1973) and *J. Mater. Sci.* **8**(11), 1527 (1973).

² R.W. Rice, "Fractographic Identification of Strength-Controlling Flaws and Microstructure," in *Fracture Mechanics of Ceramics 1*, R.C. Bradt et al., ed. (Plenum Press, NY, 1974), p. 323.

³ R.C. Pohanka, R.W. Rice, J. Pasternak, P.L. Smith and B. Walker, "Strength and Fracture of Navy Type I Sonar Ceramics," in *Proceedings of the Workshop on Sonar Transducer Materials*, Naval Research Laboratory, Washington, D.C., Nov. 13-14, 1976, p. 203.

⁴ J.R. Spann et al., "Development of Textured Antimony Sulfoiodide," *J. Mater. Sci.* **16**, 2819-30 (1981).

⁵ M. Kahn and B. Kriese, "Patterned Microvoids for Dielectric Constant Control of High Frequency Circuit Substrates," *MRS Symp. Proc.* **72**, 35-40 (1986).

⁶ M. Kahn and C. Scott, "Patterned Void for the Reduction of the Dielectric Constant of Microstrip Transmission Lines," *Adv. Ceram.* **26**, 447-54 (1989).

⁷ C.C.M. Wu et al., "Piezoelectric Ceramics with Functional Gradients: A New Application in Material Design," *J. Am. Ceram. Soc.* **79**(3), 809-12 (1996); also U.S. Patent No. 5,502,345 (1996).

⁸ C. Kim, K.M. Rittenmyer, and M. Kahn, "1-1-3 Piezocomposite for Hydrophone Transducer," *Ferroelect.* **156**, 19-24 (1994).

⁹ T. Kim and M. Kahn, "Transducers with Improved Signal Transfer," U.S. Patent No. 5,376,859 (1994).

¹⁰ M. Kahn and C. Kim, "Transducers and Method for Making Same," U.S. Patent No. 5,325,011 (1994)

¹¹ A. Glazounov, Q. M. Zhang, and C. Kim, "Piezoelectric Actuator Generating Torsional Displacement from Piezoelectric d15 Shear Response," *Appl. Phys. Ltrs.* **72**(20), 2526-8, 1998.

¹² A. Glazounov, Q.M. Zhang and C. Kim, "A New Torsional Actuator Based on Shear Piezoelectric Response," *Proc. SPIE*, **3324**, 82-91 (1998).

¹³ C.C.M. Wu et al., "Continuous Poling of PZT Bars," *Ceram. Trans.* **90**, 21-31 (1998). ★

THE AUTHORS



DAVID LEWIS III is currently head of the Active and Passive Materials and Devices Section of the Multifunctional Materials Branch in the Materials Science and Technology Division of NRL. He earned a B.S. degree in mechanical engineering and M.S. and Ph.D. degrees in mechanics at the Illinois Institute of Technology before joining the New York State College of Ceramics in 1968. After teaching at the College of Ceramics for 10 years, Dr. Lewis joined NRL in 1979 as a research engineer in the Ceramics Branch, where he became branch head in 1984. After several subsequent reorganizations, essentially the same group that comprised the Ceramics Branch now makes up the Active and Passive Materials and Devices Section, headed by Dr. Lewis. In this period, Dr. Lewis also served for one year as a Scientific Officer for the National Science Foundation, and worked for one year in the Office of Strategic Planning at NRL. Dr. Lewis has worked in the area of functional ceramics for more than 20 years, as well as in many other areas of ceramic materials research. He is a fellow of the American Ceramic Society and has well over 100 papers published in various areas of ceramic science and engineering.



CHULHO KIM joined the Naval Research Laboratory's Materials Science and Technology Division following graduation from the Rensselaer Polytechnic Institute with a Ph.D. degree in materials engineering in 1976. He earned B.S. and M.S. degrees in physics from Korea University in 1963 and 1965, joining Han Nam University in the Physics Department where he taught for 7 years. Dr. Kim has worked more than 20 years in the Materials Science and Technology Division of NRL as a materials research engineer in various R&D programs including functional ceramic devices and transducers, metallic multilayers, and metal matrix composites. He holds 7 U.S. patents and has published more than 100 papers. Recently, Dr. Kim participated in the ONR Transduction Materials Program (1992-1994) as the principal investigator of the 1-1-3 piezocomposite transducer effort and in the DARPA Smart Materials Program as the principal investigator of the Composite Piezoelectric Assemblies for Torsional Actuators project (1996-1998).



CARL C.M. WU received a B.S. degree in mechanical engineering from the National Taiwan University in Taipei and M.S. and Ph.D. degrees in materials science from Brown University in Providence, Rhode Island. After working as a postdoctoral fellow and later a visiting assistant professor at the University of Maryland, he joined the Naval Research Laboratory as a ceramic engineer in the Ceramics Branch. At NRL, for more than 10 years, his research has concentrated on structural ceramics and studies of fracture processes, fracture toughness, fatigue, failure analysis, and tribology. Currently, his research concentrates on the development and characterization of load-bearing functional materials, especially in the processing and evaluation of novel actuator designs. He is also currently a part-time program officer in the Office of Naval Research. He has made more than 70 presentations and authored and co-authored more than 70 technical papers, including a patent on unitary transducers.



TODD L. JESSEN received a B.S. degree in ceramic engineering in 1982 from Alfred University, an M.S. degree in ceramic science in 1987 from Penn State University, and a Ph.D. in ceramic science in 1995 from Rutgers University. From 1982 to 1984 he worked as a process engineer at MuRata Manufacturing Co. in State College, Pennsylvania, on production of ceramic multilayer capacitors. In 1987 he joined NRL as a member of the Ceramics Branch and is currently a member of the Multifunctional Materials Branch. Dr. Jessen's primary research interests are in the areas of structural ceramic composites and piezoelectric materials and devices. Dr. Jessen has published more than 50 refereed papers and authored 6 patents. He has won the annual best paper award from the Engineering Ceramics Division of The American Ceramic Society in both 1995 and 1997 for his work on composites.



MANFRED KAHN joined NRL as head of the Electronic Ceramics Section in the Ceramics Branch, after extensive experience as a research, development, and process engineer with AVX Ceramics and Sprague on high voltage and multilayer ceramic capacitors and semiconducting and thermally switched ceramic devices. Dr. Kahn was the first to recognize and document the importance of grain core-shell structure in doped dielectric ceramics, allowing rational design of these materials. He has published more than 50 technical papers and has over 50 patents issued concerning electronic ceramic materials and devices, including new piezoelectric actuator configurations. Dr. Kahn retired from NRL in 1997, and is now employed on functional ceramics research programs by Potomac Research International. Dr. Kahn has a B.S.E.E. degree from the University of Wisconsin, M.S.E.E. degree from Rensselaer Polytechnic Institute, and a Ph.D. in ceramic science from Penn State University.



MARK T. CHASE received a B.S. degree in mechanical engineering from the University of Maryland in 1980, and has worked on various engineering contracts at NRL since that time. His previous projects have included instrumentation and software for satellites, water purification, and SDIO survivability and vulnerability studies, among others. Since 1986, Mr. Chase has worked in the area of functional ceramics and devices at NRL on projects including: the 0-3 composite transducers, high T_c superconductor processing, pulse power switching, ordered void hydrophones, Piezogran™ transducers, torsional and telescoping high-authority actuators, characterization of PEBB capacitors, and characterization of single-crystal piezoelectric materials. Mr. Chase has published approximately 20 papers and is a co-inventor on 6 patents.



***Vorticity Remnants of the Interaction
of a Shock and a Curved Flame***

*Science-as-Art contest – Third Place winner
Submitted by: Elaine Oran and Alexei Khokhlov*

When a weak shock interacts with a curved flame, the flame is greatly distorted. The mechanism for this distortion is called the Richtmyer-Meshkov instability, which, more generally, is the result of the interaction of a pressure impulse and a density discontinuity. One result of this interaction is that vortical motions are generated, and these motions continue to evolve even when the shock is long gone. The interaction increases the surface area of the flame, and so increases the energy release rate. Subsequent interaction of shocks with the distorted flame produce a turbulent flame called a deflagration.

This graphic, showing the vorticity generated at a time after the shock-flame interaction, was obtained by solving the unsteady, reactive Navier-Stokes equations. The flame is propagating in a mixture of acetylene and air. The background color (here purple) is a region of no vorticity. The colors indicate changes in the magnitude of the vorticity.

- 71 A Search Algorithm for Resonance Anomalies (SARA)
S.A. Chin-Bing, D.B. King, R.A. Zingarelli, and A. Warn Varnas
- 72 Sound Propagation Through a Sand-Water Interface
H.J. Simpson and B.H. Houston
- 75 Estimation of Seabed Properties from Chirp Sonar Data
A. Turgut, S.N. Wolf, and M. Orr

A Search Algorithm for Resonance Anomalies (SARA)

S.A. Chin-Bing, D.B. King, and R.A. Zingarelli
Acoustics Division

A. Warn Varnas
Oceanography Division

Introduction: Radiation from the Sun penetrates the ocean surface and warms the near-surface waters to a depth of several meters. Below this depth, the water temperature is considerably cooler. The boundary separating the warmer near-surface water from the cooler deeper water is called the *thermocline*. In summer, the thermocline is well-defined and separates water masses that differ in temperature by several degrees. Since temperature affects the speed of sound in water, the water mass above the thermocline can have a significantly higher sound speed than the water mass below the thermocline. In many shallow-water, coastal, and littoral regions, the tidal action creates *internal waves* that move the ocean water masses over the rough, irregularly shaped seafloor. Water masses that flow over large seafloor protrusions undergo an upward-downward flow pattern. This flow pattern results in a sinusoidal ripple effect in the thermocline and in the related sound speed structure of the water mass (Fig. 1). This “ripple” is concentrated in a relatively small area (in the direction of the thermocline, 1 to 2 km in range; in the vertical, a height at least twice the distance from the thermocline to the sea surface; and in the cross-range direction, a length of several hundred meters). The well-defined ripple travels along the thermocline, unchanged in form, for hundreds to thousands of kilometers. These properties (large amplitude, solitary) are characteristic of a *soliton* wave

packet; hence, these shoreward traveling ripples are called *shallow-water solitons*. Conceptual insight into this effect can be obtained by attaching one end of a rope to a wall and holding the other end taut. The horizontal rope represents the thermocline. If the hand-held end of the rope is given a sudden upward-downward jerk, a ripple will travel along the rope toward the fixed end. This is analogous to the shallow-water soliton traveling along the thermocline.

Acoustic Effects of Solitons: A series of ocean acoustic experiments was performed in the Yellow Sea by researchers from the People’s Republic of China.¹ Data collected during the summer showed unexpected losses in the received acoustic signals. These “anomalous” losses were on the order of 10 to 20 dB and occurred over a fairly narrow frequency band. The Chinese researchers developed the hypothesis that large amplitude, solitary internal waves (solitons) traveling along the thermocline had interacted with the underwater acoustic signals, resulting in acoustic mode coupling and large losses in signal. Since the phenomenon occurred around a specific frequency, it was labeled by the researchers as a resonance effect. No environmental oceanographic data were taken to support the soliton resonance hypothesis.

Since this seminal paper was published, a number of researchers have used computer simulations to produce similar effects and to identify the dominant physical mechanisms that govern the anomalous signal losses caused by solitons. First, the underwater acoustic signals that interact with the shallow-water soliton packet must undergo acoustic mode conversions. These mode conversions only occur at specific acoustic frequencies (“resonance” frequencies). Next, the acoustic mode conversions must be such that strong coupling exists between the

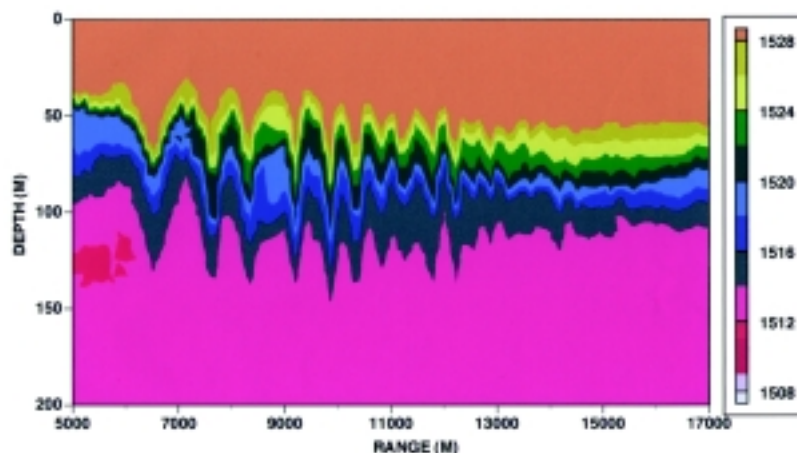


FIGURE 1
Contour plot showing the sound field for a soliton packet traveling near the Straits of Messina. The color scale is given on the right side in units of meters per second.

lower-order (waterborne) propagation modes and the higher-order, higher-loss (bottom interacting) modes. If the higher-order acoustic modes do not have significantly higher bottom attenuation than do the lower-order modes, the mode conversion will not produce the large signal losses. Finally, the range between the soliton packet (where the mode conversions occur) and the hydrophones (where the signals are measured) must be large. This long distance produces the large signal losses because the attenuated modes are continually losing energy along the entire distance.

Computer simulations have also been used to explain the “resonance” frequency phenomena. When one of the dominant spectral wave numbers, K_{sol} , of the soliton packet is approximately equal to the difference between the wave numbers of two acoustic modes, mode coupling can occur. The controlling relation can be expressed as $K_{sol} = k_n - k_m$, where k_m and k_n are the acoustic wave numbers of the m th and n th modes, respectively. Thus, when the wave number difference between two acoustic modes is approximately equal to a spectral component of the soliton packet, a transition of energy from one mode to another is possible. If significant acoustic energy is propagating in the m th mode, and the converted n th mode has a higher attenuation, then a large anomalous loss can occur.

The SARA Algorithm: From this knowledge we have developed a search algorithm for resonance anomalies (SARA) to predict resonance frequencies of shallow-water soliton packets. The SARA algorithm is based on the relationship between the spectral components of a soliton packet and the mode wave numbers. To demonstrate the SARA algorithm, we shifted our area of interest from the Yellow Sea to the Straits of Messina. While solitons are found in most of the world’s seas, many of these locations, such as the east coast of the U.S., have geometry such that multiple soliton packet interactions occur, thus complicating the analysis. In a strait, however, it is possible to get a single train of solitons. This makes the analysis process more straightforward and unambiguous.

Application: Oceanographic soliton data from an experiment performed in the Straits of Messina were obtained from the NATO SACLANT Research Centre. Using single-frequency acoustic model runs, a resonance frequency was found at 200 Hz. The SARA algorithm was applied to the same Straits of Messina oceanographic data: First, the SARA algorithm performed a spatial decomposition of the sound

speed field. The Straits of Messina data had three significant horizontal wave numbers. The SARA algorithm then calculated the acoustic wave numbers (k_n , k_m) for a series of frequencies and compared possible acoustic mode conversions with the soliton packet wave numbers (K_{sol}). At 200 Hz, a series of wave number differences ($k_n - k_m$) was found that fit the coupling equation. This prediction matched the result found by doing hundreds of single-frequency model runs.

Summary: The SARA algorithm, when applied to a soliton wave packet, can predict the existence and the frequency of soliton packet resonances. It requires far fewer calculations than do conventional systematic approaches, which require hundreds of acoustic model runs in order to determine the resonance frequency. The SARA algorithm is one of only a few models that can predict an acoustic response to a complex oceanographic event without using a full application of an acoustic propagation model.

[Sponsored by ONR]

References

- ¹J.X. Zhou, X.Z. Zhang, and P.H. Rogers, “Resonant Interaction of Sound Waves with Internal Solitons in the Coastal Zone,” *J. Acoust. Soc. Am.* **90**, 2042-2054 (1991). ★

Sound Propagation Through a Sand-Water Interface

H.J. Simpson and B.H. Houston
Acoustics Division

Introduction: The Naval Research Laboratory is using its world-renowned acoustics laboratories in advanced studies of acoustic scattering from underwater mines. Of particular interest are so-called “bottom mines” that are physically positioned on the surface of the seabed and are at times partially or fully buried. This research has led to the discovery of structural acoustics clues that may ultimately allow enhanced identification at longer ranges than are presently attainable with existing high-frequency, narrowband techniques.

A critical element of this work is developing an understanding of how broadband sound interacts with the ocean bottom. Towards this end, NRL has carried out a series of carefully controlled laboratory experiments specifically designed to quantify the broadband acoustic scattering and penetration as a function of interface topology and bottom type.¹ The

quality and environmental control associated with these experiments are unprecedented, providing to the community for the first time experimental results that have played a central role in resolving a controversy over “bottom penetration” of acoustic energy at shallow grazing angles below the critical angle discussed below.

In measurements carried out by other researchers, energy has been observed propagating into the bottom for ensonification angles below the critical angle. Controversy in the community over the physics associated with this involves two hypotheses: the first is that a slow (1200 m/s) compressional wave² predicted by Biot’s theory is supported in the sediment, and the second is that scattering from interface roughness³ leads to enhanced penetration. The Shallow Water Acoustics Laboratory at NRL is a unique environment that provides long-term environmental stability and that uses robotically scanned sources and receivers to resolve such issues. In addition, the Laboratory has unique apparatus that allows control of the bottom interface topology. The bottom can be smoothed to ~0.3 mm of rms roughness or roughened to any other value. The long-term stability of the Laboratory facilitates the use of new synthetic buried-array measurement techniques that provide a direct measurement of acoustic energy propagating in the bottom. These techniques include the use of time-domain (Fig. 2), frequency-spatial (Fig. 3), wavenumber-frequency, and two-dimensional wavenumber analyses.

Measurements: For each interface topology condition (smooth and rough), identical two-dimensional synthetic buried array measurements were conducted. These two-dimensional measurements were made using a single source and a single receiver, each attached to separate robotic scanners that positioned the transducers with 12.5 μm accuracy. Use of a single receiver eliminated many problems associated with burying a real array of receivers, including reverberation (scattering from one receiver to another receiver) and the need to manufacture and calibrate thousands of receivers that would be necessary to duplicate this synthetic array. The measurements begin with the receiver buried 90 cm below the sand-water interface and with the source directly over the receiver, 50 cm above the interface. The source was then moved horizontally, in increments of 1.5 cm, until it was 3.3 m from its start position. Upon completion of this linear scan, the source was moved back to its start position, the receiver was pulled up through the sand 1.5 cm using a vertical robotics scanner, and a subsequent scan of the source was made. At each of the source/receiver locations, an ensemble of 100 impulsive (i.e., broadband) acoustic responses was collected. Using this repetitive scanning process, 13,260 measurement points mapped out the wavefield propagating through the water-saturated sandy bottom. For the first measurement, the bottom interface was smoothed to ~0.3 mm rms, and for the second measurement, the bottom interface was roughened to ~10 mm rms.

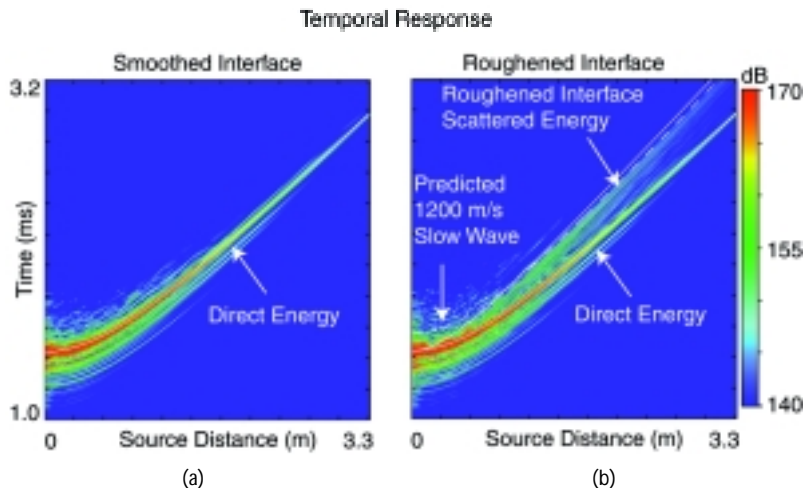


FIGURE 2
 The temporal response for a receiver at 50 cm below the water-sand interface as the source is moved from directly above the receiver to 3.3 m away for a smoothed (a) and a roughened (b) interface. The time delay for the direct compressional wave ray path is shown by the solid white line and is called Direct Energy. The dashed overlay indicates the time delay for a ray path assuming a 1200 m/s compressional wave in the sandy bottom. The other solid line (b) is the time delay associated with scattering from a roughened interface directly over the receiver.

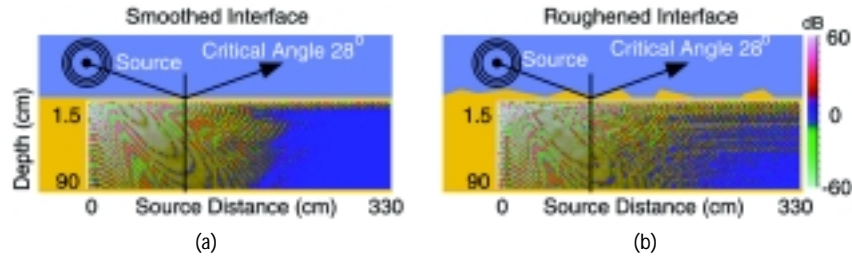


FIGURE 3 The 80 kHz frequency response of all 13,260 measurement points for a smoothed (a) and a roughened (b) interface. The log base 10 of the real part of the pressure is shown where the positive values are the top-reddish color scale and the negative values are the bottom-greenish color scale. The critical angle of 28° for this sandy bottom is indicated.

Analysis: Four analysis techniques are employed to examine the waves propagating in the sandy bottom: time-domain analysis, in which refractive ray models are used to identify the time delay associated with different paths into and through the bottom (Fig. 2); frequency-spatial analysis, in which the wavefronts propagating through the bottom are studied for each frequency bin (Fig. 3); wavenumber-frequency analysis, in which the phase and group velocities of waves traveling through the bottom are obtained; and two-dimensional wavenumber analysis, in which the phase velocity is studied for all propagation directions. The results of the analyses for the smoothed and roughened interface measurements are then compared and contrasted.

Figure 2 compares the smoothed and roughened interface measurements for the receiver buried 50 cm into the bottom and the source scanned from directly above to 3.3 m horizontally away (this scanned line of measurement points is extracted from the overall two-dimensional measurement described above). In Fig. 2(b), time-domain predictions are overlaid to show the time delays associated with three ray paths. The first ray path, designated as “Direct Energy,” assumes a water wavespeed of 1482 m/s, a bottom wavespeed of 1680 m/s, and a path assuming simple refraction at the interface. The next ray path, designated “Roughened Interface Scattered Energy,” assumes a ray path through the water column from the source to directly above the receiver. The sound is scattered from the roughened interface straight down into the bottom, with a wavespeed of 1680 m/s. The final ray path, shown by the dashed line and designated “Predicted 1200 m/s Slow Wave,” assumes simple refraction at the interface and a slower (1200 m/s) wavespeed in the bottom. For the smoothed interface, we observe no later time arrivals, thus there is only a 1680 m/s compressional wave propagating through the bottom and no slower compressional wave, as suggested in the literature.²

However, for the roughened interface, later time arrivals are seen clearly for the shallower ensonification angles. Near normal incidence, for the roughened interface, there are no later time arrivals, but as the source is moved away from the receiver, the later time arrivals track very well with the temporal response predicted for scattering from a roughened interface. We conclude from this that the roughened interface gives rise to a “virtual” slow wave, and that the bottom does not support a wave slower than the fast compressional wave at 1680 m/s.

Figure 3 compares the smoothed and roughened interface measurements using frequency-spatial analysis for 80 kHz, where all 13,260 measurement points are shown. For the wavespeeds of 1482 m/s in the water and 1680 m/s in the bottom, the critical angle is $\sim 28^\circ$ measured up from the interface. At 80 kHz, the direct fast compressional wave attenuates within ~ 1.5 m to ~ 2.0 m horizontally from the source; for ensonification angles below the critical angle, the smoothed interface exhibits a region a few centimeters below the interface and between 2.0 m and 3.3 m from the source where no energy propagates. However, with the interface roughened, measurements revealed a substantial increase in the energy penetrating into the bottom for this subcritical angle region (Fig. 3(b)).

Conclusions: The Shallow Water Acoustic Laboratory provides a unique environment in which sound propagation measurements using new synthetic array techniques can be conducted. These studies have unambiguously determined that the acoustic energy penetrating into the sandy bottom, which has been observed by others for subcritical ensonifications, is a result of scattering from interface roughness. Further, there is no evidence of a slower compressional wave, a “slow Biot wave.” These results greatly impact the design of sandy bottom theoretical models and demonstrate the importance of interface rough-

ness as a mechanism for increasing energy penetration into the bottom for subcritical ensonification angles.

[Sponsored by ONR]

References

- ¹H.J. Simpson, "Synthetic Array Measurements of Acoustical Waves Propagating into a Water-Saturated Sandy Bottom for a Smoothed and a Roughened Interface," *J. Acoust. Soc. Am.*, accepted for publication (1998).
- ²N.P. Chotiros, "Biot Model of Sound Propagation in Water-saturated Sand," *J. Acoust. Soc. Am.* **97**(1), 199-214 (1995).
- ³E.I. Thorsos, D.R. Jackson, J.E. Moe, and K.L. Williams, "Modeling of Subcritical Penetration into Sediments Due to Interface Roughness," in *High Frequency Acoustics in Shallow Water*, SAACLANTCEN Conference Proceedings Series CP-45, N.G. Pace et al., eds., June 30 to July 4, 1997, Lerici, Italy, NATO SAACLANT Undersea Research Centre, pp. 563-570. ★

Estimation of Seabed Properties from Chirp Sonar Data

A. Turgut, S.N. Wolf, and M. Orr
Acoustics Division

System Overview: Real-time estimation of seabed physical properties from chirp sonar signals is now possible due to recent developments in sonar systems, interactive data acquisition techniques, and new inversion algorithms. A typical chirp sonar system uses a broadband, high-power, and repeatable acoustic pulse, which is essential for the accurate estimation of seabed density, compressional speed, attenuation, and other physical parameters such as porosity, shear modulus, and permeability. The capability of interactive data acquisition techniques provides optimum signal transmission as well as high-quality data collection. A newly developed inversion algorithm uses high-quality chirp sonar data to estimate the sediment properties as a function of depth within the seabed.¹ Performance of the inversion algorithm has been tested numerically under noisy conditions for marine sediments ranging from mud to coarse sand, and experimentally against the sediment core data. Accurate and stable results have been obtained in both cases.²

The acoustical and mechanical properties of the seabed are required for accurate prediction of sonar performance and mine burial in the continental shelf waters adjacent to land masses. In many of the areas considered to be sites of future Navy operations, little is known of the bottom composition, particularly at depths more than a meter into the bottom. The real-time capability of remotely estimating seabed physi-

cal properties is especially important for Navy vessels operating in forward areas over previously unsurveyed bottoms. Commercial applications of this technique include surveys of bottom mechanical strength prior to cable- or pipe-laying and offshore construction. Other uses are related to selecting sites for disposal of wastes and storage of petroleum, decisions for which fluid permeability within the bottom is an important factor.

One-Dimensional Inverse Problem: Whether one is trying to map the bottom composition or to "hear the shape of a drum" from its acoustic signature, underlying concepts of the inverse problems are the same. First, a proper mathematical model is needed to capture the physics of the forward (direct) problem. Then, an inverse problem is posed to estimate the model parameters from available data. For a complete analysis, the issues of uniqueness and stability under noisy conditions should also be investigated. During the last three decades, an extensive amount of research has been done by the seismic community on the one-dimensional inversion methods to delineate Earth's interior. Several inversion methods were proposed based on the Goupillaud wave equation, inverse scattering for the Shroedinger equation, the Riccati equation, the Gopinath-Sondi integral equation, linear programming, and auto-regressive prediction. However, in inverting real data, most of these methods were reported to have little success for reasons such as sensitivity to additive noise and the requirement of a minimum phase source wavelet with infinite bandwidth. Based on a "poro-viscoelastic" seabed model, we recently developed a time-domain inversion algorithm that provides accurate and stable results for shallow subbottom applications. The inversion method's improvements over previous methods include: a) the use of an improved physical model that provides a physics-based (rather than heuristic) treatment of interaction of sound with fluid-filled porous materials; and b) the inclusion of viscous and anelastic absorption, pulse dispersion, and multiple reflections.

Procedure: First, envelope functions of the matched-filtered acoustic returns are calculated by taking the absolute values of the acoustic returns in the form of analytic signals. Then, instantaneous frequencies are calculated for a crude estimation of attenuation profile by comparing the center frequency shift in the acoustic return with that predicted by the poro-viscoelastic attenuation model. By assuming an average sound speed value (1500 m/s) in the water column, water depth is calculated from the delay time

between the transmission peak and the first return peak. Next, porosity, shear modulus, and permeability are estimated for the first sediment layer by using a global search algorithm within a model space constrained by semi-empirical relations among the model parameters. Random perturbations are applied to corresponding model parameters to minimize an objective function (quadratic deviation between the data and calculated synthetic seismogram for the first reflector). Acoustic parameters such as compressional speed and density are also calculated from the inverted model parameters by using the poro-viscoelastic theory. Then, the envelope peak of the next reflector is identified and first layer thickness is calculated using the inverted sound speed value for the first layer and the measured time lag between the first and second peaks. Again, the above procedure is used to estimate the second-layer parameters by minimizing the quadratic deviation between the amplitude of the second acoustic return and that predicted by the models. This procedure is repeated for successively deeper layers until the signal level drops below a predetermined threshold. For real-time inversions, we have also derived a simpler “fleet-oriented” sediment model from the poro-viscoelastic model. Both models provide almost the same acoustic response for a wide

frequency range and a variety of sediment types. However, inversions using the simpler sediment models are almost one order of magnitude faster.

Experimental Results: The chirp sonar system with the newly developed inversion software has been used during the SWARM-95 (Shallow Water Acoustics in Random Media) experiment in 1995. During the data collection, 2 to 5 kHz FM pulses were transmitted and received by an acoustic transducer/receiver mounted on the ship’s hull. A real-time correlation processing achieved a signal processing gain over the background noise and provided compressed matched-filter output (a processing gain of approximately two times the time-bandwidth product and a compressed pulse length equal to the inverse of the bandwidth of the transmitted pulse were obtained). Also, horizontal resolution of the system was improved by using piston-type acoustic transducers with low spatial sidelobes, thereby yielding a smaller footprint on the seafloor and reducing the effects of off-axis scatterer points. Figure 4 shows the experimental configuration and 3-D images of inverted compressional speed and density at the outer-New Jersey shelf area. Figure 5 shows the 2-D images of acoustic return and inverted compressional

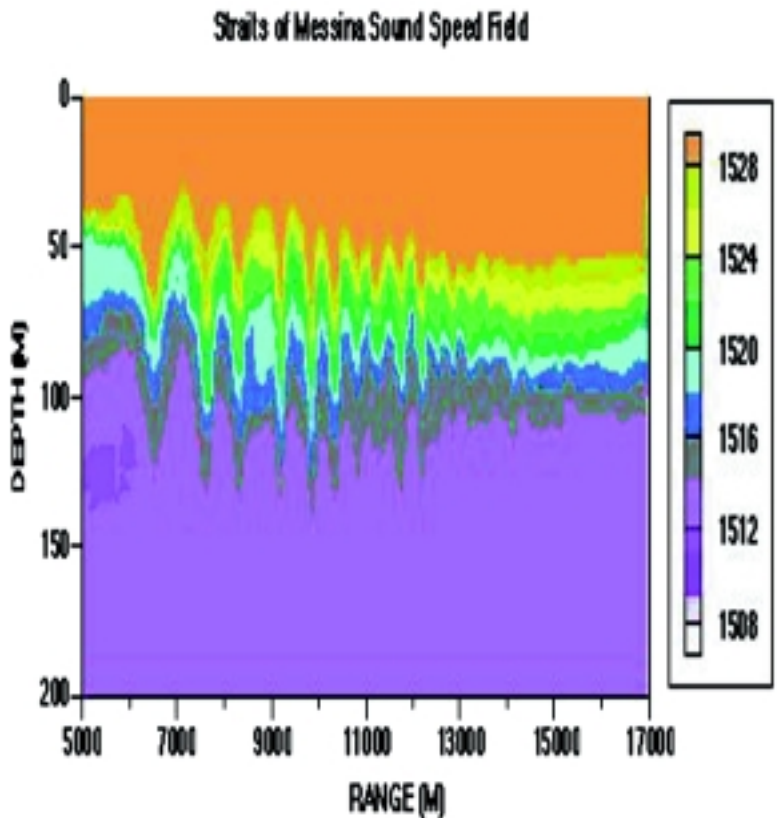


FIGURE 4
 Three-dimensional compressional speed and density structure of New Jersey shelf sediments inverted from data collected by a hull-mounted chirp sonar.

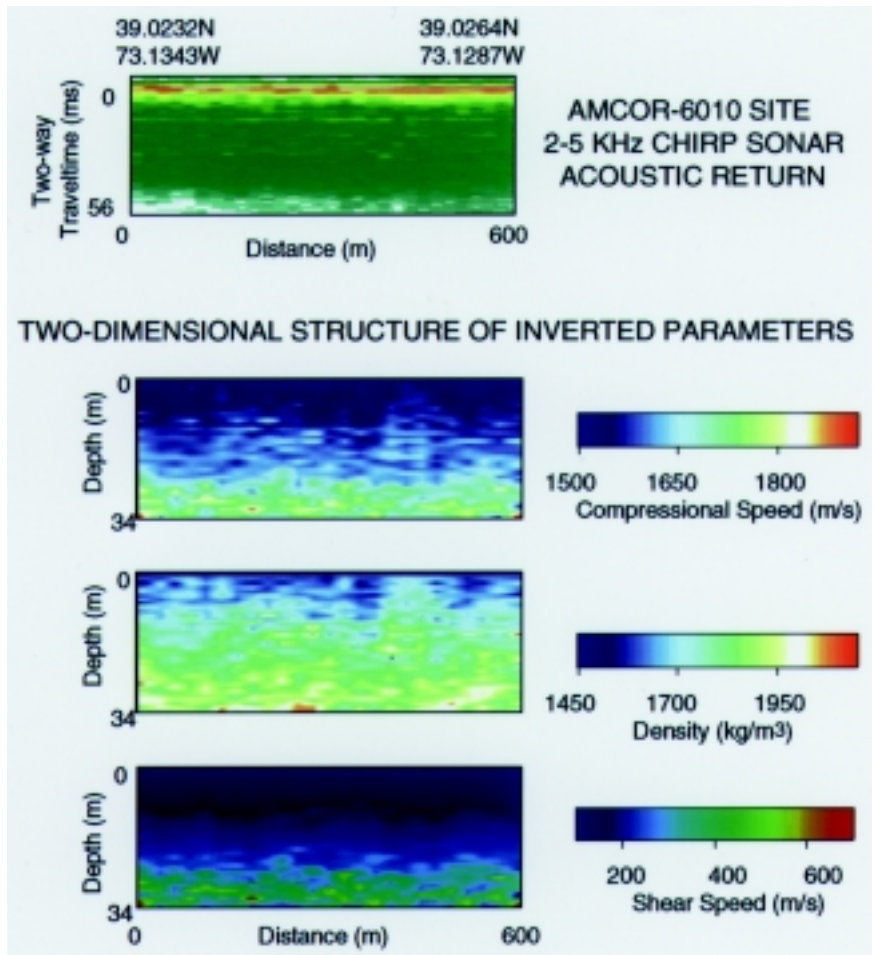


FIGURE 5 Two-dimensional subbottom images of acoustic reflectivity, compressional speed, density, and shear speed near the AMCOR-6010 site.

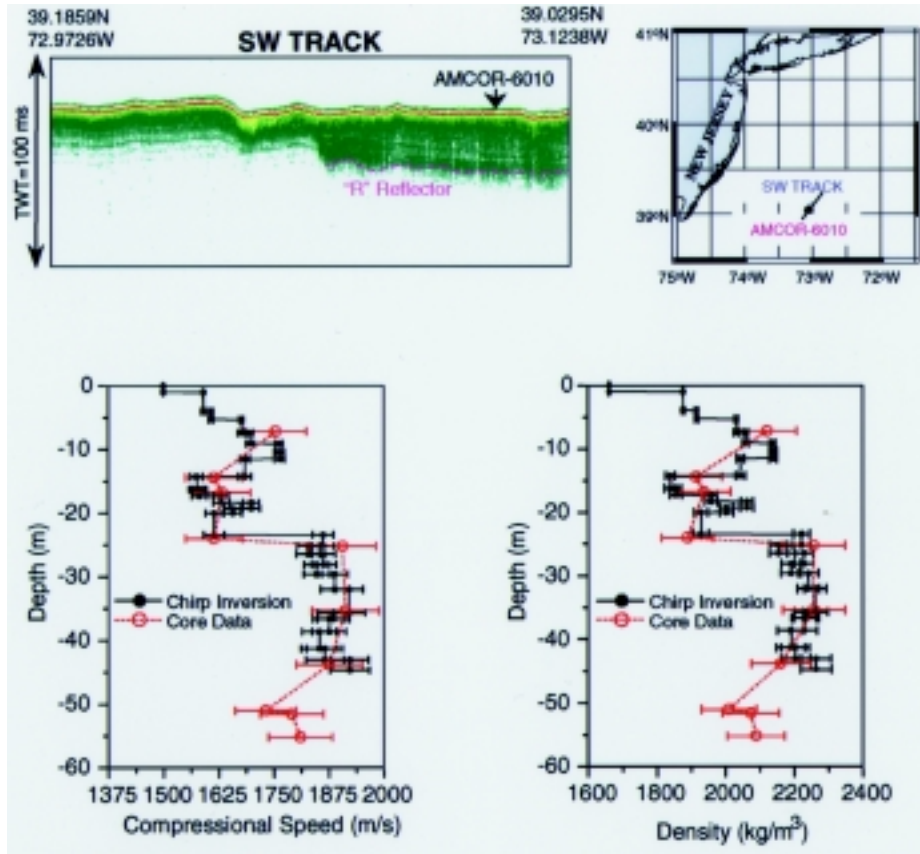


FIGURE 6
Comparison of inverted compressional speed and density profiles with those of “ground truth” core data at the AMCOR-6010 site.

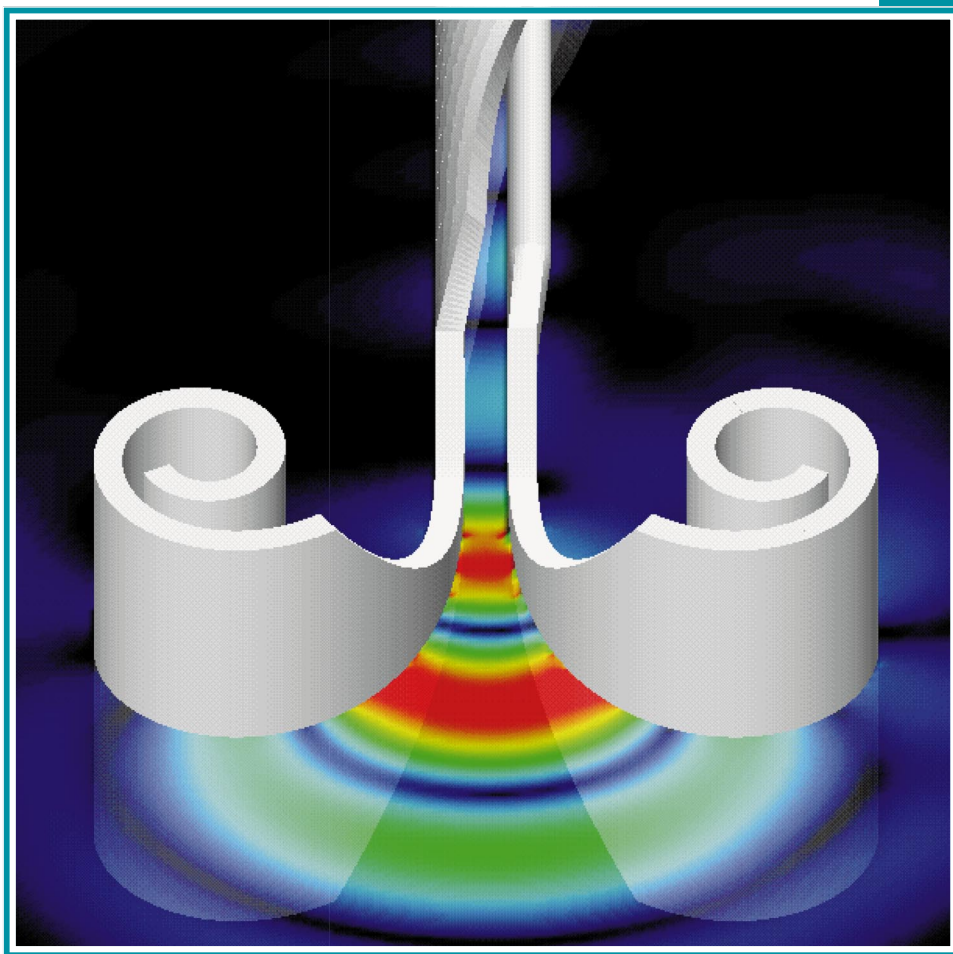
speed, density, and shear speed near the United States Geological Survey 1976 Atlantic Margin Coring Project, site number 6010 (AMCOR-6010). In the proof-of-concept testing, acoustic properties of the ocean bottom were compared with the sediment core measurements to depths up to 40 meters at the AMCOR-6010 site. Estimated compressional speed and density profiles fall within the bounds of an arbitrarily assumed $\pm 4\%$ core measurement error. Error bounds for the estimation are calculated by considering a correlation coefficient of 0.95 between porosity and shear modulus. In general, the agreement is satisfactory and both core measurements and chirp sonar inversions (Fig. 6) show an increase in compressional speed and density at the 22 m depth (R reflector), which was also confirmed by other geophysical surveys.

Summary: We have developed an accurate and stable inversion algorithm to estimate acoustical and mechanical properties of the seabed. Recent tests and analysis of SWARM-95 data indicate that our inversion results agree with the “ground-truth” sediment coring data. The agreements illustrate the feasibility of fast and accurate sediment classification in a survey mode. This capability is expected to have a significant impact on numerous Navy and commercial applications.

[Sponsored by ONR]

References

- ¹A. Turgut, U.S. Patent 5,815,465, “Method and Apparatus of Classifying Marine Sediment,” Sept. 29, 1998.
- ²A. Turgut and S. Wolf, “Determination of Seabed Statistical Properties and Their Effects on Acoustic Wave Propagation in Shallow Water,” *J. Acoust. Soc. Am.* **98**(5), Pt. 2, 2972 (1995). ★



Fields Radiated by a Cornu Flared Horn Antenna

Science-as-Art contest – Honorable Mention

Submitted by: Mark Kragalott

The Cornu flared horn antenna was designed to radiate or receive an ultrawideband electromagnetic pulse. The antenna is composed of coaxial line, a balun transition to parallel plates, and a flared horn whose profile is a scaled version of the mathematical curve known as Cornu's spiral. The Cornu spiral has the property of a linearly increasing curvature as a function of arc length. This property helps the pulse to detach from the horn with a minimum amount of reflection back down the coaxial line. In this variation, the horn is widened early along its length to facilitate the transfer of the pulse to the horn and then becomes constant in width to restrain its size. A patent application for the antenna design has been submitted by NRL. In the art work, the electric fields of the pulse are shown radiating from the Cornu flared horn in a plane through the center of the antenna.

- 81 Flight Test Data from the Sodium Sulfur Battery Cell Space Experiment
J.C. Garner
- 84 Structure/Property Relationships and Applications of Low Dielectric Cyanurate Resins
L.J. Buckley and A.W. Snow
- 86 New Materials for Heavy Metal Removal Applications
M. Pazirandeh and J.M. Mauro
- 87 Carbon Nanotubes: Experiments Catch Up with Theory
C.T. White and J.W. Mintmire

Flight Test Data from the Sodium Sulfur Battery Cell Space Experiment

J.C. Garner
Space Systems Development Department

Among the experiments in the cargo bay of the Space Shuttle Columbia as it roared off the launch pad at 2:46 p.m. on November 19, 1997, was a HitchHiker experiment. This experiment was designed to test a new rechargeable battery with three times the specific energy (Watt-hours/kg) of nickel hydrogen batteries. The experiment, the sodium sulfur battery cell experiment or NaSBE, was the last phase of a three-part U.S. Air Force Research Laboratory (AFRL) program called NaSTEC to qualify NaS battery cells for use in space by studying their performance in zero-gravity (G). After the experiments returned to Earth, the flight cells were compared to cells operated in the identical charge/discharge regime in gravity through X-ray and destructive physical analysis. Naval Center for Space Technology personnel designed, built, and tested the experiment under a 1994 Memorandum of Understanding (MOU) between NRL and AFRL. Eagle Picher Inc., of Joplin, Missouri, manufactured the cylindrical, 40 ampere-hour (Ah) NaS battery cells. The Shuttle Small Payloads Office at the NASA Goddard Space Flight Center (GSFC) provided the HitchHiker experiment interface and integration with the Shuttle Columbia.

Background: In fact, there is nothing new about NaS battery cells. They were first introduced in 1966 by the Ford Motor Company when researchers at Ford began to exploit the properties of beta alumina, a ceramic material that could be used as both a sodium ion conducting electrolyte and an electrochemical separator. NaS cell designs emerged that demonstrated specific energies of 150 Wh/kg. Ford was hoping that NaS cells would power their version of the electric car. Electric power companies in Great Britain and Japan began to use NaS cells for load-leveling applications. When the Air Force was studying how to power multi-megawatt SDIO spacecraft in the early 1980s, they needed a secondary battery with the very high specific energy of NaS. Thus for most of the 1980s, researchers at Ford, Hughes, Eagle Picher, and the Air Force Wright Aeronautical Laboratories strove to improve the durability of the beta alumina and to make the cell "fail safe." By 1991, the design was ready for the NaSTEC program. In 1993, personnel from the U.S. Air Force Phillips

Laboratory (now AFRL) visited NRL to ask the Naval Center for Space Technology (NCST) to design, build, and test a four-cell NaS space shuttle experiment. A MOU between NRL and AFRL was signed in 1994. In September 1995, Eagle Picher was awarded a contract to manufacture 30 NaS cells for the experiment. The experiment was ready to go in September 1996, but due to difficulties with an outside contractor, the experiment was manifested for a flight a year later. In May 1997, NaSBE was delivered to the NASA GSFC for final integration tests. By July, it was at the Kennedy Space Center for integration with the shuttle Columbia.

NaSBE Phase I - Heat Up To 350 °C: On STS-87 mission day 6, November 25, 1998, a command was sent from the NRL NaSBE ground equipment at the NASA GSFC Payload Operations Command and Control Center (POCC) to the experiment to begin the battery cell heat-up from their frozen state at 25 °C to the operational state of 350 °C. Almost 30 hours later, the average cell temperatures reached 350 °C. The cell voltages and temperatures during the heat-up are plotted in Fig. 1. Notice that as the temperature increases, the cell voltages increase as the sodium and sulfur change phase and the electrolyte resistance decreases.

NaSBE Phase II - Baseline Capacity Measurements: After the average cell temperatures had reached 350 °C, the first test of an NaS cell in space was initiated. A command was sent to put all four cells on-line and to turn on the 20 amp discharger for a duration of 120 minutes. All four cells discharged for the entire 120 minutes and delivered the name-plate capacity of 40 Ah. Next, the cells were charged at a C/10 = 4.0 amp rate for 10 hours. Following the charge, the cells were again discharged at the C/2 rate for 120 minutes with all four cells again producing 40 Ah. This time, the C/10 amp charge was repeated with an extra 7 minutes to see if the cells could be charged to the 2.35 volt cutoff. At 10 hours and 2 minutes, the voltage of cell #1 hit the 2.35 volt cutoff and was automatically switched off-line. At the end of the extra 7 minutes, the other three cells were still accepting charge. Figure 2 depicts the cell voltage performance over the Phase I capacity measurements.

The capacity measurements demonstrate a remarkable feature of NaS battery cells. Prior to the first -20 amp discharge, the cells had last been charged on April 9, 1997, during a thermal vacuum test at NRL. The cells were then allowed to cool down

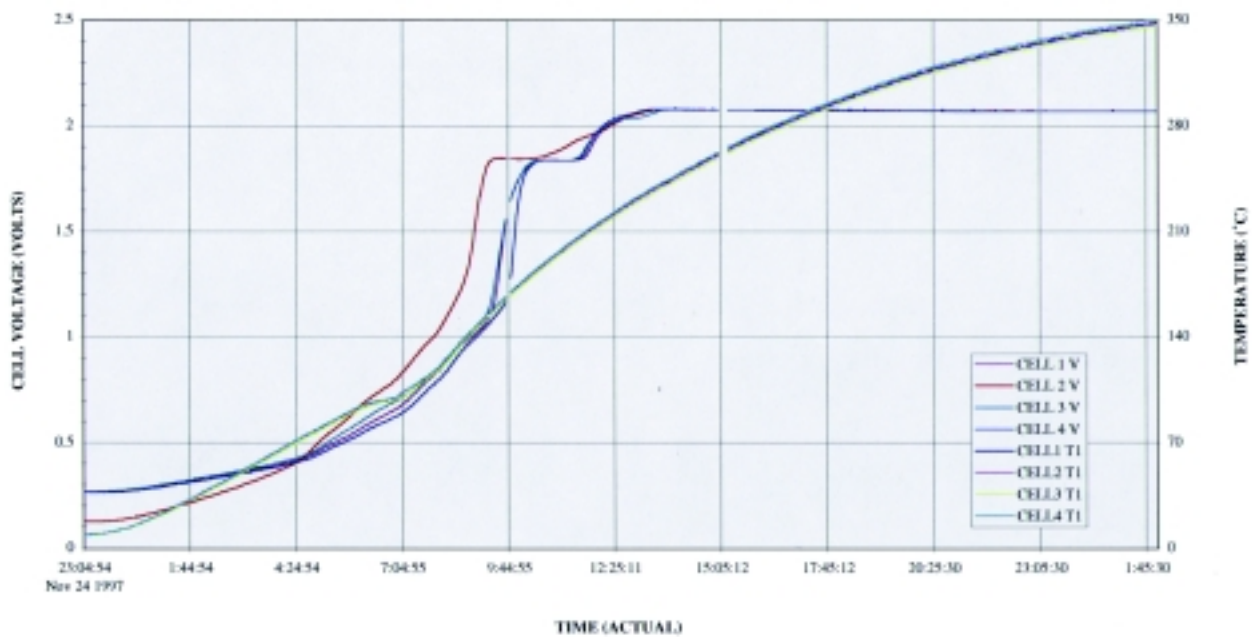


FIGURE 1
NaSBE Phase I cell voltages and temperatures.

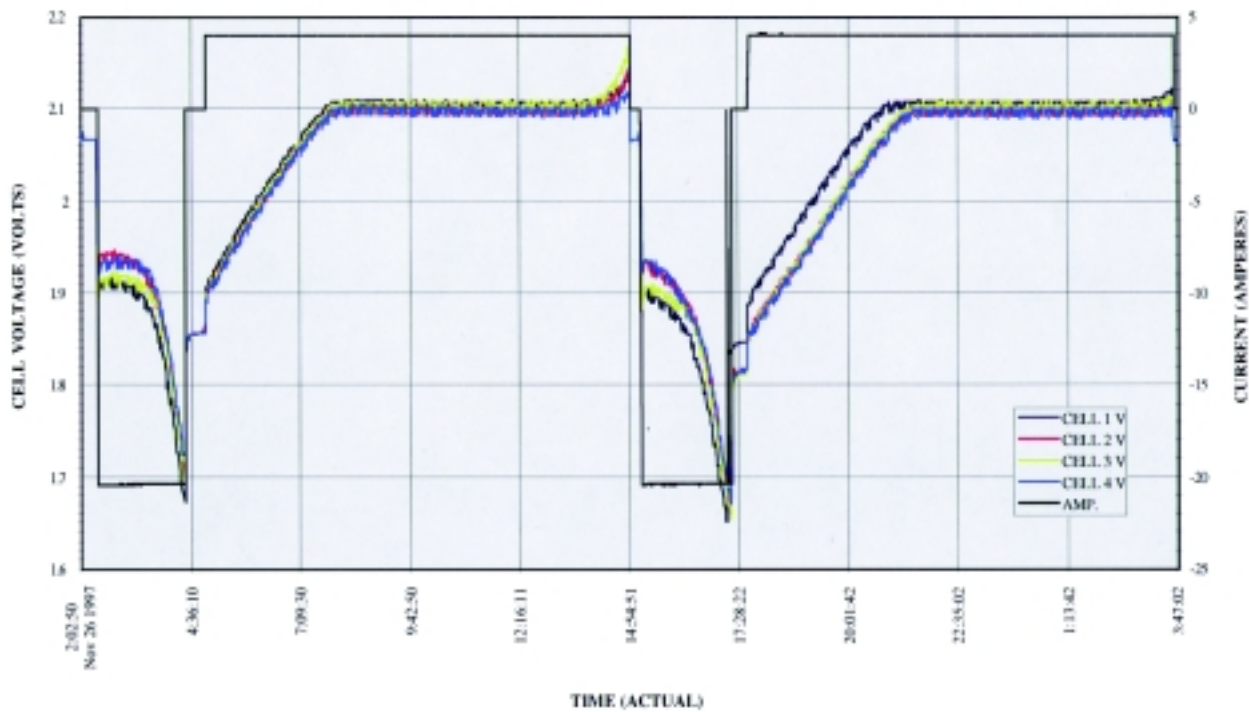


FIGURE 2
NaSBE Phase II cell voltages and temperatures.

and solidify, and then remained open circuit for 8 months (April - November). As the capacity measurements indicate, there was no open-circuit storage capacity loss over the 8-month period.

NaSBE Phase III - Simulated Geosynchronous Orbital Cycling: Phase III of the experiment consisted of cycling the battery cells at a 60% depth of discharge and quickly recharging them in a simulated geosynchronous Earth orbit (GEO) regime. The cells were discharged at 20 amps for 1.2 hours, recharged immediately at 2 amps for 12 hours, and then followed by an open-circuit stand for 10.8 hours. At the conclusion of the open-circuit stand, the sequence was repeated. The cells supported the GEO cycling without an anomaly. At the conclusion of the second open-circuit stand, the cells were ready for Phase IV.

NaSBE Phase IV - Simulated Low Earth Orbital Cycling: Phase IV of the experiment consisted of cycling the battery cells at a 40% depth of discharge and quickly recharging them in a simulated low Earth orbit (LEO) regime. The cells were discharged at -32 amps for 30 minutes and then recharged immediately at 16 amps for 60 minutes. To simulate one day's worth of cycling, 16 cycles were conducted by using a stored commanding feature included in the NaSBE Experiment Control Unit microprocessor's Embedded Command Language (ECL).

NaSBE Phase V - Final Discharge: The last test before the cells were cooled down on orbit was the final discharge of cells to different states of charge. Cell 1 was left on open circuit after the completion of the final LEO charge cycle. Cells 2, 3, and 4 were discharged at -32 amps to 80%, 60%, and 40% state of charge. As each cell completed its discharge, it was switched off-line and open-circuited. Figure 3 shows an STS-81 astronaut working over Nas BE in the shuttle bay after the completion of Phase V.

Postflight Operations: Mission STS-87 ended on the morning of December 5, 1997. Ten days later, NaSBE was removed from the cargo bay and by December 30 the experiment was returned safely to NRL. NRL technicians carefully removed the experiment from the HitchHiker canister and then opened the safety vessel to extract the NaS battery cells. The cells were clean, with no signs of stress from the operation at 350 °C. After being carefully packaged for shipment, the cells were sent to the Aerospace Corporation in El Segundo, California, for X-ray and de-



FIGURE 3
While NASA astronaut Winston Scott's experiments with some new space power tools, his image is reflected in the NRL NaSBE thermal radiator plate.

structive physical analysis (dpa). The analysis effort was a joint effort between AFRL and the NASA Lewis Research Center.

Preliminary DPA Results: The X-ray analysis shows some features in the sulfur electrode that differ between the flight and ground test cells. The distribution of voids was different between flight and ground test cells at both 100% and 40% state of charge (SOC). Also, the sodium polysulfide phases found at 40% SOC were not the same between the flight and ground test cells. No signs of sulfur leakage were found on any of the cells, nor were there any signs of cracking of the electrolyte in either the electrical or radiographic data.

Conclusions: Four 40 Ah NaS battery cells survived the launch environment of the Space Shuttle and were successfully heated to 350 °C. The cells were subjected to simulated orbital charge/discharge cycles in zero-G, and their electrical performance was comparable to that in gravity. DPA results show that the chemical composition of the sulfur electrodes in the flight cells were at least as uniform, if not more so, than the sulfur electrodes in the ground cells.

[Sponsored by USAFRL]



Structure/Property Relationships and Applications of Low Dielectric Cyanurate Resins

L.J. Buckley and A.W. Snow
Chemistry Division

Introduction: The chemical structure of cyanurate resins has evolved over the past 30 years to a state where many of the physical properties are determined by very subtle changes in the molecular structure. The processing characteristics, chemical versatility, and properties have qualified these resins for low dielectric applications such as microelectronic interconnects, radomes, and sonar domes. A review of the chemistry and structure-property relationships of cyanurate resins that are relevant to these low dielectric applications is presented with the many contributions of the NRL Chemistry Division included here. Aromatic cyanurate resins are compared to NRL-developed fluoroaliphatic cyanurates, with particular emphasis on physical structure/property relationships. The incorporation of polyfluoromethylene sequences into a network polymer offers the potential of generating a thermosetting resin with electrical properties that may approach those of polytetrafluoroethylene (PTFE; "Teflon") combined with facile thermoset processing. The properties of particular interest are the electric field permittivity, moisture resistance, thermal stability, and mechanical behavior. The thrust of the NRL effort has been to merge the facile processing characteristics of the cyanate thermoset system with the physical properties associated with perfluoromethylene sequences. Currently, this work has been transitioned to a radome application where an NRL-developed resin is being used for a quartz fiber composite in an electronic warfare component.

Aromatic Cyanurate Resins: The monomers of these thermoset resins are synthesized from any bisphenol compound by conversion of the phenolic (-OH) group to a cyanate (-OCN) group. The cyanate monomer melt is then thermally cured by a polycyclotrimerization reaction to yield a network structure of symmetrical triazine junctions (crosslinks) connected by aromatic segments. This structure is unique in that the permanent dipoles associated with it are quite small and that the molecular rigidity of the aromatic and triazine structures in this network confer a high glass transition temperature. These properties correlate with a low storage and loss of

electric field energy per frequency cycle and determine the utility of this class of resins in low dielectric applications mentioned above. As part of a 6.1 program in low dielectric polymers, the correlation of structural features of the polymer with the dielectric constant was quantitatively investigated. Figure 4 displays a correlation between the concentration of the triazine junction structure in the network with the dielectric constant. The upper curve and filled circles correspond to aromatic cyanate resins. The points connected by this curve are those corresponding to hydrocarbon segment in the resin. As this segment becomes longer and dilutes the triazine structure, the dielectric constant becomes lower. Polystyrene with a dielectric constant of 2.4 would represent a lower no-crosslinking limit. Those points lying off the curve show the effects of incorporating heteroatom (S, O, and F) containing structures in the segments. Sulfur and oxygen cause positive departures associated with dipolar structures. Fluorine causes a negative departure associated with the unique low polarizability of this atom.

Aliphatic Cyanurate Resins: Aliphatic hydrocarbon cyanate ester monomers are unstable compounds and will not form thermoset resins. The NRL Chemistry Division has recently shown that stable aliphatic fluoromethylene cyanate monomers can be synthesized and polymerized.¹ The fluoromethylene cyanurate resin system replaces the aromatic connecting groups with fluoromethylenes with the intent of further depressing the dielectric constant. Figure 4 shows this relationship to the aromatic structures and also shows the effect of fluoromethylene chain length. Polyethylene, with a dielectric constant of 2.3, would represent an infinite dilution of an aliphatic cyanurate with a hydrocarbon. Polytetrafluoroethylene, with a dielectric constant of 2.0, would represent an infinite dilution of an aliphatic cyanurate with a fluorocarbon. As seen in the figure, the F6 resin (6 fluoromethylenes) has as low a dielectric constant as the F8 and F10 compounds. This material was chosen for scale-up based on the dielectric constant and the ease of synthesis and processing when compared to the other fluoromethylene cyanurates. The synthesis, with an overall yield of 83.5%, is shown in Fig. 5. The F6 cyanurate resin has been synthesized in kilogram quantities and has been used with quartz fibers to form low dielectric composites.² With very low moisture absorption (0.3%) due to the fluoromethylene sequence, these materials show superior performance to the aromatic cyanurate resins that are commercially available.

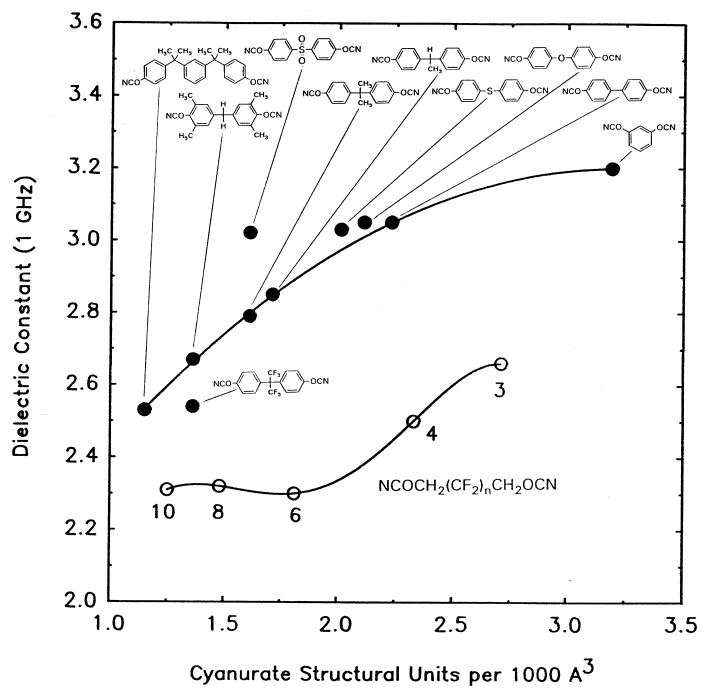


FIGURE 4
Dielectric constant vs concentration of cyanurate structural units.

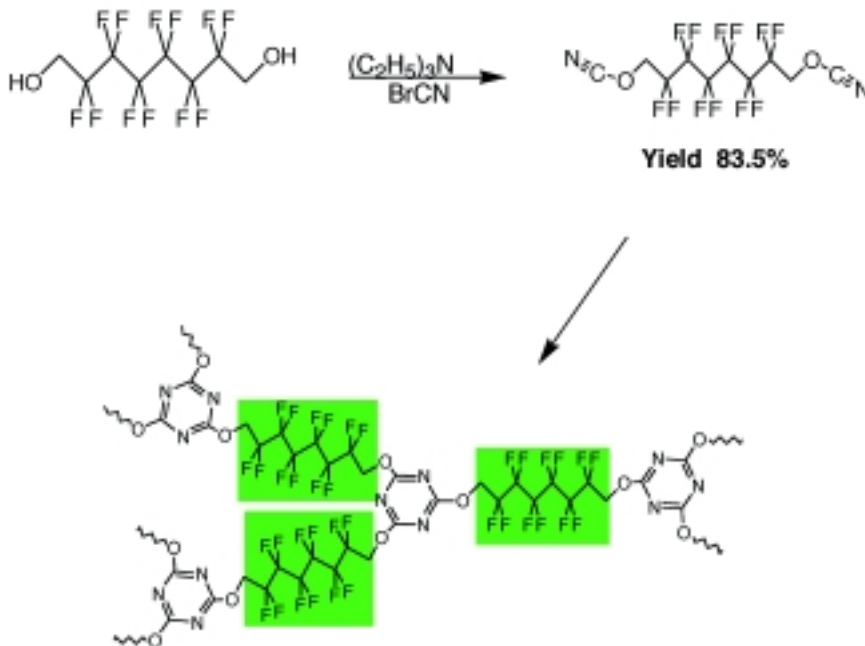


FIGURE 5
Synthesis of F6 cyanurate resin.

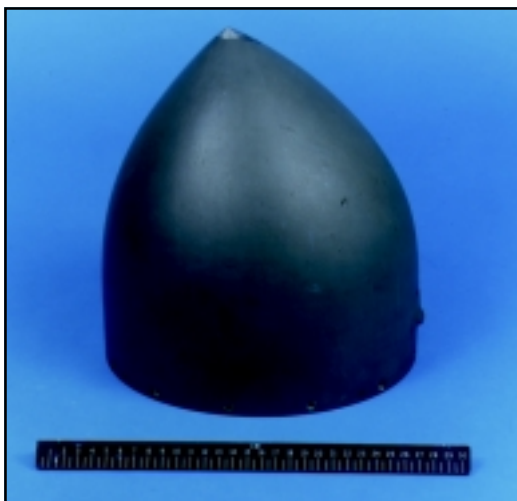


FIGURE 6
Radome for EA-6B electronic warfare pod.

Radome Application: The purpose of a radome is to protect the underlying electronics without seriously affecting the transmitted or received signal. Ideally, one would like to match the impedance of free space or air while providing mechanical and environmental protection. A low dielectric constant with low moisture absorption addresses these constraints. Figure 6 shows an ALQ-131 radome that is used on a pod for the EA-6B aircraft. In a joint effort with the Tactical Electronic Warfare Division, quartz composite sandwich structure will be fabricated using the same design as the ALQ-131 radome. The resin system will be the F6 fluoromethylene cyanurate. If successful, this system will be used to fabricate an advanced radome for the EA-6B pod.

[Sponsored by ONR]

References

¹A.W. Snow and L.J. Buckley, "Fluoromethylene Cyanate Ester Resins. Synthesis, Characterization, and Fluoromethylene Chain Length Effects," *Macromol.* **30**, 394-405 (1997).

²A.W. Snow, L.J. Buckley, and J.P. Armistead, "Fluoromethylene Cyanate Ester Resins," *Polym. Preprints* **39**, 788-789 (1998). ★

New Materials for Heavy Metal Removal Applications

M. Pazirandeh and J.M. Mauro
Center for BioMolecular Science and Engineering

Background: Current agricultural, industrial, and military operations generate large quantities of mixed

wastes containing heavy metals. Stricter environmental regulations and accelerated requirements for the remediation of contaminated sites make necessary the development of new approaches and technologies for heavy metal removal applications. Innovative methods for detoxifying waste waters require the system to be robust, cost-effective, and stable for long-term storage. Recent research in the area of heavy metal removal has focused on the development of materials with increased affinity, capacity, and selectivity for target metals. The potential for heavy metal removal by microorganisms and the use of genetic engineering to increase the efficiency of metal removal by bacterial cells is a promising technology for the development heavy metal biosorbents.^{1,2} NRL has recently developed and patented a bacterial-based technology for heavy metal removal applications.^{2,3}

Technical Concept: This approach is based the use of genetic engineering and recombinant DNA technology to design and produce peptides with high affinity and selectivity for target metals within bacterial cells. Subsequently, "biomass" is produced from these cells by the immobilization of nonviable cells or cell remnants containing the metal binding peptide within a suitable matrix. The derived product (Navsorb) may then be used for heavy metal removal applications (Fig. 7). During the initial phase of this research, a gene coding for the metallothionein from the organism *Neurospora crassa* was synthesized and expressed (produced) within *E. coli* bacterial cells. The *N. crassa* metallothionein is a small, cysteine-rich peptide with high affinity to metals such as cadmium. *E. coli* cells producing this peptide near the cell surface (NCP) were shown to efficiently and selectively remove heavy metals from simulated and actual heavy metal contaminated water samples (Fig. 8). The affinity and selectivity of the NCP for target metals was shown to be superior to that of several commercial ion exchange resins.²

Future Directions: Current efforts are focused on the large-scale and cost-effective production of heavy metal binding cells and methods for efficient immobilization of cells. Parameters being evaluated include metal binding under various flow rates, metal loading capacity, regeneration efficiency, and reusability of the biosorbent. We have also developed capabilities for bacterial production of polymeric and de-novo peptides designed for high affinity to a wide range of target compounds.⁴ Further improvements in the stability and utility of the Navsorb biosorbent is being investigated through the incorporation of amino acid sequences that are known to stabilize proteins

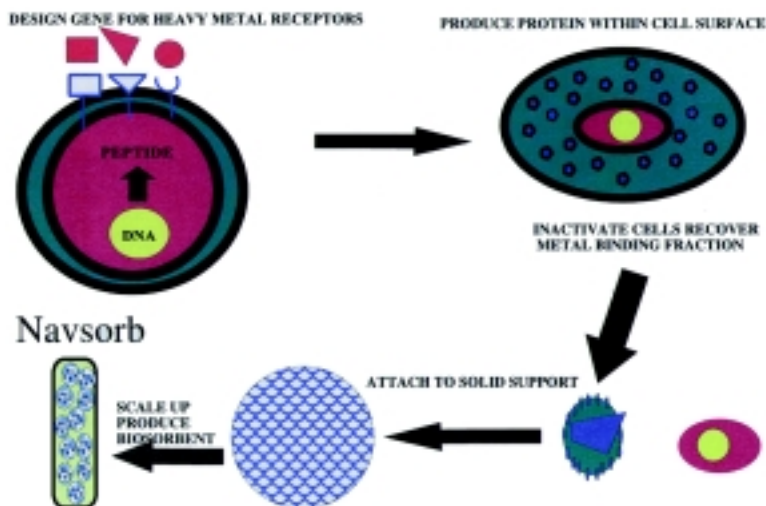


FIGURE 7
Navsorb heavy metal polisher.

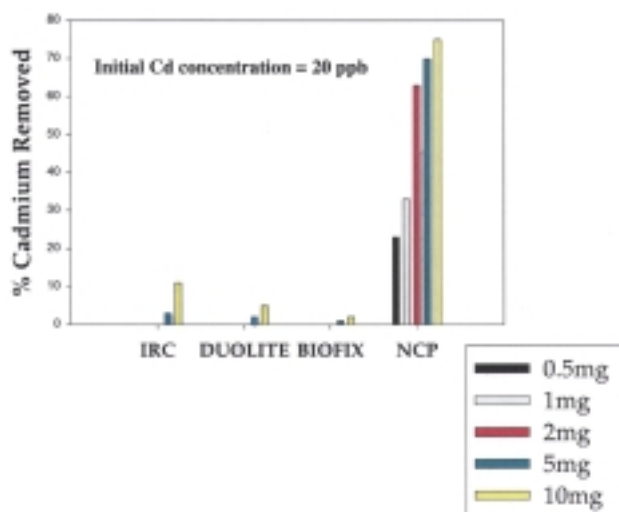


FIGURE 8
Cadmium removal by ion exchange resins and NCP.

against adverse conditions present in waste streams such as temperature and pH variability, salinity, and the presence of other contaminants.

[Sponsored by ONR]

References

- ¹G.M. Gadd, "Metal Tolerance," in *Microbiology of Extreme Environments*, C. Edwards (ed.), (McGraw-Hill, New York, NY, 1990) pp. 178-210
- ²J.B. Brower, R.L. Ryan, and M. Pazirandeh, "Comparison of Ion Exchange Resins and Biosorbents for the Removal of Heavy Metals from Plating Factory Wastewater," *Environ. Sci. Tech.* **31**, 2910-2914 (1997).
- ³M. Pazirandeh and J.R. Campbell, "Bacteria Expressing Metallothionein Gene into the Periplasmic Space, and Method of Using Such Bacteria in Environmental Cleanup," U.S. Patent 5,824,512, issued October 20, 1998.
- ⁴M. Pazirandeh, B.W. Wells, and R.L. Ryan "Development of Bacterial Based Heavy Metal Biosorbents: Enhanced Uptake of Cadmium and Mercury by an *Escherichia coli* Expressing a Metal Binding Motif," *Appl. Environ. Microbiol.* **64**, 4068-4072 (1998). ★

Carbon Nanotubes: Experiments Catch Up with Theory

C.T. White and J.W. Mintmire
Chemistry Division

At the confluence of graphite fibers and fullerenes, carbon nanotubes have exhibited exceptional mechanical and electronic properties. Even before the first reported observation of carbon nanotubes, NRL theorists predicted that these materials would provide the ultimate nanowire, with high carrier densities and mobilities. They subsequently predicted that semiconducting carbon nanotube band gaps could be engineered by varying their diameter. Recent experiments at Delft and Harvard Universities and other sites have confirmed these remarkable properties, further establishing carbon nanotubes as outstand-

ing candidates for components in 21st century molecular electronic devices. Indeed, the first single molecule transistor has already been made using nanotubes at Delft. Recent NRL work has answered several important questions raised by these experiments. How in the presence of disorder can carbon nanotubes exhibit ballistic transport over micrometers or more,¹ and why do experimental measurements indicate a universal behavior in the electronic structure near the Fermi level?^{2,3} The answers to these questions imply that carbon nanotubes will find wide use in molecular electronic devices sooner than had been anticipated.

Ballistic Transport: Any single-wall nanotube can be thought of as constructed by rolling up a single sheet of graphite (shown in Fig. 9) along one of its two-dimensional lattice vectors, $\mathbf{R} = n_1 \mathbf{R}_1 + n_2 \mathbf{R}_2$, where \mathbf{R}_1 and \mathbf{R}_2 are primitive lattice vectors of the graphite honeycomb lattice. Hence all single-wall nanotubes can be labeled by a pair of integers (n_1, n_2). Our initial work on nanotubes in 1991 predicted that a special subset of single-wall carbon nanotubes with $n_1 = n_2$, known as armchair nanotubes, should be metallic. Researchers in Delft recently obtained experimental results that not only confirm these predictions but also imply that the conduction states extend over the entire 3- μm length of the (10, 10) tube studied. This is true, in spite of the clear presence of disorder in the tube due to its interactions with the substrate and contacts. We have shown, however, that unlike normal metallic wires, conduction elec-

trons in (10,10) nanotubes (such as depicted in Fig. 10) experience an effective disorder averaged over the tube's circumference. This leads to electron mean free paths that increase with the tube's diameter.¹ This increase should result in exceptional ballistic transport properties and localization lengths of 10 μm or more for tubes with diameters that are typically produced experimentally. This surprising property of nanotubes allows them to tolerate physically reasonable amounts of disorder and still function effectively as nanowires in micrometer-size devices.

Fermi-Level Electron States: Workers at both Delft and Harvard recently reported scanning tunneling microscopy (STM) experiments on single-wall carbon nanotubes. In part, these were performed to test earlier NRL theoretical predictions that the band gaps in semiconducting carbon nanotubes should be given by $E_g = |V_0| d_0/r_T$, where $|V_0| \approx 2.5 \text{ eV}$, d_0 is the C-C bond distance, and r_T is the radius of the tube. The STM experiments give a direct experimental probe of the electron density of states (DOS) near the Fermi level. These STM experiments not only confirmed the predicted band gap dependence, but also found an unexpected similarity in the DOS for semiconducting nanotubes (those with $n_1 - n_2 \neq 3q$ with q an integer) with similar diameters but different values of n_1 and n_2 . We have shown to first-order that the DOS of single-wall carbon nanotubes can be described in the vicinity of the Fermi level in terms of a universal relationship that depends only on whether the nanotube is metallic or semiconducting.^{2,3} These

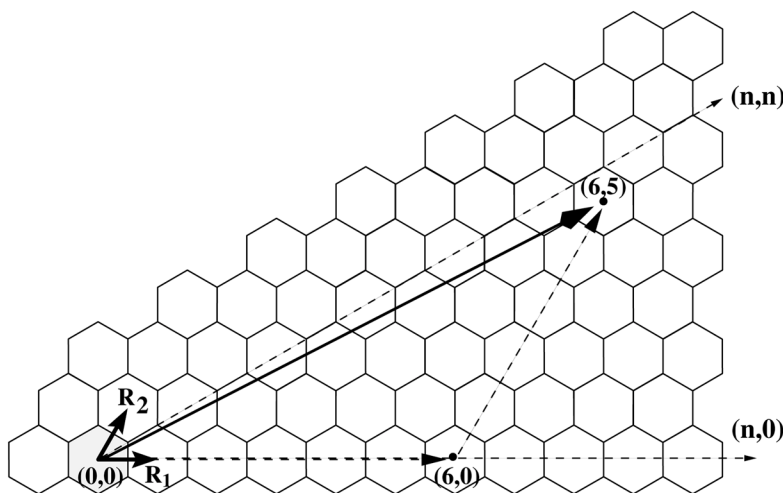


FIGURE 9 Two-dimensional graphene lattice structure. Primitive lattice vectors \mathbf{R}_1 and \mathbf{R}_2 are depicted in the origin unit cell. Rollup vector \mathbf{R} is shown for (6,5) single-wall nanotube. Armchair nanotubes are defined by rollup vectors along the (n,n) direction; zigzag nanotubes are defined by rollup vectors along the (n,0) direction. Armchair and zigzag nanotubes will possess reflection planes and be achiral, all other single-wall carbon nanotubes will be chiral.

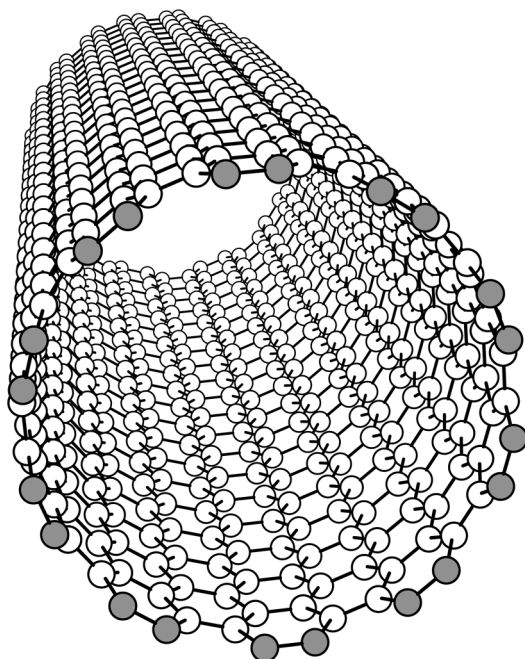


FIGURE 10
Geometry and band structure of the (10,10) armchair nanotube. A segment of the (10,10) armchair tubule with a planar 20-atom carbon containing 10 C-C bonds that can be used to generate the entire tube is depicted in gray.

results—which follow from the approximate radial symmetry of the graphite dispersion relations around the Fermi level—greatly simplify the task of sorting through semiconducting or metallic tubes of similar diameters but different helicities (n_1, n_2) to optimize a particular electronic for device applications.

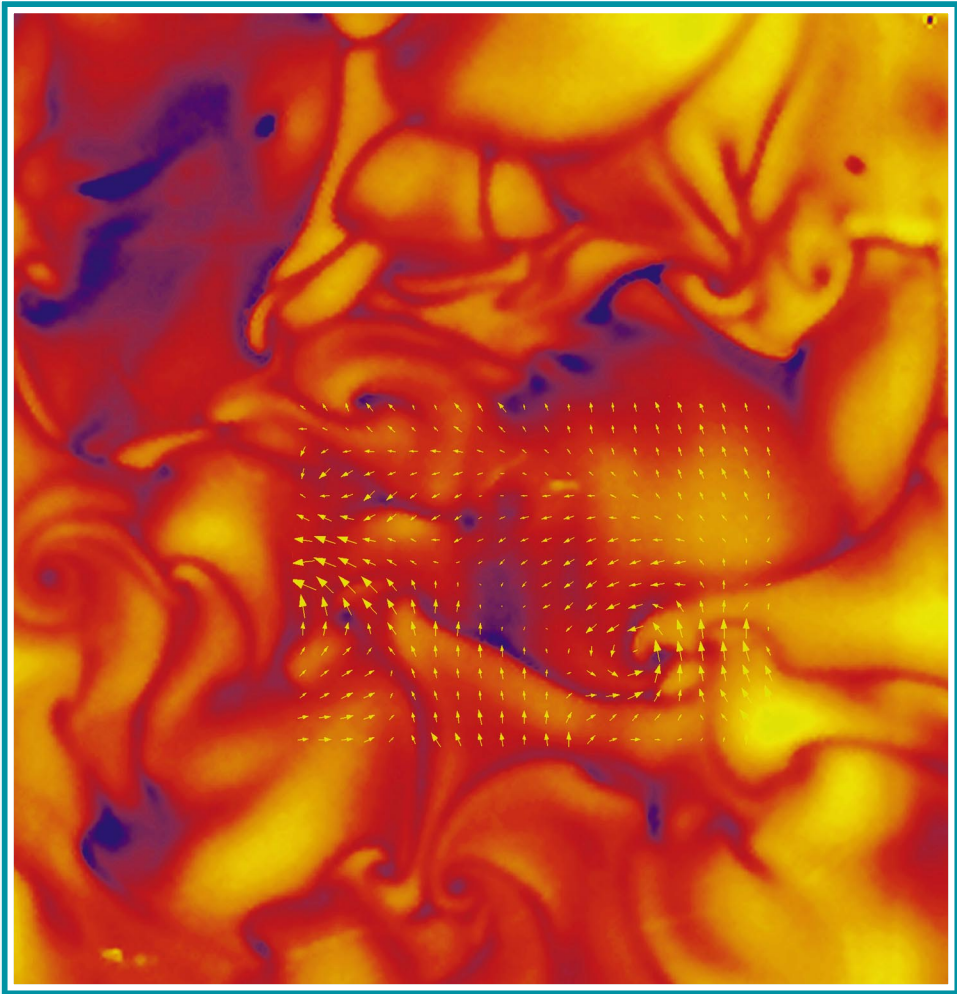
Summary: Recent experiments have confirmed NRL predictions involving the metallic and semiconducting nature of carbon nanotubes. These experiments have also stimulated new NRL theoretical work.¹⁻³ Results of these new theoretical studies imply that the conduction channels in armchair tubes are robust and able to sustain ballistic transport over unprecedented distances for such laterally confined systems in the presence of physically reasonable amounts of disorder. These theoretical results also show that the nanotube DOS near the Fermi-level—important to device applications—depends only on

the diameter of the tube and whether it is semiconducting or metallic. This dependence on diameter only, not helicity of either semiconducting or metallic tubes, removes another stumbling block previously thought to represent a significant synthetic barrier to their applications. These recently uncovered characteristics of carbon nanotubes indicate that their potential for applications in 21st century nanoscale molecular electronic devices is even higher than initially envisioned.

[Sponsored by ONR]

References

- ¹C.T. White and T.N. Todorov, “Carbon Nanotubes as Long Ballistic Conductors,” *Nature* **393**, 240-242 (1998).
- ²C.T. White and J.W. Mintmire, “Density of States Reflects Diameter in Nanotubes,” *Nature* **394**, 29-30 (1998).
- ³J. W. Mintmire and C. T. White, “Universal Density of States for Carbon Nanotubes,” *Phys. Rev. Lett.* **81**, 2506-2509 (1998). ★



Quiescent in the Infrared
Science-as-Art contest – Special Mention
Submitted by: Richard Leighton

This image was acquired in the NRL Free Surface Hydrodynamics Laboratory. The free surface of an apparently quiescent tank of water was imaged by using an infrared-sensitive camera. The lighter colors represent warmer temperatures, and the darker colors represent cooler temperatures covering the 2-degree temperature range in the 20-cm-square image. The vectors indicate the velocity of the fluid 2 mm beneath the free surface. The peak velocity is 5 mm per second. The flow is driven purely by the cooling of the free surface and the resulting instability. To the best of the authors' knowledge, these are the first laboratory measurements of this type.

- 93 Automatic Radar Periscope Detection and Discrimination
D.W. Baden, R.S. DeCampo, G. Herman, and D.W. Kerr
- 94 Development Testing of AN/SPQ-9B Radar Preproduction Model
D.J. Cardiel, L.M. Schaus, and L.M. Leibowitz
- 96 A Method for Determining the Angle of Arrival (AOA) of Impinging Radio Waves in the Presence of Multipath
J.H. Frankovich and A.Y. Tse
- 99 The Microelectronics and Photonics Test Bed Experiment
A.B. Campbell, III and S. Buchner
- 100 Fabrication of a Fast Turn-off Transistor by Wafer Bonding
K.D. Hobart, F.J. Kub, G. Dolny, M. Zafrani, and J.M. Neilson
- 102 Low-Power, High-Speed InAs-Based High Electron Mobility Transistors
J.B. Boos, B.R. Bennett, W. Kruppa, D. Park, and M.J. Yang

Automatic Radar Periscope Detection and Discrimination

D.W. Baden, R.S. DeCampo,
G. Herman, and D.W. Kerr
Radar Division

Context: In the post-Cold War era, Navy missions require ships to operate in littoral waters near hostile shores where they are at risk of attack from submarine-launched torpedoes. The risk is greater because acoustic submarine-detection sensors, usually effective in antisubmarine warfare (ASW), are impaired in shallow water. However, these same acoustic conditions require submarines to use their periscopes to launch successful torpedo attacks, and periscopes can be detected by radar. In fact, the Navy has an operational periscope-detection radar, the APS-137, installed in S-3B and P-3C aircraft. But, because the APS-137 requires human operators to distinguish sea clutter and other objects from periscopes, it is completely overwhelmed in high sea states and in dense-target littoral seas. In 1993, the Navy initiated the Automatic Radar Periscope Detection and Discrimination (ARPDD) program, an ONR Advanced Development (6.3) project to exploit new technology to meet the new ASW challenges in littoral waters.

ARPDD Team: The Naval Air Systems Command (NAVAIR) provides technical management of ARPDD, with a Navy laboratory and industry execution team that includes: NRL for radar and field test expertise; Naval Air Warfare Center (NAWC), China Lake, for automatic pattern recognition; the Applied Physics Laboratory (APL) of the Johns Hopkins University for ASW; and Raytheon TI Systems (RTIS) for equipment design and construction. Program specifications require the demonstration of technology that yields a probability of detection of briefly exposed periscopes greater than 50%, with less than one false periscope declaration per day. The technical challenge is to maintain detection sensitivity while automatically eliminating the huge number of radar reflections from sea clutter and near-shore objects (e.g., boats, buoys, and trash).

Concept: The ARPDD team selected a layered concept for eliminating nonperiscope reflections while retaining most periscope reflections. The basic radar retains the high power, fast antenna scan rate, and 1-ft range resolution of the APS-137. A novel constant false alarm rate (CFAR) processor maintains system sensitivity. A retrospective processor (RP) eliminates noise and uncorrelated sea clutter. A di-

rect discriminator (DD) applies automatic pattern recognition to a 5-s history of 1-ft range resolution signatures to eliminate correlated sea clutter and nonperiscope objects. An indirect discriminator (ID) combines the results of the DD with context information developed by a track-while-scan (TWS) processor to provide final periscope declarations.

The first driving issue was “Is there, even ideally, enough information in 1-ft signatures to distinguish real periscopes from clutter echoes and other periscope-sized objects?” The team took NRL’s Advanced Profile radar to Kauai, Hawaii, in the spring of 1993 to collect and record real signature data on periscopes, clutter, and small objects. The signature recognition experts at NAWC, after extensive laboratory processing of the data, determined that it was indeed *theoretically* possible to discriminate periscopes from other radar reflections, but there were not enough data to determine that the discrimination accuracy was sufficient to meet the system requirements.

Demonstration: The team next modified the Advanced Profile radar to implement a “breadboard” of the full ARPDD processing, but only for a limited segment of 16 nmi by 45 deg, with the RP implemented in hardware but the DD operating in the laboratory on recorded signatures. The breadboard was installed and operated in both an NRL P-3 aircraft (to investigate the applicability of the concept to airborne radar) and in a van on the shore in Kauai (for the shipboard case). The huge number of RP detections of correlated sea clutter was a tremendous challenge to the team, but refinements of the laboratory DD processing indicated that the system requirements should indeed be achievable by the ARPDD concept. Figures 1 and 2 show 5-s signature histories for both correlated sea clutter and an actual periscope, respectively.

The breadboard results justified a full implementation and operational testing of the ARPDD concept in the “brassboard” system. RTIS completed design and construction of the brassboard, and it was tested and fine-tuned in Kauai in the summer of 1997. The brassboard was installed on the USS *Stump* (DD978) in April 1998. Navy personnel operated the radar, while an onboard ARPDD team maintained the system and collected scientific data. ARPDD has now been successfully demonstrated in the course of a Fleet exercise, SHAREM-125, and other ASW events during a deployment to the Mediterranean in the summer of 1998. Performance of the system was outstanding and elicited many favorable comments from the captain of the ship and the commander of the fleet with statements such as “ARPDD

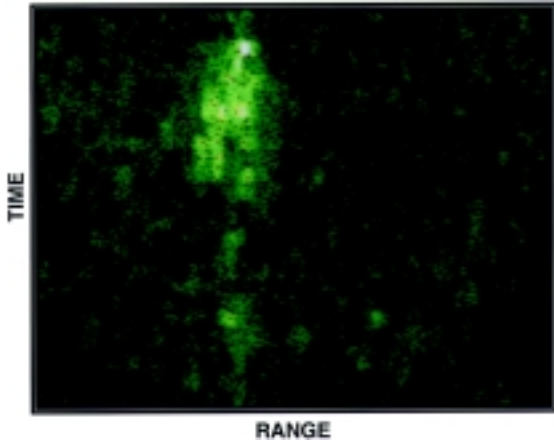


FIGURE 1
Sea spikes: clumpy returns with very wide range extents.

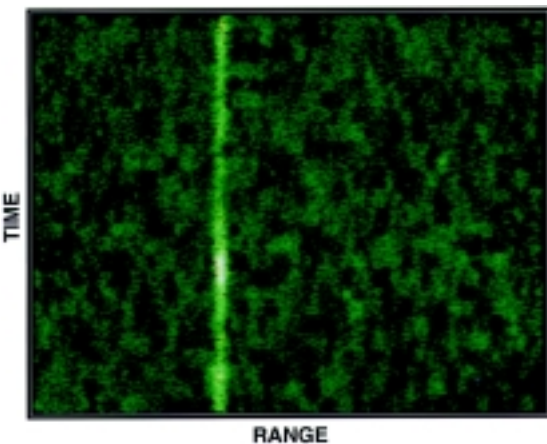


FIGURE 2
Periscopes: sharp returns with narrow range extents.

has proven itself to be an invaluable sensor in the conduct of undersea warfare.” There has been positive reaction to this new capability from all those who are exposed to it, from operating sailor to battle group commander.

Summation: The brassboard test on the USS *Stump* shows that the ARPDD outstandingly meets the shipboard ASW radar goals. The system will be tested on the NRL P-3 aircraft in the summer of 1999, where it is expected to show the same level of performance for the Airborne Maritime Surveillance application. The demonstrated ARPDD technology can either be added to existing surveillance radars, such as the APS-137 (S-3B and P-3 aircraft) and the APS-147 (LAMPS helicopters), or to new radars such as the multifunction radar for new-generation combatant ships.

[Sponsored by ONR]



Development Testing of AN/SPQ-9B Radar Preproduction Model

D.J. Cardiel, L.M. Schaus, and L.M. Leibowitz
Radar Division

Sea-skimming missiles are a major threat to U.S. Navy ships. Starting in 1991, the Naval Research Laboratory (NRL) Radar Division supported by the Program Executive Office, Theater Air Defense, developed a new AN/SPQ-9B radar concept for antiship missile defense (ASMD). This concept included both an air mode that provided a new, low-cost, quality sea-skimmer detection capability and a surface mode with improved performance in support of Gunfire Control System (GFCS) MK 86 and backup navigation. An AN/SPQ-9B advanced development model (ADM) radar was designed and assembled by NRL.¹ In 1993-94 land-based tests and 1994-95 at-sea tests conducted by NRL, the ADM radar successfully demonstrated the ability to achieve firm-track thresholds in littoral environments. An AN/SPQ-9B radar prime-item development specification (PIDS) was developed jointly by NRL, Port Hueneme Division (PHD) Naval Surface Warfare Center (NSWC), and Crane Division (CD) NSWC. Based on successful ADM testing and the PIDS, in October 1994 the Navy awarded a contract to Northrop Grumman Norden Systems (NGNS) for two AN/SPQ-9B preproduction kits (PPKs) with an option for six low-rate initial production (LRIP) kits. Following successful first-article testing, the first PPK radar unit (Fig. 3) was delivered in April 1998. With NRL as technical design agent, required land-based development testing (DT) was initiated in June 1998 at the PHD-NSWC Surface Warfare Engineering Facility (SWEF) using targets representative of sea-skimmers. These tests evaluate the AN/SPQ-9B radar’s air and surface modes, verify the interfaces to the MK 86 GFCS, and help uncover and eliminate defects in radar performance and interface operation prior to installation aboard a Spruance-class destroyer. The radar is currently planned for installation on CV/CVN, LPD-17, LHD-1, CG-47, and DDG-51 ship classes.

Development Test Objectives: The general test objective is to evaluate the ability of the AN/SPQ-9B preproduction radars to meet technical specifications in an operational environment and determine acceptability for service use. Development testing will demonstrate, to the maximum extent possible, the operational requirements, thresholds, and level of system development necessary for success in the subsequent operational test (OT) phase. The results

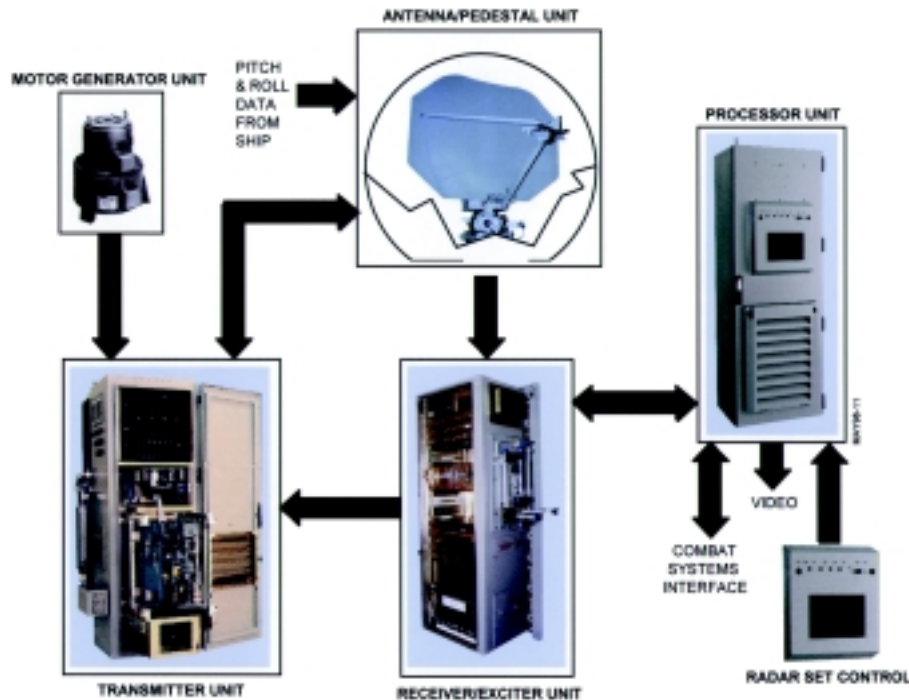


FIGURE 3
AN/SPQ-9B radar equipment description

will support a decision regarding the radar’s readiness for operational test and reflect its probability of success. The AN/SPQ-9B radar development test and evaluation will be accomplished in two phases. The first phase will be conducted at PHD-NSWC and the second phase will be conducted aboard the Spruance-class destroyer test ship. The objective of the first phase is to test the AN/SPQ-9B radar at a land-based facility to ensure that the radar will perform as required prior to shipboard testing. The air and surface modes of the radar and functional integration with the MK86 GFCS will be evaluated. This first phase is conducted using an AN/SPQ-9B preproduction radar installed at the PHD-NSWC SWEF land-based facility and tested against the critical parameters defined in the Test and Evaluation Master Plan.

In its AN/SPQ-9B TDA role, NRL reviews NGNS radar development, evaluates radar operation, and plans development testing with the support of PHD-NSWC. NRL conducts development testing and provides the test director who chairs the Test Plan Working Group and heads the development test team consisting of personnel from NGNS, NRL, and PHD-NSWC. The director also plans, manages, conducts test and evaluation related activities, and ensures communications and coordination among the test team

and other key Navy organizations. He also coordinates and conducts a Development Test Readiness Review preceding significant phases and prior to technical evaluation and conducts debriefings following each test. He will use data analysis findings of the development test team to make a recommendation regarding readiness for operational testing based on requirements.

Development Test Status: First-article testing was successfully completed on the two preproduction radar units in April and June 1998, respectively. The first unit was shipped to PHD-NSWC in April 1998 for installation at SWEF. The second unit remains at NGNS to support development testing as well as lightweight antenna development. SWEF land-based testing provides for evaluation of radar system performance and the AN/SPQ-9B/MK86 GFCS interface before conducting development and operational testing onboard an active ship. Land-based testing began in June 1998, with a scheduled January 1999 completion. Testing consists of evaluating the air and surface channels as well as the radar-to-GFCS interface and is about 75% completed with favorable preliminary results. A detailed test report with an analysis of results will be completed within 90 days of the conclusion of land-based testing.

Land-based surface-test targets include a Boghammer Iranian gunboat, Boston whaler, rigid-hull inflatable boat, and rubber raft. Air-test targets include single- and twin-propeller planes, Learjets, helicopters, and a low radar-cross-section jet aircraft. An AN/SPQ-9B LRIP radar will be installed on the USS *Oldendorf* during a scheduled shipyard availability in June-August 1999. The radar will undergo checkout and sensor alignment prior to shipboard DT/OT scheduled for late 1999. The development and operational test results will guide the Milestone III decision to begin full-scale production of the radar for introduction to the Fleet. The AN/SPQ-9B radar, with its ability to detect low-altitude threats in a clutter environment, fills a critical U.S. Navy need for a low-cost, effective ASMD radar.

[Sponsored by PEO EXW-D2]

Reference

¹B. Cantrell, L. Leibowitz, D. Cardiel, B. Connolly, S. Lessin, M. Rachuba, G. Tavik, and M. Walder, "Advanced Development Model of the AN/SPQ-9(I) Radar," NRL Memorandum Report NRL/MR/5340-94-7607, Oct. 1994. ★

A Method for Determining the Angle of Arrival (AOA) of Impinging Radio Waves in the Presence of Multipath

J.H. Frankovich and A.Y. Tse
Tactical Electronic Warfare Division

Introduction: Angle-of-arrival (AOA) estimation of radio frequency (RF) signals is an important piece of information for electronics support measures (ESM) systems. These systems, which are often used in military applications such as threat reaction, require highly accurate, real-time AOAs to correctly resolve and locate emitters immersed in a dense signal environment. A major hindrance in the estimation of AOA is the presence of multipath.

This article describes a technique that provides reliable AOA estimation of signals resident in a severe multipath environment. Whereas conventional techniques provide ambiguous results, this technique provides precision AOA accuracies of 0.1° under harsh multipath conditions. First, the multipath problem is defined as it relates to the measurement of AOA. Two methods that aid in AOA measurement in multipath environments are discussed. The first is an analytic approach that uses the maximum likelihood method to discern bad data measurements. The second is an early detection method that establishes the AOA measurement prior to the arrival of the reflected signal. The combination of these two methods is shown to provide accurate AOA measurements by making multipath effects negligible. Experimental results that use an interferometer to detect AOA by both this new method and conventional means are provided for comparison.

Multipath Defined: The measurement of AOA is severely compromised in the presence of multipath. Multipath occurs when the received signal is not only the incident RF wave, but also the summation of one or more reflected waves from different locations. Figure 4 shows an example of multipath where it occurs most often—over water.

Due to the longer distance traveled by the reflected wave, the effects of multipath are actually observed a small time after the incident wave has arrived at the receiving system. The effects observed are distortions in both phase and amplitude at the receiving system. Depending on the geometry involved, these effects are observable only nanoseconds after the leading edge of the incident RF. Since the phase is now distorted, the resulting phase measurement is no longer a reliable means of determining the AOA of the incoming plane wave.

Analytic Approach: The analytic approach is a maximum likelihood estimation (MLE) in which the

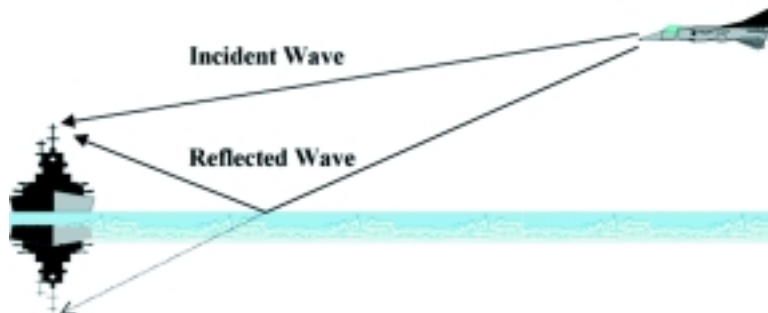


FIGURE 4
Multiple example.

estimated angle of arrival is calculated by minimizing an error function. For each bearing measurement, there is an error associated with each possible angle within the field of view. The MLE algorithm reports the angle associated with the smallest error. For each calculation of bearing, two estimates are computed—the best and second best estimates. Figure 5 shows the error plots associated with both ideal and multipath cases. In an ideal situation with no multipath, the best estimate will have a much smaller error than the second best estimate; however, in a multipath environment, the error of the second best estimate approaches the error of the best estimate. The ratio of the two errors is considered. If the error ratio is much greater than unity, an ideal case is represented. If the error ratio is near unity, two equally good answers must be assumed, which is clearly not possible (one emitter cannot be two places at the same time). In this case, the bearing calculation may be discarded as a wild bearing.

Early Detection Method: The early detection method uses the fact that with multipath interference, the reflected waves arrive after the incident RF. This implies that the multipath effects described earlier do not corrupt any angle measurement taken before the reflected wave arrives. The method described here measures phase difference between channels at the leading edge of the received pulse.

Directly sensing the intermediate frequency (IF) signal achieves the necessary precision for phase measurement. The leading edge of the IF encodes the phase for each channel in terms of near-instantaneous phase of a precision common reference oscillator. The resulting phase difference between the two reference oscillator readings contains the differential phase information—now encoded as differential reference oscillator phase. Precision AOA is then derived from the measured differential reference oscillator phase correcting for frequency differences between the IF and reference oscillator.

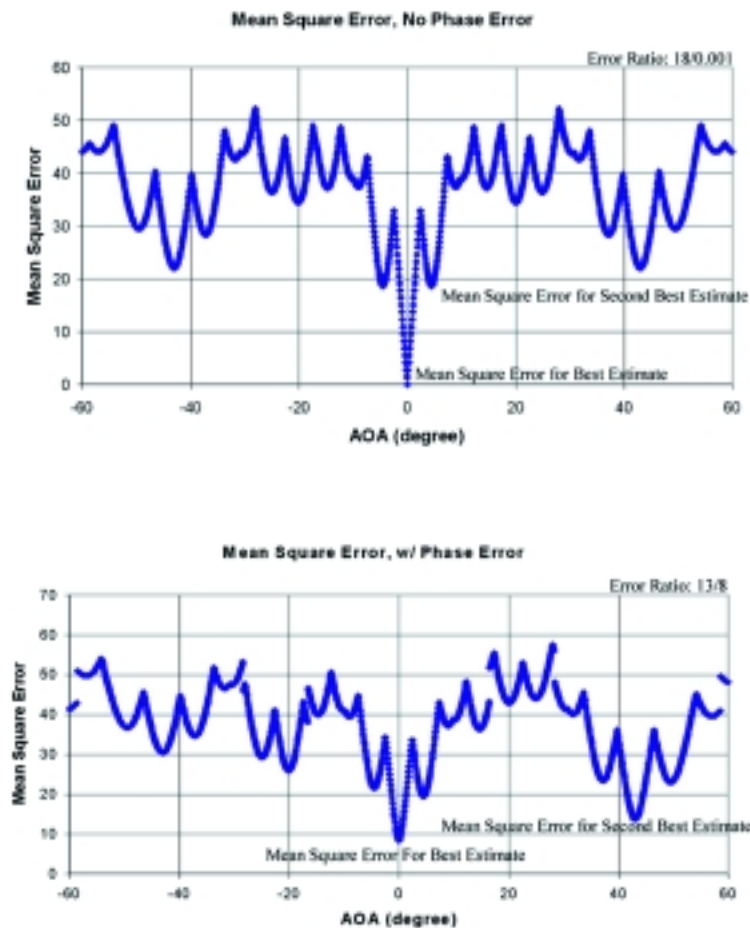


FIGURE 5 Mean square error vs angle of arrival.

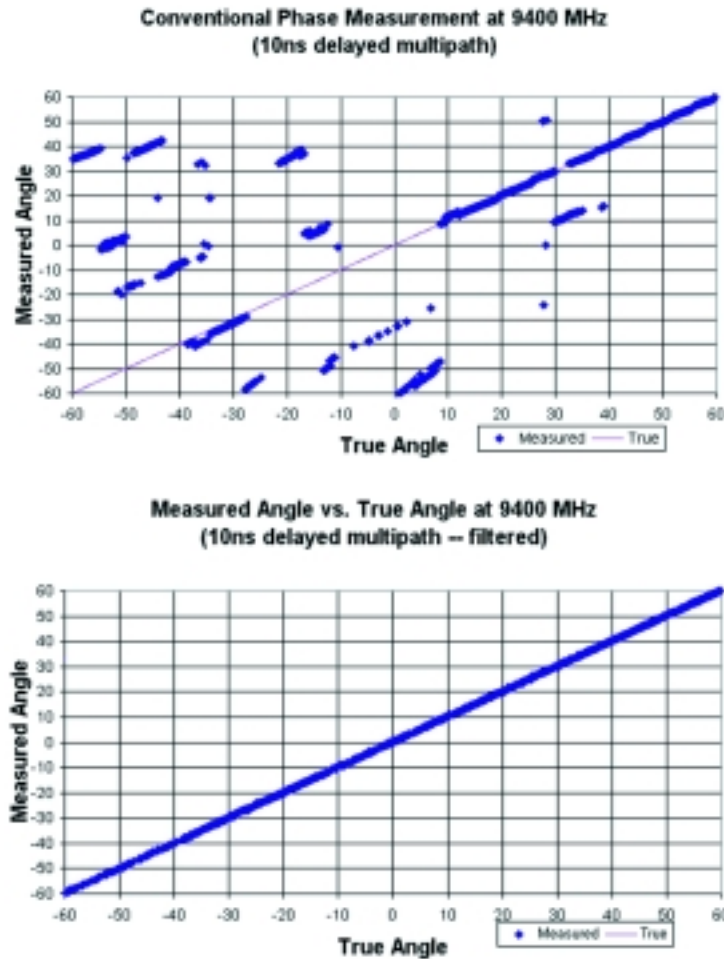


FIGURE 6
Conventional vs new method.

The concept is based on

- predetection sensing (threshold crossing) of a pulsed-carrier;
- near-instantaneous sampling of an analog reference-oscillator;
- deriving phase-difference between reference-oscillator readings (snapshots by each channel); and
- correcting phase-difference for frequency and converting the results to AOA.

It should be noted that it is possible to cycle-skip (IF cycle) while detecting the leading edge of the IF pulse. One channel could threshold on a marginal cycle peak while another crosses the threshold a complete cycle later. Proper selection of the precision reference oscillator frequency prevents this from causing problems. In the system used for this experiment, the reference oscillator and the IF frequency are matched at 160 MHz. This causes a 360° phase shift in the reference oscillator for every cycle skip in the IF. This allows the reference oscillator phase infor-

mation to remain intact, regardless of whether or not a cycle skip occurs.

A patent is pending for this method of AOA measurement. This early detection method is inherently multipath-immune. The test results prove its utility in multipath environments.

Results: A five-element interferometer was used to test AOA detection by using both the methods discussed above and conventional (IF phase detection) means. Figure 6 indicates the significant improvement gained by using the new methods. This new approach has much utility in both military and commercial applications. The most evident use is the tracking of multiple targets near a reflective surface such as water. When tracking multiple targets, AOA is an invaluable tool in discerning RF emitters. Applying the methods described in this article will alleviate many of the problems associated with AOA measurements.

[Sponsored by ONR]



The Microelectronics and Photonics Test Bed Experiment

A.B. Campbell, III
Condensed Matter and Radiation Sciences Division

S. Buchner
SFA, Inc.

Introduction: The Microelectronics and Photonics Test Bed (MPTB) has been conceived, developed, designed, and built at NRL to study the effects of the natural radiation environment of space on a variety of advanced microelectronic and photonic devices. An international group of scientists and engineers from government, university, and industrial organizations contributed ideas and experiments for MPTB, and it was funded by a large variety of government agencies. Integral parts of MPTB are coordinated space, ground test, and modeling programs. The goals of the program are to improve the prediction accuracy of radiation-induced space performance; develop a database of ground test and space data; and promote the insertion of new technologies into space systems.

MPTB is an electronic test system in space that continuously monitors 24 experiment boards including measurements of the radiation environment. MPTB's orbit is highly elliptical, extending from geosynchronous orbit where the environment is dominated by cosmic rays to below the radiation belts in which there is a large flux of protons and electrons.

MPTB Motivations: Indications based on previous space experiments and other space systems are that procedures for predicting space performance in a radiation environment are not always accurate, especially for advanced technologies. Impacts are the need for large design margins, elimination from consideration of some potentially useful technologies, and, in some cases, the use of excess shielding, which unnecessarily adds to launch costs. In addition, because of the reduced availability of radiation-hardened, radiation-tolerant, or space-qualified parts, there is increased pressure to use commercial off-the-shelf (COTS) parts. Also, a number of new phenomena such as multiple bit upsets, dose rate effects, ion track effects, and others have been discovered whose impact on space systems can be verified only through space experiments. There is always a desire for space data before system implementation to increase the accuracy of survivability and reliability calculations. New technologies are expected to be more vulner-

able to radiation effects because of the trend to reduce power, increase speed, and increase the number of functional elements per integrated circuit. Hence, MPTB's goal is to develop better ground test procedures and models to predict space performance of future technologies and to quantify the accuracy of existing procedures.

Experiments: Experiments on MPTB include looking for permanent damage in devices caused by the particle environment. The damage includes total dose changes, such as threshold voltage shifts in commercial dynamic random access memories (DRAMs) and displacement damage effects, such as dark current increases in charge-coupled devices (CCDs). Other experiments are looking at single-event effects (SEEs), including upsets and latchups—transient changes due to the passage of single particles that can sometimes result in permanent changes or damage. The flight unit includes devices and technologies such as advanced, high-speed InP test circuits, optoisolators, operational amplifiers, commercial dynamic random access memories (RAMs), neural net pattern recognition systems, analog integrated circuits, linear bipolar devices, advanced packaging technology stacked memory arrays, static RAMs including GaAs and Si devices, analog-to-digital converters, microprocessors, CCDs, a fiberoptic databus system, and field-programmable gate arrays.

Hardware: The MPTB flight system was designed and built at the NRL Navy Center for Space Technology. Experimenters either fabricated their own test cards of their experiment according to the NRL design specification or had them built at NRL. All of the control hardware and software is radiation tolerant and designed to last three years without disruptions because of the occurrence of SEE. All of the experiments, including the ones primarily looking at SEE effects, are measured for permanent damage changes.

Modeling: To improve the prediction accuracy of radiation-induced space performance requires better models for the response of microelectronic and photonic devices and systems. The inputs to these models are the data obtained from ground testing, including single-event effects cross sections from heavy ions and protons, and changes in circuit parameters from protons and cobalt-60. The results of ground measurements on the same part types as are being flown in space are combined with models of the space radiation environment and used to predict the performance of the identical parts on MPTB. Such

predictions are compared with the actual performance of the parts in the measured space environment. Accelerator testing is relatively expensive, and MPTB aims to improve the accuracy and minimize the cost of ground testing. For instance, if prediction of proton-induced SEE rates could be based on a single measurement at high energy, it would not be necessary to characterize the cross-section curve over a wide range of energies. Furthermore, methods for testing low dose rate effects observed on MPTB are also being developed.

Summary: To date, a great volume of space data have been generated and are being analyzed. Highlights include the first confirmation that dose-rate effects can result in higher damage at space dose rates compared to those in ground tests; multiple bit upsets; nonvolatile dosimetry using an electrically erasable programmable, read-only memory (EEPROM); reliable operation of a neural net system; and multiple writing of an EEPROM in the presence of radiation with no failures. The ground test and modeling programs are not complete. For further information, see the MPTB data Website at <<http://wally5.nrl.navy.mil/>> or the systems Website at <<http://ssdd.nrl.navy.mil/www/mptb/index.htmlx>>.

[Sponsored by DTRA, AF/STP, and NRO] ★

Fabrication of a Fast Turn-off Transistor by Wafer Bonding

K.D. Hobart and F.J. Kub
Electronics Science and Technology Division

G. Dolny, M. Zafrani, and J.M. Neilson
Harris Semiconductor Corporation

Introduction: A new class of electronic devices is presently under development for the Navy's Power Electronic Building Blocks (PEBB) program. One of the prime objectives of the program is to devise new power switching devices, dubbed fast turn-off transistors or FTO. Faster power switching devices are desirable on Navy platforms for several reasons: First, as switching frequencies increase, the physical size and weight of passive components used in power conditioning systems is reduced. Second, the higher switching frequencies make it easier to filter harmonics, which improves both silent operation of Navy vessels and electrical power quality. Third, the FTO is projected to reduce switching loss by a factor of 3–5 and thereby improve efficiency of power systems.

To speed the development of FTOs, NRL has developed a new wafer bonding technology and, together with Harris Semiconductor Corporation, Inc., has demonstrated a new power switching device with potential for dramatically improved performance.

The trend in FTO devices is to integrate active turn-off capability on *both* sides of the transistor, whereas conventional power switching devices have active turn-off on only one side. The benefit of the additional control gate is to reduce device switching time. Figure 7 shows the conceptual cross-section of one such FTO. The double-side insulating gate bipolar transistor (D-IGBT) is essentially two conventional single-side IGBTs (S-IGBT) placed back-to-back. This is a symmetric bipolar transistor with metal-oxide-semiconductor (MOS) gates on both sides to control vertical current flow through the device. For this device, the second gate improves turn-off characteristics by shunting the p⁺ emitter (Emitter 2) to the n⁻ drift region (n⁻ base) and effectively drains injected holes during device turn-off. In the conventional single-side device, only electron flow is terminated and holes decay through carrier recombination. The fabrication of such a device is complicated by the need for advanced semiconductor processing on the top *and* bottom of the silicon wafer. NRL recognized that the fabrication procedure could be greatly simplified if two identical devices were bonded together to produce the structure in Fig. 7. Furthermore, if the wafer bonding were performed at sufficiently low temperature (<450 °C), then fully fabricated wafers with complete device metallization could be bonded to produce the D-IGBT without compromising the integrity of the contact metal.

Direct Wafer Bonding: Direct wafer bonding for power device fabrication has been in use since the late 1980s. In all previous work, however, bonding temperatures exceeded 1000 °C. The very low

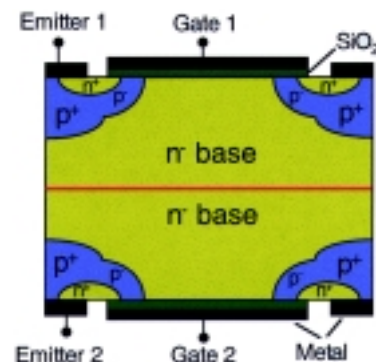


FIGURE 7
Schematic cross section of the double-side insulating gate bipolar transistor.

temperature bonding process developed at NRL uses hydrophobic bonding and long-duration, low-temperature annealing. The hydrophobic silicon surface is prepared by careful cleaning followed by etching of the native oxide in hydrofluoric acid. This process simultaneously terminates the silicon surface dangling bonds with hydrogen and renders the surface inactive to further oxidation. The wafers are then bonded by bringing the polished surfaces into close proximity and initiating contact at the center. At this point, the wafers are weakly bonded by a van der Waals-like force. Annealing at elevated temperatures increases the bond strength. The long duration (≥ 5 hour) anneals at 400 °C were found to produce sufficient bond strength to dice and package the transistors.

Interface Characterization: Beyond mechanical bond strength, the primary issue with direct wafer bonding is carrier transport across the bond interface. Carrier transport can be affected by potential barriers at the interface, which are caused by unintentional dopants and electron and hole traps. Additionally, traps can act as recombination centers, sinking current during device operation. Simple transport across the interface was characterized with the test structure shown in the inset of Fig. 8. The incremental resistance across the bonded interface was characterized as a function of anneal temperature.¹ For anneal temperatures below 800 °C, the resistance was low and no potential barriers were detected. At 800 °C, a significant potential barrier that diminished at 1000 °C was observed. This observation is consistent with boron contamination at the interface. Ubiquitous boron in low concentrations ($\sim 10^{10}$ cm⁻²) is

unavoidable, and at low temperatures the contaminant is inactive. At higher temperatures, the dopant boron becomes active, producing a p-type inversion layer in the n-type background silicon. At still higher temperatures, the interfacial boron diffuses into the bulk of the wafer, reducing the barrier. Further measurements were performed to characterize trap density at the interface. The *bulk* trap density in the region of the interface was found to be less than 10^{12} cm⁻² with no detectable traps at the interface.

FTO Fabrication: The very low temperature wafer bonding process was adopted to fabricate the D-IGBT shown in Fig. 7 (red line shows location of bonding interface). In this case, fully qualified 125-mm-diameter IGBT wafers from Harris Semiconductor were mechanically thinned to ~ 200 μ m, and the backsides were rendered atomically smooth by chemical-mechanical polishing. The wafers were cleaned and the backsides were etched in hydrofluoric acid in a spin/spray tool. Devices on the top were aligned to those on the bottom and the wafers were bonded. Low temperature annealing was performed at 400 °C for 5 hours.

The devices were diced and mounted in a custom package with leads to terminals on both sides. Static device characteristics were consistent with those of the individual IGBTs prior to bonding, and no degradation due to the bond interface was observed. The forward and reverse blocking voltage exceeded 1400 V. The forward voltage drop, $V_{E,SAT}$, was 6.2 V at 5.75 A, and was consistent with twice the nominal drop at the design current. The impact of the second gate is illustrated in Fig. 9, which shows the output of the switching waveform analyzer. The emitter cur-

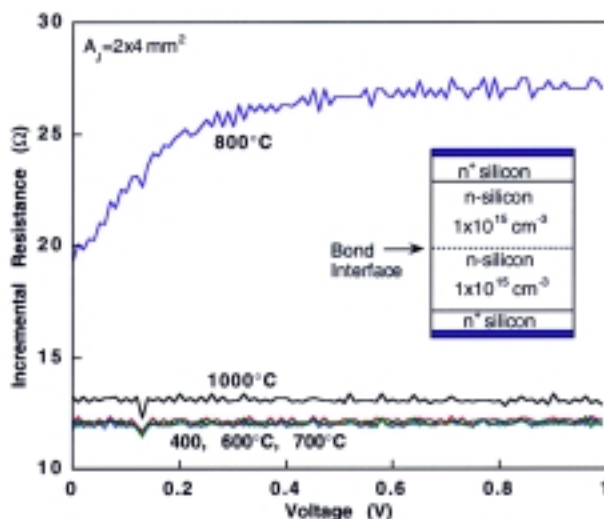
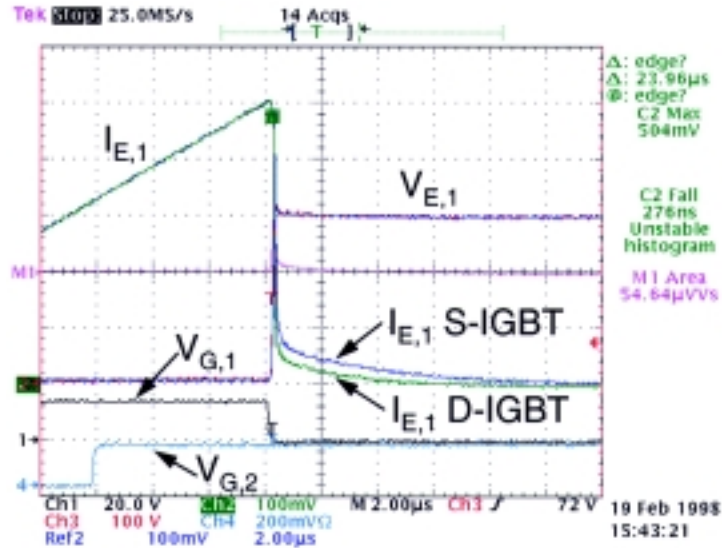


FIGURE 8 Incremental resistance vs bias as a function of anneal temperature of a n-n bonded junction. Nonlinear characteristics are evident at 800 °C and diminish at 1000 °C.

FIGURE 9
Switching waveform showing turn-off time of double-side IGBT for two cases: (1) Gate 2 (V_{G2}) always off and Gate 1 (V_{G1}) switched off (S-IGBT); and (2) Gate 2 switched on 6 μs prior to switching Gate 1 off (D-IGBT). The emitter voltage and current were 600 V and 5 A, respectively.



rent is ramped up through a series inductor by applying a pulse to Gate 1 ($V_{G,1}$). After the current reaches the design value, the device is turned off by shorting Gate 1, after which the emitter voltage ($V_{E,1}$) is restored to the supply voltage (600 V). The switching loss is defined as the time that both the emitter current and voltage are present at device terminals. In Fig. 9, the case where Gate 2 ($V_{G,2}$) remains off (S-IGBT operation) is compared to that where Gate 2 is switched on while Gate 1 is switched off (D-IGBT operation). It was found that by turning on Gate 2 *prior* to turning off Gate 1, a clear decrease in turn-off time and switching energy is observed. Gate 2 acts to short the n^- drift region to the bottom p^+ emitter (Emitter 2) and reduce the hole concentration prior to switching off the device. It was found experimentally that a delay of 6 μs produced a 50% reduction in switching energy (5.5 mJ to 2.7 mJ) at an emitter current and voltage of 5 A and 600 V, respectively. The emitter current fall time dropped from ~ 1200 ns to ~ 400 ns.

Significance: A new type of power switching device that will significantly impact many Navy power conditions systems has been demonstrated. Through the use of a novel direct wafer bonding technique developed at NRL, an advanced fast turn-off power switching transistor was realized for the first time. This demonstration indicates that the FTO indeed improves switching performance, and through standard device optimization the full performance gain should be realized.

Acknowledgment: The authors acknowledge the support of ONR and specifically the PEBB program, including George Campisi, Terry Ericson, and Al Tucker.

[Sponsored by ONR]

References

¹F.J. Kub, K.D. Hobart, and C.A. Desmond, "Electrical Characteristics of Low Temperature Direct Silicon-Silicon Bonding for Power Device Applications," *Proc. Electrochem. Soc.* **97-36**, 466 (1998). ★

Low-Power, High-Speed InAs-Based High Electron Mobility Transistors

J.B. Boos, B.R. Bennett, W. Kruppa, D. Park, and M.J. Yang
Electronics Science and Technology Division

Introduction: Low-power-consumption electronics are critical to the Navy and the Marine Corps in high-speed applications that require lightweight power supplies, long battery lifetimes, or high component density. In pursuit of electronic devices that can operate at high speed and low bias voltage, the Electronics Science and Technology Division is developing high electron mobility transistor (HEMT) technology in the AlSb/InAs material system. AlSb/InAs HEMTs have the potential to set a new standard for power consumption at room temperature.

Attractive features of this material system include high electron mobility and velocity, high sheet charge density, and good carrier confinement.¹ The HEMT is an advanced version of the common field-effect transistor, which uses band-gap engineered layer designs to precisely control the material properties of the electron channel. Accurately controlled layer designs with feature sizes on the atomic scale have been used to exploit desirable quantum confinement effects within the structure. When combined with nanoscale patterning using electron-beam lithography, HEMTs fabricated in the AlSb/InAs material system constitute the state of the art in high-frequency performance at low drain voltage.

Microwave/millimeter (mm)-wave low-noise HEMT receiver applications that would significantly benefit from reduced power consumption include: transmit/receive modules for space-based communications, mm-wave imaging arrays, remote Earth-sensing arrays, portable communications, and micro-air-vehicles. The high current drive capability and potentially low power-delay product also make the HEMTs attractive candidates for high-speed logic applications, particularly when combined with antimonide-based resonant interband tunneling diodes (RITDs). The monolithic integration of the HEMT and the RITD is a critical advancement that will provide the enabling technology needed for a new class of very dense, ultra-high-speed logic circuits with high functionality and very low power dissipation.

HEMT Design: The AlSb/InAs HEMT material was grown by molecular beam epitaxy on a semi-insulating (100) GaAs substrate in the NRL Epicen-

ter. Figure 10 shows a cross section of the layer design along with its corresponding energy band diagram for $V_{GS} = 0$. A 2.5- μm undoped AlSb buffer layer was used to accommodate the 7% lattice mismatch between the GaAs substrate and the HEMT layer structure. Key features of the design are the use of a Si-doped InAs layer and an $\text{In}_{0.4}\text{Al}_{0.6}\text{As}/\text{AlSb}$ composite barrier layer above the InAs channel, and a p^+ GaSb layer and an InAs subchannel layer below the channel. To achieve high electron mobility in a HEMT, modulation doping is used to spatially separate electrons in the narrow band-gap quantum well channel from their parent donor atoms in the wide-band-gap barrier material. The electrons in the channel can travel faster since they are not impeded by the ionized impurity scattering that would otherwise occur. A new modulation doping scheme in these HEMTs was recently demonstrated at NRL. In this approach, a high electron density in the channel is achieved through the use of Si planar-doping in an ultra-thin InAs layer located within the upper barrier material.² The large quantum confinement energy of the 12 Å InAs quantum well allows the electrons to transfer into the InAs main channel. The $\text{In}_{0.4}\text{Al}_{0.6}\text{As}/\text{AlSb}$ composite design enhances the insulating property of the barrier and enables the use of a gate recess etch into the upper barrier material prior to gate metal definition, which otherwise would be prohibited by the high reactivity of the AlSb in air. To reduce impact ionization effects in the device, we introduced a thin InAs subchannel layer that, due to quantization, has a larger effective band gap.³ In the impact ionization process, an electron in the conduction band with sufficient kinetic energy collides

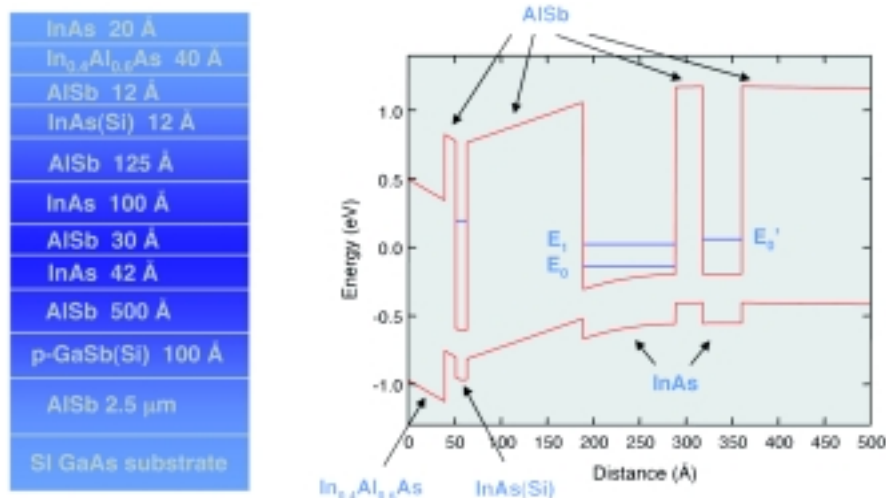


FIGURE 10 (a) HEMT starting material and (b) calculated band structure.

with an electron in the valence band. As a result, the valence-band electron is knocked into the conduction band, leaving behind a positively charged hole in the valence band. The process is multiplicative, and the additional electron and hole charges deleteriously affect device performance. In this design, electrons with high energy are transferred to a larger effective bandgap subchannel before gaining enough kinetic energy for impact ionization. As a result, the extent of impact ionization in the channel is reduced.

DC and Microwave Characterization: Figure 11 shows a typical set of drain characteristics for HEMTs with a $0.1\text{-}\mu\text{m}$ gate length. The $0.1\text{-}\mu\text{m}$ gate length was formed using electron-beam lithography in the Nanoelectronics Processing Facility. At $V_{DS} = 0.5\text{ V}$, a transconductance ($g_m = \Delta I_{DS}/\Delta V_{GS}$) above 1 S/mm is observed. The S-parameters of the HEMTs were measured on-wafer from 1 to 40 GHz and yielded f_T and f_{max} values of 180 and 80 GHz, respectively. When external parasitic effects are removed, an f_T of 250 GHz was obtained, which is the highest reported for this material system. To further optimize low-voltage operation, HEMTs with a 60-nm gate length were also fabricated. The potential for low-voltage operation in these HEMTs is demonstrated in Fig. 12, which shows the measured f_T as a function of drain voltage. At a drain voltage of only 100 mV , an f_T of 90 GHz is obtained, which is the highest reported for any FET at this drain bias.

NRL is the recognized leader in the development of this emerging technology as a result of its strong material growth and device fabrication capabilities in the antimonide-based material system. Further design improvements, particularly in the area of impact ionization management, will make the HEMTs attractive candidates in future applications where high speed and low noise at very low bias voltage will be required.

Acknowledgement: The authors thank R. Bass, S.C. Binari, H.B. Dietrich, S.W. Kirchoefer, R. Magno, C.R.K. Marrian, and B.V. Shanabrook for helpful discussions.

[Sponsored by ONR]

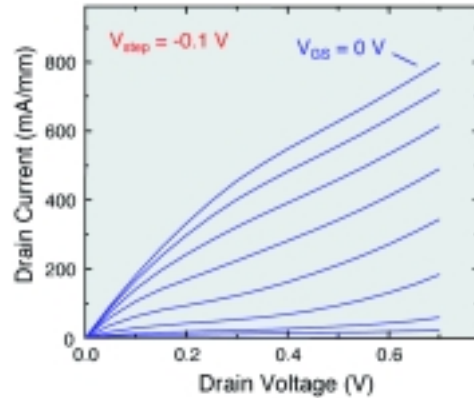


FIGURE 11
 $0.1\text{-}\mu\text{m}$ HEMT drain characteristics. $L_{DS} = 1.0\text{ }\mu\text{m}$,
 $W_G = 26\text{ }\mu\text{m}$, $V_{GS} = 0.1\text{ V/step}$.

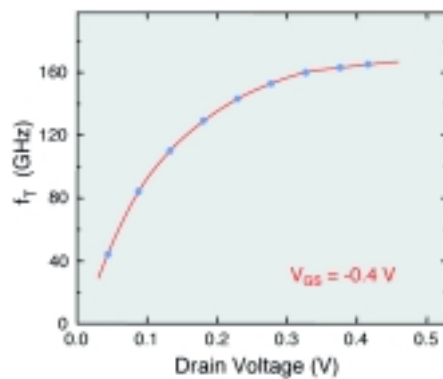
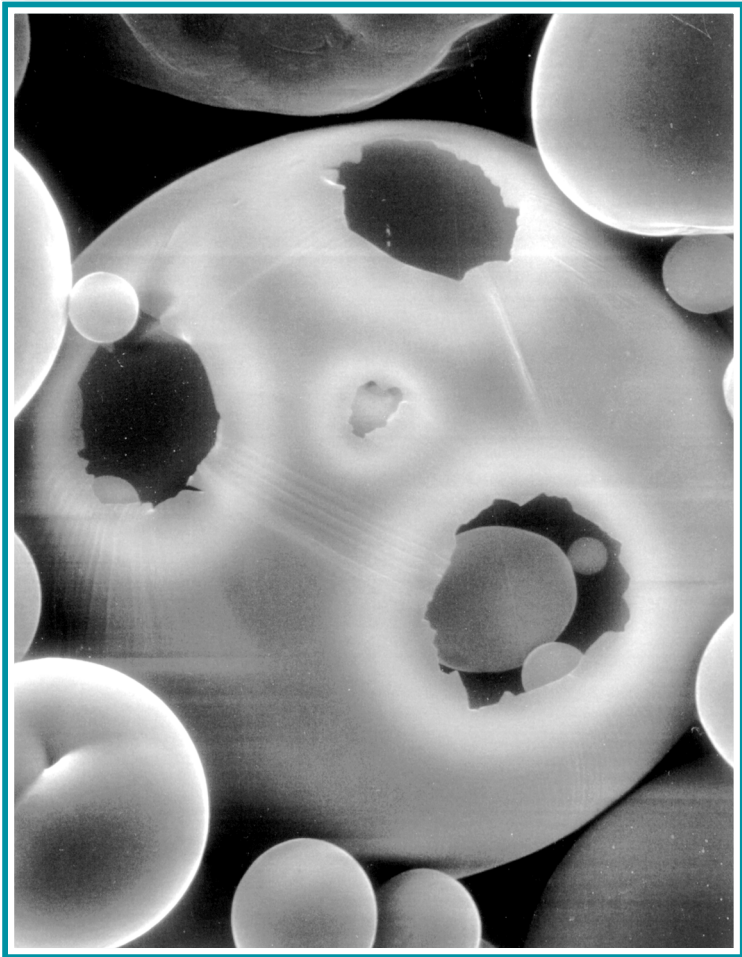


FIGURE 12
 Measured current gain cutoff frequency f_T vs drain voltage. $L_G = 60\text{ nm}$.

References

- ¹J.B. Boos, W. Kruppa, B.R. Bennett, D. Park, S. W. Kirchoefer, R. Bass, and H. B. Dietrich, "AlSb/InAs HEMT's for Low-Voltage, High-Speed Applications," *IEEE Trans. Electron Devices* **45**, 1869 (1998).
- ²B.R. Bennett, M.J. Yang, B.V. Shanabrook, J.B. Boos, and D. Park, "Modulation Doping of InAs/AlSb Quantum Wells Using Remote InAs Donor Layers," *Appl. Phys. Lett.*, **72** 1193 (1998).
- ³J.B. Boos, M.J. Yang, B.R. Bennett, D. Park, W. Kruppa, C.H. Yang, and R. Bass, " $0.1\text{ }\mu\text{m}$ AlSb/InAs HEMTs with InAs Subchannel," *Electron. Lett.*, **34** 1525 (1998). ★



I am Scared
Science-as-Art contest – Third Place winner
Submitted by: Harry Jones and Khershed Cooper

During rapidly spinning cup atomization of liquid metals, encapsulated particles form. Although the centrifugal forces are 200 g's, Stokesian analysis showed that the very fine (<5 microns) particles "sink" very little (few microns) and are trapped by the fresh incoming melt. In tin metal melt, these particles appear as spherical shells surrounding finer particles, as shown in the graphic. They are not desirable, because they tend to increase the mean particle size.

- 107 EX 252 IR Seduction Decoy
W. Humphries and M.A. Snapp
- 109 The Path to Record Kilovolt X-Ray Emission
J. Davis, J.P. Apruzese, K.G. Whitney, J.W. Thornhill, and R.W. Clark
- 112 The Behavior of Deuterium at Extreme Pressures
A.N. Mostovych

EX 252 IR Seduction Decoy

W. Humphries and M.A. Snapp
Tactical Electronic Warfare Division

Technical Concept: A new infrared (IR) decoy, the EX 252 IR seduction cartridge, has been developed and demonstrated. This decoy uses an area-extensive cloud of infrared emitting particles to generate an IR walk-off effect against missile seekers. The decoy is fully compatible with the current Navy MK 36 decoy launching system (DLS). It provides a seduction capability without relying on the relative wind or ship maneuvers to provide separation between the ship and decoy. Figure 1 shows the concept of the EX 252 IR decoy. The decoy creates hot spot movement away from the ship along a path of sequentially deployed IR chaff clouds. As the single device leaves the launcher, it deploys a series of IR chaff clouds that captures the seeker track point and pulls it away from the defending ship. The infrared energy is produced by IR chaff materials that self-heat in air to produce the “cloud” of IR radiation. The initial clouds in the series are composed of high-intensity, quick-reacting IR materials. These clouds turn on, then off, in sequence to create the hot spot movement effect away from the ship. The last cloud in the series is made up of a long-duration IR chaff material that serves as a “keeper” target to hold the seeker track point and keep it from reacquiring the ship.

Background: The EX 252 IR seduction cartridge originated in an NRL/ONR 6.2 exploratory development initiative as a concept for ship self-defense against heat-seeking missiles. Referred to as the Multi-Cloud IR decoy in 6.2 development, the initial proof-of-concept hardware demonstrated the critical ability to produce hot spot movement away from the launcher along a path of clouds sequentially deployed

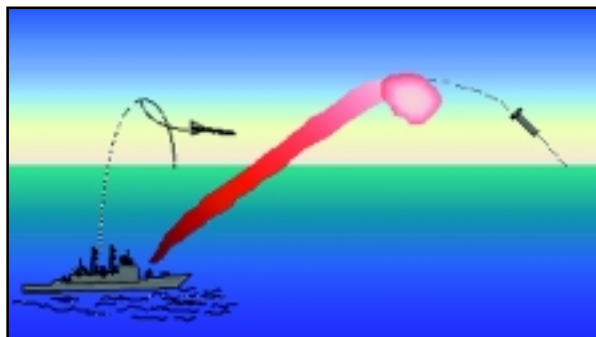


FIGURE 1
EX 252 infrared seduction decoy concept.

from a single mortar-launched shipboard decoy. Following the successful feasibility demonstration, research was conducted to develop specially tailored IR materials that enhanced the IR walk-off capabilities of the decoy. Under the 6.2 effort, the performance of the long-duration keeper target was also improved.

In FY97, funding was received from the ONR Blue Book Insertion Program to ruggedize the 6.2 Multi-Cloud hardware design; conduct safety, reliability, and effectiveness testing; and fabricate a limited quantity of devices for fleet demonstration testing. Under the Blue Book effort, the modified 6.2 hardware was assigned the nomenclature of *EX 252 Mod O IR* seduction cartridge. Figure 2 shows the EX 252 hardware.

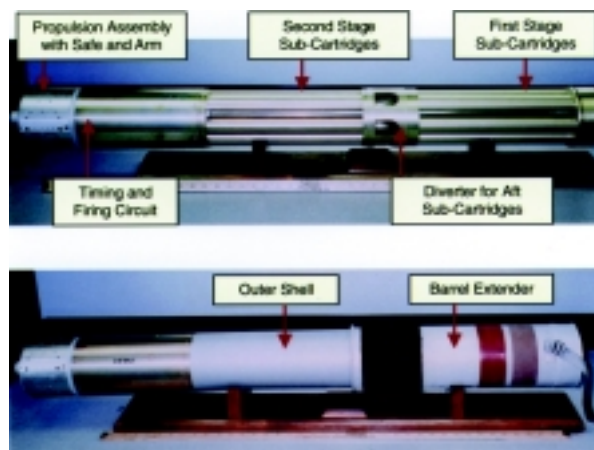


FIGURE 2
EX 252 infrared seduction decoy hardware.

Hardware Description: The EX 252 IR seduction cartridge is 5 in. in diameter, 48 in. long, and weighs 50 lb. When the cartridge is fired from the launcher barrel, a firing signal is inductively coupled to an electrically initiated device inside a firing coil assembly, which ignites the propellant propelling the cartridge out of the tube at roughly 235 ft/s. Once the cartridge exits the barrel, the safe and arm (S&A) bore rider pin is released, allowing the power supply and electronics to turn on. The electronic circuit initiates the deployment of the IR payload sub-cartridges at independent time-delay intervals as the decoy travels along its trajectory.

The EX 252 IR seduction cartridge has two payload sections. The first-stage payload section consists of sub-cartridges loaded with a fast-reacting IR chaff material and are deployed in sequence to achieve walk-off. The rear payload assembly consists of sub-cartridges loaded with a longer duration IR chaff

material. These sub-cartridges are deployed after the walk-off sub-cartridges, and are fired in rapid succession to produce the large-signature, long-duration IR target for track maintenance. When the rear sub-cartridges are fired, the IR payload material is ejected through the aft payload diverter. The EX 252 decoy uses a barrel extender, color coded with a brown and red stripe, to denote Low G explosive and IR payload, respectively. Figure 3 shows infrared imagery taken during deployment/reliability testing of the EX 252 device. The decoy was deployed from a MK 36 launcher. The test was conducted over land and shows the hot spot movement from left to right.

Current Status of Development: The tasks conducted under the Blue Book effort are complete. Hardware design modifications to the original 6.2 design were made to address High Energy Radiation to Ordnance (HERO), reliability, and effectiveness enhancements. The major hardware modifications included:

- Replacing the Launch Acceleration Threshold Sensor Safe and Arm system used in the 6.2 design with the S&A system used on the MK 214 Mod 1 and the MK 216 Mod 0 chaff decoys that are in production for the U.S. Navy and other foreign navies.
- Replacing the custom electronic timing circuit used to fire the impulse cartridges that expel the IR payload material with a modified MK 216 electronic firing circuit. This eliminates the lithium battery pack used in the 6.2 design with

a much safer thermal battery. Additionally, the thermal battery shelf life is significantly longer.

- Replacing the original “turning” cone for the aft payload sub-cartridges with a much more compact design. This enables the use of a MK 216 barrel extender, which results in the “turning” cone being completely covered by the MK 216 barrel extender once the decoy is fully assembled.
- Eliminating the “arming” wire that was used to isolate the firing circuit from the battery until the decoy was loaded into the MK 36 DLS. This function is an integral part of the MK 216 S&A.
- Modifying the design such that it is the same length and weight as a MK 216 distraction chaff decoy. This enables the MK 216 shipping container to be used for shipping the decoy. Additionally, the decoy is compatible with the MK 5 Ready Service Locker (RSL) installed onboard U.S. Navy ships.

In addition to the nonrecurring engineering, other tasks under the Blue Book effort included conducting a limited number of reliability, safety, and effectiveness tests. HERO testing of the EX 252 was conducted by Naval Surface Warfare Center (NSWC) Dahlgren, and results show that no HERO-related problems are anticipated with the EX 252. A limited number of safety tests were conducted at NSWC-Crane and no safety issues were identified. Approval

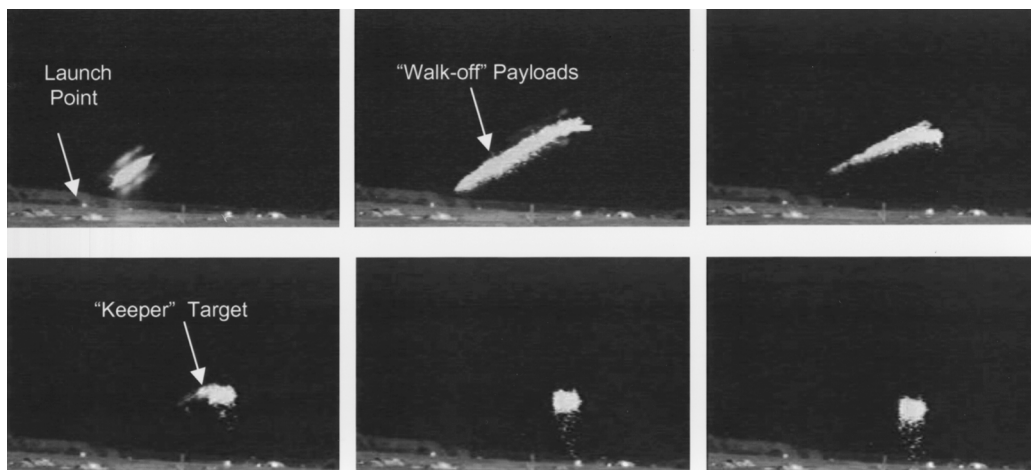


FIGURE 3
Infrared imagery of EX 252 device deployed over land from a MK 36 launcher.

to conduct the at-sea demonstration test has been received from the Weapon System Explosives Safety Review Board (WSESRB) pending the completion of minor action items by NRL and NSWC-Crane. A total of 20 units have been fabricated, and an at-sea demonstration test is scheduled for February 1999.

Summation: As a result of the ONR Blue Book Insertion effort, the Multi-Cloud decoy design has been militarized for fleet use, and 20 devices have been fabricated for an at-sea demonstration test. All technologies for the EX 252 IR decoy have been demonstrated. Twenty EX 252 IR decoy cartridges are to be deployed from a DDG AEGIS destroyer during an electronic warfare exercise in February 1999.

Development of the EX 252 IR seduction cartridge provides the U.S. Navy with an IR decoy for ship self defense against the current IR guided antiship missile threats. The decoy is simple to use in that a single round deploys a series of IR chaff sub-cartridges for track point walk off. The first cloud is placed close to the ship for a close-in seduction capability. Use of longer burning IR materials in the last cloud provides track point maintenance and a distraction decoy capability. In addition, the IR materials used in the decoy have a very low visible output, which can be useful for nighttime or covert operations.

Acknowledgments: NRL Code 5752 provided effectiveness test support. NSWC-Crane conducted safety testing of the EX 252 decoy. NSWC-Dahlgren conducted the HERO analyses. Alloy Surfaces Co., Inc., was responsible for payload/hardware fabrication. Hycor Division of Sippican, Inc., fabricated and integrated the electronics and explosive hardware components. ★

The Path to Record Kilovolt X-Ray Emission

J. Davis, J.P. Apruzese, K.G. Whitney,
J.W. Thornhill, and R.W. Clark
Plasma Physics Division

Introduction: U.S. military systems must be able to function in nuclear and space radiation environments. The end of underground nuclear testing has intensified the need for alternative methods of providing component survivability assurance in the often harsh X-ray environment of nuclear or space radiation. For nearly two decades, we have guided

experimental scientists in both the Departments of Defense and Energy in the quest to produce higher and more realistic fluxes of X rays for component testing. Some of the most useful radiation simulators have been generators that pass megamperes or more of current through wires or gas puffs, heating and compressing the material to dense, copious X-ray emitting plasmas. Recently, our work in analyzing and simulating these plasmas has been instrumental in guiding scientists at Sandia National Laboratories to achievement of record X-ray output in the 1-5 kilo-electron-volt (keV) photon energy range.¹ In addition to the vital testing of military systems, such intense X-ray sources may find application in X-ray lithography, microscopy, fusion, the pumping of short-wavelength lasers, and as sources for fundamental investigation of atomic radiation in plasmas.

Background: The most efficient method presently known to produce X rays of kilovolt or higher energies is to strip Al, or higher atomic number elements, to the one-or two-electron ionic stages called the K-shell, whose spectral lines emit copiously at the desired energies. The first large yields of Al X rays (20 kilojoules (kJ)) were obtained nearly 20 years ago at Maxwell Laboratories in San Diego by passing about 4 megamperes (MA) through 6 Al wires, and were guided by our (somewhat primitive) plasma radiation models of the time. As our analysis and simulation capability grew steadily in scope and realism, the critical roles of wire mass, spacing, number, and initial radius were revealed. Close collaboration with experimental physicists at Physics International Corporation in San Leandro, California, led to the production of 55 kJ of kilovolt (kV) X rays using the same current that previously could produce only 20 kJ. Construction of the Saturn generator at Sandia National Laboratories enabled plasma currents of 7 MA or higher, and, again in collaboration with our team at NRL, Saturn produced 88 kJ of kV X rays.² To produce X rays of 5 kV energy requires the use of Ti wires, which are six times as difficult to strip to the K-shell as Al. Saturn produced 10 kJ of 5-kV Ti photons. When the successful completion of the 16-20 MA Z generator at Sandia was announced, we looked forward to collaboratively designing and analyzing experiments that could shatter previous X-ray records established at currents of 4 and 7 MA.

Kilovolt Al Radiation on Z: For a given mass of wires, our work analyzing previous experiments had established that more and finer ones produced results superior to arrays of fewer and thicker wires.

The many-wire arrays lead to a more uniform, azimuthally symmetric plasma that provides better compression and higher resulting X-ray emissivity. Successful Al experiments on Z used more than 200 wires, producing at least 160 kJ of Al X rays, compared to the 6 wires producing a mere 20 kJ two decades earlier.³ We believe we have also achieved a much more comprehensive understanding of the compressed plasma pinch, which has been invaluable in productively guiding the experiments.³ The X-ray spectrum contains information that, when properly interpreted with detailed radiation models, provides a profile of the temperature and density of the emitting pinched plasma. Figure 4 is the emitted X-ray spectrum obtained from shot no. 70 of the Z generator; Fig. 5 is our calculated spectrum of the

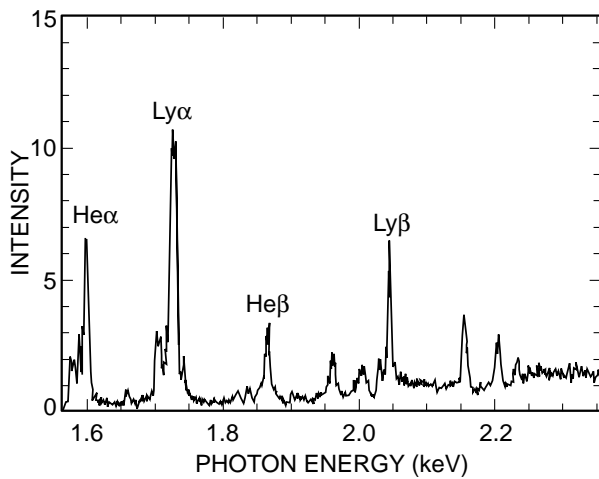


FIGURE 4
Experimental X-ray spectrum time resolved at peak power for shot Z 70.

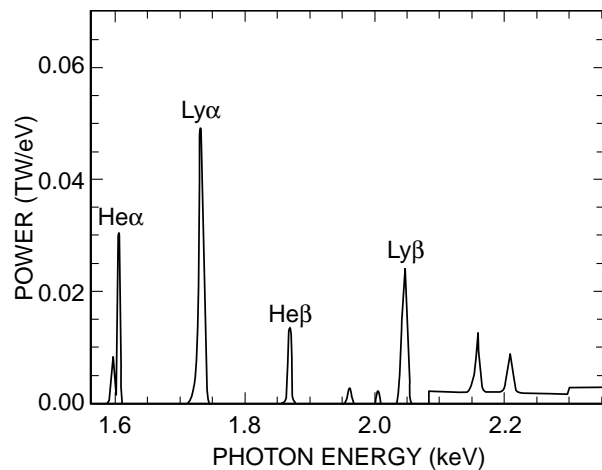


FIGURE 5
Calculated spectrum for shot Z 70.

same shot. The agreement of the two reveals that the plasma electrons were heated to a peak temperature of 19 million degrees K, and the pressure in the plasma interior was 23 million atmospheres.

5 kV Ti Radiation on Z: Based on our extensive previous analyses and experience, we recommended specific Ti wire load configurations for the Z generator. The results: the plasma crashes down on itself at about 1 million miles per hour, converting this kinetic energy of implosion into 1.2 MJ of total radiation and 5 kV photon yields of 125 kJ. This surpasses the previous record by more than an order of magnitude. In Fig. 6, both the experimental (red) and predicted (green) spectral yield in joules/eV are shown as a function of photon energy. The experimental spectrum was measured over the limited range of 1 to 5 keV. The apparent increase in yield at the photon energy of about 3.5 keV is due to backscattered X rays re-entering the spectrograph. The hydrogen- and helium-like resonance lines, Ly- α and He- α lines, are also in reasonably good agreement with the observations. In general, the calculated K-shell and total radiative yields are in good agreement with the observations. Also, a first appraisal of the ion temperature from the spectral line width, after unfolding the instrumental and opacity broadening, gives an estimate of the ion velocity at stagnation of about 60 keV. Figure 7 shows a series of composite plots of the ion and electron temperatures, density, and power density as a function of time and radius. Figure 7 is color coded with the bar code to the right of each insert. Also noted on each

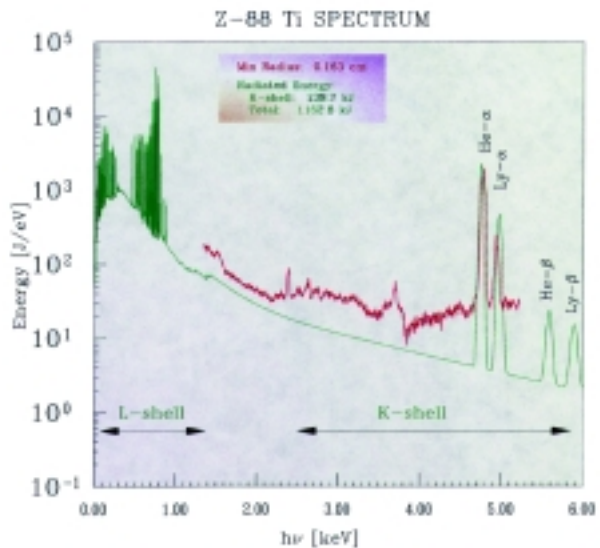


FIGURE 6
Experimental (red) and calculated (green) spectrum for shot Z88.

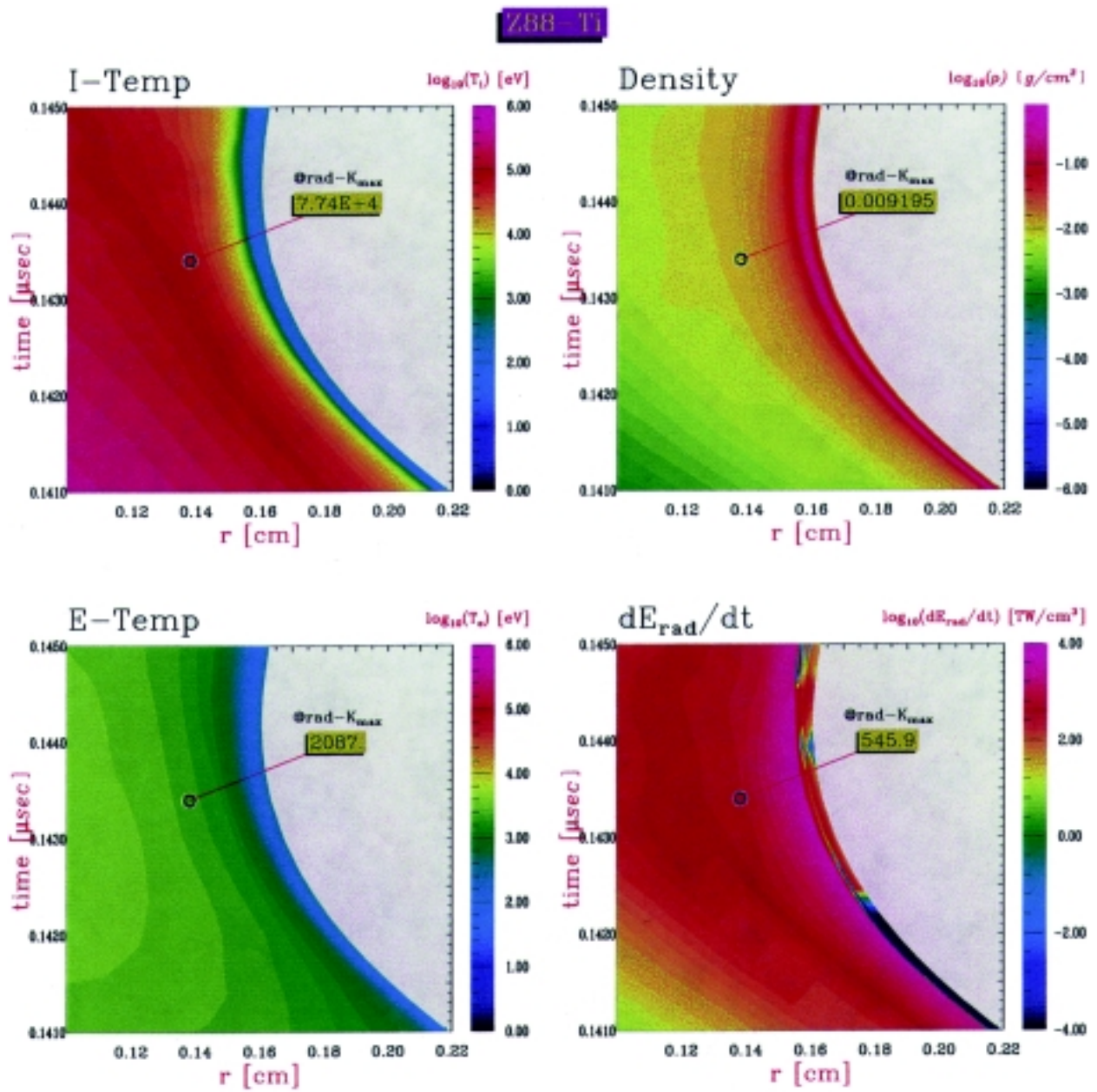


FIGURE 7
Calculated space-time history of the implosion.

insert is the position and time of peak K-shell emission accompanied by the corresponding value of each variable. At peak K-shell emission, the ion temperature is about 77 keV, in good agreement with analyses of the experimental line widths. The ions achieve enormous energies after the bounce, but this occurs where there is very little plasma density and does not significantly affect the energetics of the implosion. However, postimplosion ion dynamics may have a major impact on limiting the K-shell emission. The radiative yields of stainless steel wire loads exhibit similar dynamic behavior with slightly lower yields, in agreement with Radiation Hydrodynamics Branch scaling laws.

Acknowledgment: This work is the result of collaborations between the Plasma Physics Division, Maxwell Physics International Corporation, and Sandia National Laboratories.

[Sponsored by the Defense Threat Reduction Agency and DOE]

References

- ¹J. Davis, R.W. Clark, J.L. Giuliani, Jr., J. W. Thornhill, J.P. Apruzese, K.G. Whitney, C. Deeney, T. Nash, R. Spielman, G. Chandler, and D. Fehl, "L- and K-Shell Emission from Titanium Wire Arrays Imploded on PBFA-Z," *Bull. Amer. Phys. Soc.* **42**, 2052 (1997).
- ²J.P. Apruzese, P.E. Pulsifer, J. Davis, R. W. Clark, K.G. Whitney, J.W. Thornhill, T.W.L. Sanford, G.A. Chandler, C. Deeney, D.L. Fehl, T. Nash, R.B. Spielman, W.A. Stygar, K. W. Struve, R. C. Mock, J.L. Gilliland, D.O. Jobe, J.S. McGurn, J.F. Seaman, J.A. Torres, and M. Vargas, "K-Shell Radiation Physics in the Ultrahigh Optical Depth Pinches of the Z Generator," *Phys. Plasmas* **5**(12), 4476 (1998).
- ³K.G. Whitney, J.W. Thornhill, P.E. Pulsifer, J.P. Apruzese, T.W.L. Sanford, T.J. Nash, R.C. Mock, and R.B. Spielman, "Analyzing Time-Resolved Spectroscopic Data from an Azimuthally Symmetric, Aluminum-Wire Array Z-Pinch Implosion," *Phys. Rev. E* **56**, 3540 (1997).
- ⁴J. Davis, N. Gondarenko, and A.L. Velikovich, "Fast Commutation of High Current in Double Wire Array Z-Pinch Loads," *Appl. Phys. Lett.* **70**, 170 (1997). ★

The Behavior of Deuterium at Extreme Pressures

A.N. Mostovych
Plasma Physics Division

Introduction: At pressures of several million times atmospheric pressure, atoms and molecules become highly compressed and form different states of matter. The distance between atoms becomes smaller than typical atomic dimensions, and the electron orbits of individual atoms and molecules overlap

strongly. This can lead to large changes in the ionization, dissociation, and compressibility of matter. Compression to this extreme is common in strong explosions, proposed laser fusion implosions, and the interior of stars and large planets like Jupiter. In each of these, the overall models of the explosive, fusion, stellar, or planetary systems depend on how matter behaves at high pressure. Existing theoretical models do not agree so experiments are needed to sort out the most important equation-of-state issues. NRL has developed new techniques that permit sensitive tests of the equation-of-state of matter at high pressure. Initial measurements on deuterium samples show large changes in compressibility, confirming by a different technique the earlier work at the Lawrence Livermore National Laboratory.¹

Laser Shocks: To reach pressures of several million atmospheres, we used the Nike KrF laser to drive ultra-uniform shock waves into liquid deuterium.² Figure 8 shows the design of a typical experiment. A miniature target is constructed out of aluminum and immersed in a pool of liquid deuterium at about 20 degrees K. The aluminum plates are micromachined to a thickness less than 0.1 mm and are mounted to an accuracy of 0.0001 mm. The Nike laser irradiates the surface of the plastic-coated aluminum target at high intensities with a 1000 J laser pulse lasting 4 ns. The laser heats the plastic layer to temperatures in the range of 10,000,000 degrees K, generating a high-pressure plasma. A strong shock sets the aluminum in motion and pushes and shocks the liquid deuterium sample to about one million atmospheres, compressing it fivefold.

Experiment: The velocity of the shock in the liquid deuterium sample is measured by recording the times at which the shock exits the aluminum pusher plate and when it collides into the aluminum witness plate. These times are marked by strong emission of light. A high-speed streak camera records the light emission through diagnostic holes in the aluminum witness plate. The two open holes pass light from the aluminum pusher while the third hole is plugged so that it emits light only when hit by a shock. The shock in the deuterium reflects from the aluminum interface and gains strength while a new shock, with the same pressure, propagates through the aluminum witness plate. The known properties of aluminum and a measurement of the shock velocity in the witness plate give us the pressure of the reflected shock in the deuterium. Figure 9 displays the light emission from a typical experiment. The camera collects light from a thin strip on the target surface

FIGURE 8
Schematic of experiment to measure the equation of state of liquid deuterium at pressures above 1 million atmospheres.

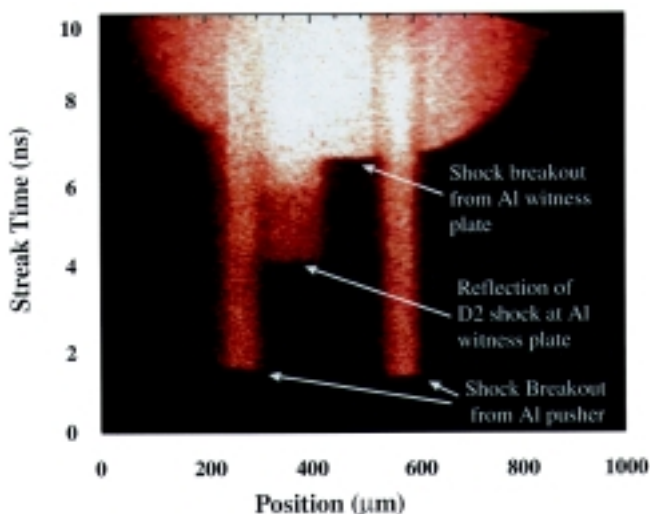
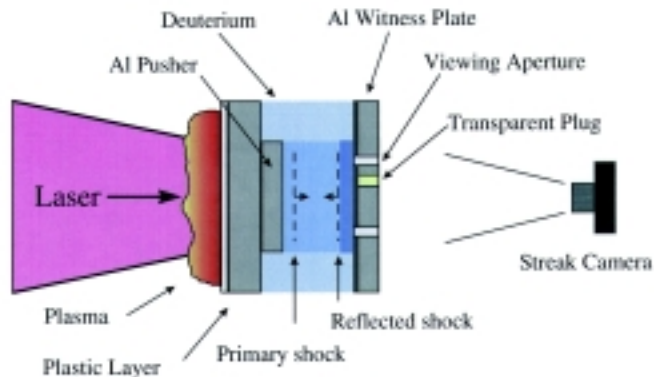


FIGURE 9
Typical streak camera data of deuterium equation-of-state shock experiments.

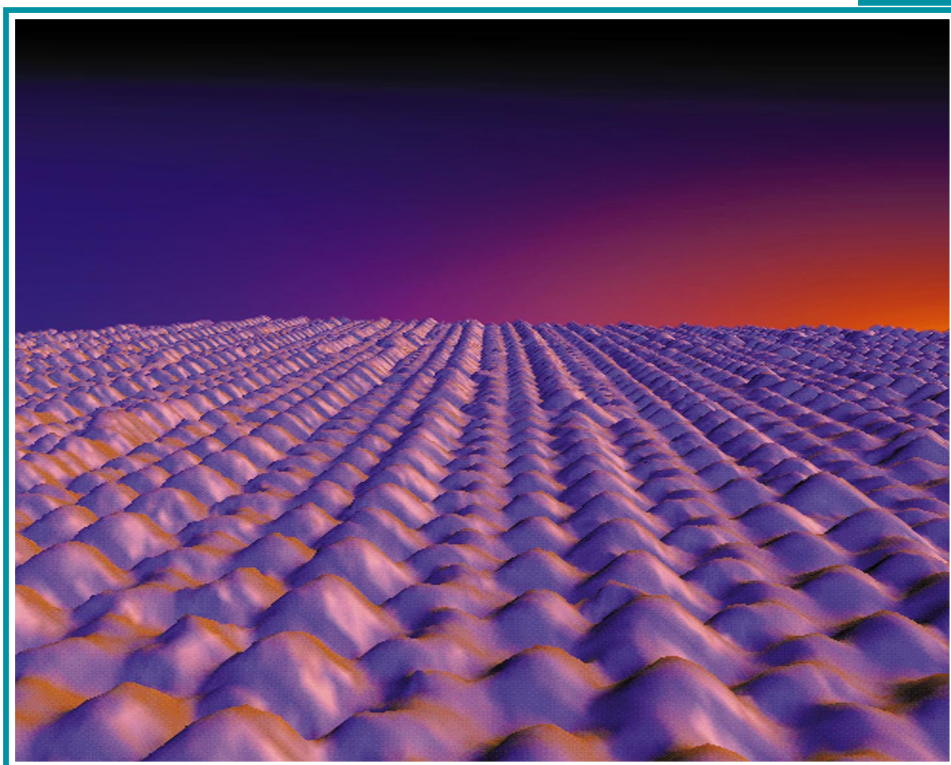
and displays the intensity of this light as a function of time. The emissions from the first shock, through the diagnostic holes, are seen as two thin columns of light. The point of shock reflection is indicated by the emission step in the middle; the emission profile at the right edge corresponds to the shock in the aluminum witness plate. As a result of the additional compression under reflection and our determination of the pressure in the aluminum witness plate, this technique gives us the advantage of enhanced sensitivity to equation-of-state physics issues. Initial measurements show that the compressibility of deuterium at a million atmospheres is strongly enhanced and is consistent with substantial molecular dissociation. This result is important because it helps resolve a standing controversy in the field of high-pressure physics.

Summary: We have demonstrated new techniques to measure equation-of-state properties of matter at high pressure with the Nike KrF laser. The use of reflected shocks gives us high sensitivity and the ability to amplify shock pressures. Initial measurements were demonstrated with liquid deuterium but these techniques can be used to similarly measure the equation-of-state of other transparent materials.

[Sponsored by DOE]

References

¹L.B. DaSilva et al., "Absolute Equation of State Measurements on Shocked Liquid Deuterium up to 200 GPa (2 Mbar)," *Phys. Rev. Lett.* **78**, 483 (1997).
²S.P. Obenschain et al., "The Nike KrF Laser Facility: Performance and Initial Target Experiment," *Phys. Plasmas* **3**, 2098 (1996).★



Sunrise over Si(114)

Science-as-Art contest – First Place winner

Submitted by: Lloyd Whitman, Steven Erwin, and A. Baski

An artistic view of the atomic-scale topography of Si(114) as revealed by scanning tunneling microscopy (STM). (An artificial background and computer-simulated lighting have been added). The tallest rows of atoms are 1.63 nm apart; the atoms visible along these rows are separated by 0.77 nm. Because of the rapidly shrinking size of electronic devices, an understanding of the atomic-scale structure of semiconductor surfaces is vital to the development of future Navy electronics. We have used STM and first-principles theoretical calculations to determine the structure of all Si surfaces oriented between the (001) and (111) planes. A number of new stable surfaces, including Si(114), have been discovered and are being investigated as possible substrates for novel Si-based electronics.

- 117 Gaiter: A Locomotion Control for Distributed Simulation
J.N. Templeman, L.E. Sibert, P.S. Denbrook, R.C Page, and J.A. McCune
- 119 Triangulation Range—Imaging Using Correlation Codes
F. Pipitone and R. Hartley
- 120 Automating CIC Communications for Reduced Manning
A. Schmidt-Nielsen, L.B Achille, and K.G. Schulze

Gaiter: A Locomotion Control for Distributed Simulation

J.N. Templeman,¹ L.E. Sibert,¹ P.S. Denbrook,²
R.C. Page,³ and J.A. McCune³

¹*Information Technology Division*

²*Independent Software Developer*

³*ITT Systems Corporation*

The Human-Computer Interface Group is developing a new virtual locomotion technique named Gaiter that allows a person to move in a natural way through a virtual environment (VE). Our approach adopts walking in place as the basis for virtual locomotion. Walking and running in place are expressive gestures that exhibit many of the attributes of a natural human gait. People feel comfortable doing it, and in-place stepping allows them to turn and change their posture in a natural manner.

Virtual locomotion is essential for constructing individual combatant simulators in which soldiers interact directly with the surrounding environment. We are developing Gaiter for use in training Marines in military operations in urban terrain (MOUT) exercises. As part of a comprehensive team simulator, Gaiter would allow Marines to practice techniques and team coordination to enhance their tactical expertise. Textbook concepts like the effectiveness of fire and movement, cover and concealment, and overlapping fields of fire can be experienced firsthand under a variety of conditions. The Marine MOUT training instructors who have tried Gaiter appreciate the full range of motion and effects facilitated by the control.

Approach: Our approach to virtual locomotion is to approximate the affordances and constraints of natural locomotion. A person afoot has a high level of maneuverability over a wide range of terrain at speeds limited by that person's strength and agility. Walking and running are compatible with other actions, including turning the head to look around and freely using both arms for manipulation. Similarly, Gaiter allows a user to make coordinated head, arm, and leg movements to look, move, and aim in concert. The control gestures also allow other body movements, including pivoting on one or both feet, actual steps, and postural changes such as bending, kneeling, and going prone. We are tuning the system so users walk and run at a rate, precision, and level of effort that is consistent with natural locomotion.

The ability to realistically simulate natural locomotion is a key element missing from most of today's

combined arms simulations. A number of developers have tried other approaches, primarily mechanical motion platforms that include one- and two-dimensional treadmills, but the systems introduce artifacts into the interaction. These platforms are quite complex, bulky, and expensive; and people have trouble maintaining their balance when the surface beneath their feet accelerates.

Implementation: With Gaiter, the user walks in place to walk through the VE. The instrumentation worn by the user is simple and unencumbering (Fig. 1). Our current implementation uses an Ascension Wireless 6 degrees-of-freedom magnetic tracking system, with a tracker at the waist to register the direction of the body and a tracker under each knee to measure the extent of knee motion. Force sensors by Interlink are positioned under the ball and heel of each foot in the user's shoes to register contact forces underfoot. The ground reaction force information is multiplexed into the wireless data stream that is transmitted to the Ascension base station. The base station is attached to a local ethernet network that includes the graphics rendering computer and Gaiter controller. The Gaiter pattern recognition software runs on a Pentium PC under Windows NT. It distinguishes actual steps, steps to turn, and in-place steps (Fig. 2). The algorithm is based on a generalized classification of human gait developed by our team from a study of the biomechanics of human walking. What makes Gaiter unique is its use of the direction, extent, and timing of each stepping leg motion to direct virtual locomotion. The result is a system that is naturally easy to use.

The visual image of the individual combatant simulator is generated on a Silicon Graphics, Inc. Onyx2 and projected on a V8 head-mounted display (HMD) from Virtual Research Corporation. The HMD presents a dynamic perspective image of the visual environment as the user moves about. Cable management is required because the HMD is tethered to the graphics rendering computer.

Features of Gaiter: Gaiter provides virtual motion in any direction, in a natural body-centric coordinate system. The interface involves the whole body, including the user's head, arm, and leg "end effectors," not just the visual and aural senses. This allows people to use their reflexes to direct their body in response to external stimuli and makes the interactive simulation more immersive and realistic. Gaiter is compatible with other actions such as manipulating or aiming at virtual objects, and the system can



FIGURE 1
 Gaiter: A sensor-based locomotion control that allows the user to move through VE by walking in place. The motion of the legs is characterized by force sensors placed on shoe insoles and 6 degrees-of-freedom trackers attached to the knees. Additional sensors attached to the waist and head track the motion of the body and viewpoint.

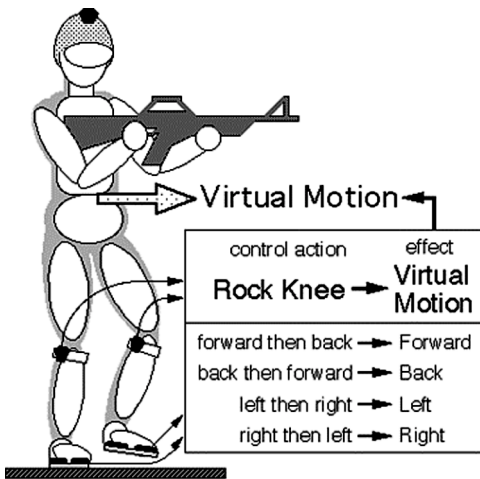


FIGURE 2
 Gaiter: The motion of the legs is used to move the body VE.

be tuned to preserve the attributes of natural locomotion. By linking optic flow directly to leg movement, the Gaiter interface feels like a simulation of walking rather than an indirect control over locomotion.

Future Developments and Challenges: We will experimentally compare Gaiter with common VE controls: one that the user moves where the head is pointed, and the other a desktop system controlled using a joystick. The experimental tasks involve stylized versions of those used in Marine training (running between cover, firing at pop-up targets while moving toward a goal, and clearing a series of rooms of enemy units). Future work includes adding more realistic collision handling based on natural constraints, developing avatar for self reference and team coordination, and networking for a multiuser training environment.

[Sponsored by ONR]



Triangulation Range—Imaging Using Correlation Codes

F. Pipitone and R. Hartley
Information Technology Division

Introduction: Imaging sensors have been vital in such computer vision applications as the recognition and localization of objects, the generation of computer models of objects, automatic inspection, autonomous vehicle navigation, and biometrics. Range-imaging sensors are particularly useful for problems involving the shapes of surfaces in the three-dimensional (3-D) world. A range image is a 2-D array of numbers that give the depth of a scene along many directions from a sensor. Instead of measuring the brightness of many points in a scene, as in a TV camera, the range sensor essentially measures the locations of visible surface points in 3-D space. In recent decades, a wide variety of range instruments have been built,¹ falling into two broad categories, triangulation and time-of-flight. Our instrument is in the first class. Measures of their performance include range accuracy, pixel rate, frame rate, motion tolerance, angular field of view, minimum and maximum measurable range, and angular pixel separation. Structured light triangulation systems such as ours use parallelism to achieve high speed and accuracy. Our design (patent pending) is particularly fast and accurate and can be built at very low cost.

The General Concept: We have conceived and prototyped a new range-imaging sensor consisting of a detector (typically a digital camera) and a structured-light projector (Fig. 3). The projector produces a nonuniform pattern of illumination stripes that is moved across the scene at a nominally constant angular velocity, during which several frames are acquired by the camera. This allows the reconstruction of one frame of range data. The projector consists of a thin light source (xenon tube and slit) on the axis of a turntable and a binary mask conforming to a cylinder coaxial with the turntable. The mask has alternate black and clear stripes parallel to the axis, forming a DeBruijn sequence. This has the key property that a few regularly spaced samples of any region of the code form a unique vector, so that we can tell where in the code they came from. The pattern can be projected over a deep field by analog smoothing of the binary pattern. This can be done without lenses by illuminating the binary mask with a thick line source, and the smooth function allows substripe accuracy. To produce range data, a computer pro-

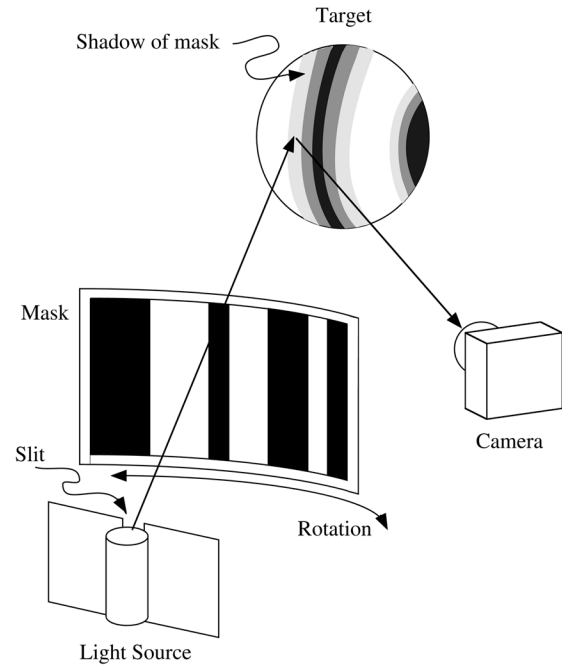


Figure 3
 Simplified schematic illustration of system.

gram generates one range point for each photodetector element by determining which place in the code the sequence of samples from a given photodetector element matches. Range is a monotonic function of this position. Essentially, range is computed by determining which plane containing the axis of the projector is being observed by a given photodetecting element. Then the line of sight of that element intersects that plane at a unique place, which is the location of the desired range sample. This system can be scaled to accommodate a wide range of depth of field and angular field.

Experimental Work: We have built two prototype systems based on Fig. 3. The first (described in detail in Ref. 2) is the basis of the following results. A second (Fig. 4) is a more robust version intended for a mobile robot and for experiments in high-accuracy object recognition and pose estimation. Our prototype uses a 512×512 Dalsa camera with a 12.5 mm lens. The DeBruijn sequence is of Order 6, so that six camera images generate one range image:

111111000001000011000101001111010001110010010110111011001101010

Here, 1 represents opacity and 0 represents transparency. For optimal smoothing, the width of one mask stripe (one bit), now 0.5 mm, is about one-half

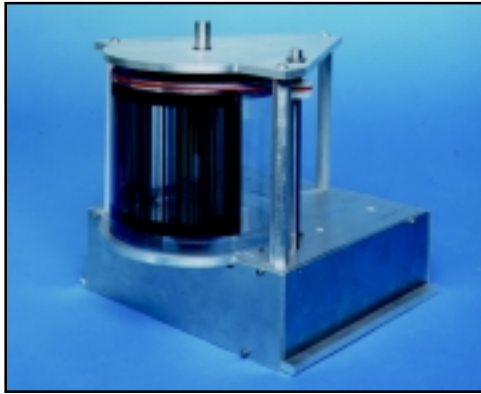


Figure 4
The second prototype projector.

the light source width. The baseline distance between camera and projector is currently approximately 275 mm. Other geometric design parameters include the camera and lens parameters and the distance between light source and mask (now 95 mm). Figure 5 shows a range image produced by the prototype system, which is shaded to highlight range error. The statue is 11 cm in height. The uniform region to its left is in the shadow of the structured light; range data are not available there.

Conclusion: We have built, tested, and submitted for patent a triangulation range-imaging sensor based on a moving structured-light code pattern. A range accuracy of approximately 0.1 mm was



Figure 5
Shaded rendering of a range image.

achieved at a standoff of about 1 ft. Only six frames of camera data were needed to form a range image. The cost is extremely low. The main cost is for the camera and computer, which are standard off-the-shelf components whose costs are dropping rapidly. The system is easily reconfigured to a different scale. Potential applications include robot navigation, industrial robot vision, and biometrics.

[Sponsored by ONR]

References

¹P. Besl, "Active, Optical Range Imaging Sensors," in *Machine Vision and Applications*, Vol. 1 (Springer-Verlag, 1998), pp. 127-152.
²F. Pipitone and R. Hartley, "Moving-Correlation-Code Triangulation Range Imaging," *Proceedings of Conference on Sensors and Controls for Advanced Manufacturing*, Oct. 1997, SPIE, Pittsburgh, PA, Vol. 3201. ★

Automating CIC Communications for Reduced Manning

A. Schmidt-Nielsen and L.B. Achille
Information Technology Division

K.G. Schulze
U.S. Naval Academy

Verbal communications are used to coordinate team decision making in the Combat Information Center (CIC) on Navy ships. In times of stress, many people talking at once can overload the communication net. This research is an effort to identify the types of communication tasks that are best suited for automation. Originally intended to reduce communication load in larger teams, the results are timely for reduced manning efforts. With smaller CIC teams, many functions currently performed by humans will have to be automated.

In collaboration with the U.S. Naval Academy, we developed a networked Wizard-of-Oz experiment to study the effects of automating aspects of CIC team communications. Previous work that classified CIC communications according to function¹ was used to select two types of communication (acknowledgments and attribute information) for study. The task is a one-person version of a team decision-making task, based on a similar task developed by Hollenbeck and Ilgen.²

Experiment Description: The participant plays the role of the Anti-Air Warfare Officer and collects information about eight attributes (altitude, corridor,

radar) of two targets, determining the threat level of each in a two-tiered decision-making process. The team members from whom the information is collected are simulated on a second networked computer (controlled by a human, the “wizard”). The responses can be verbal or text, and acknowledgments can be verbal or a button light. Delays are included to simulate that the information might not always be immediately available. Time-stamped log files track everything the participant and the wizard do during the experiment, allowing us to collect and analyze performance data—completion time, correct decisions, and repeated requests.

A study was conducted using 60 volunteers, naval officers stationed at the U.S. Naval Academy. Although participants knew that they were interacting with a computer simulation, it was clear from their comments that they responded as though they were interacting with two officers.

Correct Decisions: Communication mode had very little effect on the number of correct decisions (Table 1), and the number of correct decisions also did not change systematically over trials. This is a positive result and indicates that the officers were able to make good decisions even under conditions in which communicating required more time and effort.

Completion Time: The time to complete the task was faster for text responses than for verbal responses (Fig. 6). The verbal response mode caused users to take extra steps that were not needed in the computer response mode. Most participants in the verbal response conditions took extra time to type in attribute values and looked up the associated threat levels only after they had collected all attribute data. The task could be performed accurately without extra typing by selecting the appropriate threat level for each attribute value. As is the case in real life, it also takes longer to say than to display responses.

TABLE 1
Total Number of Correct Responses and Standard Errors (S.E.) for Each Group

Acknowledge Response	Computer		Verbal	
	Mean	S.E.	Mean	S.E.
Text	18.00	0.414	17.13	0.380
Verbal	17.80	0.380	17.00	0.602

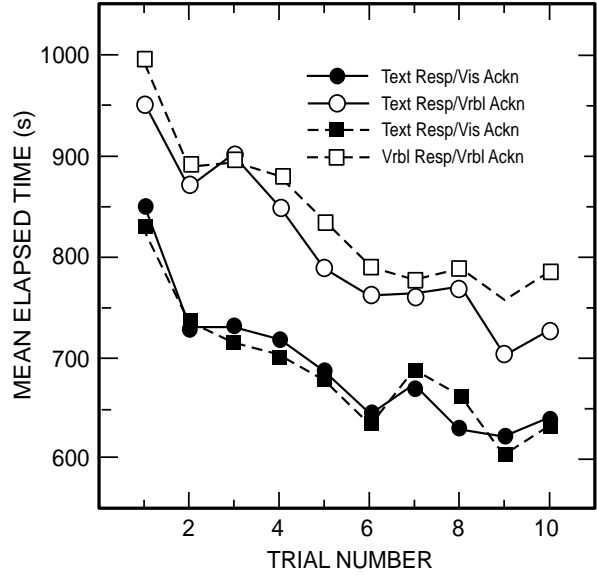


FIGURE 6
Average time to complete the task over trials for each group.

Whether acknowledgments were made verbally or by computer had little effect on the time it took to complete the task.

Another common source of delay is repeating a request. Text responses and, when the response was delayed, verbal acknowledgments resulted in fewer repeated requests (Fig. 7).

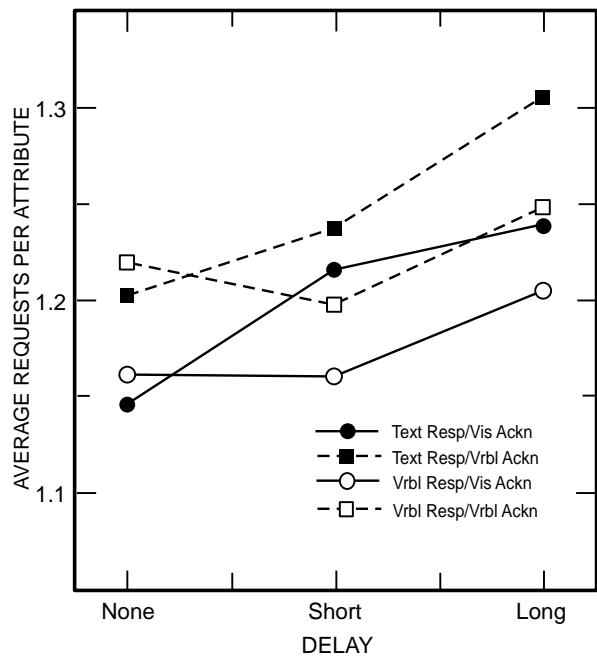


FIGURE 7
Average number of requests per attribute for each of the four groups.

Strategies: Participants were told to deal with the most threatening target first. Communication mode did not significantly affect the order in which decisions were made, but the computer response groups were more likely to request information on more than one attribute at a time.

Conclusions: This experiment studied the effects of communication mode on information gathering and decision making. A study using naval officers showed no significant change in decision accuracy, but decision time and strategies were significantly affected by communication mode.

- Text presentation of numerical attribute information reduced task completion time, and this type of communication is a good candidate for automation.
- Presenting numerical information in text or visual form helps reduce memory load and reduces the need for repeated requests.
- When there is a delay before a response is received, acknowledgments are crucial and should be in a form that will be paid attention to. Unless auditory overload is a problem, verbal acknowledgments are preferable.

The results of this study will help determine the feasibility of automating certain information that is currently delivered verbally. A second study using civilians will compare the performance of civilian users with that of naval officers. The outcome of the second study will have implications for the Navy's use of civilians in research to test technology intended for future Fleet use.

Acknowledgments: Funding for this project was provided by SPAWAR and by the Office of Naval Research (ONR). The authors thank CAPT F. G. Farrell for serving as a naval consultant during the development of this project; Dr. Manuel Pérez-Quiñones for valuable Macintosh assistance; and Thomas R. Schulze and Derek Brock for recording the verbal responses.

[Sponsored by ONR and SPAWAR]

References

¹L.B. Achille, K.G. Schulze, and A. Schmidt-Nielsen, "An Analysis of Communications and the Use of Military Terms in Navy Team Training," *Mil. Psychol.* **7**, 95-107 (1995).
²J.R. Hollenbeck, D.J. Segó, D.R. Ilgen, D.A. Major, J. Hedlund, and J. Phillips, "Team Decision Making Accuracy Under Difficult Conditions: Construct Validation of Potential Manipulations Using the TIDE Simulation," in *New Directions in Team Measurement*, M. Brannick, E. Salas, and C. Price, eds. (Jossey-Bass, San Francisco, 1995), pp. 111-136. ★



Microscopic Features of Alkyl Ether of Tartaric Acid Formed by Self-assembling Process

*Science-as-Art contest – First Place winner
Submitted by: Alok Singh and Jean-Marie Lehn*

The physical properties and microscopic texture of a material are dependent on the nature of their molecular building blocks and their arrangement at the molecular level. Chemists design and make interesting materials by learning through relationship between chemical structures and the arrangement of those molecules in the morphologies they form. This picture is a result of one such investigation where polycrystalline powder of chemically altered tartaric acid was examined at 90 °C under an optical microscope. Polymolecular association took place involving carboxylic acid groups of tartaric acid.

- 125 Protein Crystal Growth Cessation and Reinitiation
M.A. Perozzo and J.H. Konnert
- 127 Novel Aerogel Materials
D.R. Rolison and C.I. Merzbacher
- 128 A New Way to Measure Spin Polarization
R.J. Soulen, Jr., M.S. Osofsky, B. Nadgorny, and J. Byers
- 130 Computational Screening of Candidate Thermoelectric Materials
D.J. Singh
- 132 Disorder-Induced Colossal Magnetoresistance
R. Stroud, V. Browning, J. Byers, V. Harris, and W. Fuller-Mora

Protein Crystal Growth Cessation and Reinitiation

M.A. Perozzo and J.H. Konnert
Laboratory for Structure of Matter

Background: The technique of choice for determining the three-dimensional structure of a protein at atomic resolution is X-ray diffraction crystallography. In this technique, a single protein crystal is impinged with a monochromatic X-ray beam and the diffraction that arises from the interaction of the X rays and the crystal are collected for all unique crystal orientations. Because the diffracted X rays cannot be refocused to form an image of the structure, theoretical methods were developed at the Naval Research Laboratory in the 1950s and early 1960s and resulted in the Nobel Prize. These methods provided the breakthrough to obtaining molecular models.¹⁻³ In the past 30 years, thousands of protein structures have been solved in this way. Information obtained from these structures has led to the elucidation of “molecular diseases” such as sickle cell anemia, the genetic engineering of new proteins with specific functions, and an understanding of the mechanism of action of large molecular complexes such as the photosynthetic reaction center of green plants. Structural information also forms a foundation for the development of biosensors, whereby the proteins can be placed in a substrate and used to assay for the presence of disease-causing agents, toxins, or energetic materials.

The protein crystals of sufficient size and quality needed for a structure determination are prepared using trial and error methods. Conditions are sought that will produce crystals by slowly approaching protein supersaturation in the presence of various salts, buffers, or organic molecules in an aqueous medium. Each protein behaves differently, and when crystals are obtained, it is often only after hundreds of unique experiments have been performed. We are studying the process of protein crystal growth using the atomic force microscope (AFM) to gain better control in the routine production of high-quality crystals.

Atomic Force Microscopy: Atomic force microscopy is a technique used to obtain surface structural information. The height profile of an area is measured by scanning successive lines across the sample with a flexible cantilevered tip. The deflection of a laser beam reflected off the cantilever is kept constant by means of a feedback loop, and the

height changes necessary to do this are recorded as the relative height of the sample. Surface structures can be imaged with height resolutions as good as 0.1 nm. Our laboratory has used the AFM to measure growth rates of lysozyme crystals as well as to obtain details regarding the orientation of molecules at the surface.⁴ The regular steps associated with the crystal growth unit can be observed as the crystal continues to grow during imaging. Defect formations such as screw dislocations are observed as well. Figure 1 shows a growing screw dislocation spiral on the [110] face of lysozyme. The step height of the ledges corresponds to two molecules thickness: 5.6 nm.

Crystal Growth Cessation: The reason crystals sometimes only grow to a limited size and then stop is not well understood. Crystals were observed by use of the AFM over the course of several days as the surface growth changed from regular, repeating growth steps to a roughened surface, and finally stopped growing altogether. It was found that the surface of the growing crystal was smooth and contained characteristic growth steps corresponding to the growth unit thickness. Upon growth cessation, the surface no longer had the smooth regular repeat of molecules aligned in an organized array. Instead, the area was roughened and bumpy. Fresh protein solution would not induce growth on the roughened surface, indicating that it is the surface, not the solution, that inhibits further growth.

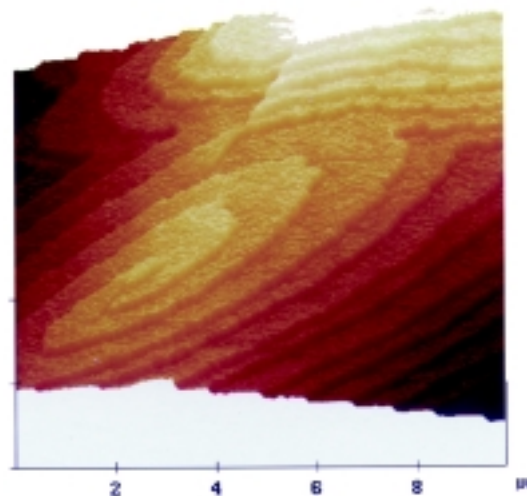


FIGURE 1
Screw dislocation on the [110] face of a lysozyme crystal. The steps correspond to one growth unit of 5.6 nm in height. The height dimension is exaggerated to emphasize detail.

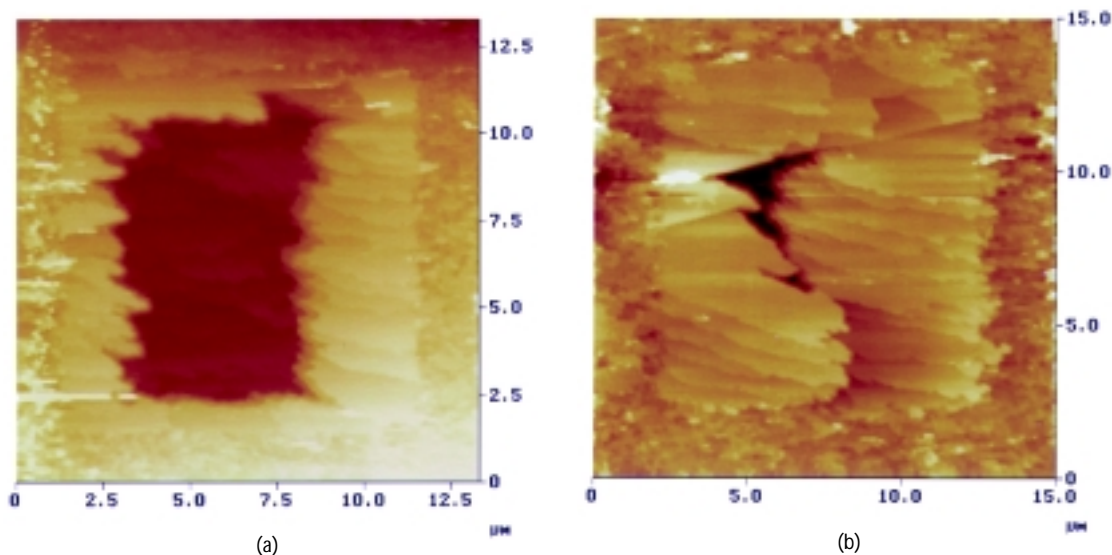


FIGURE 2
Surface etching of the [110] face of a lysozyme crystal that had stopped growing. Etching of a $10 \times 10 \mu\text{m}$ section of the roughened surface resulted in new growth in that area: (a) 33 minutes and (b) 114 minutes after etching. The bottom of the etched pit (orange) is approximately 60 nm lower than the crystal face.

Crystal Etching: To obtain the smooth surface conducive for crystal growth, the AFM tip was used to scrape away an area of roughened surface. A force of 30 nN was applied downward onto the surface, while the linear scan rate was increased from 5 to 10 Hz. The force was large enough to remove several layers of crystalline and noncrystalline material. Figure 2(a) shows the $10 \times 10 \mu\text{m}^2$ area etched from the [110] face of lysozyme crystal 33 minutes after etching. The surrounding crystal surface shows the roughened area where no growth occurred. The crystal was etched to a depth of 60 nm, corresponding to roughly 10 growth layers. Growth layer ledges can be seen in the surface of the etched pit.

Regrowth: Growth on the etched surface begins immediately. In Fig. 2, growth is seen to occur from the pit sides and to fill the pit from the opposing walls toward the center. Figure 2(b) shows the same surface 81 minutes later. The pit is filled except for a small volume, which still maintains the same initial depth of 60 nm. Note that no new growth occurs on the roughened surface where etching was not performed.

Conclusions: Crystals stop growing for various reasons: protein in solution may be depleted, the

conditions in solution may change, or material may add to the surface in a manner that inhibits further growth. In the case of lysozyme, the appearance of a layer of noncrystalline material on the surface of less than 12 growth units in thickness is enough to stop growth. By replacing the growth solution and removing a layer of the crystal that shows no crystal step ledges, we are able to reinitiate crystal growth. A practical application of this method could be developed whereby chemical means of removing this layer of the outer surface of nongrowing crystals would induce further growth.

[Sponsored by NASA]

References

- ¹J. Karle and H. Hauptman, "The Phases and Magnitudes of the Structure Factors," *Acta Cryst.* **3**, 181 (1950).
- ²I. Karle, H. Hauptman, J. Karle, and A.B. Wing, "Crystal and Molecular Structure of p,p'-dimethoxybenzophenone by the Direct Probability Method," *Acta Cryst. (Note)* **10**, 481 (1957).
- ³J. Karle and I. Karle, "The Symbolic Addition Procedure for Phase Determination for Centrosymmetric and Noncentrosymmetric Crystals," *Acta Cryst.* **21**, 849 (1966).
- ⁴J.H. Konnert, P. D'Antonio, and K.B. Ward, "Observation of Growth Steps, Spiral Dislocations and Molecular Packing on the Surface of Lysozyme Crystals with the Atomic Force Microscope," *Acta Cryst.* **D50**, 603-13 (1994). ★

Novel Aerogel Materials

D.R. Rolison
Chemistry Division

C.I. Merzbacher
Optical Sciences Division

Aerogels are a class of materials composed of approximately 10-nm particles connected in a highly porous (80-99% by volume), three-dimensional network. Aerogels combine being and nothingness (i.e., particles and pores), which is the key to their unique properties. Because aerogels provide both high surface area (up to 1000 m²/g) and highly open space, they are especially well-suited to catalytic and sensing applications, where rapid transport of reactants (or detectable species) and large, accessible surface areas are critical to performance. We are developing aerogels as advanced materials for use as high-surface-area electrodes, catalysts, battery structures, and advanced thermoelectric materials, and as architectures around which to design chemical, physical, and optical sensors.

Preparing Composite Aerogels Using a Nanoglue: The most widely studied aerogel composition is silica, which is prepared by supercritically removing the liquid from a wet silica gel.¹ Over the past year, our research team has provided design flexibility and expanded the range of aerogel properties by using the gel's building block (colloidal silica sol) as a "nanoglue" to trap suspended particles or colloids of a second phase as the colloidal silica forms the network of the wet gel. This technique has been used to make composite aerogels of silica plus a range of physically and chemically diverse particulates (Fig. 3). To date, these include: 5-100-nm gold colloids (Fig. 4), ~2-nm platinum colloids, photoconductive titanium dioxide colloids or aerogel powder, 1- μ m-sized metal or semiconductor particles, electron-transfer-modified zeolites, polymers, and conductive carbon blacks.

When the second phase of the composite is present above a certain threshold, its transport characteristics (e.g., conduction of electrons) are imparted to the composite aerogel, even though it retains the low density and openness characteristic of pure silica aerogels. Although the carbon-silica composite aerogel seen in Fig. 3 is ~80% open space, its blackness blocks transmission of He-Ne laser light, even though a pure silica aerogel transmits the beam of laser light with minimal scattering (Fig. 5).

Aerogels as a Tool to Control Materials Properties: Our synthesis of ruthenium oxide-based aerogels permitted an unambiguous assignment of mixed electron/proton conductivity for the surface of technologically important RuO₂ (which is used for the commodity production of chlorine gas). By expressing RuO₂ as an aerogel, we decoupled the dominating electronic conductivity of the bulk oxide from the mixed conductivity of its amorphous surface.² The surface character of a material is amplified by the high surface-to-volume ratio of aerogels, so that the aerogel solid behaves in ways distinct from the bulk solid. We see aerogels as a new tool to isolate, stabilize, characterize, and ultimately design the surfaces of electrically conductive metal oxides. These materials are of critical importance in batteries, fuel cells, and supercapacitors.

Determining Properties on the Nanoscale: To characterize these novel nanoscale materials, a combination of techniques has been brought to bear, including transmission electron microscopy, X-ray diffraction, microprobe Raman spectroscopy, X-ray photoelectron spectroscopy, impedance spectroscopy, voltammetry, gas adsorption and chemisorption, and small-angle neutron scattering (SANS). Although all of these techniques are widely used, researchers at NRL have been the first to adapt the technique of "contrast-matching" SANS for independent structural characterization of two solid phases in a composite aerogel. The pores of the aerogel are filled with a H₂O/D₂O mixture that matches the

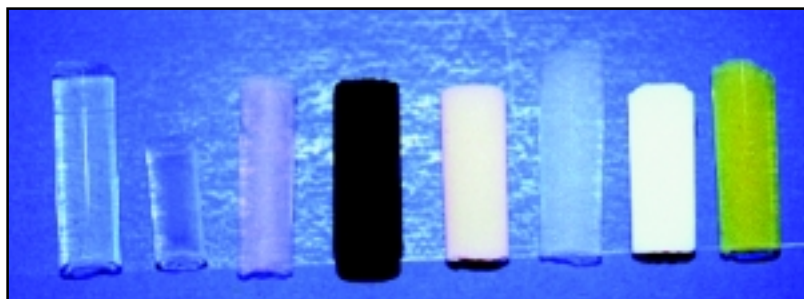


FIGURE 3
Silica-based composite aerogels (from left to right): SiO₂; colloidal Pt-SiO₂; colloidal Au-SiO₂; Vulcan carbon-SiO₂; Fe^{II}(bpy)₃-modified zeolite NaY-SiO₂; TiO₂(aerogel)-SiO₂; Degussa titania-SiO₂; and PMMA-SiO₂.

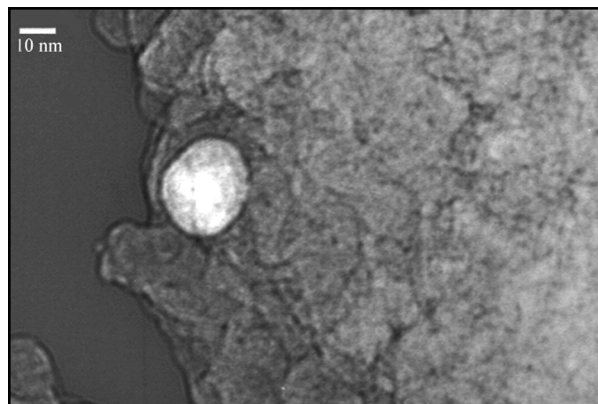


FIGURE 4
Transmission electron micrograph of a ~20-nm gold colloid in silica aerogel.

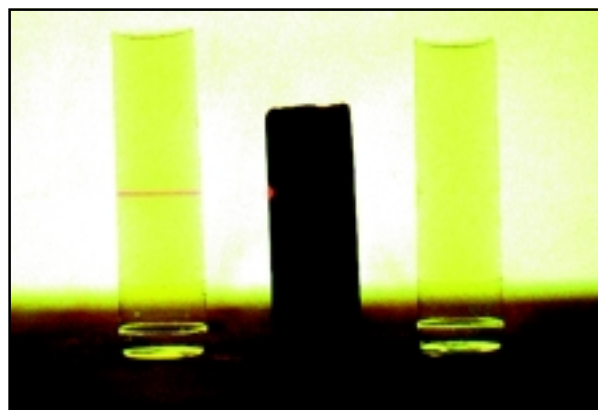


FIGURE 5
Preparing black materials from being and nothingness: He-Ne laser (from left) irradiating air, SiO₂ aerogel, and Vulcan carbon-SiO₂; no light is transmitted through the carbon-SiO₂ composite aerogel to the SiO₂ aerogel on the right, even though the carbon-SiO₂ composite aerogel is 80% open space.

neutron scattering properties of one phase. The observed scattering is therefore solely due to the unmatched phase. The scattered intensity as a function of wavevector reveals morphologies on the nanoscale and distinguishes smooth vs rough (or fractal) structures. Contrast-matching SANS studies have also shown that aerogels with ~15% the density of the bulk material can be re-wetted, even in high-surface-energy liquids such as water, without structural damage to the aerogel.³ This assurance of structural stability permits development of aerogel-derived catalysts, electrode materials, and sensors for liquid-phase applications.

The Promise of the Nothingness of Aerogels: Real-world surfaces are actually nanoscale domains that differ from the underlying bulk and that

dictate many of the technologically most relevant catalytic and electrical properties of the material. Our research program on aerogels demonstrates how a fundamental effort to design and characterize nanostructured platforms leads to improvements in the properties of technologically relevant materials and the design of new materials.

[Sponsored by DARPA and ONR]

Acknowledgments: Special acknowledgments to our postdoctoral associates, K.E. Swider, J.W. Long, M.L. Anderson, and V.M. Cepak; our visiting faculty, N. Leventis and J. Fontanella; our undergraduate research students, C.A. Morris, R.A. Bernstein, J.V. Ryan, and M. Korwin; our NRL colleagues, R.M. Stroud, A.D. Berry, and P.L. Hagans; and our NIST colleague, J.G. Barker.

References

- ¹N. Hüsing and U. Schubert, "Aerogels—Airy Materials: Chemistry, Structure, and Properties," *Angew. Chem. Int. Ed.* **37**, 22-45 (1998).
- ²K.E. Swider, C.I. Merzbacher, P.L. Hagans, and D.R. Rolison, "Synthesis of Ruthenium Dioxide-Titanium Dioxide Aerogels: Redistribution of Electrical Properties on the Nanoscale," *Chem. Mater.* **9**, 1248-1255 (1997).
- ³C.I. Merzbacher, J.G. Barker, K.E. Swider, and D.R. Rolison, "Effect of Re-wetting on Silica Aerogel Structure: A SANS Study," *J. Non-Cryst. Solids* **224**, 92-96 (1998). ★

A New Way to Measure Spin Polarization

R.J. Soulen, Jr., M.S. Osofsky, and B. Nadgorny
Materials Science and Technology Division

J. Byers
George Washington University

The Search: Spin-polarized transport has recently emerged as an important new phenomenon in solid state physics as well as forming the basis for a new class of electronics.¹ Progress on both fronts has been severely impeded, however, by the paucity of materials whose spin polarization P is sufficiently large to make the phenomenon practical. Accordingly, researchers are actively looking for new, highly spin-polarized materials, in which the "holy grail" is a fully spin-polarized material ($P = 100\%$).

This search is frustrated by the fact that determining P for candidate materials is very difficult. Theoretical calculations can give some guidance but, at the present state of the art, cannot yield completely

adequate results. Photoemission offers an experimental means to determine P , but it lacks the necessary energy resolution (~ 1 meV) and requires very careful surface preparation. An alternative experimental method incorporates the material into a planar tunnel junction, which offers the high-energy resolution and has thus produced the most data on P for many materials. This method, however, does place rather stringent requirements on the sample because it must be incorporated into a tunnel junction. Consequently, the spin polarization of many of the newer materials cannot be determined by this method.

New Techniques: We report here on a new technique discovered at NRL.² In this technique, the conductance G of a point contact made between a sharpened superconducting point and a metallic sample is used to determine P . This technique is based on the phenomenon known as Andreev reflection, which is shown schematically in Fig. 6. An electron e in the normal metal N is shown approaching the interface. For the electron to enter the superconductor S, it must pair up with a second electron to form a Cooper pair in S. The second electron (with opposite spin) required for the pair is obtained from the N metal, thus leaving behind a hole h at the interface. This hole has the opposite momentum of the incident electron and propagates away from the interface. Previous studies of Andreev reflection have dealt only with unpolarized N metals. We have reexam-

ined the problem for the case where the N metal is spin polarized. Then the conductance due to Andreev reflection is suppressed, since it is limited by a spin minority population. We have developed a model that allows us to determine the spin polarization to within a few percent for all experimental conditions.

This method, referred to as PCAR (Point Contact Andreev Reflection), is extremely simple to implement, its energy resolution matches the tunneling experiments, no special surface preparation is necessary, and there are no special requirements on the sample geometry. Indeed, we have measured thin film samples, foils, and arc-melted samples of irregular shapes with equal facility. Thus, in a very short time we have been able to measure the spin polarization of several familiar metals whose spin polarization has been determined by tunneling: $\text{Ni}_x\text{Fe}_{1-x}$, Ni, Co, and Fe. We have pressed on to measure P for several new materials beyond the reach of tunneling experiments: NiMnSb, $\text{La}_{0.7}\text{Sr}_{0.3}\text{MnO}_3$, $\text{La}_{0.7}\text{Ca}_{0.3}\text{MnO}_3$, and CrO_2 . Figure 7 shows some of our results.

Wherever possible, we have compared our results with previous tunneling experiments. Also, our results for the conventional ferromagnets (Ni and Co) were confirmed very recently by Upadhyay, et al.,³ who observed the suppression of Andreev reflection in microlithographically fashioned superconductive/ferromagnet junctions. A summary of the comparison is shown in Fig. 8 where we have already dem-

FIGURE 6
Schematic representation of current flow across an interface between a normal metal (N) and superconductor (S).

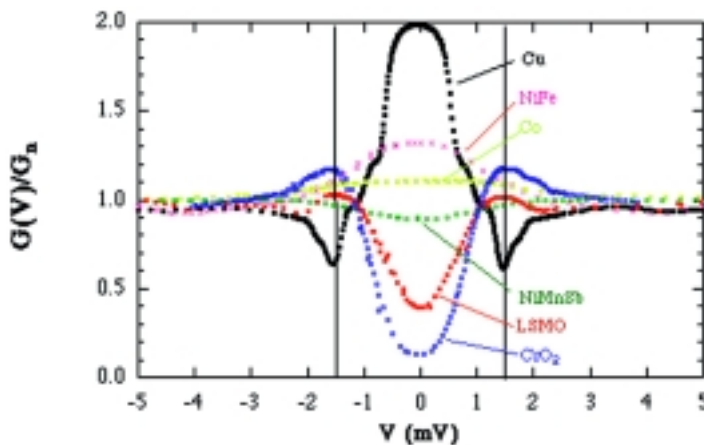
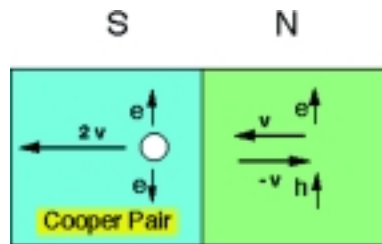


FIGURE 7
The normalized conductance $G(V)/G_n$ as a function of voltage V for several spin polarized metals showing the suppression of Andreev reflection with increasing P .

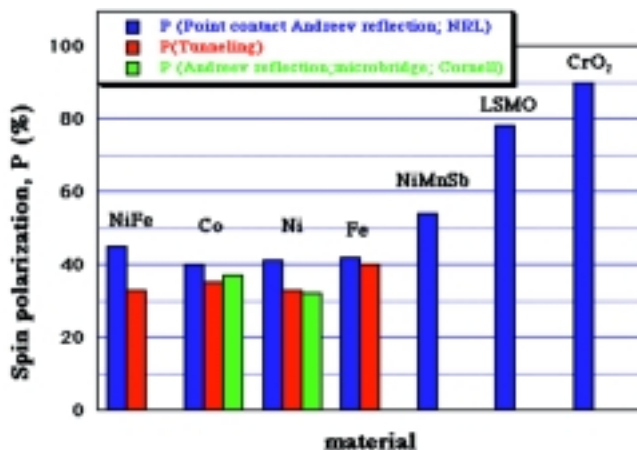


FIGURE 8
Comparison of the spin polarization obtained by three different methods.

onstrated $P = 90\%$ in CrO_2 . We find that, although there are differences as large as 10%, the overall agreement among the various methods is very encouraging.

Summary: At the moment, NRL is in a truly unique position to harness the PCAR method to open up a wide range of new areas both in fundamental research and in applications. Collaborations are underway between our laboratory at NRL and several sample-preparation laboratories throughout the world to conduct the search for fully spin-polarized materials.

[Sponsored by DARPA and ONR]

References

- ¹G. Prinz, "Spin-Polarized Transport," *Physics Today* **48**, 58 (1995).
- ²R.J. Soulen, Jr., J.M. Byers, M.S. Osofsky, B. Nadgorny, T. Ambrose, S.F. Cheng, P.R. Broussard, C.T. Tanaka, J. Nowak, J.S. Moodera, A. Barry, and J.M.D. Coey, "Measuring the Spin Polarization of a Metal with a Superconducting Point Contact," *Science* **282**, 85 (1998).
- ³S.K. Upadhyay, A. Palanisami, R.N. Louie, and R.A. Buhrman, "Probing Ferromagnets with Andreev Reflection," *Phys. Rev. Lett.* **81**, 3247 (1998). ★

Computational Screening of Candidate Thermoelectric Materials

D.J. Singh
*Condensed Matter and Radiation
Sciences Division*

The Navy has a strong interest in spot cooling technologies for electronic applications. Next-generation and beyond electronic technology will benefit greatly from operation below room temperature.

There is also considerable commercial interest because lowering microprocessor junction temperatures by 100 °C can yield 30% or better speedups.

Thermoelectric Challenges: Conventional refrigerators are ill-suited to electronic applications. Besides cost, maintenance, and noise, it is hard to make small low-power refrigerators appropriate to cooling integrated circuits while retaining reasonable efficiencies. Here, solid state thermoelectric coolers offer several advantages: they are simple, reliable, noise-free, and readily scalable to the power and size needed.^{1,2} Unfortunately, they suffer a crucial drawback: they have inordinately high power consumption relative to cooling capacity. This is directly related to properties of the materials that are used in the active elements. The currently used Bi-Te-Sb alloys have dimensionless figures of merit, $ZT \sim 1$. New materials with higher ZT must be found to improve the efficiency of thermoelectric coolers.

Finding New Materials: Discovering a material that meets given specifications is akin to finding the proverbial needle in a haystack. For thermoelectrics, this is further complicated by seemingly contradictory requirements — high thermopower, like a semiconductor; high electrical conductivity, like a metal; and low thermal conductivity, like a glass. The bias to complex multi-component compounds inherent in the need for low thermal conductivity, and the fact that electrical conductivity and thermopower are strong functions of doping level make the Edisonian approach of making and testing all candidates impractical. Instead, to sort through the haystack, NRL uses simulations on high-performance computers to identify promising materials, find trends, winnow out poor candidates, and suggest avenues for optimization.

Calculating Materials Properties: Our work is based on density functional theory, developed by Walter Kohn and others with ONR support. When implemented computationally, this theory, for which Kohn won the 1998 Nobel Prize for Chemistry, allows calculation of properties of materials from composition and crystal structure alone.

We use the linearized augmented planewave implementation³ to calculate electronic structures (for electrical conductivity and thermopower) and vibrational modes (for thermal conductivity). We obtain microscopic understanding of thermoelectric properties, and determine whether or not given materials are good candidates for experimental investigation and what the optimum doping levels are. This is illustrated by examples like Zn_4Sb_3 where we showed that higher values of ZT could be obtained in this NASA-discovered material via lower carrier density. However, this approach is still an Edisonian approach, albeit with calculations, not experiments.

Designer Materials: Calculations connect thermoelectric properties to the atomic scale, providing understanding of origins and trends but requiring idealizations; measurements are the acid test. The “designer materials” concept connects these to solve the haystack problem (Fig. 9). The idea is to use materials classes where properties depend strongly on chemical degrees of freedom that can be adjusted more or less continuously. These are regarded as “knobs.” The goal is to understand the effects of the different knobs and find high performance “settings.” Theory is used to understand the thermoelectric properties and their variation; experiments test predictions, establish what “knob” settings are realizable, and ultimately define success. Filled skutterudites (prototype $\text{LaFe}_4\text{Sb}_{12}$) are a focus of NRL work. These feature complex but high symmetry crystal structure (Fig. 10), electrical and thermal properties spanning the desired range and extraordinarily many chemical modifications through substitutions and alloying. NRL calculations and experiments at the Jet Propulsion Laboratory, Oak Ridge National Laboratory, and elsewhere are being used to unravel the connections between these and thermoelectric properties.² Initially, it was thought that things might be fairly simple: Skutterudites may all have similar band structures, with the doping level adjusted via the transition metal (Fe) site and the thermal properties via the filling (La) site. NRL calculations revealed a much richer picture; the thermal conductivity is strongly affected by the interaction of vibrational modes associated with the filling site and the Sb_4 rings, while the electronic

properties are strongly and differently modified according to the specific filler (Fig. 11).

Payoff: Besides the detailed understanding of skutterudites emerging from the calculations and from experimental work elsewhere, two new high ZT materials have been discovered, including $\text{CeFe}_4\text{Sb}_{12}$ found by JPL to have $\text{ZT} > 1.4$, following NRL calculations. Although $\text{CeFe}_4\text{Sb}_{12}$ is not well-suited to room temperature operation, our results indicate that several avenues remain to further increase ZT in skutterudites, ranging from doping level optimization

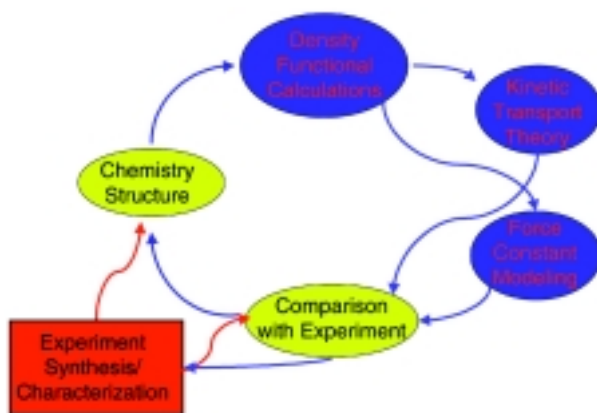


FIGURE 9

The “designer materials” concept, consisting of the interplay of simulation and experiment within a materials class, as applied to NRL theory effort on skutterudite thermoelectrics.

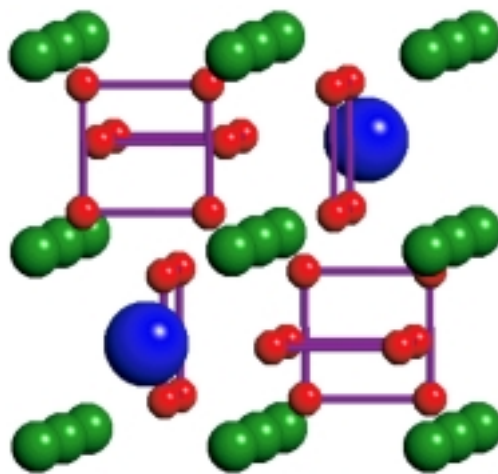


FIGURE 10

The filled-skutterudite structure showing the various crystallographic sites. For the prototype, $\text{LaFe}_4\text{Sb}_{12}$, La is blue, Fe is green, and Sb is red. Note the prominent Sb_4 rings. Electronic states associated with these covalent units are heavily involved in the electrical properties.

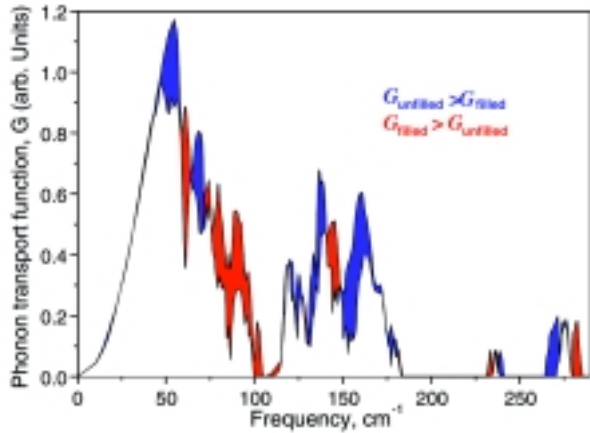


FIGURE 11 Phonon (thermal) transport function of $\text{LaFe}_4\text{Sb}_{12}$ compared with $\text{Co}_4\text{Sb}_{12}$ showing the role of the filling atom in scattering Sb_4 ring derived modes that are involved in heat conduction.

to new chemical modifications. Discovery of ZT values exceeding 2 at room temperature will pave the way for new, actively cooled Navy electronics concepts.

Acknowledgments: I am grateful for support from ONR and DARPA and contributions of my co-workers: J.L. Feldman, I.I. Mazin, W.E. Pickett, L. Nordstrom, R. Nunes, and S. Kim.

[Sponsored by ONR and DARPA]

References

- ¹D.M. Rowe, *Handbook of Thermoelectrics* (CRC Press, Boca Raton, 1995).
- ²T. Caillat, ed. *Proc. 15th International Conference on Thermoelectrics*, (IEEE Press, Piscataway, NJ, 1996).
- ³D.J. Singh, *Planewaves, Pseudopotentials and the LAPW Method* (Kluwer, Boston, MA, 1994). ★

Disorder-Induced Colossal Magnetoresistance

R. Stroud
Condensed Matter and Radiation Sciences Division

V. Browning, J. Byers, V. Harris, and W. Fuller-Mora
Materials Science and Technology Division

Introduction: The electrical resistance of a magnetoresistive material changes in response to an applied magnetic field. Magnetoresistive materials therefore make excellent magnetic field sensors and

are currently used in applications ranging from metal detectors to hard disk read heads. A new type of magnetoresistance, called colossal magnetoresistance, was recently observed for doped manganese oxides of the form $\text{A}_{1-x}^{+3}\text{A}_x^{+2}\text{MnO}_{3-\delta}$, $\text{A}^{+3} = \text{La, Nd, Pr}$; $\text{A}^{+2} = \text{Ca, Sr, Ba}$. The magnitude of the magnetoresistance, $\text{MR} = \{\rho(\text{T,H}) - \rho(\text{T},0)\} / \rho(\text{T},0)$, of some $\text{La}_{0.7}\text{Ca}_{0.3}\text{MnO}_{3-\delta}$ thin films exceeds 10⁶%, six orders of magnitude larger than that of conventional materials. However, for bulk $\text{La}_{0.7}\text{Ca}_{0.3}\text{MnO}_{3-\delta}$ samples, the magnitude of the MR is as low as 10%. Previous theories of the origin of the MR could not explain MR values as large as 10⁶%, or the huge variation in MR values for different samples of the same composition. As part of the Oxide Electronics Advance Research Initiative, NRL researchers from the Surface Modification (6670) and Materials Physics (6340) branches have succeeded in explaining both the magnitude and the variability of the MR. The joint study demonstrates a strong correlation between the magnitude of the MR and the level of atomic disorder in the samples, illustrating a serious obstacle for the utilization of these materials as sensors.

The T_p - Δ_p Characteristic Curve: The structure, transport, and magnetism of doped manganites are interdependent; small external perturbations such as an applied magnetic field, change in temperature, or defect concentration produce large variations in transport properties. In zero applied field, $\text{La}_{0.7}\text{Ca}_{0.3}\text{MnO}_{3-\delta}$ (LCMO) undergoes a phase transition from a paramagnetic nonmetal at high temperature to a ferromagnetic quasi-metal at low temperature. The onset temperature of the transition, indicated by a peak in the resistivity, varies from 0 to 280 K, depending on the sample. Under an applied magnetic field, the temperature of the transition increases, leading to a large decrease in the resistivity compared to zero-field values, i.e., large negative MR values ranging from -10% to -10⁶%.

NRL researchers were the first to show that the variation in LCMO transport properties is systematic. In Fig. 12, a large volume of resistivity data is summarized by plotting the activation energy of resistance Δ_p as function of the peak resistivity temperature T_p for single crystal, thin film, and powder samples. The activation energy is a measure of the binding energy of localized carriers in the nonmetallic phase, and T_p indicates the onset temperature of carrier delocalization. For samples grown and processed under conditions that minimize strain and defect concentration, such as single crystals and annealed films, T_p is high, ~280 K, and Δ_p is low, 30-60 meV. The values of T_p decrease and Δ_p increase

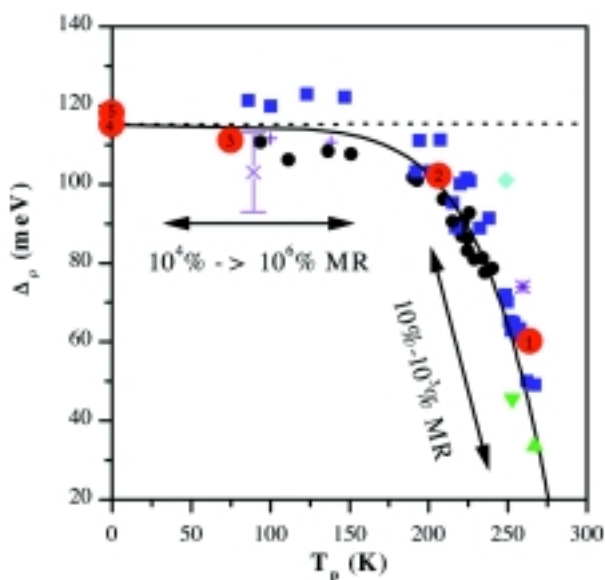


FIGURE 12

Resistivity activation energy vs peak resistivity temperature for $\text{La}_{0.7}\text{Ca}_{0.3}\text{MnO}_{3-\delta}$. The activation energy is calculated by fitting the resistivity data for $T > T_p$ to the form $\rho = \rho_0 \exp[\Delta_p/k_B T]$. Samples include pulsed laser deposited (PLD) (●) and sputtered films (■) grown at NRL, and single crystals (▼,▲), MBE films (+), an as-grown PLD film (+), an annealed PLD film, and a sintered $\text{La}_{0.75}\text{Ca}_{0.25}\text{MnO}_3$ powder (*), grown elsewhere.

for samples grown under less ideal conditions, such as as-grown pulsed laser deposited thin films (●), or strained MBE films (+). The magnitude of the MR of the samples also increases from 10% to $>10^6\%$ as the level of disorder increases.

Disorder-Induced Polaron Formation: The existence of the LCMO Δ_p - T_p characteristic curve is a strong indication that disorder is important to the physics of doped manganites. In fact, doped manganites are inherently disordered, due to the cation doping, Jahn-Teller distortions of the Mn-O octahedra, and Mn-core-spin ordering fluctuations. To varying degrees, extrinsic defects, such as dislocations, oxygen vacancies, and strain, will also occur in every sample. All of these types of atomic-scale disorder can contribute to the localization of carriers and accompanying lattice distortions known as polaron formation.

Included in Fig. 12 are samples (①–⑤) in which the extrinsic disorder was externally controlled. A single annealed film, produced in the Code 6672 Pulsed Laser Deposition Laboratory, was divided into five pieces and four were irradiated with 10 MeV iodine ions using the Code 6670 ion accelerator. These samples provide a uniform test set with a range of disorder that spans the characteristic curve.

Detailed studies of the irradiated films, making extensive cross-divisional use of NRL facilities, were conducted to prove that disorder controls T_p and the magnitude of the MR by triggering polaron formation. The structure of the films was characterized using the Code 6680 rotating anode X-ray dif-

fractometer, Code 6324 analytical transmission electron microscope (TEM), Code 6812 high-resolution TEM, and Code 6340 extended X-ray absorption fine structure spectrometer at the NRL beam line at Brookhaven. Resistivity, thermopower, and magnetization measurements were made using Code 6340 facilities.

The resistivity (Fig. 13(a)), MR (Fig. 13(a) inset) and local Mn-O bonding arrangement (Fig. 13(b)) of the films vary with the level of induced disorder. As the induced disorder increases, Δ_p increases, T_p is suppressed, the magnitude of the MR increases, and the severity of the distortions of the Mn-O bonds also increases. The increase in Δ_p indicates increased localization of carriers, which together with the distortions in Mn-O bonding, clearly demonstrates polaron formation. Furthermore, the EXAFS data are also in close quantitative agreement with those reported in the literature for LCMO and $\text{La}_{0.75}\text{Ca}_{0.25}\text{MnO}_3$ samples, indicating that the disorder-induced polaron formation is intrinsic to doped manganites, not an artifact of the radiation.

Conclusion: Colossal magnetoresistance is the product of interdependent structural, electronic, and magnetic properties of doped manganites. It is a complex phenomenon that requires a multifaceted research program. Together, researchers from Surface Modification (6670) and Materials Physics (6340) branches have explained one of the fundamental problems in CMR, the mechanism that produces MR values ranging over six orders of magnitude. By showing that the magnetoresistance of LCMO is driven

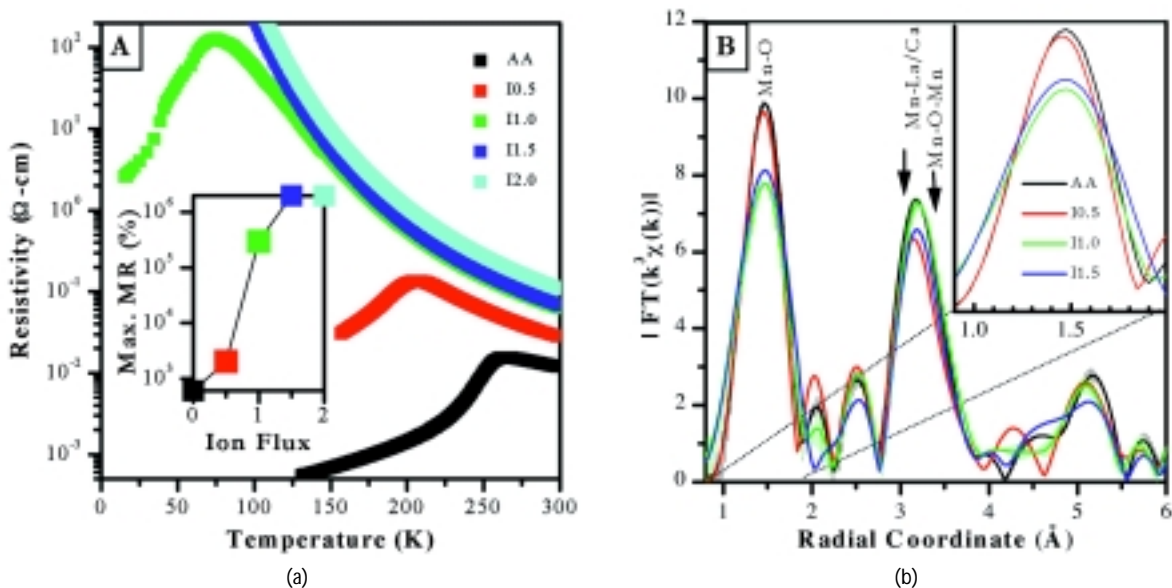


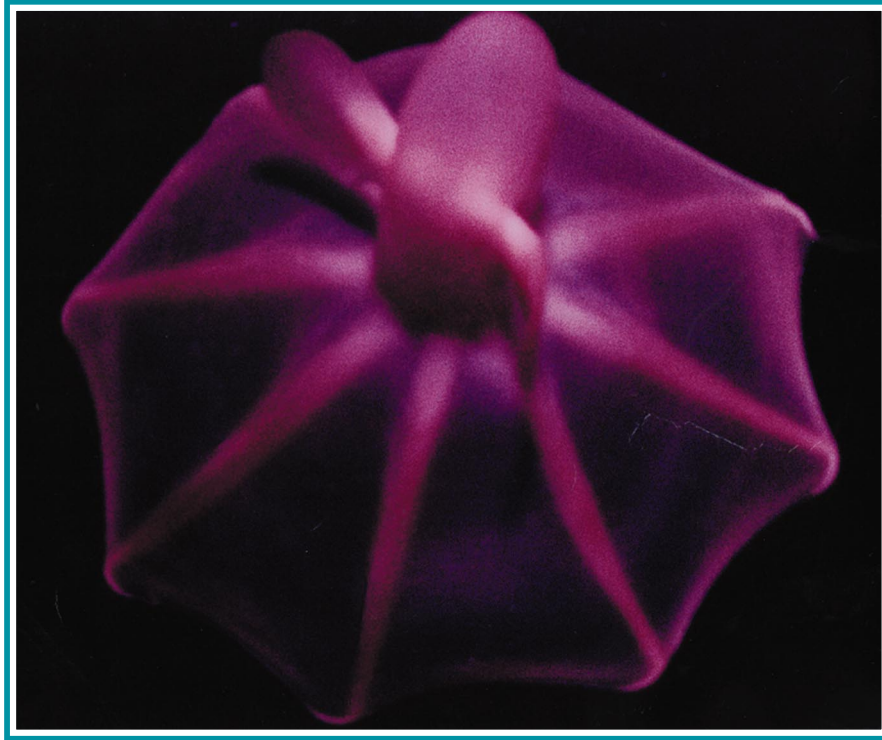
FIGURE 13 Temperature dependence of the resistivity of disordered $\text{La}_{0.7}\text{Ca}_{0.3}\text{MnO}_{3-\delta}$ films. Data labels AA, I0.5, ..., I2.0 indicate the as-annealed film and film pieces irradiated with 0.5×10^{13} to 2.0×10^{13} 10 MeV iodine ions/cm². **A** INSET: Maximum magnetoresistance of disordered $\text{La}_{0.7}\text{Ca}_{0.3}\text{MnO}_{3-\delta}$. **B** Fourier transform amplitude of Mn K-edge EXAFS for the disorder series (AA –I1.5). INSET: The Mn-O nearest-neighbor peak broadens with increasing disorder.

by disorder-induced polaron formation, NRL researchers have provided a defining question for future manganite studies: can this unique sensitivity to disorder be exploited to “tune” the magnetoresistance properties for specific applications, or do the negative consequences, e.g., low operating temperature and large noise signals, prevent future applications?

Acknowledgments: The authors gratefully acknowledge contributions of funding, time, and equipment from: P. Broussard, D. Knies, K. Grabowski, J. Horwitz, D. Chrisey, J. Kim, D. Koller, M. Osofsky, J. Cross, D. Fonda, and M. Twigg.

[Sponsored by ONR]





Serpendipity in Science: A Deep-Sea Cirrate Octopod
Science-as-Art contest – Second Place winner
Submitted by: Peter Vogt

A deep-tow Benthos camera system with black and white and color still photography as well as color video was one of the research tools used on the NRL-led 1996 geophysical expedition to the Norwegian-Greenland Sea. The cruise took place on board the Russian vessel *NIS Professor Logachev* and carried a tri-national scientific party (US-Russian-Norwegian) to examine seafloor geological processes.

Seafloor photography, other imaging, and sampling is still, like extraterrestrial planetary probes, a kind of “fishing expedition” where there are invariably surprises—giving these sciences a potential for “scientific serendipity.” On the *Logachev* expedition, we first tested the camera system in the Lofoten Basin, northwest of Norway, on 1 August 1996. Due to technical problems, the entire film was exposed in the water column perhaps 10 meters off the bottom, not a few meters as planned, so the seafloor is mostly invisible on the exposed film. By chance, however, an umbrella-shaped cirrate octopod happened to be in the field of view and was immortalized in one of the exposures. The exact size of the animal is unknown, but they are known to reach 4 ft in size as they slowly drift along the bottom, their “umbrella” unfurled to net unsuspecting prey.

This cirrate octopod (suborder Cirroteuthoidei) was thus immortalized in about 2310 m water depth at 70°, 24.7'N, 15°, 09.9'E. The color print from the 35-mm film was slightly cleaned up by computer scanning and removing little spots, maybe marine snow or plankton drifting by.

- 137 POAM III Monitors the Polar Stratosphere
J.S. Hornstein, R.M. Bevilacqua, R.L. Lucke, E.P. Shettle, M. Daehler, K.W. Hoppel, G. Nedoluha, D.T. Chen, D.R. Korwan, M.D. Fromm, and J.D. Lumpe
- 141 Nuclear Contamination Studies in the Russian Arctic
D.R. Johnson, S.E. King, M. Krosshavn, and T.A. McClimans
- 143 The Dynamics of Unusual Coastal Wave Clouds
S.D. Burk and T. Haack
- 145 Baroclinic Oscillations on the Louisiana Continental Shelf During Hurricane Andrew
T.R. Keen and S.E. Allen
- 148 High-Resolution Observations of Foreshore Morphodynamics
K.T. Holland and J. Puleo

POAM III Monitors the Polar Stratosphere

J.S. Hornstein, R.M. Bevilacqua, R.L. Lucke,
E.P. Shettle, M. Daehler, K.W. Hoppel,
G. Nedoluha, and D.T. Chen
Remote Sensing Division

D.R. Korwan, M.D. Fromm, and J.D. Lumpe
Computational Physics, Incorporated

Widespread Thinning of the Ozone Layer:

Absorption of sunlight by the ozone layer creates a worldwide temperature inversion, known as the stratosphere, that caps widespread upward motions in the lower atmosphere, and thereby limits the strength of thunderstorms, hurricanes, and other low pressure systems. Spatial variations in ultraviolet absorption and infrared cooling by the ozone layer influence the winds at high altitudes, eventually affecting weather in the lower atmosphere. Ozone also filters out ultraviolet solar radiation which, if left unfiltered, would have made life on land impossible, and which, when insufficiently filtered, causes skin cancers and cataracts. Clearly, the ozone layer is important.

Stratospheric winds cause ozone to pool in the wintertime polar stratosphere, so until recently the ozone layer was always densest during the polar winter and early spring. But during the past 15 years or so, during each southern hemisphere spring, the ozone layer over a continent-sized area of the southern polar regions has virtually disappeared at those altitudes where it is usually densest. This is called the Antarctic Ozone Hole. There have also been noticeable widespread depletions during the northern hemisphere spring during those years when the wintertime stratosphere has been unusually cold.

The abnormal ozone depletions are found to be tightly correlated with the abundance of chlorine monoxide, identifying chlorine in the stratosphere as the primary culprit. Although volcanos inject a small amount of chlorine into the stratosphere, by far the largest sources of chlorine in the stratosphere are chlorofluorocarbons (CFCs), manmade compounds that are used as refrigerants and fire extinguishers because of their extreme chemical inertness. (Unless your car is a recent model, its air conditioner uses CFCs.) The same inertness that makes CFCs desirable as refrigerants and fire extinguishers allows them to reach the stratosphere without being intercepted by the chemical processes that usually prevent chlorine compounds in the lower atmosphere from reaching the stratosphere. Once in the stratosphere, the CFCs are exposed to intense ultraviolet radiation from the Sun and are broken into much less inert forms of

chlorine. Reactions on the surfaces of polar stratospheric cloud particles, and to a lesser extent on the surfaces of non-cloud stratospheric aerosol particles, convert the less inert forms of chlorine into forms that catalytically destroy large amounts of ozone when sunlight returns to the polar regions in the spring. Thus, polar stratospheric clouds (PSCs) and stratospheric aerosols are important factors in the widespread loss of ozone from the springtime polar stratospheres of both hemispheres.

Several other components of the atmosphere also play a role. These include NO_2 , which can combine with ClO to interrupt the catalytic cycle, and water vapor, which at low temperatures swells the stratospheric aerosol, increasing its surface area and—at low enough temperatures—converting the aerosol particles into PSC particles of various compositions. A significant second effect of PSCs is the removal of nitrogen compounds from the ozone layer by sedimentation; this prevents NO_2 from interrupting the catalytic destruction of ozone.

Because of their crucial role in destroying the ozone shield, CFCs are being phased out, in accordance with the Montreal Protocol and subsequent international agreements. The phasing out of CFCs for fire extinguishers and other applications has required the Navy to embark on a costly and time-consuming search for replacements. The Navy and national policy makers therefore have a major interest in monitoring the effects on ozone of the phasing out of CFCs.

NRL's Polar Ozone and Aerosol Monitor (POAM) III is monitoring the ozone layer in the polar regions, as well as PSCs, stratospheric aerosols, NO_2 , water vapor, and temperature, as described below. In addition to their value in monitoring ozone depletion, POAM III data provide valuable information on atmospheric parameters that limit the performance of DoD systems.

POAM III Monitors the Stratosphere: POAM III is carried on an Earth-orbiting platform and works by measuring the changing attenuation of sunlight as the instrument watches the Sun rise and set behind the Earth's atmosphere. Measurements are made in nine narrow spectral channels spaced across the near-UV, visible, and near-IR portions of the spectrum, from 354 to 1018 nm.¹

The limb-viewing geometry provides excellent vertical resolution (about 1 km), and also makes POAM sensitive to aerosol layers and optically thin clouds, because it looks through their long dimension. POAM can detect clouds and aerosol layers that would be invisible to nadir-viewing sensors or to observers on the ground. These subvisual layers can

substantially affect the performance of off-nadir optical systems.

POAM III is on the SPOT-4 remote sensing satellite, which is owned and operated by the Centre National d'Etudes Spatiales (CNES, the French Space Agency), and was launched on March 24, 1998. SPOT is in a polar Sun-synchronous orbit, so there is one sunrise and one sunset per orbit, for a total of 14 sunrises and 14 sunsets per day. During each day, the sunrises occur around a circle of latitude in the northern polar region and the sunsets occur around a circle of latitude in the southern hemisphere. The two circles of latitude vary slowly from day to day, with a seasonal dependence that repeats from year to year.

POAM III is an improved version of NRL's very successful POAM II instrument,² which was carried by SPOT-3 and obtained data from October 8, 1993 until the spacecraft failed on November 13, 1996.

POAM III Observations: The following discussion analyzes the POAM III data on ozone, PSCs, and water vapor.

Figure 1 shows how the concentration of ozone changed during the most recent southern hemisphere fall, winter, and spring (May to November, 1998). The red area between 15 and 20 km shows the ozone layer. Notice that the concentration plummets beginning in early September, reaching extremely low values in late September and October. This phenomenon is called the Antarctic Ozone Hole.

Figure 2 shows the changing ozone concentration more quantitatively, at selected altitudes. The points for 1998 in each of the four plots in this figure correspond to a horizontal slice through Fig. 1. This type of plot is able to compare 1998 data as

observed by POAM III to data from three years (1994 to 1996) as observed by POAM II. At 16 km, 1998 started out with more ozone than in 1994 to 1996, and the ozone initially disappeared more slowly; however, by October the abundance of ozone at this altitude was as small as in the other years. At successively higher altitudes, the abundance of ozone switches from being more than in previous years to being less. At all altitudes, the disappearance of ozone is later but steeper in 1998 than in the other years, and at the highest altitude, the ozone recovers more rapidly in 1998.

Figure 3 shows POAM observations during the late winter of 1998. Every POAM observation during this period contained a PSC, as indicated by the heavy dots. This is remarkable, as can be seen in Fig. 4, which shows the fraction of POAM observations that contained PSCs for 1998 (POAM III) and for three earlier years (1994 to 1996, POAM II). PSCs were common from July through early September in all four years, but the red area (1998) saturating at 100% shows that PSCs were significantly more pervasive than normal in 1998.

Figure 5 shows POAM III measurements of water vapor in 1998. Note the dark area, corresponding to unusually dry air, from 12 to 21 km from late July through early October. This dehydration is due to the removal of water by the sedimentation of cloud particles. Most types of PSC particles remove nitric acid along with water vapor, reducing the feedstock for NO₂ that could have protected the ozone from chlorine.

Discussion: As the above figures illustrate, thanks to SPOT's orbit, POAM III is well placed for monitoring the strongest ozone depletions in the

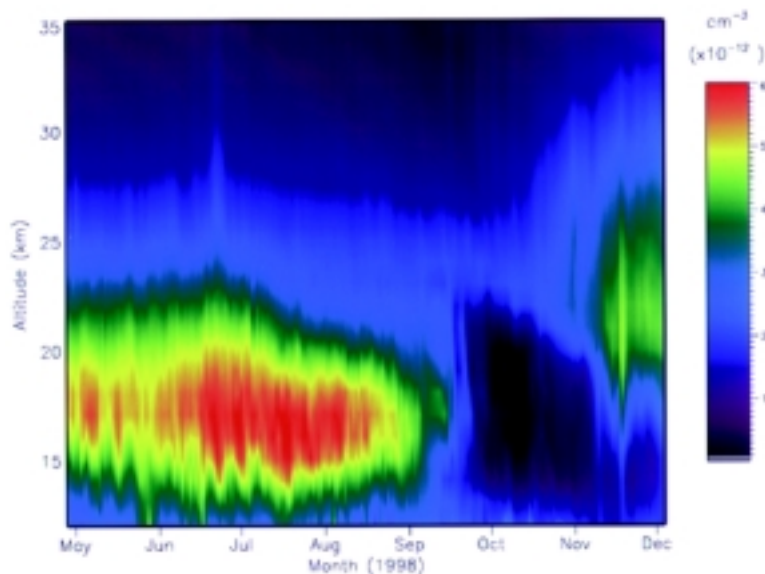


FIGURE 1
The vertical distribution of ozone at the latitudes of POAM III as a function of time during 1998. The ozone hole is the dark area between 14 and 23 km that forms at the end of September; the normal ozone layer is the red area at these same altitudes earlier in the year.

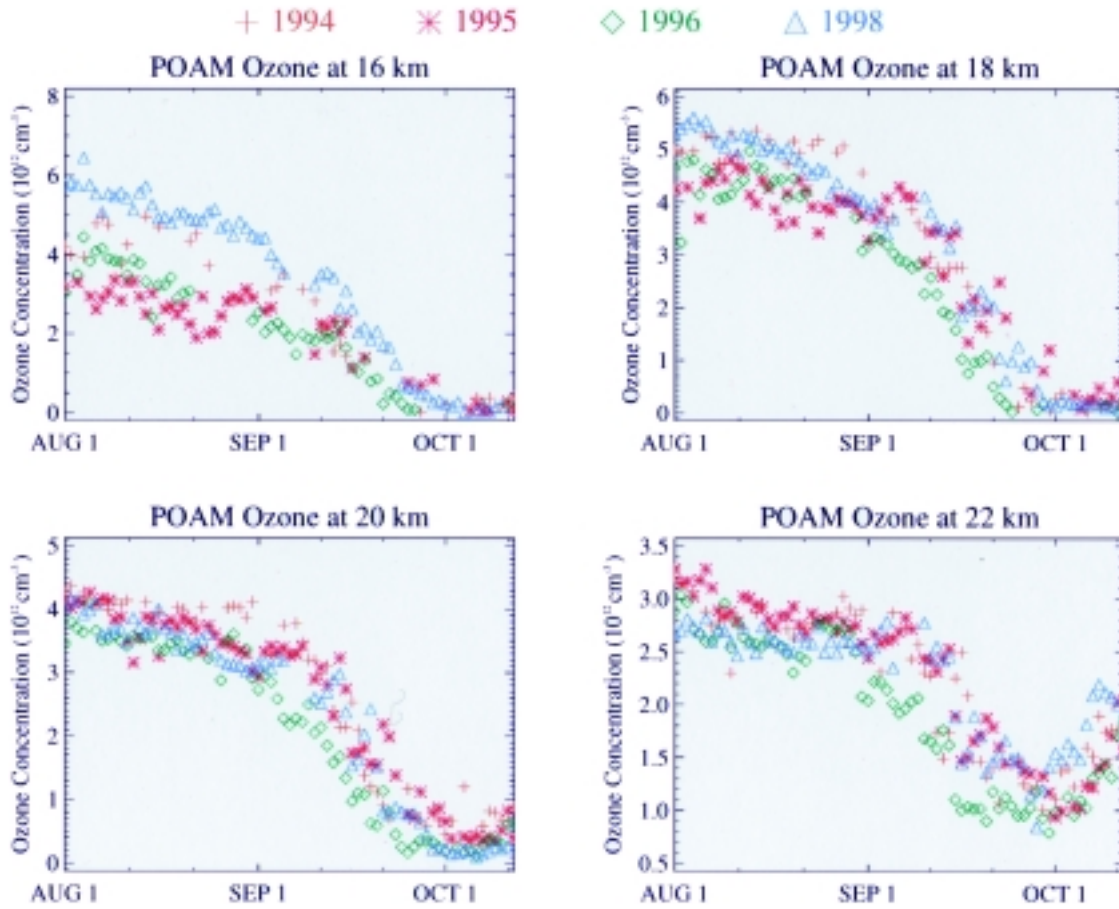


FIGURE 2
The decrease of ozone during the formation of the ozone hole, at several altitudes in the ozone layer. POAM II data for three years are shown alongside POAM III data for the current year, allowing year-to-year differences to be identified.

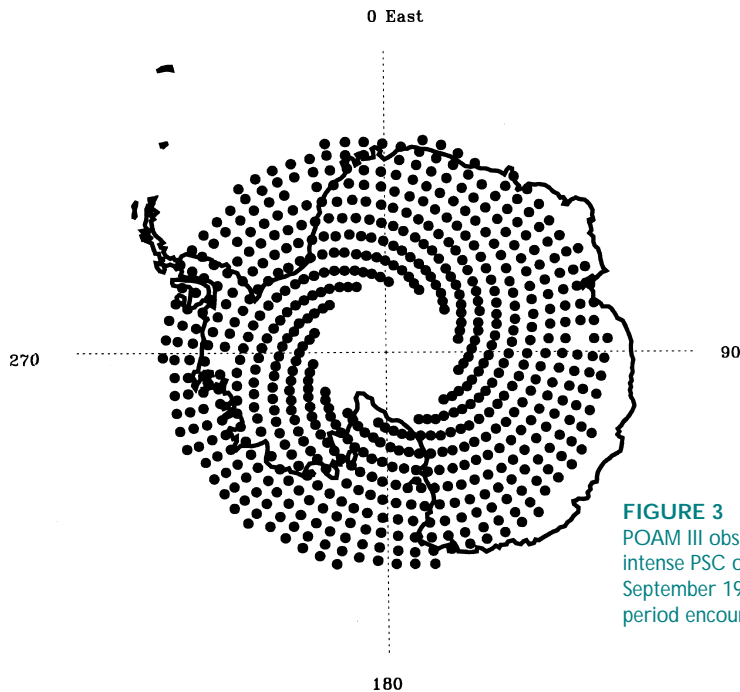


FIGURE 3
POAM III observations of PSCs during the unusually intense PSC outbreak that occurred from July to September 1998. Every POAM III observation during this period encountered a PSC, as indicated by a heavy dot.

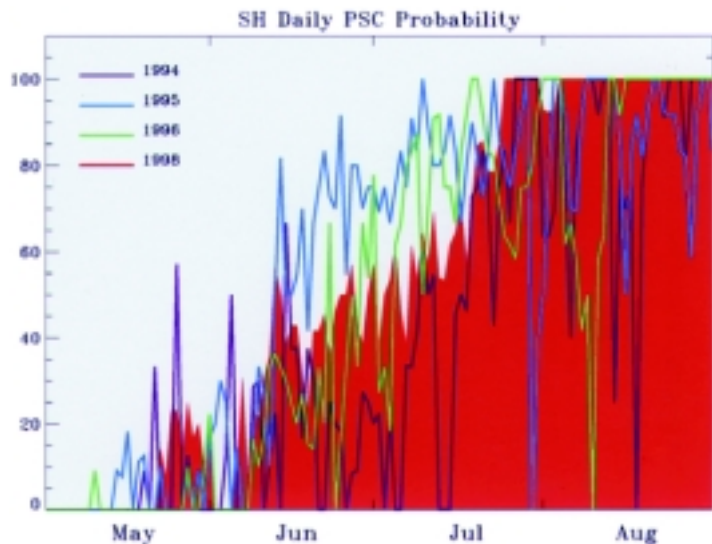
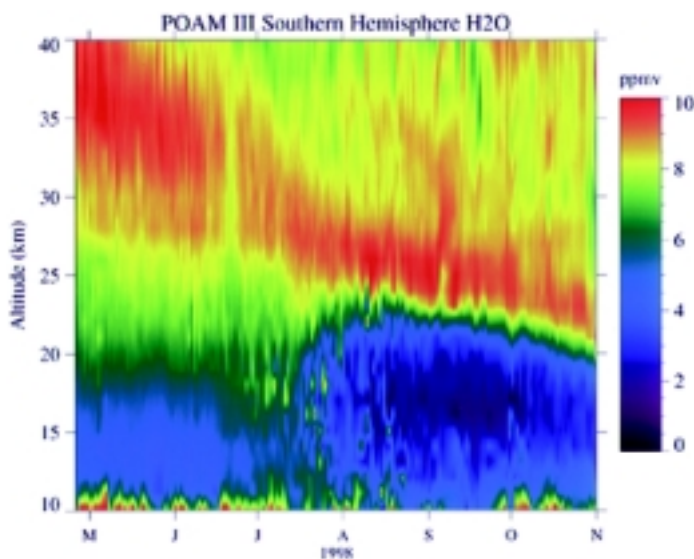


FIGURE 4
The probability that a POAM observation contained a PSC, contrasting three years of POAM II data to POAM III data for the most recent year. The red area saturating at 100% for an extended period shows that PSCs were unusually frequent this year.

FIGURE 5
POAM III measurements of the vertical distribution of water vapor for the same period covered in Fig. 1. The descent of air inside the wintertime stratospheric vortex is evident. A dry hole develops from 12 to 21 km in late July. It is caused by the sedimentation of PSC particles, which take water away from the region where the PSCs form.



atmosphere, including the Antarctic Ozone Hole. In addition to providing high quality data on massive ozone depletions, POAM III has already observed many polar stratospheric clouds, as well as the removal—due to the settling of cloud particles—of NO₂ and water vapor from the altitudes occupied by the ozone layer. These phenomena largely control the intensity and duration of the large-scale springtime depletions of stratospheric ozone in both polar regions. POAM III data in combination with data from the very successful POAM II mission are producing a valuable long-term data set that should be particularly useful for detecting long-term trends in ozone, including those due to the phasing out of CFCs in accordance with the Montreal Protocol. The latter issue is of great interest to the Navy and to policy makers. The data set is contributing to scientific un-

derstanding of other upper tropospheric, stratospheric, and mesospheric phenomena, as well. NASA will be using POAM III data as part of the upcoming THESEO and SOLVE campaigns. The high thin clouds, stratospheric aerosols, and ozone measured by POAM also affect the performance of ultraviolet, visible, and infrared systems of interest to DoD.
[Sponsored by ONR]

References

¹R.L. Lucke, D.R. Korwan, R.M. Bevilacqua, J.S. Hornstein, E.P. Shettle, D.T. Chen, J.D. Lumpe, M.D. Fromm, D. Debrestian, B. Neff, and M. Squire, "The Polar Ozone and Aerosol Monitor (POAM III) Instrument and Early Validation Results," submitted to the *J. Geophys. Res.*
²R.M. Bevilacqua, "Introduction to the Special Section: Polar Ozone and Aerosol Measurement (POAM II)," *J. Geophys. Res.* **102**, 23615-23627 (1997). ★

Nuclear Contamination Studies in the Russian Arctic

D.R. Johnson,¹ S.E. King,² M. Krosshavn,³ and T.A. McClimans⁴

¹Oceanography Division

²Condensed Matter and Radiation Sciences Division

³Norwegian Defence Research Establishment, Kjeller, Norway

⁴SINTEF-CEE, Trondheim, Norway

Background: In the early years of the Cold War, tests of nuclear weapons were conducted on and around Novaya Zemlya, an island separating the Eastern Barents Sea from the Kara Sea in the Russian Arctic continental shelf regime (Fig. 6). After the breakup of the Former Soviet Union, it became known that considerable dumping of nuclear waste material had additionally occurred in the Kara Sea and its environs. Much of this material, such as fuelled and defuelled nuclear reactors and containers with radioactive waste, was sunk into the East Novaya Zemlya Trough (ENZT) and into fjords along the island of Novaya Zemlya. Additional sources of radioactive as well as industrial pollution for the Kara Sea are associated with the inflow of the Ob and the Yenisey Rivers, whose drainage covers extensive industrialized watersheds containing nuclear power plants and nuclear weapons facilities.

It is of considerable importance to understand both the present levels of radioactive contamination of the Kara Sea and the transport routes out of the Kara Sea in order to better address future container breachments or accidents in impoundments along the watershed. To gain this understanding, a series of joint military/scientific expeditions was conducted in the Kara Sea aboard the Norwegian research vessel *H.U. Sverdrup II* during the late summer months of 1993 through 1996. These expeditions involved scientists from the Naval Research Laboratory and the Norwegian Defence Research Establishment (NDRE). A rotating laboratory model of the Kara Sea was also constructed and the general circulation was simulated (Fig. 6) at SINTEF (The Foundation of Scientific and Industrial Research of the Norwegian Institute of Technology) in Trondheim, Norway.

Circulation: Figure 7 shows the near-surface circulation constructed from four yearly expeditions, which included a total of 17,000 km of shipboard Acoustic Doppler Current Profiler (ADCP) measurements combined with 23 seasonal current meter moorings. The resulting circulation pattern, with tides removed, shows an unexpected left-turning outflow from the rivers converging with a weaker flow from the southwest along the ENZT, a subsequent exit toward the north with an increase in speed along the northern tip of Novaya Zemlya and then westward into the Barents Sea. A

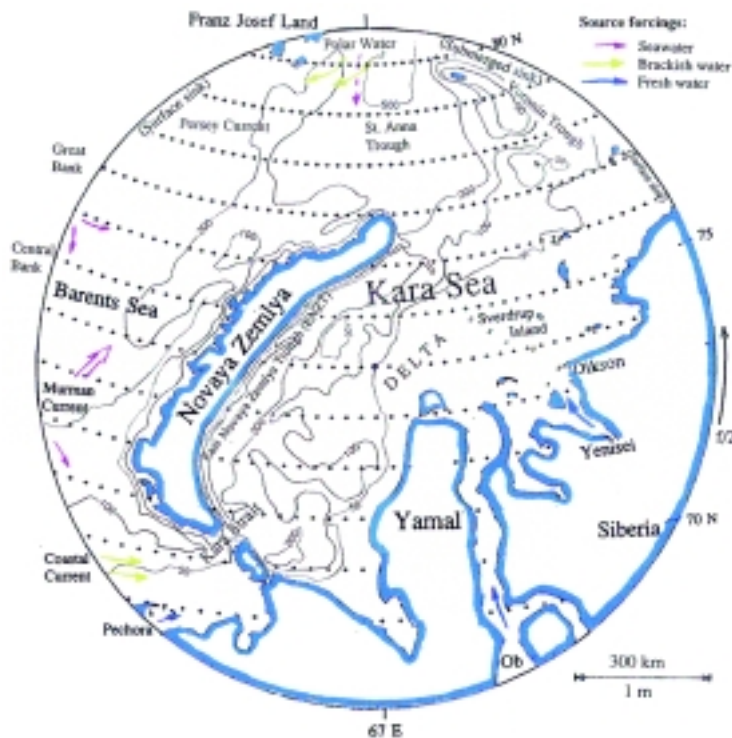


FIGURE 6
The laboratory model domain on a 5-m diameter rotating table. Bottom topography is given in meters.

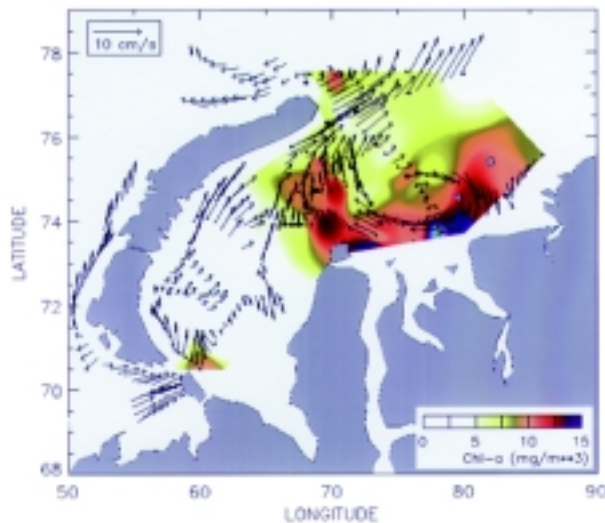


FIGURE 7
Near-surface circulation vectors composited from ADCP and moored current meters from data obtained from 1993 to 1996. Chlorophyll-a as a fresh water tracer is mapped by the 1995 expedition only within the Kara Sea.

weaker eastward return flow forms the final leg of a 200 to 300 km diameter anticyclone (clockwise rotation) north of the rivers. Chlorophyll-a measurements at a 5-m depth (Fig. 7) tracked river water and coincided well with the observed currents. In addition, satellite-tracked ice drifter beacons (not shown) demonstrated that the pattern, although very sluggish, continues over the winter, when river discharge is low. This pattern contradicts the circulation shown in Russian atlases, which depict an inward flow around the tip of Novaya Zemlya and a southward flow along its coast. The flow of Kara Sea water to the Barents Sea is more significant in the north than had been expected from the atlases.

The left-turning tendency of the river outflow has been recently explained in a numerical modeling effort.¹ The river outflow is exceptionally impulsive, with the major outflow occurring during local ice breakup in June. This outflow turns right and builds up along the coast of the Taymyr Peninsula (the eastern border of the Kara Sea). As the outflow relaxes toward mid- to late summer, this high pressure mound moves back westward to a position north of the river mouths, creating the anticyclonic/high pressure-centered motion that was observed during this period. Tidal residuals may also contribute to the current structure.

In the southwestern basin of the Kara Sea, water from the Pechora Sea with relatively high chlorophyll-a content enters through the Kara Strait and appears to mix quickly into a sluggish northward motion. Although moorings showed wind-forced and tidal fluctuations of 30 cm/s, the mean circulation is quite

weak, especially in the southwestern basin. Deeper currents showed the same general patterns. The laboratory model simulation also produced the general circulation pattern shown here, but in addition showed a relatively consistent northward flow along the river delta slope (50-m isobath in Fig. 6). This flow was too narrow to be seen in the smoothed and synthesized observations.

Sediment Suspension and Removal: Figure 8 shows light attenuation at the bottom as observed during the 1995 expedition. Two regions are of significant interest in this figure. First, the extremely high light attenuation levels near the delta bottom coincide with high levels of chlorophyll-a and suggest that strong removal of both biological and sedimentary materials from the surface freshwater outflow is occurring, with material deposits in mid-delta. Although the stirring is sufficient to keep this material in suspension in a bottom nepheloid layer, it is not sufficient to mix it throughout the water column or to remove it from the delta except by anomalous events. Second, the relatively high light attenuation at the bottom in the southwestern part of the ENZT can be traced to fjord outflow from Novaya Zemlya and suggests that a stronger connection exists between these fjords and the Kara Sea than had been expected.

Figure 9 shows the distribution of ¹³⁷Cs measured in the bottom water layers. Waters that flow in through the Kara Strait along the 50 to 100-m isobaths contain the lowest levels of ¹³⁷Cs. Lower levels of ¹³⁷Cs along the delta slope reveal this water route, as had been suggested in the laboratory model.

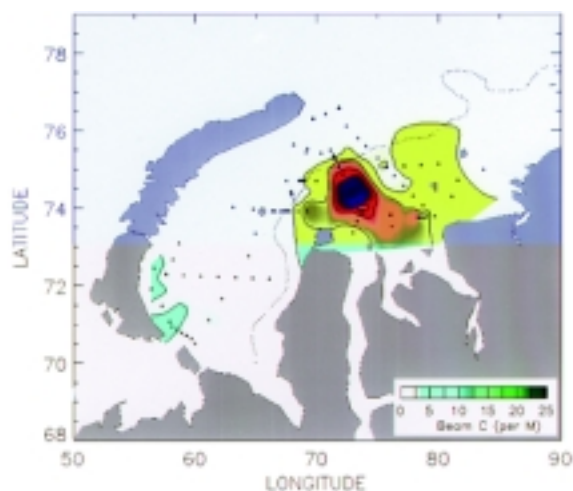


FIGURE 8
Light attenuation at 660-nm wavelength at the bottom. A beam attenuation of 20 per meter means that light is diminished to 1% of its intensity over a 23-cm path.

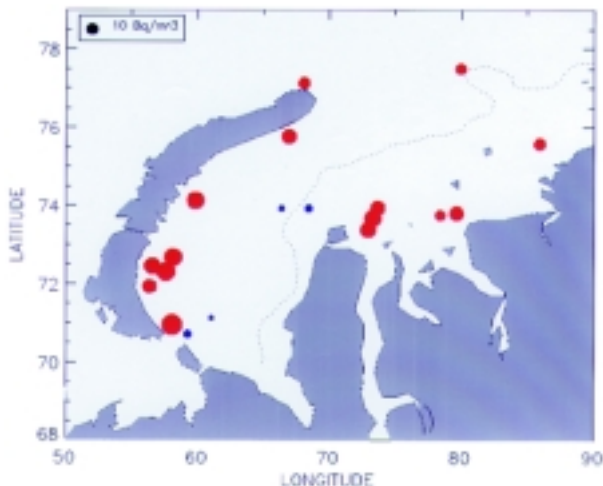


FIGURE 9
 ^{137}Cs distribution in the lower layer of the water column. Size of circles represents concentration. Circles are blue for concentrations of less than 6 Bq/m³.

Although the levels of ^{137}Cs are generally higher in the ENZT and over the river delta, they are not of present concern. Modeling studies² have shown that even catastrophic releases from the reactors in the Kara Sea will lead to local but not basin-wide problems. The principal concern along the watershed is the possible breach of containers or of impoundments that contain large amounts of isotopes.

[Sponsored by ONR]

References

- ¹I.D. James, "A Numerical Model of the Development of Anticyclonic Circulation in a Gulf-type Region of Freshwater Influence," *Cont. Shelf Res.* **17**, 1803-1816 (1998).
- ²R.H. Preller and P.G. Posey, "Modeling the Dispersion of Radioactive Contaminants in the Arctic," *1997 NRL Review*, Naval Research Laboratory, Washington, DC, April 1997, pp. 41-48. ★

The Dynamics of Unusual Coastal Wave Clouds

S.D. Burk and T. Haack
Marine Meteorology Division

Introduction: Numerical weather prediction (NWP) models at the Fleet Numerical Meteorology and Oceanography Center (FNMOC) currently provide operational forecasts that span a resolution scale from global down to ~10 km. Atmospheric predictability at finer scales is an active research area of enormous practical significance to the Navy. Kilo-

meter-scale variations in wind, wind shear, clouds and visibility, precipitation, turbulent transport and dispersion, aerosols, and refractivity greatly impact naval operations, communications, and weapons systems. The NRL Coupled Ocean/Atmosphere Mesoscale Prediction System (COAMPS),¹ FNMOC's operational mesoscale NWP model, is used in this study to investigate cloud formations having substantial fine scale structure, not only in cloudiness but in wind speed and direction, as well as boundary layer depth. The fundamental dynamics producing these clouds are this study's primary focus, but a secondary benefit is the testing and validation of COAMPS at extremely high resolution.

Wave Clouds: Unusual long, linear marine boundary layer (MBL) cloud formations, extending offshore from certain orographic features along the California coast, occur generally in the summer months. These clouds often are 50 to 100 km long; they are substantially longer and more linear than Kelvin-Helmholtz billows and, similar to mountain lee waves, they are stationary relative to the orography forcing them. Unlike lee waves, however, these wave clouds occur *upwind* of terrain. A substantial body of observations, modeling, and theory exists concerning mountain lee waves, but coastal wave clouds of the type addressed here have not been explained. Figure 10 shows an occurrence of these wave clouds off the Monterey/Big Sur, California, coastline in a GOES-9 visible image at 2324 UTC June 23, 1996.

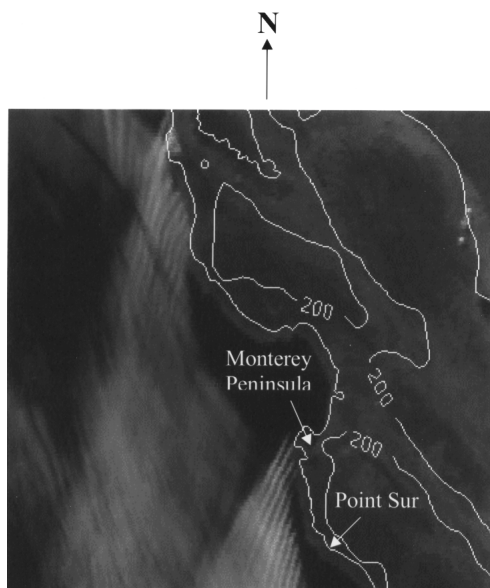


FIGURE 10
 Wave clouds along the California coast. Monterey Bay in the center of the photo is clear.

The prevailing wind is northwesterly, paralleling the coast, and the horizontal wavelength between cloud lines is ~3 to 4 km. These cloud lines first appeared off of Monterey around 2100 UTC and were absent the following morning. Such wave clouds tend to occur at locations where the coastline turns into, and blocks, the prevailing wind. Further, they are seen repeatedly in the same locations and their orientation relative to the coastline tends to be invariant.

Observations and Model Simulations: The wave clouds in Fig. 10 occurred during the ONR-sponsored Coastal Waves field experiment² and were the subject of extensive observation with the NCAR EC130Q research aircraft (D. Rogers and C. Dorman, co-principal investigators, Scripps Institute of Oceanography). Aircraft measurements indicate that upwind of the cloud waves, the inversion-capped MBL is ~150 m deep and topped by a prominent low-level jet of ~20 m s⁻¹. The MBL depth increases abruptly to ~350 m at the leading edge of the wave clouds, and undergoes sinusoidal amplitude variations of ~100 m in conjunction with the ~4 km horizontal wavelength.

To resolve the fine scale structure and variations of these clouds, COAMPS was run with five grid meshes nested down to an inner grid having 1/3 km spacing. This simulation is the highest resolution real-data COAMPS forecast to date. Initial fields are given by NOGAPS, the Navy's global atmospheric model, 30 hours prior to the period of interest (1800 UTC June 23 to 00 UTC June 24). The COAMPS 12-hr forecasts are produced in an operational manner with lateral boundary conditions supplied by NOGAPS every 6 hours on the outer grid and by the parent grid every time step for each inner mesh.

Results: As the low-level winds intensify with the afternoon sea breeze, a remarkable feature appears in the forecast winds. The 10-m wind field (Fig. 11) develops a strong shock front that coincides well with the leading edge of the wave clouds in Fig. 10. Abrupt deceleration and directional wind changes occur across the shock, and the isotachs display fingerlike variations consistent with the wave cloud spacing and orientation. The model-computed Froude number, *Fr* (ratio of wind speed to gravity wave phase speed), changes from supercritical (*Fr* > 1) upwind of the flow discontinuity to subcritical (*Fr* < 1) within the wave cloud region. For simple layered fluids, such a *Fr* transition generally is accompanied by a hydraulic

jump. Figure 12(a) shows the model forecast vertical velocity field, *w* (m s⁻¹), at 425 m, while Fig. 12(b) is a vertical cross section of potential temperature (K) and vertical velocity along section A-B of Fig. 11. COAMPS forecasts a series of trapped internal waves having a horizontal wavelength of ~3.3 km, in good agreement with observations.

Conclusions: The atmosphere, with its variable stratification and wind shear, is considerably more complex than a simple layered fluid, but changes in flow criticality and trapping of internal gravity wave energy can permit the atmosphere to exhibit responses typical of a shallow-water flow, including hydraulic jumps. COAMPS forecasts a hydraulic jump of nearly the observed depth and in the correct position, followed by a set of trapped internal waves of approximately the observed length, orientation, and spacing. Pronounced variation of vertical wind shear, which creates refraction of vertically propagating gravity waves, is primarily responsible for internal energy trapping rather than thermal stratification effects. In the process of unveiling the basic physics/dynamics associated with these peculiar cloud formations, this study has demonstrated the impressive capability of COAMPS to accurately forecast meteorological structures down to the kilometer scale, which has pro-

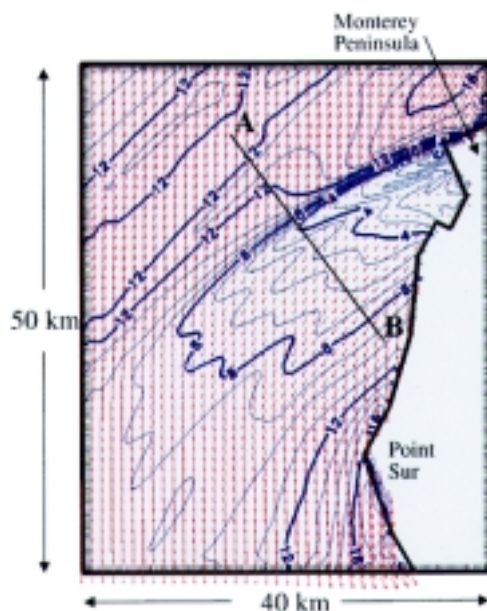


FIGURE 11
10-m wind forecast (DX = 1/3 km) valid 00 UTC June 24, 1996.

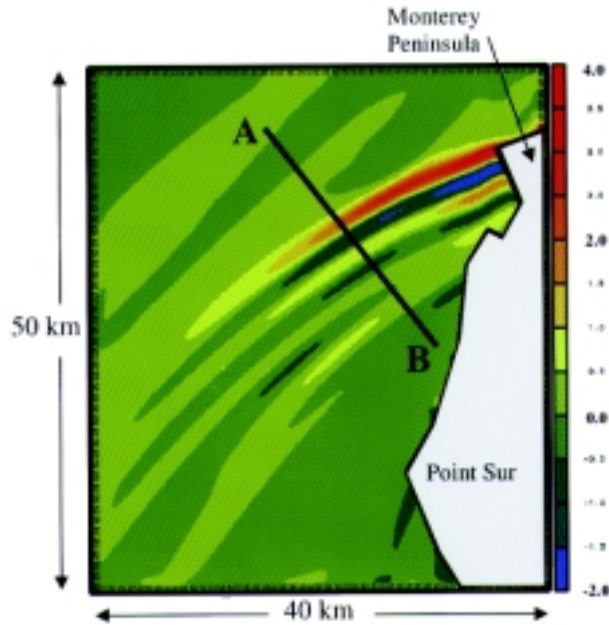


FIGURE 12(a)
Plan view of vertical velocity field (ms^{-1}) at 425 m. Forecasts valid 00 UTC June 24, 1996.

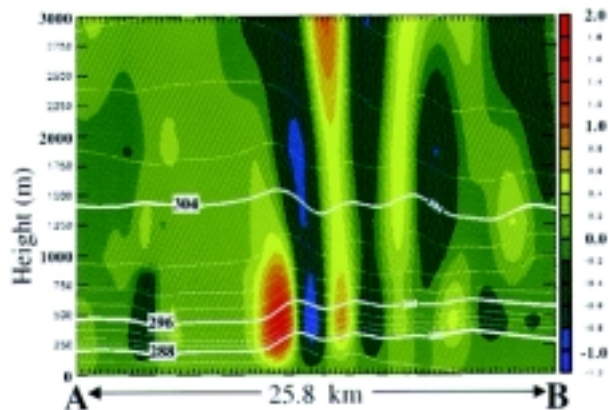


FIGURE 12(b)
Potential temperature (K) and vertical velocity (ms^{-1}) along A-B. Forecasts valid 00 UTC June 24, 1996.

found implications for the future of operational Naval meteorological support.

[Sponsored by ONR]

References

¹R.M. Hodur, "The Naval Research Laboratory's Coupled Ocean/Atmosphere Mesoscale Prediction System (COAMPS)," *Mon. Wea. Rev.* **125**, 1414-1430 (1997).
²D.P. Rogers, C.E. Dorman, K.A. Edwards, I.M. Brooks, W.K. Melville, S.D. Burk, W.T. Thompson, T. Holt, L.M. Strom, M. Tjernstrom, B. Grisogono, J.M. Bane, W.A. Nuss, B.M. Morley, and A.J. Schanot, "Highlights of Coastal Waves 1996," *Bull. Amer. Meteor. Soc.* **79**, 1307-1326 (1998). ★

Baroclinic Oscillations on the Louisiana Continental Shelf During Hurricane Andrew

T.R. Keen
Oceanography Division

S.E. Allen
University of British Columbia

As a hurricane passes over a stratified ocean, near-inertial oscillations are generated by displacement of the free surface and thermocline. Further complexities are introduced by the presence of a coastline and bottom topography.¹ Hurricane Andrew is an interesting example because of the strength of the shallow-water response. The hurricane eye crossed the Louisiana continental shelf on August 26, 1992 (Fig. 13(a)). This article describes baroclinic oscillations during this storm and proposes several generating mechanisms.

Observations of Temperature: A time series of temperature (Fig. 13(b)) reveals the presence of internal waves from the continental slope (mooring 12) to the inner shelf (mooring 15). The mixed layer temperature at the shelf break (mooring 13) decreased 6 °C as the eye approached, but inertial oscillations with a period of 22 to 28 hours were weak. Higher frequency internal waves were common. The temperature at a depth of 100 m reveals 5 °C inertial oscillations, which weakened substantially over the next 5 days.

Turbulent mixing on the middle shelf (mooring 14) decreased the mixed layer temperature by 5 °C. Furthermore, a near-bottom temperature increase of 4 °C coincided with a 1 °C increase at the surface. This oscillation may have been a baroclinic shelf wave that was superimposed on turbulent mixing. The surface temperature on the inner shelf (mooring 15) was decreasing when the instrument failed, but a spike of almost 3 °C at the bottom suggests that an internal wave passed this mooring, as was observed on the middle shelf.

Numerical Simulations: The Princeton Ocean Model (POM) was used to simulate the storm currents using realistic topography and wind forcing.² As the eye passed over the moorings, isotherm displacements (Fig. 14(a)) increase with depth within the Mississippi Canyon. East of the canyon, the displacement is apparent below the 16 °C isotherm, suggesting that the lower thermocline was important in

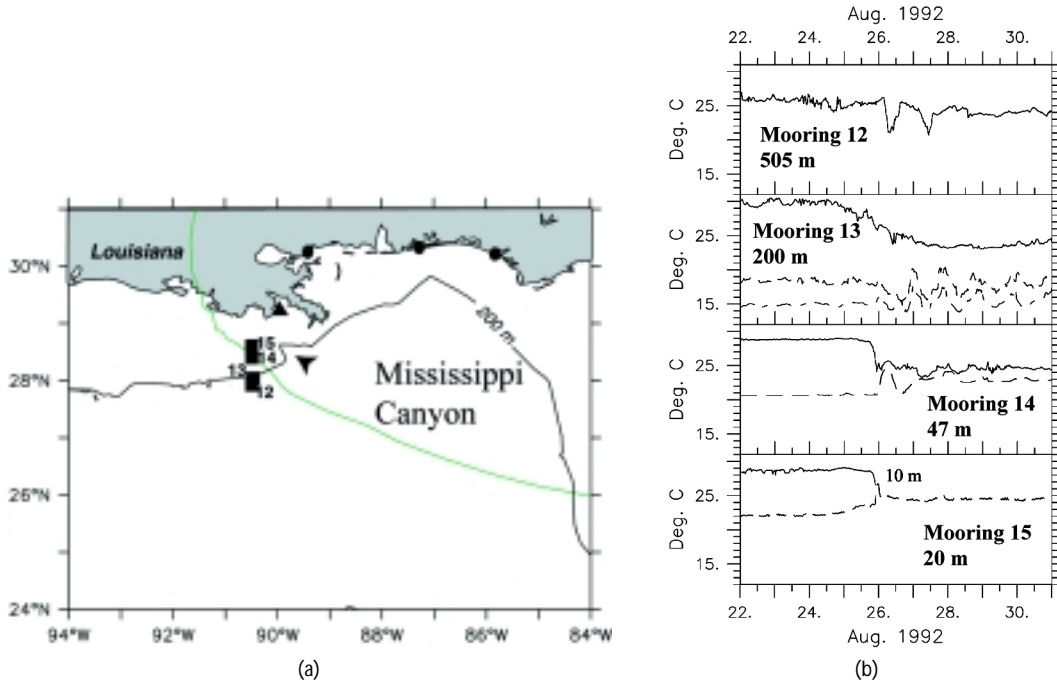


FIGURE 13 (a) North central Gulf of Mexico, showing the path of Hurricane Andrew and the moorings discussed in the text. (b) Time series (GMT) of observed temperatures at the moorings. For moorings 12, 14, and 15, the black line is 10 m below the surface and the green line is 10 m above the bottom. For mooring 13, the dashed line is at 100 m and the long-short dashed line is at the bottom.

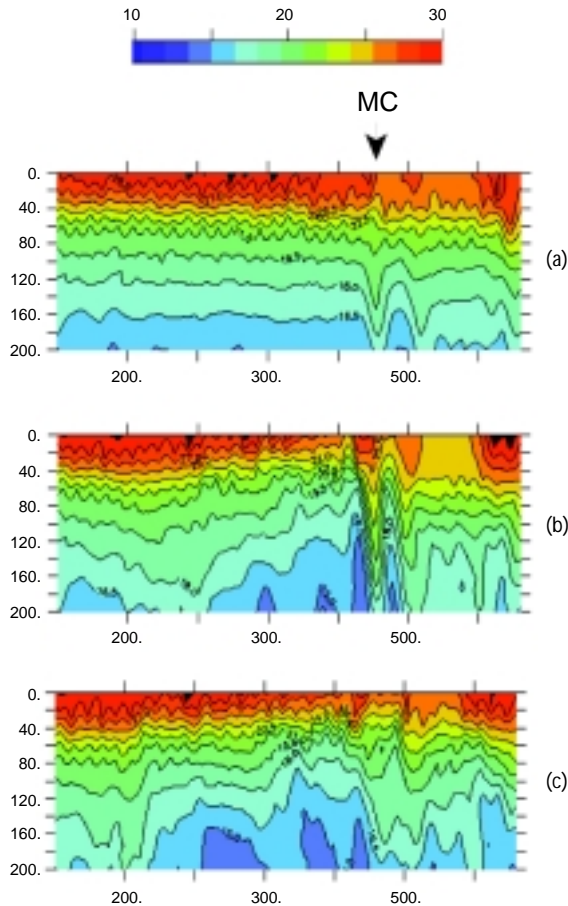


FIGURE 14 Temperature predicted by the POM along the 200 m isobath: (a) at 2100 GMT on Aug. 25; (b) at 0900 GMT on Aug. 26; and (c) at 1430 GMT on Aug. 26. MC = Mississippi Canyon.

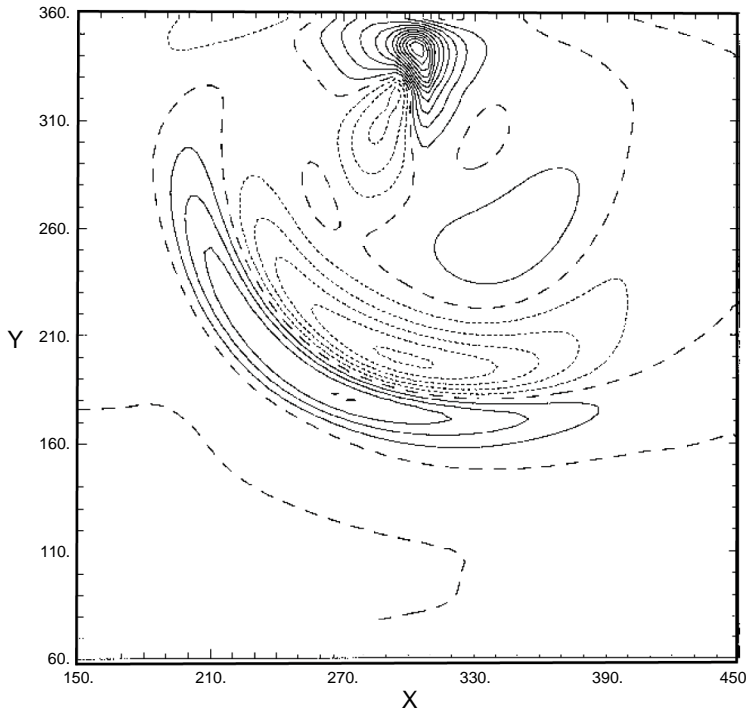


FIGURE 15
Results from the idealized model. The interface variation shown is at 1200 GMT on Aug. 27. Contoured from 0.5 m to 1.1 m. Contour interval is 0.1 m. Dashed lines are negative contours. The canyon is located at $X = 300$ and extends from $Y = 270$ to 350 .

the generation of internal waves. Internal waves that propagated into the canyon were reinforced by downwelling near the canyon head.

After the storm, the inner shelf is well mixed west of the canyon, but 26 °C water is predicted at the surface on the outer shelf (Fig. 14(b)), where a long-wavelength internal wave is present along the upper thermocline. A cold plume is predicted within the canyon (Fig. 14(c)) after downwelling stops, and the 16 °C isotherm is displaced 75 m upward. Deep internal waves are generally less than 20 km in length, as opposed to the long wavelength predicted above the thermocline.

Generating Mechanisms: A two-layer isopycnal model³ with idealized topography and wind was used to investigate generation mechanisms for internal waves during Hurricane Andrew. Four principal origins have been identified: 1) deep-ocean baroclinic oscillations, which generate flow at the same frequency over the slope and shelf; 2) a trapped edge wave that is generated over the shelf; 3) inertial oscillations that generate internal waves at the shelf break. (A trough in the thermocline forms when the flow there is eastward. The trough bifurcates, with one trough moving shoreward and the other towards the deep ocean. Conversely, a crest forms when the flow there is westward. This crest moves offshore

only.); and 4) the strong downwelling currents within the canyon, which generate Poincaré waves (Fig. 15). Within the canyon, the waves move seaward at about 0.5 m/s. After the wave exits the canyon, the crest is bent westward and it becomes curvilinear.

Summary: It has been possible to gain insight into the complex coastal dynamics during short time intervals in this study by using observations in combination with a simple two-layer model and a fully three-dimensional baroclinic numerical model. This approach requires an initial effort to set up and validate the numerical model, although the generality of models like the Princeton Ocean Model is such that very little tuning was required to reproduce the range of coastal processes encountered. Further research is needed to understand the relationship between the response of the idealized and realistic models.

[Sponsored by ONR]

References

¹E.T. Petrunco, "Observations and Modeling of the Internal Tide in a Submarine Canyon," *J. Phys. Oceanogr.* **28**, 1873-1903 (1998).
²T.R. Keen and S.M. Glenn, "Factors Influencing Model Skill for Hindcasting Shallow Water Currents During Hurricane Andrew," *J. Atmos. Oceanic Tech.* **15**, 221-236 (1998).
³S.E. Allen, "Topographically Generated, Subinertial Flows within a Finite Length Canyon," *J. Phys. Oceanogr.* **26**, 1608-1632 (1996). ★

High-Resolution Observations of Foreshore Morphodynamics

K.T. Holland and J. Puleo
Marine Geosciences Division

Introduction: Amphibious landings, many special operations, and some aspects of counterterrorism warfare depend upon knowledge of the littoral region at the land–ocean interface known as the foreshore. Societal interest in the foreshore is immense in that beaches serve as recreational areas, contribute to biological diversity, and stand as protective buffers for infrastructure against storms. However, this so-called “biting edge of the sea” is highly dynamic. Changes in foreshore profile elevation of more than a meter have been observed to occur over time scales as short as one day. In addition, shoreline motions at a variety of temporal and spatial scales have been linked to alongshore-rhythmic morphologic patterns such as beach cusps. Given the strong potential for variability in the foreshore region, a predictive capability for how foreshore morphology evolves in response to hydrodynamic forcing is greatly desired.

Understanding foreshore evolution requires detailed observations of foreshore morphodynamic and hydrodynamic change. Unfortunately, most prior foreshore measurements have lacked either the temporal resolution necessary to sample both the fluid forcing and sediment response, the spatial resolution necessary to parameterize alongshore processes, or both. For example, sedimentological data collec-

tion often lags measurements of waves and currents by several days because of the difficulty of collecting morphodynamic information during storms. In contrast, a stereometric video technique, recently demonstrated by the Naval Research Laboratory, provides rapid, high-resolution measurements of foreshore processes over relatively large spatial scales. The technique utilizes image processing and remote sensing to permit data collection even under extremely harsh conditions.

Stereometric Intersection: The specifics of this method rely upon the strong contrast between the bright, often-foamy swash edge and the dark, underlying sand surface that serves as a feature for edge detection image processing. Simultaneous views of this edge by multiple cameras (Fig. 16) allow the recovery of the three-dimensional (3-D) surface beneath the edge through a process known as stereometric intersection.¹ This intersection method is similar to triangulation in that views of the same object from multiple perspectives define the object position in space. Since the edge is not a one-dimensional point object, an epipolar constraint is applied to allow the correspondence between pixels in each of the cameras to be determined. Through time, as the swash edge moves landward, the foreshore morphology is resolved using sequential edges. In addition, the method provides simultaneous measurements of the swash motion, which is the main hydrodynamic signal. This automated process can be repeated on a nearly wave-by-wave basis and typically results in several thousand estimates per swash cycle.

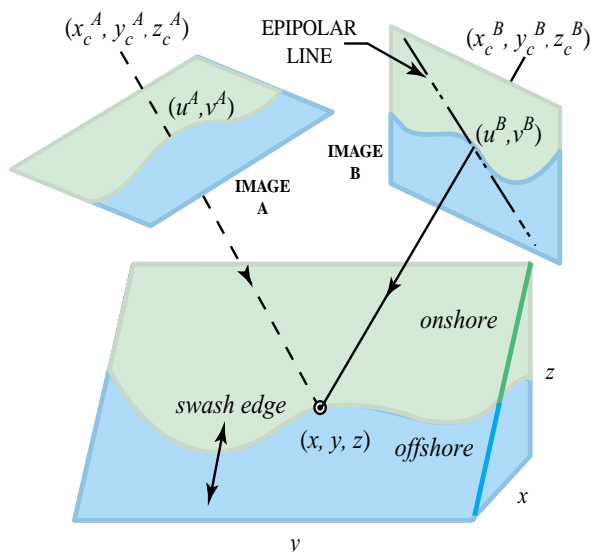


FIGURE 16
 A schematic showing the application of the stereometric method using multiple cameras. The pixel coordinates in image A (u^A, v^A) define corresponding coordinates in image B at the intersection of the epipolar line (dashed) and the swash edge. Pairs of matching coordinates are used to determine the world coordinates (x, y, z) of the foreshore surface at the selected point. The process is repeated for all other pixels in the swash edge and for all successive edges as the swash moves landward and seaward (double-sided arrow).

Foreshore Morphodynamics: This capability was used as part of the Duck94 and SandyDuck'97 field experiments at Duck, North Carolina. Up to five video cameras were used to sample 3-D morphology over a study region of approximately 100 m in the alongshore. These measurements, obtained to roughly centimeter accuracy, showed distinctive patterns of net sediment transport and morphologic change over an approximately 20-day interval during each experiment. The morphologic measurements made using the video method showed good correspondence to somewhat coarser estimates made using more traditional surveying technology (Fig. 17). However, since the stereo measurements could be repeated more frequently than the daily surveys, measurements of 3-D foreshore surface at approximately quarter-hourly intervals were obtained. Changes between successive surfaces indicated that either erosion or accretion had occurred and bounded the magnitude of spatial gradients in foreshore sediment transport. Figure 18 shows one particularly dramatic example.

Sediment Transport Modeling: Given estimates of both the hydrodynamic forcing (swash motions) and sediment response (foreshore morphodynamic change), it is possible to develop and validate models of foreshore sediment transport. Limited success has been shown through the use of energetics-based models that quantify sediment transport largely as a function of fluid particle velocity. Video-derived estimates of fluid velocity at multiple cross-shore and alongshore locations can be used with models such as these for comparison with the observed gradients in sediment transport. Initial analysis of the over 1200 hours of video data has shown that predictions using the energetics-based equations were dissimilar to observations, suggesting that factors other than velocity could also be important. Of particular interest were instances where forcing conditions were approximately equivalent, yet morphologic response was dramatically different.

Summary: The stereometric video method described above is useful in providing high-resolution

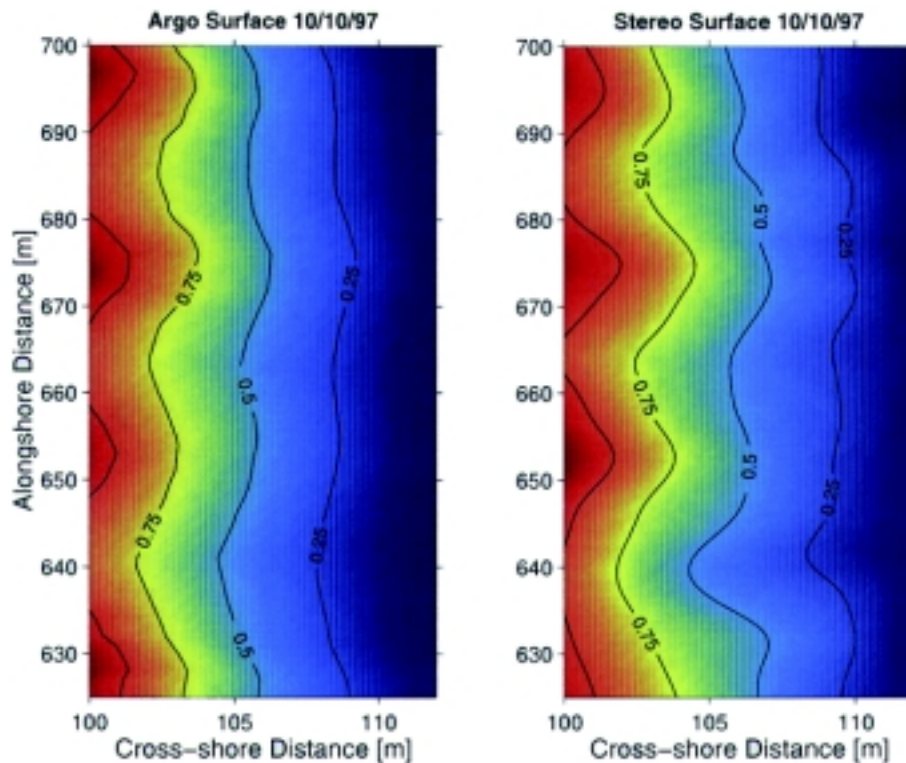


FIGURE 17 Comparison of a video-derived foreshore surface (right panel) with that from a more traditional surveying method (left panel). Contour lines represent elevation values above mean lower low water in meters. The higher resolution (approximately 5 cm horizontally) of the video method shows finer detail than the more poorly resolved (approximately 2.5 m horizontally) survey.

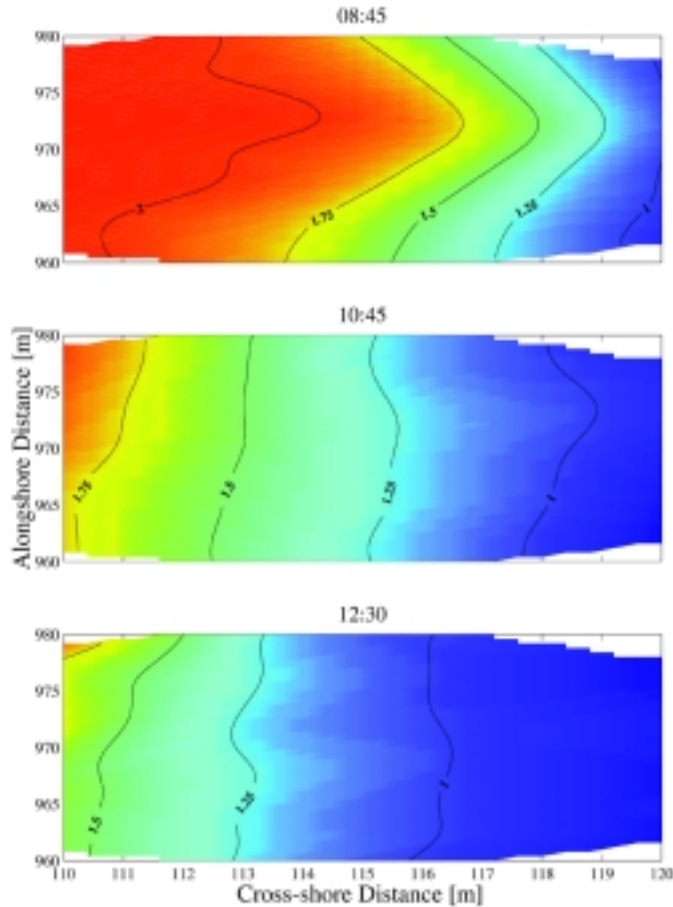


FIGURE 18
 Example of the rapid change in foreshore morphology over an approximately four-hour period. Times at which the surfaces were estimated are given above each plot. Contour lines represent elevation values above mean lower low water in meters. The erosion of the beach cusp corresponded to a cross-shore gradient in sediment transport of $0.25 \text{ m}^3/\text{hr}$.

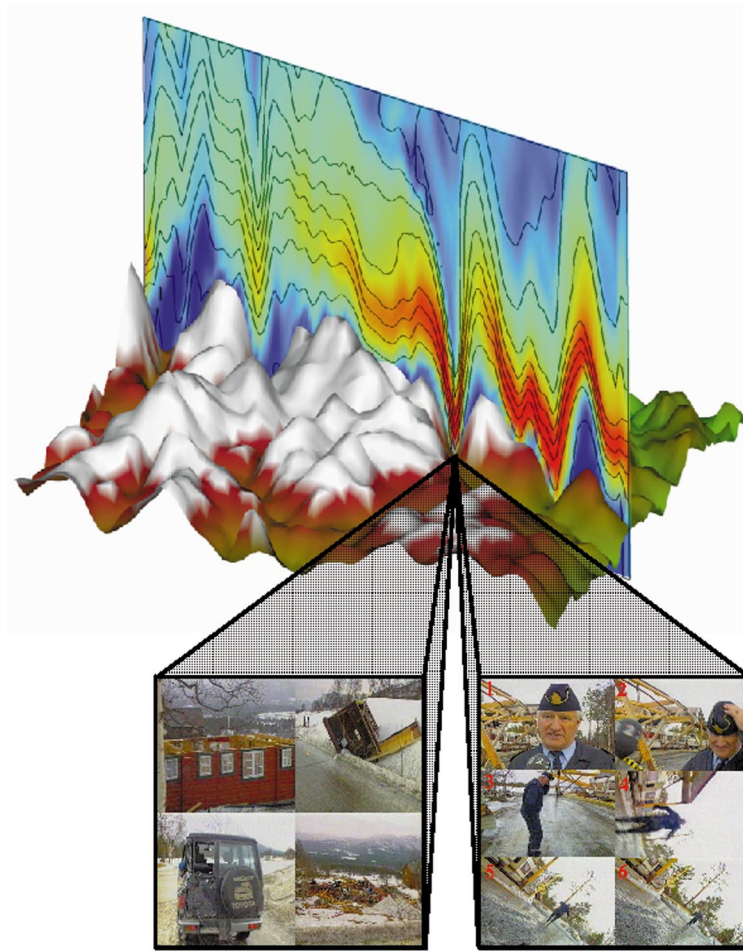
measurements of foreshore morphodynamic behavior. These measurements are preferable to estimates from other techniques, such as traditional surveying, because of the large spatial coverage and rapid sampling capability. This remote-sensing method is also advantageous in that it requires almost no human interaction and is therefore extremely affordable. We plan to use the field observations obtained using this method to further develop and validate models of

foreshore sediment transport. The value in such models would be in the prediction of beach change over fairly short time intervals, from days to weeks.

[Sponsored by ONR]

Reference

¹K.T. Holland and R.A. Holman, "Video Estimation of Foreshore Topography Using Trinocular Stereo," *J. Coastal Research* **13**, 81-87 (1997). ★



***Numerical Simulation and Unique Validation of a
Downslope Windstorm in Complex Topography***

Science-as-Art contest – Second Place winner

Submitted by: James Doyle and Melvyn Shapiro

This graphic is a three-dimensional representation of a downslope windstorm, as viewed from the northwest. The data used to create the figure are produced from a high-resolution numerical simulation using NRL's Coupled Ocean Atmosphere Mesoscale Prediction System (COAMPS) with a horizontal grid increment of 1 km. The windstorm occurred in a complex topographical region of central Norway on 31 January 1995. The cross section extends up to 4 km in the vertical and is 145 km wide in the horizontal. Color shading in the vertical cross-section plane represents the simulated horizontal wind speed, with indigo equivalent to speeds less than 5 ms^{-1} . Isentropes in the cross-section plane are shown in black at an interval of 3 K. As an intense prefrontal low-level jet passed over the Norwegian highlands, which contain mountain peaks in excess of 2 km, substantial internal gravity waves are generated and trapped beneath a critical level. Internal hydraulic jump structures form on the lee slopes of the mountains and contain wind speeds in excess of 60 ms^{-1} just above the surface.

The largest mountain wave and internal hydraulic jump is centered in the Oppdal Valley, in agreement with structural damage reports. Video footage (courtesy of TV-2 in Bergen, Norway) indicated that substantial damage occurred in the valley (left box). A remarkable validation of the model-simulated windstorm was provided by a television interview with a Norwegian police officer in the Oppdal Valley that was taken nearly simultaneously as the high winds occurred in the numerical simulation. Six still frames extracted from this interview (right box) illustrate the strength of the downslope windstorm, which initially caused the camera person to lose balance and fall down (frames 4-6) and subsequently blew the police officer rapidly down an icy road (frames 3-6). This unique validation highlights the exciting weather prediction capabilities of the new generation of mesoscale models such as COAMPS.

- 153 Confined Photons in Semiconductor Microcavities
T.L. Reinecke, P.A. Knipp, M. Bayer, and A. Forchel
- 155 Optical Detection of Defects Below the Surface of Nontransparent Materials
M. Bashkansky, M.D. Duncan, and J.F. Reintjes
- 156 Dark HORSE (Hyperspectral Overhead Reconnaissance—Surveillance Experiment)
J.V. Michalowicz and F. Bucholtz
- 159 The NRL Infrared Range Facility
K.A. Snail and R.G. Priest

Confined Photons in Semiconductor Microcavities

T.L. Reinecke,¹ P.A. Knipp,² M. Bayer,³ and A. Forchel³

¹Electronics Science and Technology Division

²Christopher Newport University

³University of Würzburg

Centimeter-sized cavities with metallic walls can be used to modify the coupling between electronic excitations, such as those in atoms, and the electromagnetic modes of the cavity, called photons, by modifying the photon density of states. This occurs because the electric fields of the photons must be zero at the cavity walls, which gives a discrete photon energy spectrum in the cavity. In this way, for example, spontaneous emission involving the atomic transitions can be reduced, which is of interest in connection with laser action. Such metal cavities are used in the microwave frequency range because the photon wavelengths there are of the order of the cavity size.

Semiconductor microcavities with dimensions on the order of microns might offer the opportunity to modify the photon spectrum for frequencies in the infrared and visible part of the spectrum. The structures are of interest in connection with applications ranging from thresholdless lasers to optical switching and quantum computation. In addition, semiconductor structures have the advantage that they can be a part of integrated optoelectronics in applications. To date, however, it has not been demonstrated that semiconductor structures can be fabricated with the ability to provide such control of the photonic properties.

Semiconductor Microcavities: The behavior of semiconductor microcavities is being studied in a collaboration involving theoretical work at the Naval Research Laboratory and fabrication and experimental work at the University of Würzburg in Germany. In these structures, a layered GaAs cavity of thickness on the order of microns is grown by molecular beam epitaxy between two highly reflecting mirrors provided by GaAs/AlAs superlattices grown above and below it. A 5-nm InGaAs quantum well is grown in the center of the cavity to provide the optically active electronic states, which are in the form of excitons. Then lithographic techniques and etching are used to fabricate a square structure by removing the material down through the GaAs cavity (see insert in Fig. 3).

The energies of the photons in these structures are studied by photoluminescence, which arises when excitons recombine into photons. The energies are shown as functions of lateral cavity size in Fig. 1.¹ The results of detailed calculations with no fitable parameters are given by the solid lines in the figure. Several photon modes are confined for each cavity size, and their energies are found to increase for decreasing lateral size. These effects result from the confinement of the photons by the large differences in refractive index between the semiconductor and the surrounding vacuum. This increase in energy is similar to that observed for electronic states confined by potential offsets in quantum dots, and thus the microcavities can be thought of as “photonic dots.” This work provides the first demonstration of confined photon states in three-dimensionally structured semiconductor microcavities.

Structures with Several Microcavities: Pairs of microcavities have been fabricated in which the photonic coupling between the cavities is given by an unetched bridge between them.² Their photonic modes have been studied as functions of this coupling, which is varied by changing the length and width of the bridges. An interpretation of the experimental results is given by calculations of photonic modes shown in Fig. 2. The two lowest lying modes are analogous to the *s*-bonding and *s*-antibonding

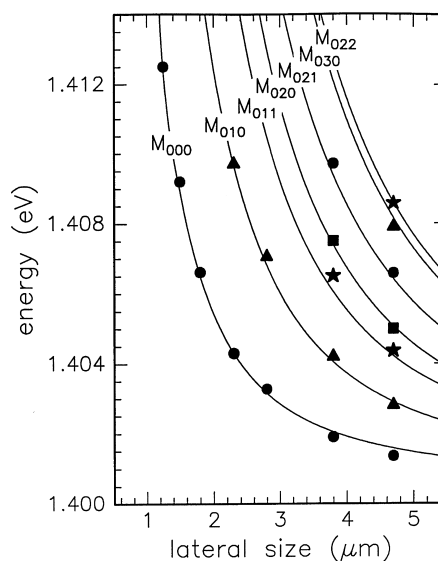


FIGURE 1 Photoluminescence results for the energies of confined photon modes as functions of lateral microcavity size compared with detailed calculations given by the solid lines.¹

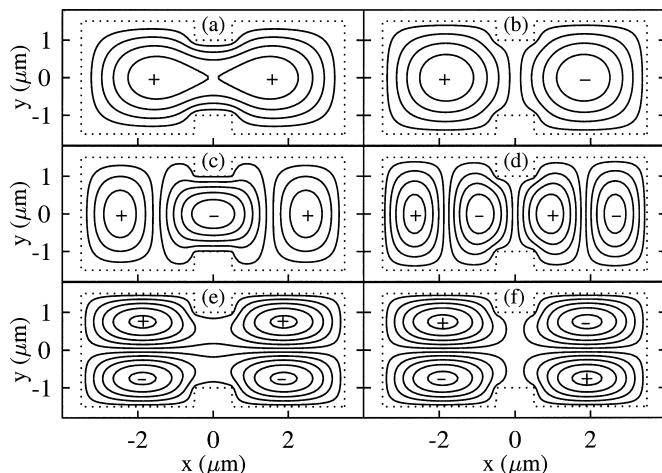


FIGURE 2
Calculated photon modes of photonic molecules given by pairs of coupled microcavities.²

states of electrons in molecules (Fig. 2(a),(b)), and higher lying modes are analogous to bonding and antibonding combinations of p_x and p_y states of molecules (Fig. 2(c)-(f)). For this reason, these structures can be thought of as “photonic molecules.” In this work, the wavefunctions in these photonic systems can be observed directly, and they provide novel insight into bonding effects in molecules.

Chains of up to 50 microcavities have been fabricated and studied by measuring their photoluminescence at varying tilt angles along the chain. This gives the dependence of the photon energy on the wavevector along the chain. In Fig. 3, the photon energies are seen to increase with increasing wavevector and to exhibit discontinuities near values of wavevector given by $n\pi/a$, where a is the repeat period of the chain and $n = 1, 2, \dots$. These wavevectors determine the edges of the Brillouin zones in the photonic chains. The gaps in the photon dispersions are analogous to the band gaps at the Brillouin zone edges of electronic states in solids. Such gaps are the hallmark of periodic structures, and they demonstrate that a “photonic crystal” has been achieved. Photonic band gap structures have been a focus of research for several decades, and this is the first demonstration of such a photonic crystal for energies in the optical regime. In very recent work, photonic defect states, which are analogous to electronic donor and acceptor states in solids, have been introduced into the photon band gaps by placing a single cavity that has a larger or smaller size in the chains.

This work has demonstrated that discrete, confined photon states can be obtained and understood in detail in semiconductor microcavity systems and that their photonic properties can be tailored to a remarkable degree, even to creating photonic molecules and photonic crystals.

[Sponsored by ONR]

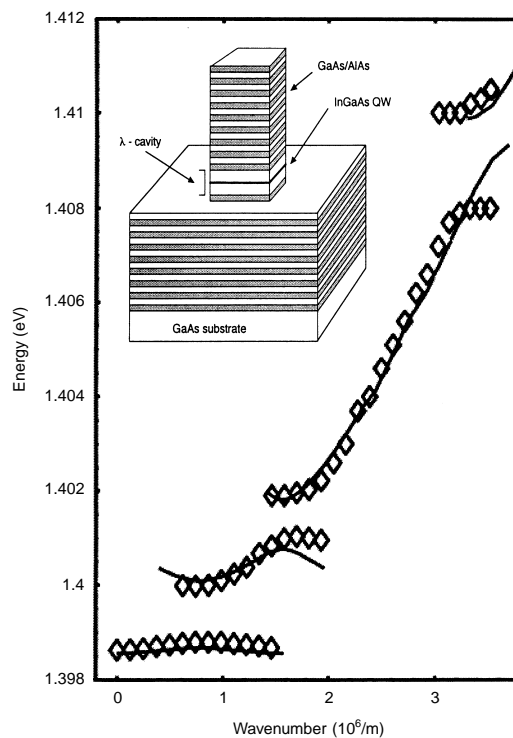


FIGURE 3
Energies of photon states of one-dimensional chain microcavities as functions of wavevector along the chains (lateral cavity size, $3.0 \mu\text{m}$). Gaps occur in the photon dispersions for wavevectors at the Brillouin zone edges of the one-dimensional photonic crystals. Insert shows the structure of each cavity.

References

- ¹J.-P. Reithmaier, M. Röhner, H. Zull, F. Schäfer, A. Forchel, P. A. Knipp, and T. L. Reinecke, “Size Dependence of Confined Optical Modes in Photonic Quantum Dots,” *Phys. Rev. Lett.* **78**, 378 (1997).
- ²M. Bayer, T. Gutbrod, J.-P. Reithmaier, A. Forchel, T. L. Reinecke, P. A. Knipp, A. A. Dremin, and V. D. Kulakovskii, “Optical Modes in Photonic Molecules,” *Phys. Rev. Lett.* **81**, 2582 (1998). ★

Optical Detection of Defects Below the Surface of Nontransparent Materials

M. Bashkansky, M.D. Duncan, and J.F. Reintjes
Optical Sciences Division

Modern military and industrial equipment rely extensively on advanced, highly engineered materials. These materials include ceramics, plastics, composites, and other, even more exotic materials such as diamond films. These materials are designed to have improved thermomechanical, chemical, and electrical properties. They are often expensive to manufacture, and they are used mainly in critical applications. For example, advanced ceramics are used as bearing components in the Space Shuttle and for high-energy density piezoelectric drivers in Navy sonar systems. It is important that the materials used in these applications be free from imperfections, since the presence of defects can cause a drastic reduction of component lifetime and can lead to catastrophic failures. It appears that structural defects in the near-surface region of these components are the most important since the operational stresses there are greatest. Conventional nondestructive evaluation techniques, however, are not well suited for the near-surface detection of small defects. To address this need, we have adapted an optical technique used in the biomedical community and demonstrated that it can be used to determine, nondestructively, the size and location of small subsurface defects in advanced ceramic and other materials. We have used this technique to find defects as small as $7\ \mu\text{m}$ in size and 1 mm below the surface in ceramic materials.

Technique: The optical technique we use is based on optical coherence domain reflectometry. A

variant of this technique has been developed by biomedical researchers and is used to image structures in the eye and in the near-surface regions of other tissue. We have pioneered the application of this technique to advanced ceramics and other materials. Figure 4 is a schematic diagram of our device. A broadband light source with a short coherence length is used in a fiber-based Michelson interferometer. In one arm of the interferometer, the reference mirror defines the position of a temporal gate, where the gate width is given by the coherence length. The other arm of the interferometer contains the sample. A signal is detected only when various reflecting structures on or inside the sample are positioned to match the length of the reference arm. The lateral resolution is determined by the focus of the signal beam, and an image is acquired by raster scanning over the sample or by scanning in one lateral direction and moving the sample in the Z direction. One of our contributions to this technology was the use of a very fast piezoelectric modulator in the reference arm that decouples the modulated signal from the Z motion of the sample. Coupled with a fast galvanometer mirror, this allows us to produce planar images in any direction in less than one second while still staying at the focus of the lens. We also developed a special optical scanning technique that allows imaging over a spherical convex surface. This is important for imaging the surface and subsurface regions of curved components such as ball bearings and rods.

Results: Figure 5 demonstrates the application of our technique to the detection of defects in ceramic ball bearings. Ceramic balls containing four types of critical defects were provided by a major ceramic manufacturer. The current inspection technique, used in the industry to identify these defects, consists of a human using an optical microscope. This

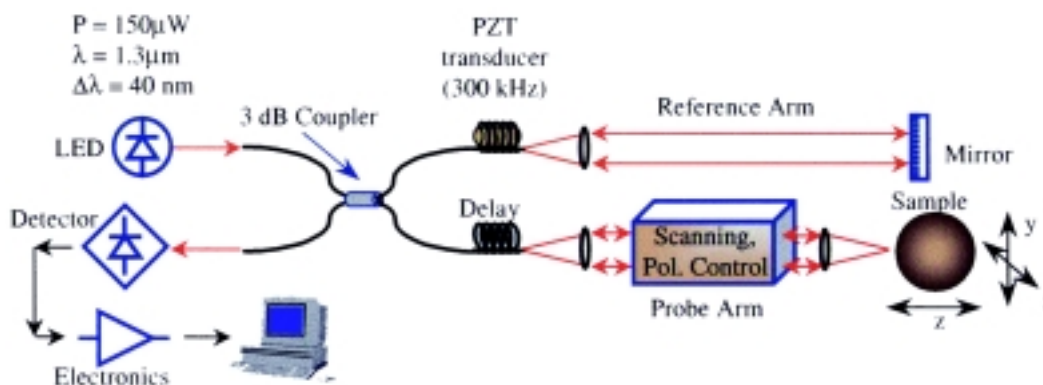


FIGURE 4
Schematic of the device.

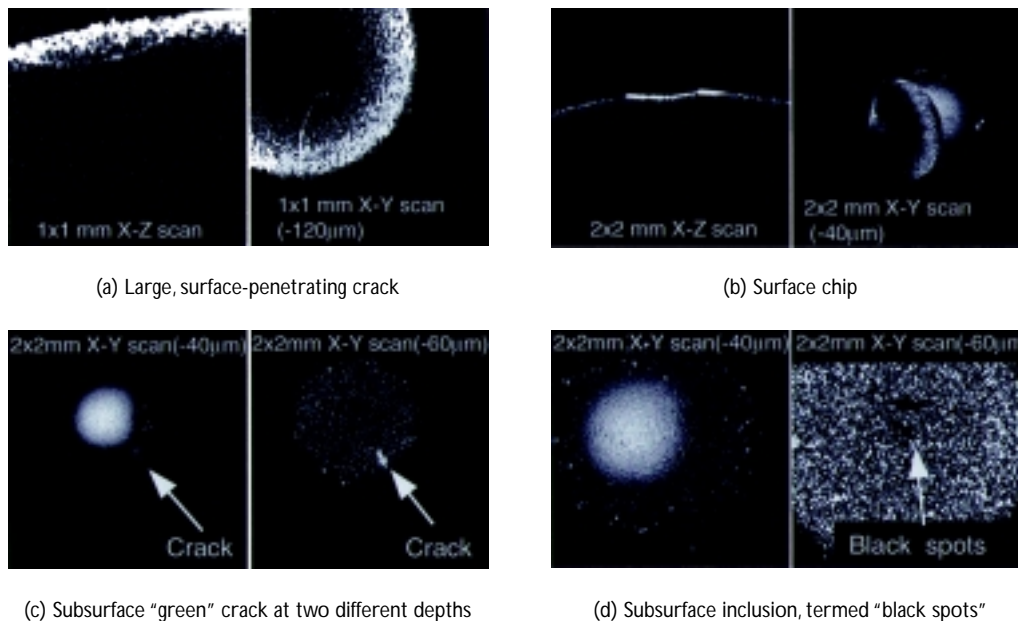


FIGURE 5
Two-dimensional scans showing various defects.

process is labor intensive and subjective, is affected by fatigue and illumination conditions, and produces low contrast images of some, but not all, of the important defects. As shown in Fig. 5, the images produced by our technique have high contrast and allow us to pinpoint the location of defects in three dimensions. With our current device we can detect defects as deep as $75\ \mu\text{m}$ in this particular material. Figure 5(a) shows scans of a large crack. The depth and the extent of the crack below the surface can be determined precisely. Figure 5(b) shows scans of a surface chip. Using our technique, the shape and extent of surface imperfections are determined easily. Figure 5(c) shows scans of a small "green" crack. This small subsurface crack can barely be seen under a microscope and is often missed using purely visual inspection. Our technique provides images with greatly improved contrast. Figure 5(d) shows scans of a small dark spot. In this case we can determine the location and the structure of the defect, information that can be used to identify the origin of the defect.

Summary: We have demonstrated the use of an optical technique for defect detection and localization in the near-surface region of advanced ceramic materials. In particular, we have identified four critical types of defects in ceramic ball bearings. This optical technique is currently in use in the biomedical field. Using improvements pioneered by NRL, we have shown how this technique has potential for the nondestructive evaluation of materials with important military and industrial applications. One of the

challenges for this technique is the limited depth of penetration into most samples. We plan to address this problem by increasing the power of the optical source and by extending the wavelength of our device further into the infrared, where both the absorption and the scattering are reduced for many materials of interest.

[Sponsored by ONR]



Dark HORSE (Hyperspectral Overhead Reconnaissance—Surveillance Experiment)

J.V. Michalowicz and F. Bucholtz
Optical Sciences Division

The Navy clearly recognizes the need for tactical military surveillance and reconnaissance of critical ground targets. If an aircraft has a high-resolution camera and knows exactly where to look, it may be able to obtain an image in which to identify and then strike a target. However, these are "soda-straw" systems: to get detailed resolution they can image only a small area at a time. As was evident in the search for mobile Scud missile launchers in Operation Desert Storm, tactical airborne systems must be able to cover wide areas and then strike immediately upon detecting the target. However, an increase in the search rate produces a concomitant loss in spatial resolution. A proven way to compensate for this loss of

spatial information is to exploit the spectral differences between targets of interest and local backgrounds as a detection discriminant. As part of the tri-service Joint MultiSpectral Program (JMSP), the Optical Sciences Division has been developing algorithms over the last several years that use the natural background correlations in multiple wavebands to detect unresolved and barely resolved targets in clutter and camouflage. These algorithms have various mathematical bases; some use filters matched to the spectral signatures of the targets, others search the scene for spectral anomalies. Both visible and infrared bands are used so that the systems will have day-night capability. With the maturation of these algorithms and parallel developments in highly sensitive multispectral/hyperspectral sensors and computational power, the time was ripe to demonstrate the feasibility of a tactical surveillance system that could provide timely and detailed reconnaissance information about the battlefield. In the Dark HORSE project, NRL became the first to successfully evince this tactical capability—to demonstrate, from an airborne platform, autonomous real-time cueing of a high-resolution framing camera for target identification using a hyperspectral imaging sensor with a real-time processor to provide the initial detections. At the same time, the real-time processor cued a pulsed laser mounted on a ball gimbal to designate the detected target as a simulation of target kill.

Dark HORSE Components: The first Dark HORSE demonstration was accomplished in October 1997 and used a rebuilt PHILLS sensor, a visible

grating spectrometer with a 512×512 charge coupled device (CCD) array fabricated by NRL's Plasma Physics Division, as the hyperspectral instrument. Cued visible panchromatic high-resolution imagery was obtained using the CA-260 25-megapixel framing camera built for NRL by Recon Optical Inc. (ROI). The real-time on-board processor was developed by Space Computer Corporation (SCC); it consists of a 200 MHz Pentium Pro with 8 SHARC boards and provides up to 1 Gflop/s of processing power. The ball gimbal laser designator, supplied by the Applied Physics Laboratory, Johns Hopkins University, consists of a custom near-infrared (NIR) pulsed laser mounted to the gimbal platform. Also on board was a long-wavelength infrared (LWIR) QWIP camera provided by the Jet Propulsion Laboratory. Data were transmitted to a ground station at NRL, Washington, D.C., using the Advanced Tactical Airborne Reconnaissance System Common Data Line (CDL).

The Dark HORSE 1 Collection: The flight tests were staged out of the Patuxent River Naval Air Station, Maryland, and flew over Fort A.P. Hill, Virginia, where ground vehicle targets had been deployed. The platform was a P-3 supplied by NRL's Flight Support Detachment (Fig. 6). The Dark HORSE data are displayed both in the airplane and the ground station (Fig. 7). Data from the hyperspectral sensor are analyzed by the real-time processor and shown as a continuous 3-color waterfall display. When a target is detected, the high-resolution camera takes a picture; in Fig. 7, two pictures

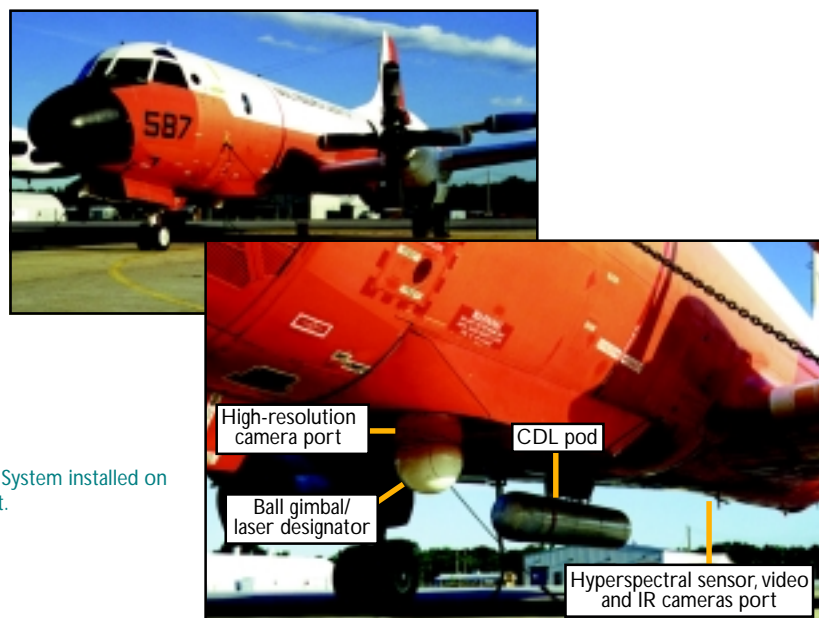


FIGURE 6
Dark HORSE 1 System installed on
NRL P-3 aircraft.

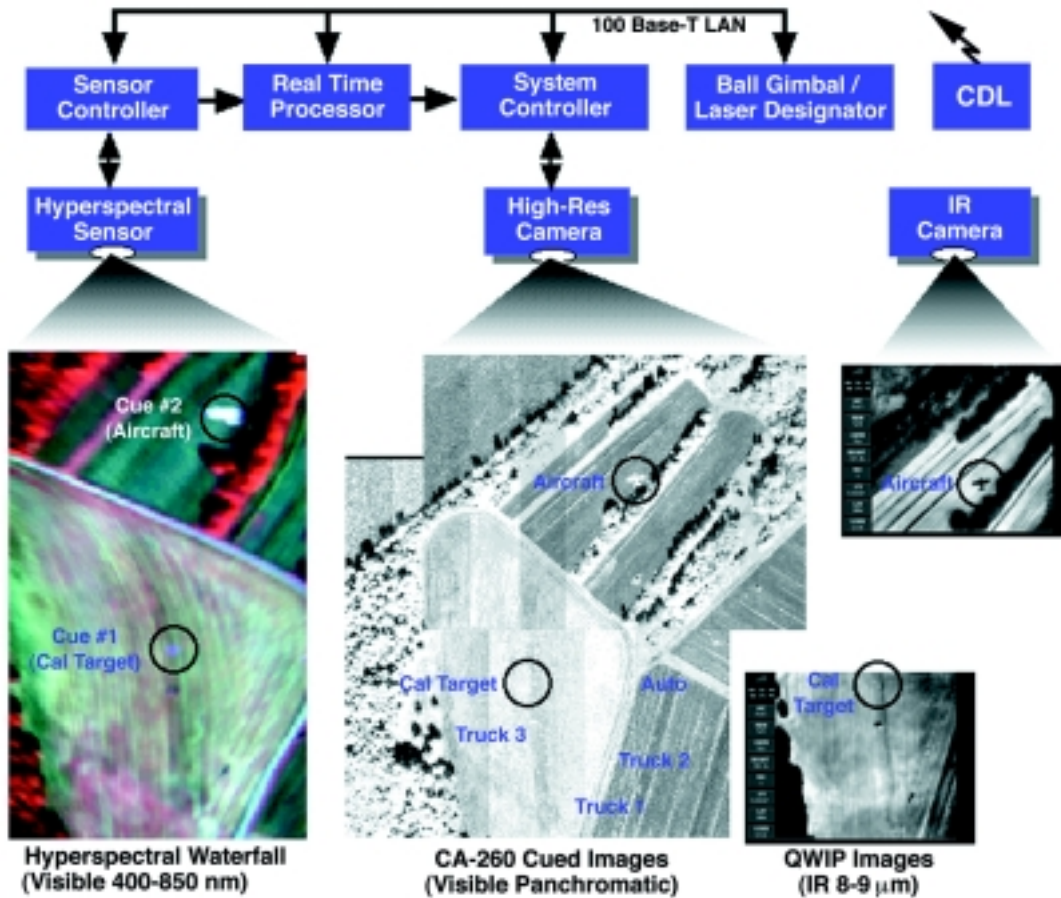


FIGURE 7
Dark HORSE 1 display.

are shown, one cued by a ground target and one by an airplane flying 4000 ft below the P-3 flight altitude of 7100 ft. Figure 8 is a full-resolution CA-260 picture of the target area.

False Alarm Mitigation: The real-time processor incorporated two simultaneous algorithms: a subspace R-X anomaly detector and a clustering algorithm, both with 3×3 -pixel spatial filtering. These algorithms were operated in combination to reduce false alarms; this was effective, as is shown in Fig. 9, where pixels detected by a single algorithm are shown in either red or blue and pixels detected by both are in white. Over the 5 sq. km strip containing our six target vehicles and six other manmade objects, the Dark HORSE 1 collection registered 20 natural features (generally trees dressed in their fall colors) as false alarms.

Future Plans: The Dark HORSE 1 collection demonstrated daytime operation in a nadir-looking mode. The Dark HORSE 2 collection at Eglin Air Force Base, Florida, in November 1998 is showing day/night operation with Aerospace Corporation's SEBASS (Spatially Enhanced Broadband Array Spectrograph System) LWIR/MWIR dispersive imaging spectrometer as the hyperspectral sensor. Subsequent Dark HORSE collections will be at long range and oblique angles.

Summary: NRL has successfully demonstrated, from an airborne platform, autonomous real-time hyperspectral detection of airborne and military ground targets, with autonomous cueing of a high-resolution framing camera for target identification and a gimbal-mounted pulsed laser for target designation.



FIGURE 8
Full-resolution ROI camera image.

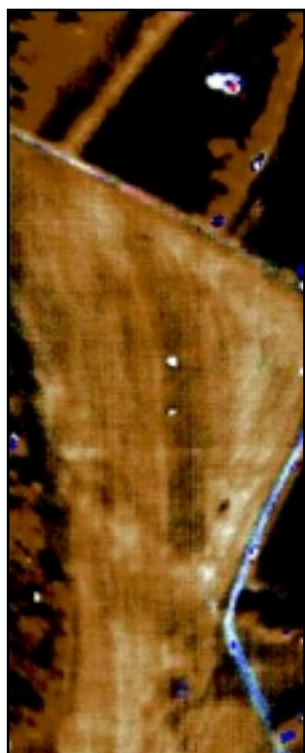


FIGURE 9
Detection pixels in multispectral waterfall display.

Acknowledgment: The authors acknowledge the other members of the Dark HORSE team: B. Brown, D. Brown, G. Hazel, J. Kershenstein, J. Lee, G. Lynn, C. Stellman, and N. Stone, all of NRL's Optical Sciences Division, and R. York of Sachs Freeman Associates (SFA).

[Sponsored by ONR]



The NRL Infrared Range Facility

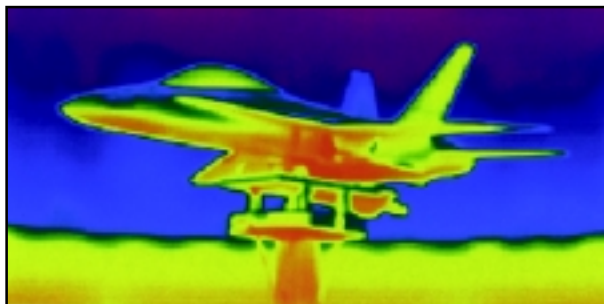
K.A. Snail and R.G. Priest
Optical Sciences Division

Background: Low observables (LO), countermeasures, and tactics are the primary approaches to improving a military vehicle's probability of surviving in combat. Over the last three decades, there has been a concerted tri-service effort to reduce the radar cross section (RCS) of military vehicles. One of the key techniques for reducing vehicle signatures in the radar frequency (RF) regime has been the testing of scale models in outdoor and indoor RF ranges. Range facilities provide a set of highly controlled conditions under which different LO materials and techniques can be evaluated. Although RF signatures have decreased, the fraction of U.S. aircraft losses in combat attributed to infrared (IR) missiles has increased. Consequently, there is a growing awareness of the need for new tools and techniques for dealing with the IR threat. In response, NRL started a Capital Procurement Program project in FY95 to design and build an infrared range. The objectives of this project were to provide a realistic simulation of uncluttered infrared backgrounds from sea level to 30 kft altitudes, viewing angles representative of standard IR threats, versatile control of a test article's temperature and orientation, and a low-cost alternative to IR field testing.

Range Features: The NRL Infrared Range Facility was brought on-line in late 1997 and has recently become fully functional. The chamber itself is 20 ft in diameter and 13 ft high (Fig. 10). The dry air atmosphere within the chamber has a dewpoint of approximately -60°C and a CO_2 level of below one PPM. The low dewpoints are needed to minimize frost formation on the chamber walls when they are configured for high-altitude conditions (e.g., 30 kft). The chamber walls used to simulate the zenith sky can attain temperatures as low as -110°C . Low CO_2 levels are needed to minimize absorption in the CO_2 doublet near $4.2\ \mu\text{m}$. The sky panels are coated with a new type of flocked black coating, with a reflectance below 0.2% throughout the infrared. Without such a coating, the thermal radiation from the warm Earth panels would reflect from the sky panels and overwhelm the emitted radiation from the sky. Test articles are inserted through the roof of the chamber and can be viewed over a range of elevation angles from -20° to $+20^{\circ}$. The test article itself can be rotated through $\pm 180^{\circ}$, be tilted through $\pm 45^{\circ}$, and



FIGURE 10
NRL Infrared Range Facility with operator console (lower right), primary IR camera port (next to operator on stairs), and midwave solar simulator port (next to operator on stairs).



(a)



(b)

FIGURE 11
(a) Thermal infrared image of a similar model in the NRL Infrared Range Facility; (b) stereolithographic model of an F/A-18 aircraft.

have its temperature controlled through a variety of heaters and/or temperature-conditioned fluids.

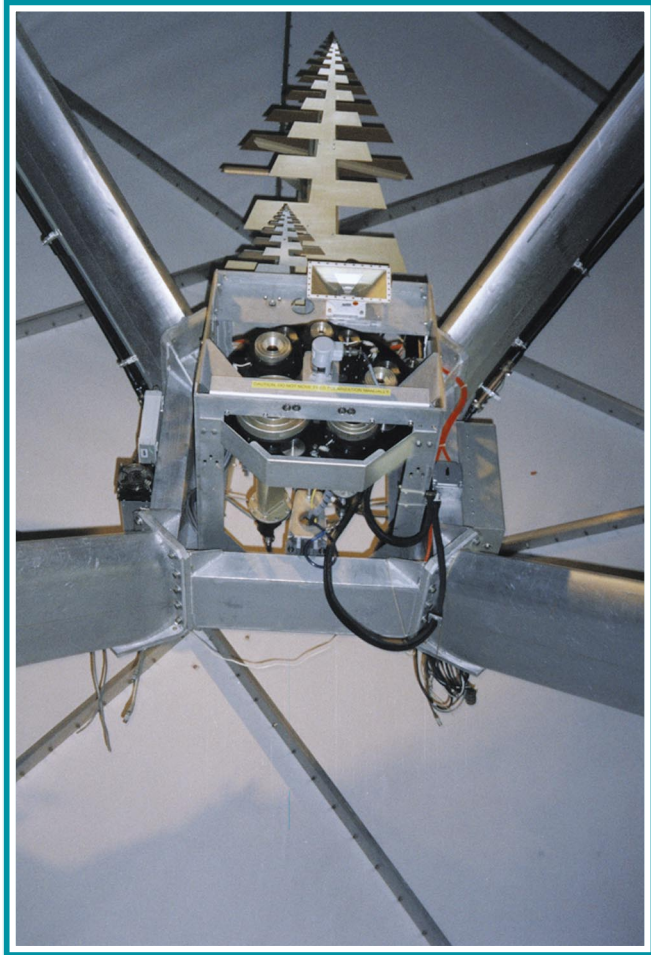
Sample Imagery: Scale models designed for use in the NRL IR Range Facility use internal fluid passages to achieve isothermal skin temperatures, and heaters to simulate the localized hot parts associated with engines and other internal heat sources. Temperature control of the model's skin is needed for accurately simulating aerodynamic heating of air vehicles and solar loading effects for ship and ground vehicles. Figure 11 shows a stereolithographic model of an F/A-18D aircraft along with an infrared image

of a similar model measured in the NRL IR Range Facility. Range measurements can be used to estimate the maximum detection range of standard IR threats, including man-portable missiles.

Summary: A new type of infrared simulation facility has been developed at NRL. The NRL IR Range Facility is currently being used by LO engineers to reduce the IR signature of numerous military weapons systems. The availability of this facility will hasten the transition of new IR LO technologies to operational use.

[Sponsored by NRL]





Midway Research Center – Antenna Tracking System
Science-as-Art contest – Third Place winner
Submitted by: Robert McKnight, Edward Becke, and Roger Eisinger

This photograph shows the feed antenna assembly inside Antenna Tracking System I at the Midway Research Center (MRC), located near Quantico, Virginia. The Naval Center for Space Technology operates the MRC as a facility for transmitting accurate calibration signals. Each of the three ATS units includes a 60-ft diameter parabolic reflector antenna enclosed in a large radome. Shown here is the feed assembly at the focal point of one of these antennas, which is mounted on four spars on the front of the reflector. The collection of antenna feeds can transmit signals ranging in frequency from 200 MHz to 18 GHz. The geometric “jumble” includes two NRL-built log-periodic antennas (the pyramids at the top of the photo), and five round scalar feeds built onto a turntable (a black disk known as the “pizza wheel”), which rotates a selected feed into the exact focal point of the antenna. This photo was taken from a lift some 45 ft above the ground as part of the multiyear upgrade effort currently being performed by NCST to improve the capabilities of the facility.

- 163 Multifrequency Polarimetric SAR Images of Gulf Stream Features from Space
S.R. Chubb, T.F. Donato, F. Askari, A.L. Cooper, and S.A. Mango
- 164 Autonomous Survey System
B.S. Bourgeois and A.B. Martinez

Multifrequency Polarimetric SAR Images of Gulf Stream Features from Space

S.R. Chubb, T.F. Donato, F. Askari, A.L. Cooper, and S.A. Mango
Remote Sensing Division

Introduction: Synthetic aperture radars (SARs) produce fine-resolution images of the Earth from space, day or night, regardless of weather conditions. These characteristics make SARs especially attractive for environmental and tactical surveillance. For this reason, the Navy, Air Force, and Army have targeted SAR as an important technology for tomorrow's Armed Forces.

Recent advances in processing, data storage, and hardware are providing new capabilities that enhance the usefulness of SAR. For surveillance purposes, an especially promising new procedure has resulted from these enhancements. It involves synthesizing different SAR images of a single scene from space by using multiple radar polarizations and frequencies. In this article, we examine the results of applying this new technique for the first time to a particular problem in ocean surveillance: the identification and characterization of strong ocean frontal features from space, using multifrequency, polarimetric SAR images.¹

Setting the Scene: During NASA's first Shuttle Radar Laboratory (SRL-1) experiment, members of the Shuttle crew obtained a unique set of SAR images of wave and current features at the boundary of the Gulf Stream (GS). The set is unique because: NRL scientists simultaneously measured the local environmental conditions; the crew collected the data using three different frequencies and four polarizations; and in the resulting imagery, a pronounced increase in radar intensity occurs at one frequency and polarization near the GS boundary in one image but not in the remaining images.

Gulf Stream Boundary Imagery/Ground Truth: On 17 April 1994, members of NASA's SRL-1 Shuttle team collected SAR imagery data from an area near the northern boundary of the GS. They used three radar frequencies: L-band (1.25 GHz), C-band (5 GHz), and X-band (10 GHz), and a combination of horizontally (H) and vertically (V) polarized signals. Using this information, scientists from the Jet Propulsion Laboratory (JPL) constructed L-band

and C-band images in which both the received and transmitted signals are either H polarized (which we refer to as H-H imagery) or V polarized (V-V imagery). In addition, these scientists constructed L-band images in which the transmitted signal is H polarized and the received signal is V polarized (H-V imagery); while German scientists from Deutschen Zentrum für Luft-und Raumfahrt (DLR) synthesized X-band V-V imagery. Simultaneously, NRL scientists aboard the research vessel R/V *Cape Hatteras* performed in situ measurements of the local environmental conditions in the same area.²

Figure 1 shows the L-band H-V image. The arrows indicate a number of prominent submesoscale features. In the remaining L-band and C-band H-H and V-V images, and in the X-band V-V image, we find the same features, in the same locations² with one important exception: the feature that we have marked "Thermal Front," which appears as a bright line in the H-V image in Fig. 1, either disappears or appears as a dark line.

Modeling: From the environmental information that NRL scientists collected during the experiment, we have performed detailed radar simulations.² These

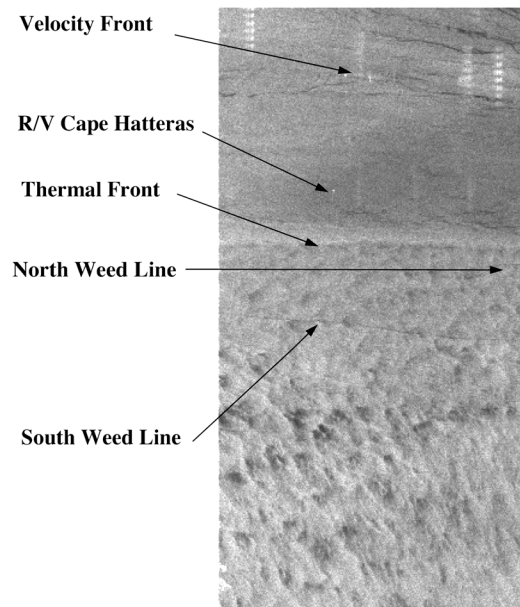


FIGURE 1
L-band H-V image of region near north boundary of the GS, derived by JPL from data collected during NASA's SRL-1 mission. Arrows mark prominent features that NRL scientists have identified from measurements performed during the experiment.

calculations explain why the “Thermal Front” feature is bright only in the L-band H-V image. Specifically, in this image, polarization-dependent filtering takes place that accentuates local variations in wave slope. The filtering occurs because the dominant (resonant Bragg scattering) reflection processes that take place at the ocean surface conserve the polarization (or angular momentum) of the incident signal, except when considerable local tilting from longer waves is present.¹ The radar intensity variations in H-V images result from processes that do not conserve polarization. For this reason, pronounced variations in intensity occur in these images in regions involving appreciable tilt; in comparable images in which the transmitted and received signals have the same polarization, these variations are absent.

Conclusion: For the first time, we have identified relationships between strong frontal features at the ocean surface and variations in radar intensity in SAR imagery obtained with multiple polarizations and frequencies from space. An important result of the work is that, near fronts, environmental forcing from currents and wind frequently causes enhancements in radar intensity in images in which the transmitted and received signals have different polarizations. This conclusion has important implications in the design and application of future SAR systems for surveillance purposes.

[Sponsored by ONR]

References

- ¹J.-S. Lee, R.W. Jansen, D.L. Schuler, T.L. Ainsworth, G.O. Marmorino, and S.R. Chubb, “Polarimetric Analysis and Modeling of Multifrequency SAR Signatures from Gulf Stream Fronts,” *IEEE J. Ocean. Eng.*, **23**, 322-333 (1998).
- ²S.R. Chubb, T. Donato, F. Askari, R. Romeiser, S. Ufermann, A.L. Cooper, W. Alpers, and S.A. Mango, “Study of Gulf Stream Features with a Multi-Frequency Polarimetric SAR from the Space Shuttle,” *IEEE Trans. Geos. Rem. Sen.*, in press (1998). ★

Autonomous Survey System

B.S. Bourgeois
Marine Geosciences Division

A.B. Martinez
Tulane University

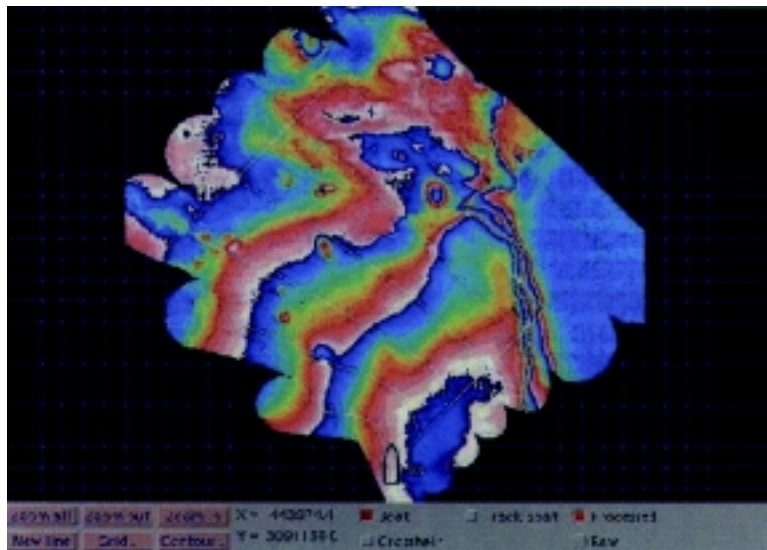
Bathymetric Surveying: For many decades, bathymetric surveys have been conducted using vertical single-beam sonar systems. Surveys were conducted using a series of preplanned navigation lines based on historical knowledge of an area’s depth.

Acoustic imaging systems were used to ensure that shallower areas did not exist between the sounding lines. Modern swath bathymetry systems provide multiple soundings with each sonar ping, within a narrow swath perpendicular to the ship’s track. Compared with single-beam systems, swath systems can provide 100% bottom coverage, yielding denser soundings and faster coverage of an area. Swath systems are typically operated at or near the ocean surface to maximize bottom coverage with time. Since a swath sonar covers an angular sector (as large as 150° for some systems), the actual swath width on the ocean floor varies with ocean depth—narrower in shallow water and wider in deep water. Also, the effective swath width of these systems is adversely affected by environmental conditions such as sea state, sound velocity profile, bottom morphology, and bottom composition. The consequence of these factors is that it is difficult to predict a priori the effective swath width and to preplan navigation lines for minimum survey time while ensuring complete bottom coverage. Consider a simple case in which a series of parallel lines are to be run over an area with a slope, and the lines are oriented perpendicular to the contour of the slope. If planned line spacing is computed using the average depth and the nominal swath width, the result will be excessive overlap between swaths in the deep areas (wasted survey time) and gaps between swaths in the shallow areas (missing data).

AutoSurvey: The AutoSurvey system was developed to provide more efficient deployment of swath bathymetry systems through an environmentally adaptive approach—minimizing total survey time while ensuring complete area coverage and adequate data quality. Building on the real-time swath bathymetry processing system developed by C&C Technologies, Inc., functionality has been added to estimate the actual swath width after the completion of each survey line, and to automatically generate the next line’s waypoints.

Real-time processing of the data involves georectification of the depths and across-track ranges generated by the sonar using vessel position and heading, as well as correction for tide, sonar head depth, and ray bending. Part of this processing step includes the numeric analysis of the data to ensure that the final corrected results achieve specified quality standards in terms of horizontal and vertical accuracy. When gridded, these data can be used to create a color contour bathymetry display (Fig. 2). Figure 2 is the result of a simulator run using previously collected data over the East Flower Garden near Corpus Christi, Texas.

FIGURE 2
 Simulator-generated color contour bathymetry.



Processed data that meet the specified quality constraints are then analyzed to find the effective swath edge. This edge, along with a user-specified percent overlap between swaths, is used to generate the waypoints for the next survey line. Three approaches are provided for generation of the next survey line to allow for flexibility in the execution of the surveys. Each approach involves fitting line segments to the previous swath's edge: (1) Straight line—adaptively spaced parallel straight lines; (2) Linear Regression—nonparallel straight lines; and (3) Piecewise Linear—a series of joined line segments. All three methods are computationally efficient and can be performed in real time through the use of adaptive spatial reduction. Figure 2 shows the results of a simu-

lation run using the Piecewise Linear method, where the white lines are the generated tracklines. In this simulation, the survey was started on the upper right edge of the survey boundary (identified by the white box). Figure 3 shows the bathymetric coverage for this simulation run. The darker areas are regions where adjacent swaths overlap, and areas with missing data are black. It is evident from Fig. 3 that there is minimal overcoverage and missed data.

Results: The AutoSurvey system has been fully implemented on the ORCA, an unmanned semi-submersible equipped with a multibeam bathymetry system. With the ORCA, AutoSurvey-generated waypoints are fed directly into the control system

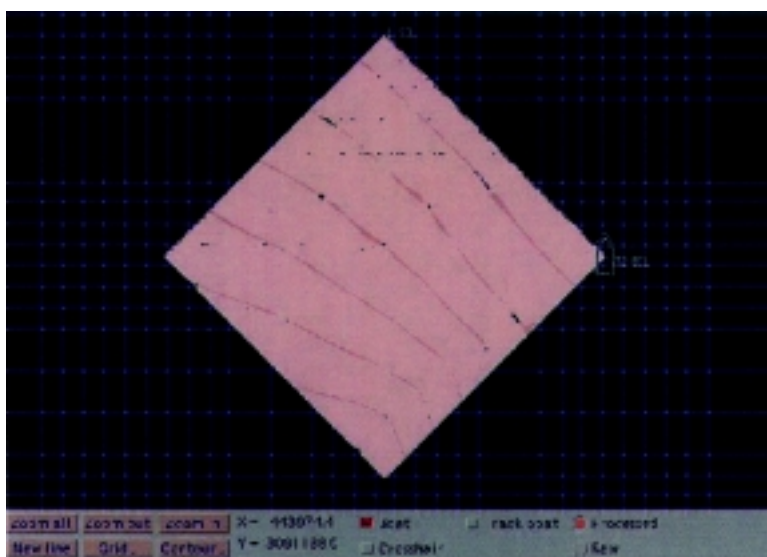


FIGURE 3
 Simulator-generated bathymetry data coverage.

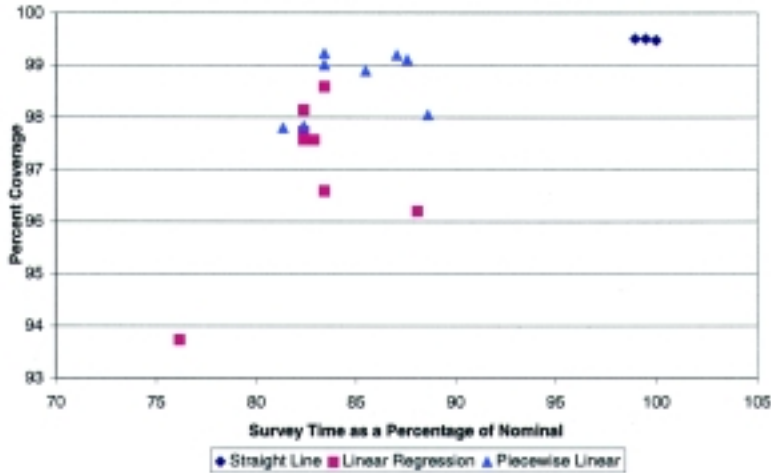


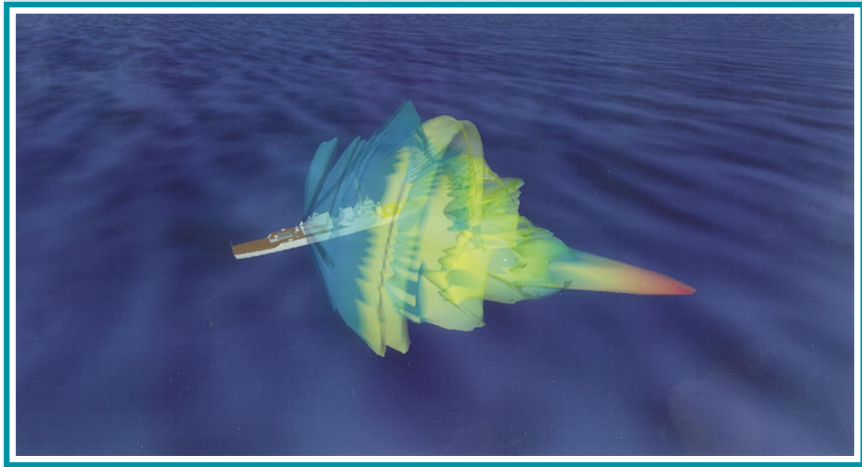
FIGURE 4
AutoSurvey simulation results.

autopilot, allowing a completely autonomous “hands-off” survey of a region. To conduct a survey, the operator designates a survey region by drawing a polygon on the system’s geographic display and then initializes the software processes. Once started, ORCA will conduct the entire survey without intervention.

Figure 4 shows simulation results using the East Flower Gardens data, comparing the time for survey completion between the Straight Line, Linear Regression, and Piecewise Linear approaches. The nominal survey time was arbitrarily chosen to be the

cluster of the 3-Straight Line results. Note that the Straight Line method used here involves adaptive spacing of the tracklines, which would be expected to yield shorter survey times than if a constant spacing were used over the entire survey region. The simulation results clearly indicate that this approach to swath surveying can reduce survey time by 15% or greater, while ensuring sufficient area coverage *and* data quality. This translates into significant savings in terms of ship cost for bathymetric surveys.

[Sponsored by Oceanographer of the Navy] ★



Mark-51 Fire Control Radar Antenna Pattern
Science-as-Art contest – Third Place winner
Submitted by: Mike Zyracki

Three-dimensional antenna pattern of a fire-control radar aboard a *Burke*-class ship. The colors of the antenna pattern highlight the strength with which other objects, such as incoming missiles, defensive decoys, or other ships, would be illuminated in the side and back lobes as well as the main beam. This frame is from an animated visualization of data from an at-sea test of the fire control system.

- 169 Ground Truth Reference System
A.C. Hosmer
- 170 Master Stability Functions for Synchronizing Systems
L.M. Pecora and T.L. Carroll
- 174 Reduced Manning—Its Impact on Damage Control
P.A. Tatem and F.W. Williams
- 175 Transition to Detonation in Turbulent Flames
A.M. Khokhlov and E.S. Oran
- 177 Atmospheric RF Propagation Effects on Tracking, Navigation, and Communication Links
J. Choi and M. Regan

Ground Truth Reference System

A.C. Hosmer

Tactical Electronic Warfare Division

Requirements: A primary focus of the Tactical Electronic Warfare Division at NRL is countering the missile threat to the Navy. The radar-guided antiship cruise missile (ASCM) is of particular interest. Engineers and scientists at NRL develop, test, and deploy effective countermeasures or electronic attack (EA) techniques to defeat these missile guidance systems through an extensive research and development process. NRL conducts tests using ASCM simulators at major points in the development cycle. Initially, these tests are conducted in the controlled and repeatable laboratory environment. As development continues, testing becomes more realistic and less controlled. The development cycle culminates in an at-sea flight test that includes simulators carried aboard NRL's NP-3D aircraft, one or more ships, and various offboard decoys (Fig. 1). Laboratory data analysis is relatively straightforward since the position of all targets is precisely known. On the other hand, at-sea data analysis is labor-intensive, in part due to the inability to precisely locate the test platforms in a fixed coordinate system.

Approaches: One possible solution for obtaining ship location is to record data from a Global Positioning System (GPS) on the ship. However, logistics and the timeliness of data retrieval complicate the issue, and it is not an option for offboard decoys such as chaff. A dedicated tracking radar on the aircraft is another solution for recording the positions of moving objects on the test range precisely as a

function of time. However, a radar system is expensive to obtain, install, and maintain, can interfere with test results, and reduces the number of simulators the aircraft can carry. Distributed sensor, time-space-position information systems provide an ideal solution for obtaining the required position data. These systems use multiple sensors separated from each other by a fixed distance, with each sensor measuring the range and angle to the targets. They are complex and costly to implement; they involve multiple hardware installations, complex mathematical computations for extraction of coordinate information, synchronization of individual sensor measurements, and independent calibration of the different measurement stations. Consequently, the accuracy of the resolved target positions can be severely degraded. This degree of coordination and structure is also not a realistic solution for most electronic warfare (EW) field tests since the Navy conducts at-sea tests on many different test ranges, and assets are limited.

Several years ago, NRL personnel conceived the novel idea of using existing data from the NP-3D mounted simulators to determine platform locations. This approach offered the promise of providing the required information without the cost, technical complexity, or logistical impact of the alternatives. By design, however, missile-seeker simulators are optimized for terminal homing but not for target tracking. Therefore, identifying precise target locations using only one simulator is not realistic. Integrating data from several simulators, however, improves target location accuracy to the point where closely spaced target returns can be resolved. By using the P-3 Inertial Navigation System (INS) and GPS data, the locations are translated to a fixed coordinate system.

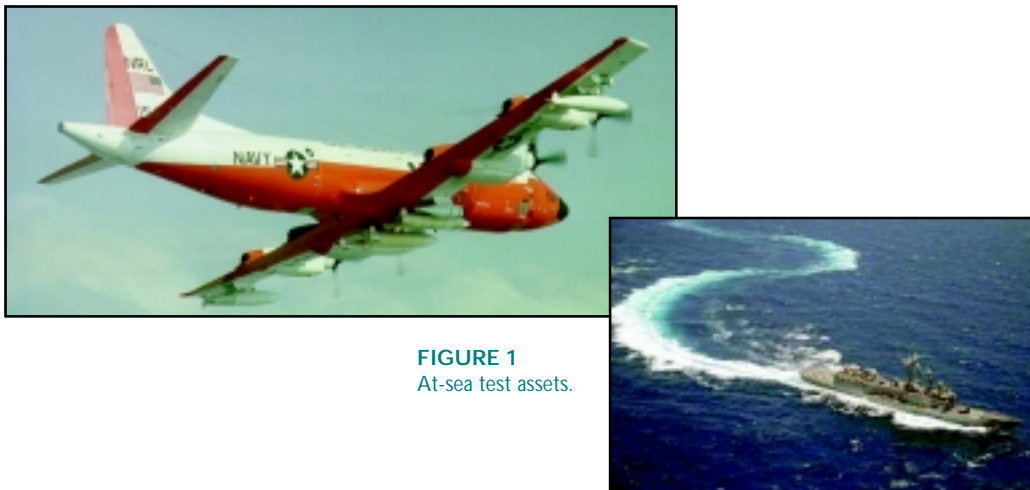


FIGURE 1
At-sea test assets.

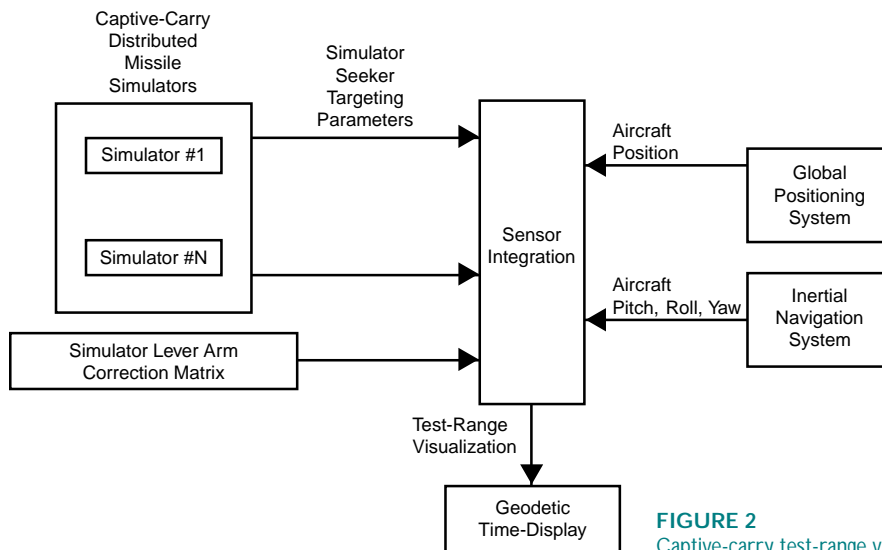


FIGURE 2
Captive-carry test-range visualization process.

Implementation: The Ground Truth Reference System (GTRS) accurately displays, in geodetic coordinates, a complete pictorial presentation of a field test experiment using only the onboard simulators of the captive-carry aircraft (Fig. 2). The GTRS architecture uses the body fixed, navigation, and tangent plane coordinate systems to process the simulator track data. A new digital interface records the Euler angles (pitch, roll, and yaw) from the INS on the aircraft. After time correlation, GTRS uses these angles to translate the simulator data between these coordinate systems. GTRS also performs a series of lever-arm corrections to translate each simulator's mounting position and orientation to the reference of the GPS antenna. The algorithm creates an error bubble centered on the expected ship location using the drift angle (the difference between the INS heading and the direction of travel), the simulator reported range to target, and the knowledge that the aircraft flies toward the test ship. When the simulator reports a track within this bubble, it is marked as the ship. Finally, the GTRS features a new digital interface to the aircraft GPS. After time correlating these data, GTRS maps the entire engagement into a geodetic display. The output of the algorithm is a graphical display of the P-3 flight path, the recorded path of the tracked target, and the derived path of the ship. If the latter two paths coincide, the ship was "hit."

Using the GTRS enables the data analyst to determine whether a specific engagement was effective more quickly, reliably, and objectively than previously possible. Future development should allow the GTRS to display successful decoy geometries, further enhancing the analysis efforts.

[Sponsored by NAVAIR]



Master Stability Functions for Synchronizing Systems

L.M. Pecora and T.L. Carroll
Materials Science and Technology Division

Introduction: Networks in which nearly identical elements are connected in some fashion and which evolve and influence each other are ubiquitous in nature and manmade systems. Biologists often consider nerve cells as coupled oscillators, and coupled arrays of Josephson junctions are being considered for voltage standards. Coupled arrays of laser diodes may increase the power available from solid-state lasers. Researchers are also studying clusters of coupled nonlinear circuits to take the place of mechanical phase shifters in phased-array antennas.

One common and important type of behavior in all these systems is synchronous behavior in which all the elements or nodes of the network do the same thing at the same time. This can often lead to coherence, efficiency, and increased power output, for example. A key question that comes up in the study or design of networks is, for what types of coupling between elements and what parameter settings is the synchronous state stable? Such analysis is often carried out in intensive modeling of the network and is often done on a case-by-case basis.

We have shown that for many types of coupled networks of systems we can calculate a master stability function for each particular node or oscillator in the network and each coupling function that, once and for all, solves the problem of stability for any configuration of those oscillators with any number of oscillators present. In fact, finding the stability of a

particular oscillator configuration becomes a simple matter of finding eigenvalues of a connection matrix rather than a brute force calculation of the stability exponents from scratch. This work was recently published in *Physical Review Letters*¹ and we review the basic results from that work here.

The Network: Here we set up the mathematical system that models a network of oscillators (see Fig. 3, for example), one oscillator at each node of the network and all oscillators assumed identical. Each oscillator has an output function (assumed the same for all oscillators), but we assume the output is fed to other nodes in the system by a general set of connections that we do not specify, yet. Our goal will be to generate a set of evolution (differential) equations that let us estimate the stability of the synchronous state.

Let there be N nodes in the network. Each node will contain an oscillator that is represented by m dynamical variables. The i th node will have a vector of variables $\mathbf{x}^{(i)} = (x_1^{(i)}, x_2^{(i)}, \dots, x_m^{(i)})$. We assume that the dynamics of each isolated node is given by an ordinary differential equation (ODE):

$$\frac{d\mathbf{x}^{(i)}}{dt} = \mathbf{F}(\mathbf{x}^{(i)}). \quad (1)$$

Suppose each node has an output given by the vector function $\mathbf{H}(m$ components), so that $\mathbf{H}(\mathbf{x}^{(i)})$ is the output of the i th node.

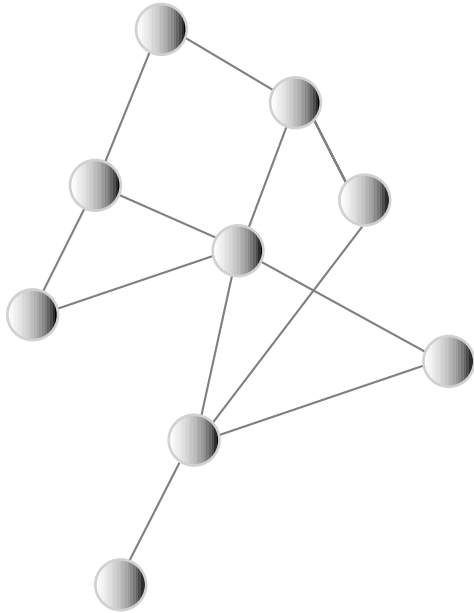


FIGURE 3
Example of a configuration of nodes and coupling connections between them.

We build the network by connecting the nodes (oscillators) as follows. We modify the equation of motion for each node (Eq. (1)) by adding a weighted sum of outputs (using \mathbf{H}) from all other nodes (some weights may be zero):

$$\frac{d\mathbf{x}^{(i)}}{dt} = \mathbf{F}(\mathbf{x}^{(i)}) + \sum_{j=1}^N G_{ij} \mathbf{H}(\mathbf{x}^{(j)}), \quad (2)$$

where the weights G_{ij} make up a connection matrix \mathbf{G} . We can actually use much more general coupling than the linear combinations of Eq. (2), but we keep to this simpler form for clarity.

The Synchronization Problem: Given this network (Eq. (2)), we now seek to answer the question, when is the synchronous state stable? The synchronous state is defined as the case when $\mathbf{x}^{(1)} = \mathbf{x}^{(2)} = \dots = \mathbf{x}^{(N)}$ at all times. This latter set of equalities defines a set of $N - 1$ constraints that specifies a “hyperplane” or flat subspace in the overall state space of the system. The dimension of the overall state space is mN since that is how many dynamical variables there are. The synchronization constraints dictate that the motion all takes place on an m -dimensional flat subspace, which we call the synchronization manifold. The question of the stability of this state comes down to confirming that if we perturb the system to go slightly off the synchronization manifold, the system will return to the subspace and the synchronous state.

The last statement allows us to derive an equation of motion for the perturbations away from the desired synchronous state and use it to test for the stability. Suppose the synchronous state is represented by the m -dimensional vector $\mathbf{s}(t)$, so that $\mathbf{x}^{(1)} = \mathbf{x}^{(2)} = \dots = \mathbf{x}^{(N)} = \mathbf{s}(t)$. Let $\mathbf{y}^{(i)} = \mathbf{s}(t) + \xi^{(i)}$ be a perturbed vector of the i th node. Differentiating each \mathbf{y} equation, using the ODEs for these and subtracting Eq. (2) gives a set of equations for the perturbations $\xi^{(i)}$, $i = 1, 2, \dots, N$:

$$\begin{aligned} \frac{d\xi^{(i)}}{dt} &= \mathbf{F}(\mathbf{x}^{(i)} + \xi^{(i)}) - \mathbf{F}(\mathbf{x}^{(i)}) \\ &+ \sum_{j=1}^N G_{ij} [\mathbf{H}(\mathbf{x}^{(j)} + \xi^{(i)}) - \mathbf{H}(\mathbf{x}^{(j)})]. \end{aligned} \quad (3)$$

If we use the Taylor series to expand in small $\xi^{(i)}$ we get the following form for the evolution equation of the perturbations:

$$\frac{d\xi^{(i)}}{dt} = \left[\mathbf{J}(\mathbf{x}^{(i)}) + \sum_{j=1}^N G_{ij} [\mathbf{DH}(\mathbf{x}^{(j)})] \right] \cdot \xi^{(i)}, \quad (4)$$

where $\mathbf{J}(\mathbf{x}^{(i)})$ is the Jacobian of \mathbf{F} , the linear term in the Taylor expansion, and $D\mathbf{H}(\mathbf{x}^{(i)})$ is the Jacobian of \mathbf{H} . Note that since all node variables equal $\mathbf{s}(t)$, these Jacobians are the same for all nodes. The equations for the evolution of the perturbations are usually called the variational equations.

The problem now is to calculate the evolution of perturbations orthogonal to the synchronization manifold using the variational equations. If these damp out, the synchronization state is stable. If not, then any small defect in the network or noise in the system will cause the synchronous motion to go away. The main problem is that the perturbations orthogonal to the synchronization manifold are mixed into the perturbations on each node $\xi^{(i)}$ in a nontrivial way. In the next section we show how to separate out the perturbations orthogonal to the synchronization manifold from those in the synchronization manifold that do not determine the stability of the synchronous state.

The Synchronization Solution: A Master Stability Function: We could solve our problem by a brute-force numerical simulation of Eq. (4) (involving mN variables) and at each time step project out the orthogonal component of the perturbations, but we now derive a more elegant and very general approach.

First, for the motion to be consistent with synchronous behavior we must have $\sum_j G_{ij} = 0$ (zero row sum) so that when all $\mathbf{x}^{(i)} = \mathbf{s}(t)$, the coupling vanishes and all motions are the same.

Next we note that we can block-diagonalize the variational equations, Eq. (4), by diagonalizing the matrix \mathbf{G} . This gives a set of m -dimensional blocks that are now uncoupled:

$$\frac{d\zeta^{(k)}}{dt} = [\mathbf{J} + \gamma_k D\mathbf{H}] \cdot \zeta^{(k)}, \quad (5)$$

where γ_k are the eigenvalues of \mathbf{G} , $k = 0, 1, 2, \dots, N - 1$ and ζ 's are the new variables in the eigencoordinates. Now, because of the zero row-sum requirement on \mathbf{G} we know that one of the eigenvalues must be zero, and we associate γ_0 with that value. This is important since that eigenvalue is associated with the m -dimensional block that represents perturbations that are in the synchronization manifold. The remaining $N - 1$ blocks are associated with perturbations orthogonal to the synchronization manifold. In this way we have succeeded in separating out the perturbation directions we want to study.

We can do even more if we notice the following. All the m -dimensional blocks like Eq. (5) have the same form. In fact, the only difference between them

is the numerical (complex) eigenvalue. Hence, we propose the following. Solve the “generic” block variational equation

$$\frac{d\zeta}{dt} = [\mathbf{J} + (\alpha + i\beta)D\mathbf{H}] \cdot \zeta \quad (6)$$

for all (or a wide range of) α and β values, i.e., over the whole complex plane. These solutions will tell us whether the generic perturbations ζ will damp out or grow. Their behavior either way will be determined by a stability exponent λ (the Lyapunov exponent), which will be negative for damping and positive for growing. This exponent will be a function of α and β , i.e., it will determine a surface over the complex plane. We call this generic stability exponent the Master Stability Function (MSF). To get the stability of a particular eigen-equation, Eq. (5), we merely see what the value of λ is at the complex point γ_k . If the function λ is negative at all the points $\{\gamma_k, k = 1, 2, \dots, N - 1\}$, then the synchronous state is stable.

Once determined, λ is useful in an infinite number of cases. To see why $\lambda(\alpha, \beta)$ has such utility, we note that once we know λ , then if we reconfigure the network, we are changing the connection matrix \mathbf{G} . To test the stability of the synchronous state in the new configuration, we need only get the eigenvalues of the new \mathbf{G} and see what the sign of λ is at those points in the complex plane. Thus the name, Master Stability Function. In the next section we show some numerical and experimental determinations of an MSF for a particular oscillator.

Experimental Analysis of Synchronization for a Chaotic Oscillator:

We chose a nonlinear oscillator circuit that generates a chaotic signal to show what the Master Stability Function looks like for a typical system and to test its shape experimentally. The system is the following (the equations for each node, $\mathbf{x}^{(i)} = (x, y, z)$):

$$\begin{aligned} \frac{dx}{dt} &= -\alpha(rx + \beta y + z) \\ \frac{dy}{dt} &= -\alpha(\gamma y - x + ay) \\ \frac{dz}{dt} &= -\alpha(z - g(x)) \end{aligned} \quad (7)$$

$$g(x) = \begin{cases} 0 & \text{if } x < 3 \\ 15(x - 3) & \text{if } x \geq 3, \end{cases}$$

which is a circuit version of a well-known chaotic system, the Rössler system. As an output function,

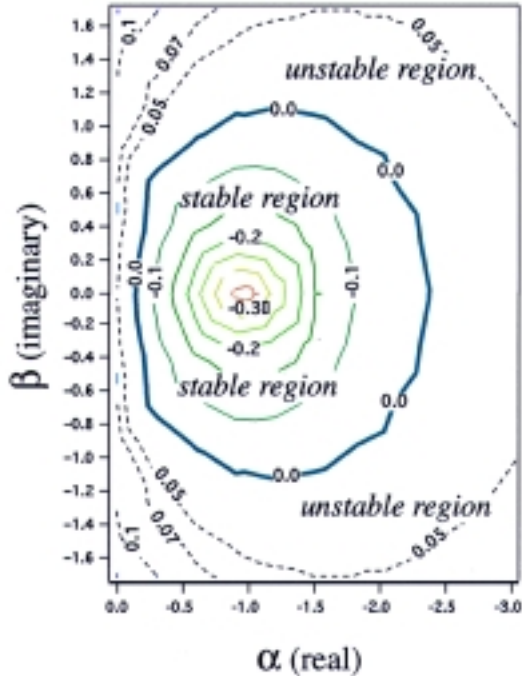


FIGURE 4
The master stability function for chaotic circuits calculated on computer from model. The dashed lines show contours in the unstable region. The solid lines are contours in the stable region. The thick line is the threshold for stable synchronization.

we chose coupling the circuit nodes via their x -components. This gives a matrix form for \mathbf{H} , namely

$$\mathbf{H} = \begin{pmatrix} 1 & 0 & 0 \\ 0 & 0 & 0 \\ 0 & 0 & 0 \end{pmatrix}. \quad (8)$$

We used these expressions in the generic variational equation (Eq. (6)) to calculate the MSF for this oscillator circuit.

Figure 4 shows the MSF as a contour plot of the λ surface over the complex plane. We see that there is a central region of stability. If we have a configuration \mathbf{G} whose eigenvalues all fall in that stable region, the synchronous state is stable for that configuration. If we change \mathbf{G} so that one eigenvalue, at least, moves into the unstable region, we will destabilize the synchronous state and, if the system is in the synchronous state, the pattern that will go unstable first is that particular mode. So we can also predict the spatial pattern that will emerge when we bifurcate into an unstable situation.

We tested the shape of the stable region of the MSF function in an experiment in which we coupled

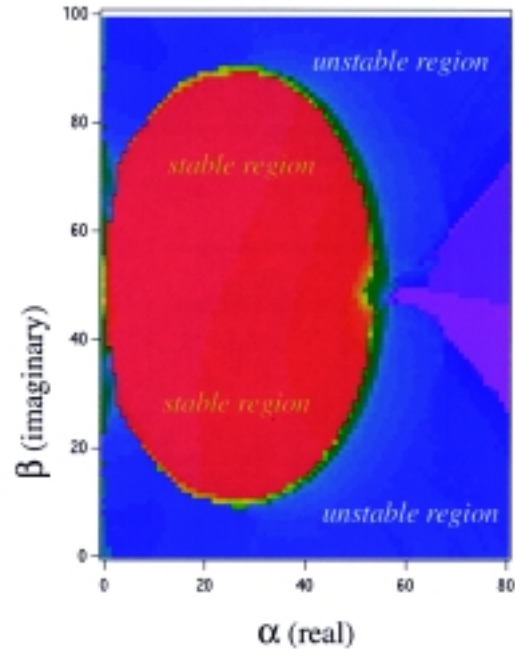


FIGURE 5
The master stability function for chaotic circuits as determined from experiment. The blue and purple area shows the unstable region. The solid red area shows the stable region. Note that this confirms the shape shown in Fig. 4.

three circuits and varied the symmetric and antisymmetric parts of the coupling matrix \mathbf{G} for those three circuits. This is equivalent to varying the real and imaginary parts of the generic coupling in Eq. (6). We keep track of which coupling setting resulted in stable synchronous behavior. This is mapped out in Fig. 5, which we see has the correct shape according to Fig. 4.

Conclusions: We have provided an approach to the problem of stability of the synchronous state in a network of dynamical systems that solves that problem for a large class of systems. The investigation of the MSF for any oscillator also leads to conclusions about large and small coupling regimes and proof of effective decoupling of subsystems in those ranges. We are currently continuing the research and preparing other papers for publication on this rich topic.

[Sponsored by ONR]

References

¹L.M. Pecora, T.L. Carroll, G. Johnson et al., “Master Stability Functions for Synchronized Coupled Systems,” *Phys. Rev. Lett.* **80**(10), 2109 (1998). ★

Reduced Manning—Its Impact on Damage Control

P.A. Tatem and F.W. Williams
Chemistry Division

Introduction: Reduced manning and affordability have become drivers for the ships of the future. These benefits can be attained in the area of damage control by capitalizing on existing technologies as well as those under development that demonstrate the viability of automating functions of detection, reasoning, and casualty response operations. The impact on the ship can be realized through not only life-cycle cost reductions resulting from reduced manning, but also through improved personnel safety and ship survivability resulting from reduced exposure of personnel and quicker responses in casualty control efforts. To meet the challenges to damage control efforts by a minimally manned combatant, the Office of Naval Research has funded the Damage Control-Automation for Reduced Manning (DC-ARM) program to develop the technologies required to automate sensing, decision making, and control and actuation. Products from the DC-ARM program will provide improved “fight through” capability through damage resilience of DC systems. War-fighting payoffs derive from more effective use of personnel, material, and sensor resources.

Objective: The objective of the DC-ARM program is to demonstrate the capability to reliably automate sensing, decision making, control, and actuation technologies that relate to fire protection and fluid systems control to effect up to an 85% reduction in damage control manning for future ships. The goal that will be achieved by satisfying this objective is to provide a timely mitigation of shipboard fire and flooding conditions by the (1) elimination of primary attack, boundary cooling, and smoke control teams; (2) elimination of the need for a manned response to isolate, reconfigure, and restore damaged fluid systems; and (3) augmentation or replacement of the reasoning and directed commands of present day crew members.

Technical Approach: Damage control (DC) in Condition I is the primary manning driver for surface combatants. To reduce the Condition I DC manning requirements, the DC-ARM program will integrate an automated system for detection and analysis with proactive correction of casualty situations from remote locations throughout the ship. This will be achieved by using state-of-art technologies to auto-

mate those functions of the damage control problem that have traditionally been manpower-intensive. Key technology areas are smart sensors, automated reasoning, and reliable/survivable topologies for fire protection and fluid system restoration. These key technologies will be demonstrated on ex-USS *Shadwell*, the Navy’s test site for DC. A series of DC actions for live fires and flooding will be executed to display what the Navy is presently capable of, what the near-term capability will be, and what the DC-ARM program will provide the Navy in the 21st century.

The DC-ARM program will use demonstrations as “proof of concept.” Full-scale products will be demonstrated under actual live fire/flooding conditions on ex-USS *Shadwell* using Fleet personnel as test participants. These demonstrations will be conducted for a representative mix of simulated weapons-induced fire, self-inflicted damage, and uncontrolled fluid casualty scenarios. It is also essential for the demonstration protocol to provide opportunity for the end-users to play an active role throughout the developmental and evaluation process to ensure that the final products meet the future needs of the Fleet. This program will capitalize on existing technologies as well as those under development. Many of the technologies that will be transitioned to DC-ARM have been developed under numerous activities. These demonstrations will take place as three major full-scale exercises aboard the ex-USS *Shadwell*. This type of test methodology has been used over the years on *Shadwell* and has been successful in evaluating DC equipment and doctrine improvement exercises.

The DC-ARM demonstration exercises will use a building-block approach whereby the initial actions for shipboard fire fighting and fluid system(s) control and restoration will be incrementally shifted from a manual to a fully automated response. The following provides a brief synopsis of the planned DC-ARM exercises:

Pre-DC-ARM “Baseline” FY98 Demonstration: The initial demonstration series focused on decentralized control with a modified DC organization. A modified Smart Ship-like organization was exercised that supports a 35% manning reduction using current DDG-51 state-of-the-art technologies. The organization and doctrine used was based on lessons learned from the Smart Ship (USS *Yorktown*), Fleet testing aboard *Shadwell*, and Fleet practices aboard submarines. This demonstration was completed in September 1998 and the results are described below.

DC-ARM “Remote Manual” FY00 Demonstration: The DC-ARM “remote manual” demonstration will be achieved with centralized control and remote

shock reflections, boundary layers, and all of their interactions with each other. Recent experiments carried out at the Centre for Explosion Studies at Aberystwyth (UK) indicate that the turbulent flame acceleration behind a shock and coupling of the shock with a turbulent flame appear to be a part of the DDT process.¹ In these shock-tube experiments, an initially laminar flame was distorted by repeated shock interactions, thereby producing a turbulent deflagration (a turbulent flame brush). Under certain conditions, DDT occurred in the experiments. However, even modern flow diagnostics lack the spatial and temporal resolution to resolve the actual process of DDT.

Highly resolved numerical simulations of these DDT experiments have now been performed at NRL with resources from the High Performance Computing Modernization Program and the San Diego National Supercomputer Center. The numerical model solved multidimensional time-dependent Navier-Stokes equations describing fluid convection, chemical reactions, thermal conduction, molecular diffusion, and viscosity.²⁻⁴ The solution of this problem required resolving scales from the thickness of a flame front (microns) to the size of the experimental apparatus (meters). A Fully Threaded Tree (FTT) adaptive mesh refinement algorithm was incorporated to increase both spatial and temporal resolution of the model at shocks, flame fronts, and other regions of high spatial gradients in the solution.⁵

The Turbulent Flame and DDT: Numerical simulations were carried for acetylene-air (Fig. 6) and ethylene-air mixtures. The simulations reproduced the formation of a turbulent flame brush, flame acceleration and the transition to detonation seen in the experiments. In particular, we were able to experimentally reproduce the observed dependence of the location of DDT on the strength of the incident shock. The results indicate that the two main elements of the DDT process are the generation of the turbulence by the Richtmyer-Meshkov instability and the formation and explosion of hot spots in the pockets of unreacted material inside the turbulent flame.

The simulations showed that the shock-flame interactions, through the Richtmyer-Meshkov instability, create and maintain a highly-turbulent flame brush. The interactions of an incident shock with the initially laminar flame lead to the initial flame distortions and to the formation of secondary shocks and rarefactions. These shocks and rarefactions then interact with the distorted flame surface, generating new shocks and rarefactions, and further distorting the flame. The turbulence is not Kolmogorov turbu-

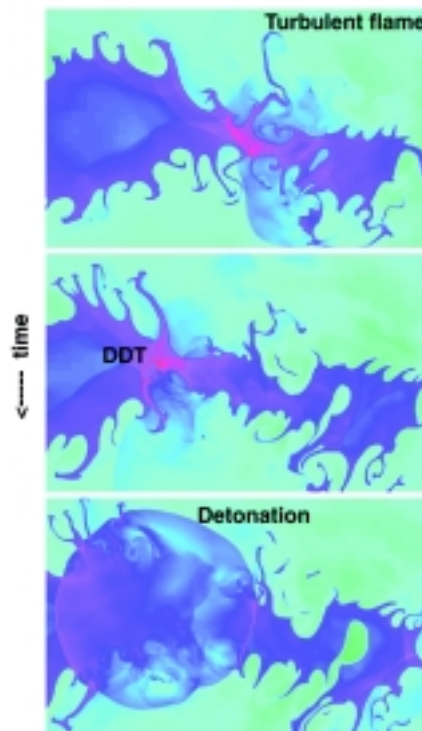


FIGURE 6
Deflagration-to-detonation transition in an acetylene-air mixture.

lence, but it is driven at all scales by repeated shock-flame interactions. Repeated shock-flame interactions and merging shocks in unreacted material lead to the increase of the energy generation in the flame and to the development of a high-speed shock that moves out in front of the turbulent flame. The region between this shock and the flame is subject to intense fluctuations generated in the flame.⁴

Pressure fluctuations generated in the region of the turbulent flame brush create, in turn, hot spots in unreacted material. These hot spots may then transition to DDT under the proper conditions. The simulations showed that these hot spots transitioned to a detonation when the gradients in induction time in the hot spot allowed the formation of supersonic reaction waves, which later transition to a detonation. An unsuccessful explosion in hot spots formed a shock with a flame left behind it. As the strength of the initial incident shock was increased, the location of DDT shifted from outside the flame brush to inside the flame brush.⁵

Conclusions: We carried out first-principle multidimensional numerical simulations of the transition of a turbulent premixed flame to a detonation and reproduced the process of DDT observed in the ex-

simply defined as the height at which the value of the geopotential local refractivity is computed as N_s/e (where e is the natural logarithm number, 2.71828), where the height h is equal to the scale height H . Any local refractivity $N(h)$ at the altitude h meters (or km) in space, can thus be computed by

$$N(h) = N_s \times \exp(-h/H)$$

$$N_s = [77.6/T_s] \times [p_s + 4,810 \times e_s/T_s]$$

$$e_s = RH_s \times 6.105 \times \exp(x)$$

$$x = 25.22 \times (T_s - 273.2)/T_s - 5.32 \times \log_e(T_s/273.2),$$

where H is a scale or reference height and is calculated adaptively for each designated grid square, subscript “s” represents the surface pressure (p_s), temperature (T_s in Kelvin), and water vapor pressure (e_s), and RH_s is a relative humidity.

The refractive effect on RF propagation of ray-bending and time delay beyond this reference height is minimal since the temperature and relative humidity (zero humidity above 9.0 km) do not change drastically enough to extend the effect of refractive bending beyond the troposphere region (tropopause to ionosphere region) above the 1.0 GHz frequency range. This coincides with the fact that most ray-bending and refractive phenomena occur within this region (beneath the reference height, approximately 9.0 km) from the surface of the Earth. Therefore,

the proposed simple modified exponential model (i.e., empirical data-driven model) has adopted the fact that RF ray-bending can be approximated with the reference height H without loss of any significant physical principles.

Performance Analysis and Simulation Results:

Several models, including a radar model (Barton and Ward model), have been examined and compared with the modified exponential model to show the advantages and improvements of the new approach. The radar model produces much larger errors of both range and angle on the order of magnitude than those of propagation models (stratified, Cains, Goad, and Blake). Figure 7 shows global time delay errors for 0° elevation angle during August based on 10-year average climatology data from ECMWF. Time delays vary from 330 ns in the lower range to 490 ns in the upper range. This error reflects a 160-ft range error for the ideal cases without consideration of other atmospheric effects. Time delays at 20° elevation angle are about 30 ns. These kinds of propagation error data from -5° to +90° can be provided within 35 minutes for both local and worldwide statistics of mean and standard deviation with 6-hour diurnal as well as climatology data. A radar or antenna operator can then calibrate their equipment by correcting both range and time delay errors for any given instant of time and geographical location.

Figure 8 is worldwide map of the angle-of-arrival (or simply angle) error for the 0° elevation angle in

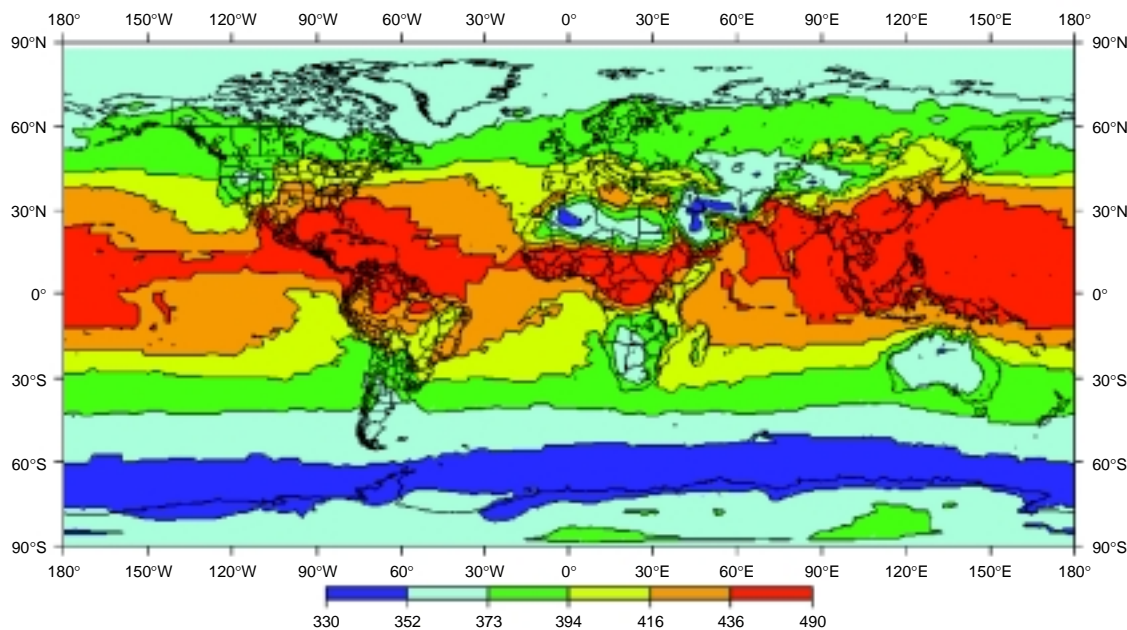
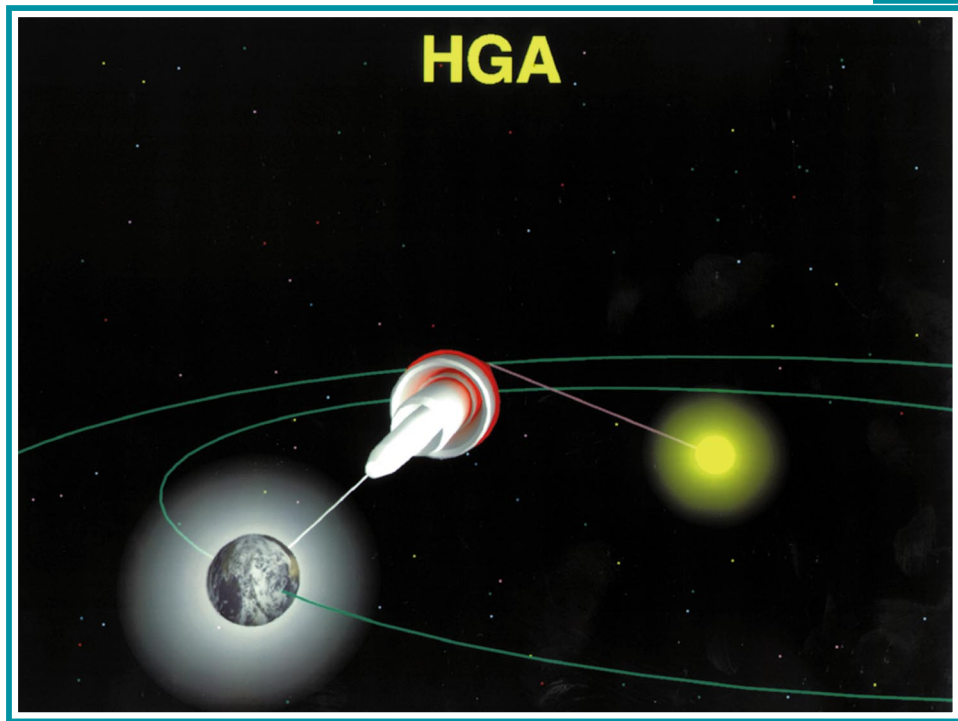


FIGURE 7
Global time delay errors for 0° elevation angle (10-year average).



***Mars Observer Spacecraft with Antenna Beam**
Science-as-Art contest – Honorable Mention
Submitted by: Brian Solan*

Earth, Sun, and the Mars Observer High Gain Antenna beam pointed toward Earth. This image is part of the Mars Observer Investigation that was performed through NRL. This view, when animated and combined with the postulated tumbling of the Mars Observer in the fuel-system-rupture scenario, illustrated the improbability of being able to achieve communication with Earth. After extensive analyses, it was concluded that the most probable cause of communication loss was a rupture in the fuel system.

- 183 Ionospheric Forecasting with Dynamic GPS Assimilation
M.J. Keskinen
- 186 Far-Infrared Spectroscopy of Colliding Galaxies
J. Fischer and M. Luhman
- 188 Modelling Radiation Effects on Spacecraft: CREME96
A.J. Tylka
- 190 Interim Control Module (ICM)
A.B. Jacoby
- 192 First U.S. Flight Hall Thruster Electric Propulsion System
P.R. Lynn, Jr. and M.F. Osborn II

Ionospheric Forecasting with Dynamic GPS Assimilation

M.J. Keskinen
Plasma Physics Division

Introduction: A growing number of Navy, Department of Defense (DoD), and commercial space systems will depend on or are now affected by paths passing through the ionosphere and upper atmosphere, e.g., in communications high-frequency (HF) and ultrahigh frequency (UHF), mobile wireless); navigation Global Positioning System (GPS); surveillance (space-based radars, passive geopositioning; synthetic aperture radars, and over-the-horizon radars), and satellite ocean radar altimetry. For example, in the communications area, specific Navy needs include forecast of the reliability and quality of UHF and HF satellite-to-ship and ship-to-ship communications links. The Navy is increasingly relying on GPS for precise navigation and needs accurate forecasts of GPS outages and position errors. There is well-defined need for the accurate and timely specification and forecasting of both global and regional ionospheric conditions. Figure 1 shows new space-based ionospheric and upper-atmospheric remote-sensing technologies (e.g., GPS¹ and satellite ultraviolet imaging^{2,3}) have been developed that will provide a wealth of new data concerning the ionospheric and upper-atmospheric state. In addition, radio-tomographic imaging methods will also play a role in ionospheric specification. For many years, the meteorological community has relied on both space- and ground-based data and has developed techniques to assimilate these data into dynamical first-principles forecast models, e.g., to predict the intensity and track

of a hurricane. Forecasting accuracy has been improved by the merging of numerical forecast models and data derived from space- and ground-based sources. A similar need for the ionosphere and upper atmosphere exists, but it is still in its infancy. Analogous atmospheric weather features also exist in the ionosphere, e.g., rising equatorial bubbles.⁴ A challenging problem in the next millennium will be to merge new ionospheric sampling observations with global models to improve ionospheric and upper-atmospheric specification and forecasting. This article describes the assimilation of GPS data into global first-principles ionospheric models.

GPS—A Space-Based Dataset: GPS is a constellation of 24 satellites orbiting at approximately 10,980 nmi (20, 334 km). The GPS signal frequencies at 1.57542 and 1.2276 GHz can be affected by the plasmasphere, ionosphere, and lower atmosphere (Fig. 2). The primary propagation effects are group delay caused by the total electron content of the ionosphere and plasmasphere, and temperature and water vapor in the atmosphere. The presence of the ionosphere changes the velocity of propagation according to the refractive index. The refractive index varies in turn along the propagation path (Fig. 3). At large elevation angles, the group delay is proportional to the integrated plasma electron content from transmitter to receiver. By knowing the group delay, the total electron content of the ionosphere can be derived.

Ionospheric Forecast Model: We have developed a global ionospheric forecast model, the Global Ionospheric Prediction Model (GIPM), using the primitive equations describing the dynamics of the

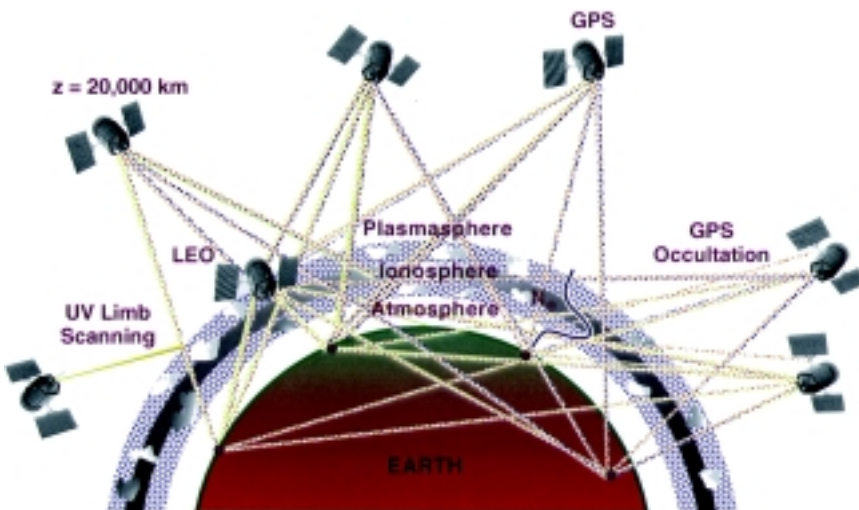


FIGURE 1
The GPS constellation and UV imaging satellites.

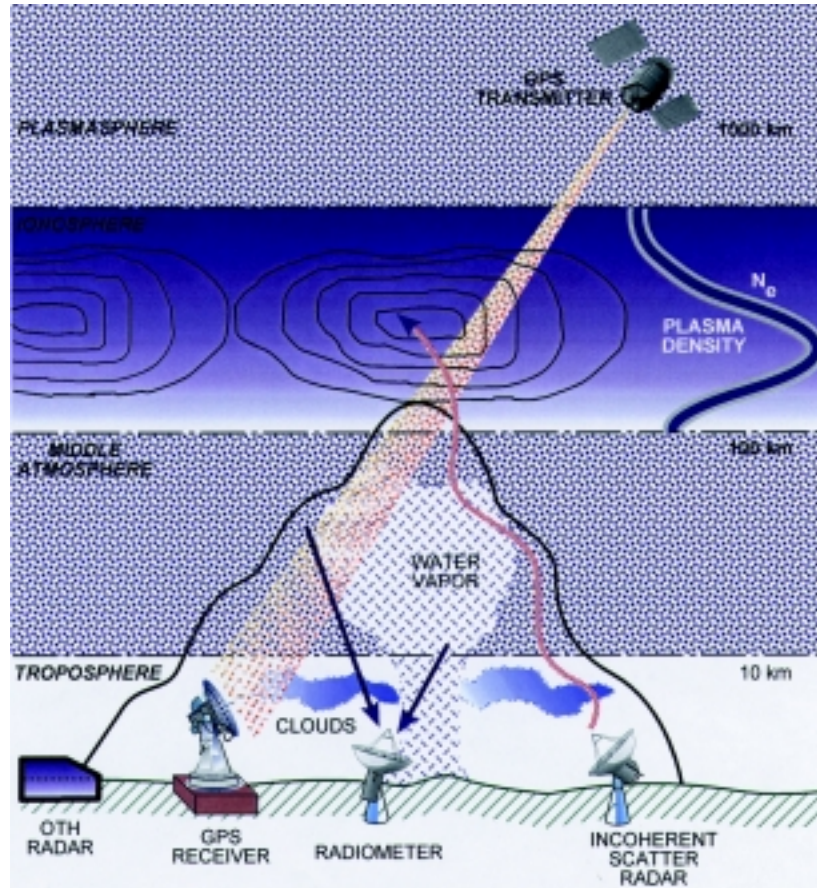


FIGURE 2
GPS is affected by the ionized space plasma and neutral atmosphere.

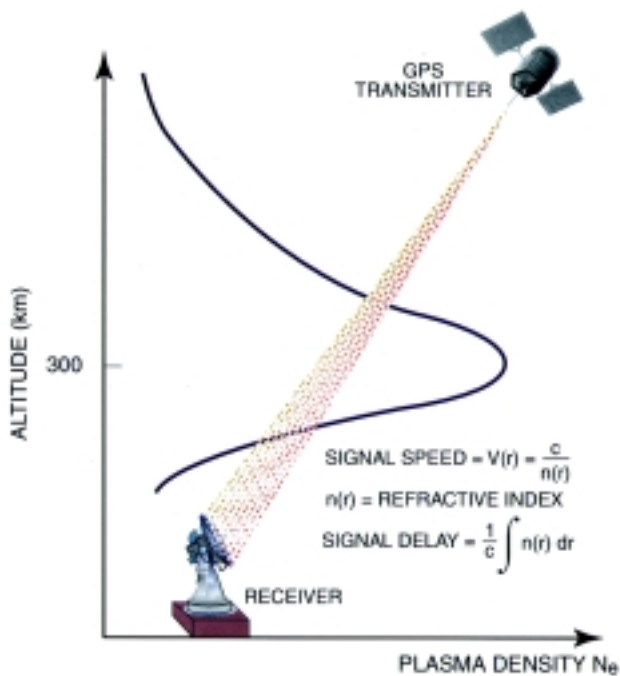


FIGURE 3
GPS suffers a signal delay as it propagates through the ionosphere proportional to the total electron content in the signal path.

ionosphere. A set of equations of continuity, momentum, and energy have been solved using finite-difference techniques. The model is three-dimensional and time-dependent. A high-altitude plasmaspheric extension to the model has been developed based on existing empirical models and data. The model physics includes ion production due to solar extreme ultraviolet (EUV), resonantly scattered radiation, auroral processes, ion-neutral chemical reactions, thermal conduction, neutral composition changes, thermospheric wind inputs, electrodynamic drifts, field-aligned diffusion, and local heating and cooling processes. Some inputs to the model are taken from existing empirical models.

Ionospheric Forecasting with GPS Assimilation: The approach is to assimilate GPS differential phase-path data, which are proportional to total electron content, into the global ionospheric forecast model using a Newtonian relaxation technique. Here we relax the model prediction of an ionospheric parameter at a specific place and time to that obtained by GPS using a characteristic relaxation time. We use data from a GPS receiver located near the Millstone Hill incoherent scatter radar at Westford, Massachusetts, near Boston. The assimilation of total electron content is analogous to the assimilation of precipitable water used in meteorological forecasting. GPS data have been assimilated into the GIPM forecast code for a range of relaxation parameters. The ionospheric F-region electron density profile forecast at the Millstone Hill location is dependent on the relaxation parameter used in the model. For a specific range of relaxation parameter, we have found that the assimilation method improves the model prediction. Figure 4 compares the model prediction

of the ionospheric F-region electron density profile and the profile obtained using the Millstone Hill facility.

Summary: We have developed techniques to assimilate space-based GPS data into a global time-dependent ionospheric first-principles forecast model. We have compared and validated the model prediction with independently derived data from a midlatitude incoherent scatter radar. Preliminary results of this work indicate that space-based GPS data assimilation can potentially improve the forecast of ionospheric parameters, i.e., F-region density profiles, under specific conditions. Multiple GPS data inputs should be included in the analysis, and the fusion of GPS and other data sources is needed.

Acknowledgments: Contributions from M.H. Reilly and M. Singh of Geoloc Corporation are acknowledged.

[Sponsored by ONR]

References

- ¹B.W. Parkinson, "Introduction and Heritage of NAVSTAR, the Global Positioning System," in *Global Positioning System: Theory and Applications, Vol. 1*, B.W. Parkinson and J.J. Spilker, eds. (American Institute of Aeronautics and Astronautics, New York, 1996), pp. 101-123).
- ²K.F. Dymond, S.E. Thonnard, R.P. McCoy, and R.J. Thomas, "An Optical Remote Sensing Technique for Determining Nighttime F-Region Electron Density," *Radio Sci.* **32**, 725-743 (1997).
- ³R.R. Meier and J.M. Picone, "Retrieval of Absolute Thermospheric Concentrations from the Far UV Dayglow: An Application of Discrete Inverse Theory," *J. Geophys. Res.* **99**, 6307 (1994).
- ⁴M.J. Keskinen, S.L. Ossakow, S. Basu, and P.J. Sultan, "Magnetic-Flux-Tube-Integrated Evolution of Equatorial Ionospheric Plasma Bubbles," *J. Geophys. Res.* **103**, 3957 (1998). ★

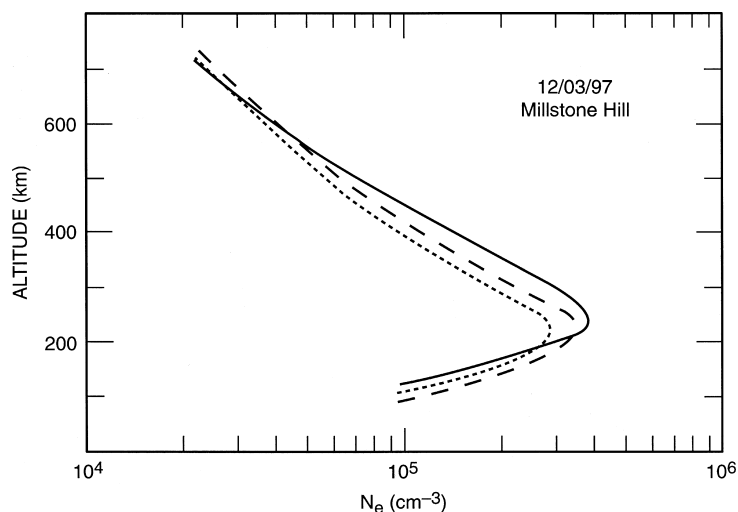


FIGURE 4
Comparison between ionospheric electron density profile observed by Millstone Hill incoherent scatter radar (solid line), model prediction without assimilation (dotted line), and including assimilation (dashed line).

Far-Infrared Spectroscopy of Colliding Galaxies

J. Fischer
Remote Sensing Division

M. Luhman
National Research Council Associate

Introduction: One of the most important discoveries resulting from NASA's Infrared Astronomical Satellite (IRAS) sky survey, launched and operated in 1983, was that many galaxies emit a large fraction of their energy in the far-infrared and that a significant number of these have luminosities greater than 10^{12} times that of our Sun. Optical images of these infrared-bright galaxies show tidal tails and double nuclei, indicating that most of these are interacting or colliding pairs of galaxies. The most luminous of these, known as the ultraluminous infrared galaxies (ULIGs), appear to be more advanced, merging galaxies. Both observational evidence and theoretical models suggest that dissipative collapse induced by collisions between gaseous disk galaxies may lead to important phases in galaxy evolution such as the formation and/or fueling of massive black holes in the centers of galaxies and the formation of elliptical galaxies. The luminous far-infrared (FIR) continuum emission emanating from the centers of these galaxy systems is due to thermal re-radiation by dust heated by ultraviolet light. What is the fate of the infalling clouds of material at the centers of the ultraluminous galaxies and what powers their luminous far-infrared emission? Do they form stars or luminous quasars as they contract due to self-gravity? Conclusive answers to these questions are elusive because of obscuration of the energy source of the ultraviolet light by these same infalling, dusty clouds. At longer FIR wavelengths, the dust becomes optically thin, making far-infrared spectroscopy a powerful diagnostic tool.

FIR Spectroscopy from Space: In November 1995, the European Space Agency (ESA) launched the Infrared Space Observatory (ISO) equipped with a 60-cm telescope and four infrared (IR) (2.5 to 200 μm) astronomical instruments cooled to temperatures of 2 to 4 K by superfluid helium. The observatory was operational for 2.5 years, until its helium supply was exhausted in April 1998. IR astronomers from NRL's IR Sensors Section have participated as co-investigators on the Long Wavelength Spectrometer (LWS) team in an international consortium, including scientists from the United Kingdom, France, and

Italy. The LWS is a FIR scanning grating spectrometer that covers the 43 to 197 μm wavelength range at low spectral resolution using 10 photoconducting Ge:Be and Ge:Ga detectors, with a complementary high-resolution Fabry-Perot mode. NRL scientists contributed to the development of metal-mesh reflector technology¹ for the spectrometer's high-resolution Fabry-Perot mode and lead the team's investigation on the infrared (IR)-bright galaxies.

Discovery of a Spectral Sequence of IR-Bright Galaxies: Figure 5 shows full spectra of six IR-bright galaxies taken with ISO's LWS. They reveal a dramatic progression in emission and absorption-line characteristics, extending from galaxies with

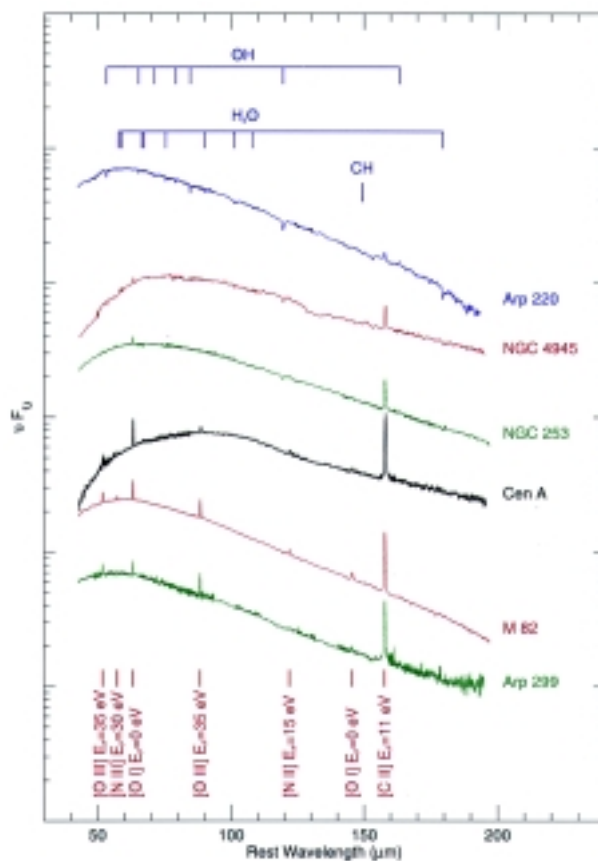


FIGURE 5 The full Infrared Space Observatory (ISO) Long Wavelength Spectrometer (LWS) spectra of six infrared (IR)-bright galaxies.² The spectra have been shifted and ordered vertically according to apparent excitation. The ionization state and energy required for ionization to that state for detected emission lines are indicated in red (e.g. [O I] refers to unionized oxygen, while [O III] refers to twice ionized oxygen). Molecular transitions, mostly in absorption, are indicated in blue.

strong-line emission from highly ionized gas (doubly ionized oxygen and nitrogen) to galaxies with only faint-line emission from gas in photodissociation regions (from singly ionized carbon).² The several ultraluminous galaxies included in the small full spectral sample (i.e., the galaxy Arp 220 shown in Fig. 5) have the weakest emission-line characteristics and show absorption lines of molecular and atomic species such as OH, H₂O, and atomic oxygen. We were able to further substantiate this result by measuring the strength of the spectral line of singly ionized carbon at 158 μm in a sample of ultraluminous galaxies extending to larger distances.³ Figure 6 illustrates that indeed, relative to the thermal dust continuum, the 158-μm emission line is an order of magnitude fainter in the class of ultraluminous galaxies than in other IR-bright galaxies.

Our results suggest that dust-enshrouded starbursts, rather than quasars, are responsible for powering the bright-IR emission in the ultraluminous galaxies. This is because quasars have harder spectra than hot, young stars and would be expected to produce strong lines from high-excitation species. Analysis of the emission-line ratios in individual objects in the sequence lead us to conclude that neither density nor FIR extinction effects play dominant roles

in the sequence. Rather, we infer from these spectra that softer radiation fields due to starburst evolution are responsible for the apparent progression to low excitation. For example, an older starburst or one with a deficit in massive young stars could be present in the ultraluminous and the other low-excitation galaxies. A soft radiation field may also explain the low 158-μm ionized carbon line flux relative to total FIR flux and the molecular absorption due to the presence of cold molecular material seen in these galaxies.

Future Directions: These results raise new questions and have important implications for future astronomy missions. How long does the starburst phase last? If galaxy mergers do lead to the formation of relatively gas-free elliptical galaxies or quasars, how do these merging systems rid themselves of the gas and dust? How similar are these galaxy collisions to those that occurred when the universe was young, when collisions and mergers are thought to have been more common? IR Sensors Section scientists are working on the development of IR spectrometers and with scientists of the Nanoelectronics Processing Facility on filter technology for future IR space missions.

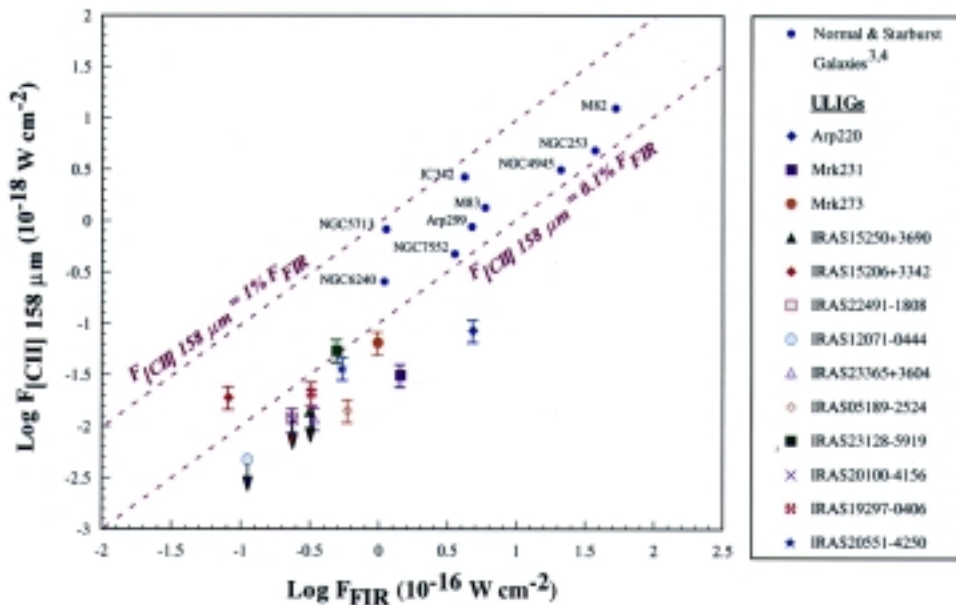


FIGURE 6
 [C II] 158-μm line plotted against the Infrared Astronomical Satellite (IRAS) far-infrared (FIR) flux for a sample of normal/starburst galaxies (blue dots) and the observed ultraluminous infrared galaxies (ULIGs). The two dashed lines depict the observed F[C II]/F_{FIR} regime typical of normal/starburst galaxies. The ultraluminous galaxies as a group fall well below this regime.

Acknowledgments: This work is based on observations with ISO, an ESA project with instruments funded by ESA member states, especially the Principal Investigator countries: France, Germany, the Netherlands, and the United Kingdom, with the participation of the Institute of Space and Astronautical Science and the National Aeronautics and Space Administration.

[Sponsored by ONR and NASA]

References

- ¹M. Rebbert, P. Isaacson, J. Fischer, M.A. Greenhouse, J. Grossman, M. Peckerar, and H.A. Smith, "Microstructure Technology for Fabrication of Metal-Mesh Grids," *Appl. Opt.* **33**, 1286 (1994).
- ²J. Fischer, M.L. Luhman, S. Satyapal, M.A. Greenhouse, G.J. Stacey, C.M. Bradford, S.D. Lord, J.R. Brauher, S.J. Unger, P.E. Clegg, J.W. Colbert, M.A. Malkan, P. Cox, G. Melnick, and H.A. Smith, "A FIR Spectroscopic Survey of Infrared-Bright Galaxies," in *Astrophysics with IR Surveys: Prelude to SIRTf*, *Astronomical Society of the Pacific Conference Series*, Proceedings from ASP Conference, Pasadena, Calif., June 22-24, 1998 (in press).
- ³M. Luhman, S. Satyapal, J. Fischer, M.G. Wolfire, P. Cox, S.D. Lord, H.A. Smith, G.J. Stacey, and S.J. Unger, "Infrared Space Observatory Measurements of a [C II] 158 Micron Line Deficit in Ultraluminous Infrared Galaxies," *Astrophys. J.* **504**, L11 (1998).
- ⁴S.D. Lord, D.J. Hollenbach, M.R. Haas, R.H. Rubin, S.W. Colgan, and E.F. Ericson, "Interstellar Properties of a Dual Nuclear Starburst: Far-Infrared Spectroscopy of M82," *Astrophys. J.* **465**, 703 (1996). ★

Modelling Radiation Effects on Spacecraft: CREME96

A.J. Tylka
Space Science Division

Radiation Effects on Satellites: The ionizing radiation environment in space poses severe challenges for the design and operation of satellites. Accumulated long-term radiation damage causes gradual deterioration and eventual failure of most spacecraft systems. Transient solar-wind disturbances sometimes produce large, temporary increases in the intensity of >1 MeV electrons in Earth's outer radiation belt. Interior charge build-up, due to exposure to these enhanced electron fluxes for a few days or more, has been implicated in several sudden satellite failures, including the Galaxy-4 loss that disrupted pager service across the United States on May 19, 1998.¹ Another type of sudden, random anomaly is the "single-event effect," in which a *single* high-energy (> 30 MeV) nucleus (such as a galactic cosmic ray, a solar energetic particle, or a proton trapped in Earth's

radiation belts) passes through a microelectronic device. Depending on the type of device and its function, these single-event effects have numerous consequences, ranging from recoverable data corruption to temporary interruption in operations, to permanently degraded capabilities, or even to catastrophic loss of the satellite.

CREME96: Because of the complexity of the space radiation environment and its effects, engineers and mission planners use numerical models to ensure that space systems will meet mission requirements. The development of such numerical models was pioneered by Dr. James H. Adams, Jr. and colleagues at NRL, who published the original Cosmic Ray Effects on Micro-Electronics (CREME) code in 1981.² CREME literally became an industry standard for evaluating single-event effects. MILSTD-1809 mandated its use for Department of Defense (DoD) systems, and CREME is often a contractual requirement in NASA and commercial programs. Elements of the original CREME have also been incorporated into commercial software packages.

Discoveries of the past decade, including those from NRL-sponsored experiments, have substantially reduced uncertainties about some space radiation hazards. In 1998, NRL's Space Science Division completed a 3-year effort to make these new discoveries available to spacecraft designers through a revision of the CREME code. This revision, known as CREME96,³ is now available as an operational space-system design tool at <<http://crsp3.nrl.navy.mil/creme96>>. During development, this Website was also used for extensive beta testing by volunteers from the aerospace community. Comments from these beta testers helped to ensure that the final product would be easy to use and properly targeted on the most pressing needs of space-system designers.

Solar Energetic Particles: Solar particle events (or, as colloquially known, "flares") endanger spacecraft by increasing high-energy interplanetary particle intensities by 3 to 4 orders of magnitude for as long as a week. The past decade produced major discoveries about solar particles, including the fact that the events that affect spacecraft are caused by shocks driven by very fast coronal mass ejections (CMEs).

Figure 7 illustrates how a discovery about solar particles from an NRL basic-research experiment contributed directly to CREME96. NRL's Heavy Ions In Space (HIIS) experiment⁴ showed that solar iron ions above 200 MeV/nucleon are not fully stripped of electrons but rather have mean ionic charge state of

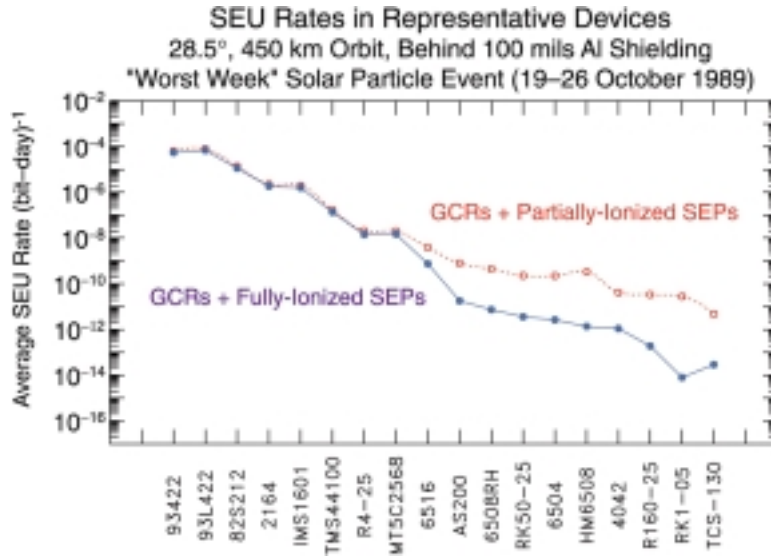


FIGURE 7 Calculated single-event upset rates in representative microelectronic devices in a low-inclination orbit during a very large solar energetic particle event.³ The incorrect calculations (in blue) assume that the solar energetic iron ions are fully ionized. The correct calculations (in red, from CREME96) correctly take into account the partially ionized charge state of solar-energetic iron ions.

~14. This ionization state is characteristic of the ~2-million kelvin coronal plasma from which the ions were accelerated. As a result of this partially ionized state, high-energy solar iron ions penetrate Earth’s magnetic field and reach satellites in low-inclination orbits.

Figure 7 shows single-event upset rate calculations for various kinds of microchips in such an orbit. In this figure, devices at the left are vulnerable to upset by lightly ionizing particles, such as very fast galactic cosmic rays (GCRs). Devices at the right, however, are affected only by heavily ionizing particles, such as stopping iron nuclei. The blue curve shows

incorrect calculations in which the solar iron ions are assumed to be fully ionized. The red curve shows correct calculations from CREME96 in which the partially ionized charge state is taken into account. Correct treatment of the solar iron charge states increases the predicted single-event upset (SEU)-vulnerability of some devices on the right by a factor of ~100 or more.³

Figure 8 shows an on-orbit validation of the new CREME96 algorithms for calculating single-event effects on geosynchronous satellites due to solar particles.⁵ The datapoints show reported rates of single-event upsets (“bit flips”) aboard NASA’s TDRS-1 sat-

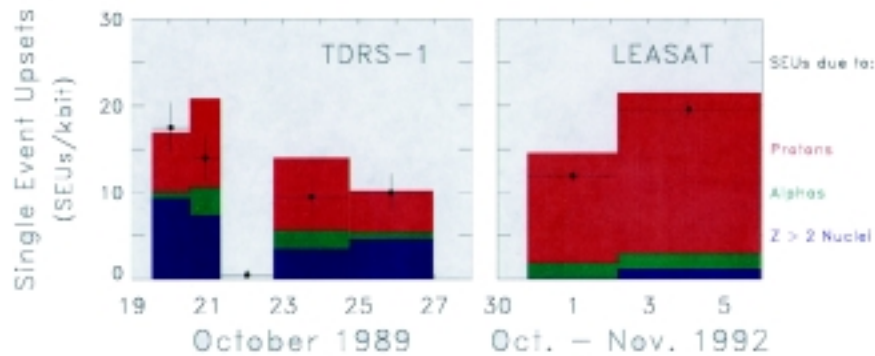


FIGURE 8 Datapoints with statistical error bars show observed SEU rates in microchips aboard NASA’s TDRS-1 satellite (left) and the Navy’s LEASATs (right) during some large solar particle events of Solar Cycle 22. Bar graphs show calculated contributions of energetic solar protons (red), alpha particles (green), and heavy ions (blue) to the observed rate.

ellite and the Navy's LEASAT fleet-communications satellites during some of the largest solar particle events of the previous Solar Maximum. The color-coded bar graphs show the calculated contributions from protons, alpha particles, and heavy ions (with atomic number $Z > 2$) to the observed rates. The "gap" in the TDRS-1 rate corresponds to a period in which the high-energy solar particle intensities fell to low levels. The few SEUs observed in that period are consistent with the typical rate expected from GCRs. The relative importance of different particles in causing the upsets on TDRS-1 and LEASATs reflects differences between the microchips aboard the satellites.

Technology Transfer: Like the original CREME model, CREME96 has become an authoritative source of information on space radiation effects. The CREME96 website provides not only tutorial information but also on-line access to tools needed for computationally intensive space-system design calculations. The Website has proven to be a highly efficient way of making the new code available to the aerospace community. To date, nearly 600 scientists and engineers (mostly from U.S. aerospace companies but also from universities and DoD and National Aeronautics and Space Administration (NASA) laboratories) have registered as CREME96 users. CREME96 was recognized with an NRL Technology Transfer Award in June 1998. CREME96 is also the subject of a currently pending U.S. patent application.

Acknowledgments: Members of the CREME96 development team were James H. Adams, Jr. (NRL), Paul R. Boberg (Universities Space Research Association), Buddy Brownstein (Softech, Inc.), William F. Dietrich (U. Chicago), Erwin O. Flueckiger (U. Bern, Switzerland), Edward L. Petersen (consultant), Margaret A. Shea and Don F. Smart (Phillips Laboratory), and Edward C. Smith (consultant).

[Sponsored by ONR and NASA]

References

- ¹D.N. Baker, J.H. Allen, S.G. Kanekal, and G.D. Reeves, "Disturbed Space Environment May Have Been Related to Pager Satellite Failure," *Eos. Trans. Am. Geophys. Union* **79**, 477-483 (1998).
- ²J.H. Adams, Jr., R. Silberberg, and C.H. Tsao, "Cosmic Ray Effects on Micro-Electronics: The Near-Earth Particle Environment," NRL Memorandum Report 4506, Aug. 1981.
- ³A.J. Tylka, J.H. Adams, Jr., P.R. Boberg, B. Brownstein, W.F. Dietrich, E.O. Flueckiger, E.L. Petersen, M.A. Shea, D.F. Smart, and E.C. Smith, "CREME96: A Revision of the Cosmic Ray Effects on Micro-Electronics Code," *IEEE Trans. Nucl. Sci.* **44**, 2150-2160 (1997).

⁴A.J. Tylka, P.R. Boberg, J.H. Adams, Jr., L.P. Beahm, W.F. Dietrich, and T.Kleis, "The Mean Ionic Charge State of Solar Energetic Fe Ions Above 200 MeV per Nucleon," *Astrophys. J. Lett.* **444**, L109-L113 (1995).

⁵A.J. Tylka, W.F. Dietrich, P.R. Boberg, E.C. Smith, and J.H. Adams, Jr., "Single Event Upsets Caused by Solar Energetic Heavy Ions," *IEEE Trans. Nucl. Sci.* **43**, 2758-2766 (1996).★

Interim Control Module (ICM)

A.B. Jacoby

Spacecraft Engineering Department

Introduction: The Naval Center for Space Technology (NCST) has been tasked by the National Aeronautics and Space Administration (NASA) to provide a propulsion module for attitude control (spacecraft pointing and control) and reboost (altitude increase/orbit adjustments) of the International Space Station (ISS). In response to this requirement, the interim control module (ICM) is being developed. The ICM is based on residual government hardware from a previous NCST spacecraft. This spacecraft was originally developed for a Space Shuttle launch but was redirected following the Challenger incident. The ICM could be used as early as the third assembly element of the ISS and will be preceded by the Russian-built FGB (function cargo block, currently called Zarya) and U.S. node 1.

The ISS is a significant and technically demanding, multinational space program with team members consisting of the United States, Russia, Canada, Japan, and a European consortium. The ICM represents a timely, cost-effective, and technically responsive contingency solution to temporarily replace the Russian service module (RSM). The RSM was to provide the initial habitable area as well as to supplement the FGB for attitude control and reboost. The ICM, as shown in Fig. 9, replaces the RSM and provides for the uninterrupted assembly of the ISS. The ICM is to be launched on the Space Shuttle with an anticipated launch date of March 2000. NRL works jointly with NASA team members consisting of representatives from the Kennedy Space Center (KSC), Johnson Space Center (JSC), Marshall Space Flight Center, Goddard Space Flight Center, and the Russian Space Agency. NRL has prime program responsibility for the design and delivery of the ICM.

Mission Overview: The ICM is primarily a propulsion vehicle that carries 11,700 lb of nitrogen tetroxide and mono-methyl hydrazine along with necessary plumbing and control electronics to navi-

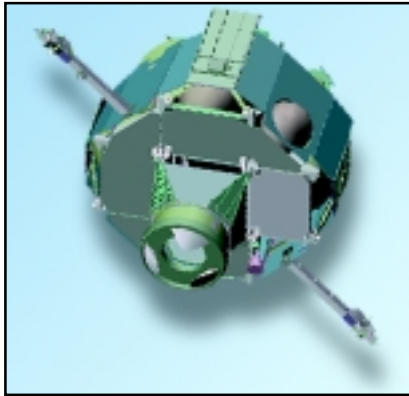


FIGURE 9
NRL's solution to NASA's requirement for an interim control module (ICM).

gate and operate 5- and 25-lb force engines for attitude control. A single 110-lb force thruster is used for ISS reboost. The ICM is fitted with Russian docking mechanisms to attach to the Shuttle and ultimately the ISS. With a total liftoff weight of 24,000 lbs at launch (including propellants and airborne support equipment), the ICM represents a large and complex deployment challenge. The mission deployment and mating sequence calls for

- launch of the ICM via the space Shuttle;
- storage of the ICM in its canister cargo element (Fig. 10) during in-route Space Shuttle flight operations; and
- extraction of the ICM from the canister with attachment to the Shuttle's orbital docking system (ODS), with subsequent mating of the ICM via Shuttle maneuvering to the ISS's FGB or pressurized mating adapter (PMA).

The ICM, once deployed and attached to the ISS, weighs 19,000 lb. Figure 11 illustrates the ICM attached to the FGB and functioning in a fully operational mode. The precise configuration and attach-

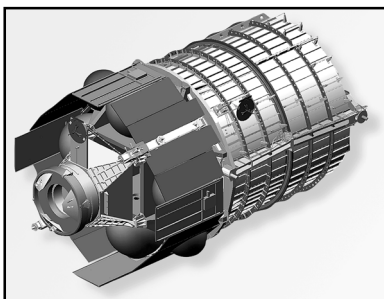


FIGURE 10
The ICM and canister mated together for Shuttle launch and predeployment maneuvers.

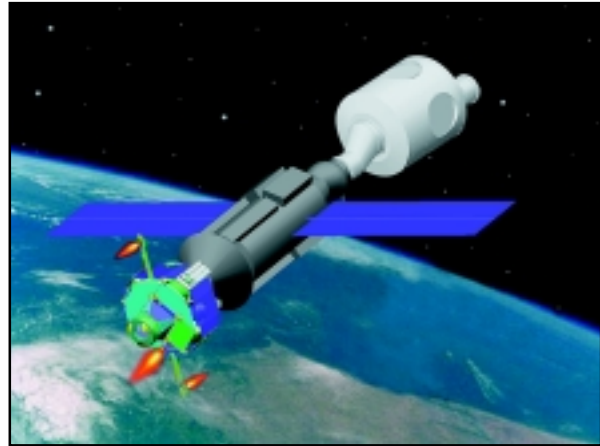


FIGURE 11
Artist conception of a fully operational ICM in a thrusting and maneuvering mode.

ment to the ISS will be determined when the ICM is officially manifested by NASA for a specific Shuttle launch.

Technical Challenges and Solutions: Significant challenges encountered on the ICM program include:

- converting the NRL bus from a spinning spacecraft to a 3-axis stabilized system;
- the design, qualification, and installation of propellant management devices (PMDs) into existing fuel tanks;
- significant changes to the sensor suite and thermal design;
- incorporation of fault detection, isolation, and recovery circuitry (FDIR);
- astronaut extra vehicular activity (EVA) contingency mission scenarios; and
- extensive safety and hazard conditions associated with a Shuttle launch and subsequent ISS assembly mission environment.

Conversion to a 3-axis stabilized spacecraft required the design and installation of PMDs necessary to allow the fuel and oxidizer to be extracted from the tanks in zero gravity (G). Because new tanks designed around a PMD could not support mission schedules, the challenge presented to ICM, as shown in Fig. 12, was to design a PMD that could be installed through the 5-in. diameter openings of the existing 52-in. diameter tanks.

The "bar-b-que rotisserie" thermal mode of a spinning spacecraft was no longer applicable. Therefore, the thermal control system was completely redesigned for the 3-axis stabilized spacecraft to include heat pipes, radiators, and a computer control system.



FIGURE 12
With approximately the same diameter and circumference as the propellant tank (52-in. diameter), the PMD on the left must be packaged to allow for insertion into the propellant tank through a 5-in. diameter opening.

Simulations and rigorous analytical models were required as some of the heat pipes are not testable in 1 G. FDIR is a NASA requirement that forces problem solving onboard the vehicle due to “man rating.” Loss of attitude control because of an onboard failure could quickly place the ISS in a power or thermal condition that could not be corrected. Potential failures and their effects are analyzed and hardware or software fixes are incorporated as necessary to prevent propagation of effects.

Summary: The ICM provides a working solution for a program of national and global interest. It allows NRL to continue the advancement of spacecraft technologies with technology transfer to DoD and industry. Potential follow-on programs associated with ICM include the assessment of refueling capabilities for extended and sustained operations, application of the ICM for de-orbiting spacecraft structures that are approaching mission-life exhaustion, and the provision for follow-on ICMs either for ISS use or as a Shuttle-qualified space tug.

[Sponsored by NASA] ★

First U.S. Flight Hall Thruster Electric Propulsion System

P.R. Lynn, Jr. and M.F. Osborn II
Spacecraft Engineering Department

Introduction: The Naval Center for Space Technology (NCST) is demonstrating advanced spacecraft propulsion for use on future Navy, Department of Defense (DoD) and National Reconnaissance Office

(NRO) satellites. Today, the fractional mass of a propulsion system aboard a satellite is between 20% to 50%. Electric propulsion is an advanced technology that promises to significantly decrease the propulsion mass and maximize the amount of payload aboard satellites. The Electric Propulsion Demonstration Module (EPDM) program is based on advanced Hall thruster propulsion technologies developed in the former Soviet Union. The Ballistic Missile Defense Office (BMDO) and National Aeronautics and Space Administration (NASA) Lewis Research Center (LERC) started the Russian Hall Effect Thruster Technology (RHETT) project that performed extensive testing of Hall thrusters to understand spacecraft interaction issues, lifetime capability, power handling, and stability.¹ These investments were the “seedcorn” for the EPDM program. With the launch of EPDM aboard the NRO’s Space Technology Experiment (STEX) spacecraft, the first U.S. Hall thruster electric propulsion system is now operational.

Mission Description: The EPDM mission consists of two parts, an orbit transfer phase and a stationkeeping phase. The EPDM system will perform a coplanar orbit raising of 20 km over a several-week period, after which it will provide 3 years of precision stationkeeping. The EPDM system operates at 600 W of discharge for firing times between 5 and 15 min. Thrust time depends on spacecraft energy available, which varies with spacecraft attitude and Sun angle conditions. A minimum of 300 W-hr per orbit is available for each set of maneuvers. To maintain a precise orbit, stationkeeping burns will be made on a varying basis, depending on environmental drag effects. The frequency of adjustments will be between 1 day to 1 week. The duration of firings will vary from 10 s to 15 min., accordingly, with a potential for 1200 on-off cycles.

System Description: The EPDM system consists of four major subassemblies: the power processing unit (PPU), the auxiliary interface unit (AIU), the engine assembly, and the xenon flow system (XFS) (Fig. 13). The AIU provides command and telemetry interfacing with the spacecraft, while the PPU provides all primary power processing for the Hall thruster. The PPU is a 90% efficient unit consisting of five separate but interrelated power supplies to operate the anode discharge, the engine magnets, the cathode heater, and the keeper/ignitor circuit.

The EPDM XFS is a high-pressure storage system with regulated pressure and mass flow developed by NRL. The xenon is stored in a spherical tank at 900 pounds per square inch absolute (psia) with flow

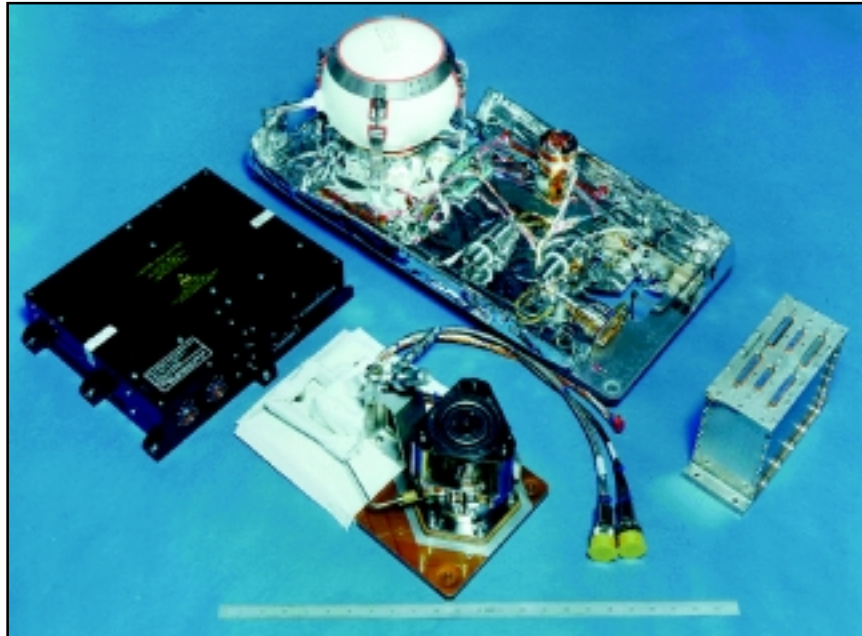


FIGURE 13
Modular components of the EPDM system. From center, clockwise: xenon flow system (XFS), auxiliary interface unit (AIU), TAL-D55 engine assembly, and power processing unit (PPU).

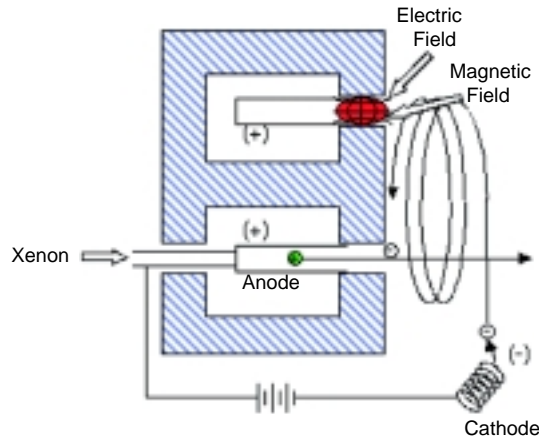
control provided by two solenoid valves upstream of the pressure regulator. The regulator is a bellows type with an outlet pressure of 37 ± 1.5 psia. Thermostatically controlled heaters are located at multiple points on the XFS to provide thermal conditioning of the system prior to use and to eliminate the possibility of any two-phase flow within the system.

The Hall thruster is an electrostatic type of electric propulsion, specifically a thruster with anode layer TAL-D55. EPDM operates the TAL-D55 at 600 W of discharge power. This setting provides a thrust level of 38 mN at 1550 s of specific impulse, excluding cathode flow. The thruster is mounted on top of a titanium thermal and electrical isolator. Low-pressure xenon is fed into precision orifices with tight temperature control to accurately maintain the xenon mass flow setting. A hollow cathode, similar to the International Space Station plasma contactor, is mounted near the exit plane of the TAL.

The EPDM system is operated by a set of stored spacecraft commands to initialize the system, thermally condition the system, and fire the thruster. Operating the electric propulsion system begins with a 20-min. thermal conditioning of the xenon flow system. During the last 7 min., the cathode is preheated to self-emission temperature. Then xenon flow is started to the engine, and the discharge is initiated. In operation, an electrical discharge is established between the anode and the cathode. The elec-

trons flowing from the cathode to the anode interact with the magnetic field and generate the electric field within the discharge plasma. These electrons also generate xenon ions in collision with neutral xenon propellant atoms. In the presence of the +300 V anode, the xenon ions are accelerated from the engine. Some of the electrons from the cathode go to the ion beam and both charge and current neutralize the ions in that beam.² Figure 14 shows the theory of operation; Fig. 15 is a photograph of the engine in operation.

Summary: The EPDM program was an 18-month “design to cost” program that provided an acceptable risk level to the sponsor while demonstrating Hall thruster electric propulsion. The EPDM development, test, and verification approach was to achieve the highest level of systems testing possible prior to delivery for integration on the spacecraft. The data gathered on the system’s operational performance will guide future users of Hall thruster systems and advance the Hall thruster technology base. The EPDM program is the culmination of a large effort on the behalf of many organizations and individuals. The technology of EPDM demonstrates to potential users that Hall thruster electric propulsion systems are ready for application. By replacing chemical systems with Hall thruster systems to perform orbit functions such as insertion, orbit maintenance,



- Annular Discharge Between Cathode (-) and Anode (+)
- Crossed Magnetic Field Cause Complex Electron Motion - Closed Circular Drift Shown
- Electric Field Results From Magnetic Effect On Electrons and Anode Sheath Layer
- Heavy Ions Are Unaffected By Magnetic Field and Are Accelerated By Electric Field

FIGURE 14
Hall thruster theory of operation.

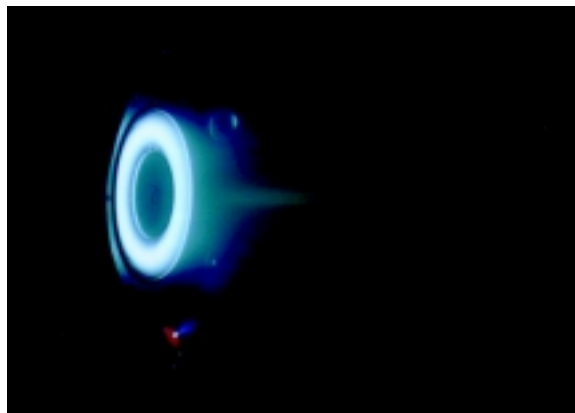


FIGURE 15
EPDM performance characterization testing in vacuum chamber.

and de-orbit, the spacecraft mass can be reduced to the extent that new and enabling missions are made possible.

Acknowledgments: The EPDM program is run by the NCST at NRL. BMDO in conjunction with the NASA LECR has sponsored the development of the TAL thruster, power processor, and flow system technology being used by EPDM. NASA LECR assisted in the qualification and testing of the EPDM hardware. The TAL thruster is a Russian Hall thruster technology developed by the Central Scientific Research Institute of Machine Building (TsNIIMash) in

Korolev, Russia. The EPDM program is a cooperative DoD/NASA effort with expertise, fiscal sponsorship, and national space test beds from across the government used to successfully implement the program.

[Sponsored by NRO]

References

¹J.M. Sankovic, L.H. Caveny, and P.R. Lynn, "The BMDO Russian Hall Electric Thruster Technology (RHETT) Program: From Laboratory to Orbit," AIAA-Paper-97-2917, American Institute of Aeronautics and Astronautics, July 1997.
²V.V. Zhurin, H.R. Kaufman, and R.S. Robinson, "Physics of Closed Drift Thrusters," IEPC-97-191, August 1997. ★



The Clementine Concept
Science-as-Art contest – First place winner
Submitted by: Richard Cooksey and Dennis Brooks

Artist's rendering of the Deep Space Program Science Experiment (DSPSE), otherwise known as *Clementine*. *Clementine* was the first satellite to incorporate the “better, cheaper, faster” management style. The time from its conception to its launch was an incredible 22 months. One aspect of this mission was the mapping of the Moon. *Clementine* generated 1.8 million images of the Moon. As a result of this work, scientists determined that water ice may be found on the Moon. In early 1998, NASA's Lunar Prospector confirmed the existence of water ice on the South Pole of the Moon.

197 Special Awards and Recognition

209 Alan Berman Research Publication and Edison Patent Awards

Special Awards and Recognition

NRL is proud of its many distinguished scientists, engineers, and support staff. Here we feature some who have received awards from prestigious institutions, the Department of the Navy, and NRL.

Outside Awards



Mr. Robert Eisenhauer
Space Systems Development
Department

PRESIDENTIAL RANK OF MERITORIOUS EXECUTIVE IN THE SENIOR EXECUTIVE SERVICE (SES)

The President of the United States of America has conferred on Mr. Eisenhauer the rank of Meritorious Executive in the Senior Executive Service for sustained superior accomplishment in management of programs of the United States Government and for noteworthy achievement of quality and efficiency in the public service.



Mr. Roger Easton
Former NRL engineer—
Naval Center for Space
Technology

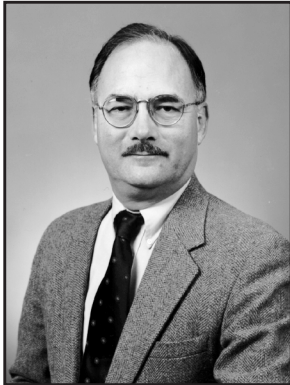
AMERICAN PHILOSOPHICAL SOCIETY MAGELLANIC PREMIUM AWARD

The Magellanic Premium Award was established by John Hyacinth de Magellan of London in 1786 for a medal to be awarded from time to time under prescribed terms, to the author of the best discovery or most useful invention relating to navigation, astronomy, or natural philosophy. Mr. Easton shares the award equally with Stanford University professor Bradford Parkinson (retired, USAF), who was the first GPS program manager. Mr. Easton was cited for “contributions to creating the Global Positioning System.” The award recognizes the significance of GPS outside of its military uses.

SPACE TECHNOLOGY HALL OF FAME

The Space Technology Hall of Fame was established in 1988 by the United States Space Foundation, in cooperation with NASA, to honor innovators who have transformed technology originally developed for space use into commercial products, to increase public awareness of the benefits of space spin-off technology, and to encourage further innovation. NRL’s Naval Center for Space Technology has been inducted into the Space Technology Hall of Fame for its contributions related to the Global Positioning System (GPS), specifically the *TIMATION* program. CAPT Bruce W. Buckley and Mr. Roger Easton were presented with commemorative medallions in recognition of this achievement.





Mr. David Pettit
Space Systems Development
Department

NATIONAL RECONNAISSANCE OFFICE GOLD AWARD FOR DISTINGUISHED SERVICE

The National Reconnaissance Office (NRO) Gold Award for Distinguished Service, which is the highest award given by the National Reconnaissance Office, is awarded in recognition of distinguished service to the mission of the NRO. The citation states, “Mr. David L. Pettit distinguished himself by sustained exceptional service as a space systems engineer and mission manager for the Low Earth Orbit Systems Program Office. ...Senior officials in the Department of Defense and the Intelligence Community continually recognized Mr. Pettit for his expertise and sought his advice. As a consummate engineer, innovator, and team player, Mr. Pettit contributed greatly to the defense of the United States. The distinctive accomplishments of Mr. Pettit reflect great credit upon himself, the Naval Research Laboratory, and the National Reconnaissance Office.”



Dr. John Montgomery
Tactical Electronic Warfare Division

DR. ARTHUR E. BISSON PRIZE FOR NAVAL TECHNOLOGY ACHIEVEMENT

Dr. Montgomery is the second recipient of the Dr. Arthur E. Bisson Prize for Naval Technology Achievement, which recognizes a person who has successfully translated research findings into substantive fleet programs that meet critical Navy requirements. Dr. Montgomery leads the Navy’s premier laboratory for electronic warfare (EW) technology, which conducts a comprehensive program of research and development. He has orchestrated the transition from concept to prototype to fielded capability of a great number of EW technologies, developed the Navy’s solution to the Wartime Reserve Mode problem, and initiated successful ship and aircraft decoy programs.



Dr. Robert Conway
Space Science Division

SIGMA XI 1998 PURE SCIENCE AWARD

Dr. Conway was recognized for his accomplishments as the principal investigator of the Middle Atmosphere High Resolution Spectrograph Investigation (MAHRSI), a high-spectral-resolution remote sensing instrument. The award noted that Dr. “Conway’s achievements have led to the identification of the cause of discrepancy in our understanding of the distribution of ozone, a matter of intense importance to the national program and the global community. ...Building on advanced detector and optical design technology developed at NRL, Conway led an intensive effort at NRL for nine years to develop an instrument to measure hydroxyl in the Earth’s middle atmosphere. His scientific acumen, technical capability, unselfish dedication to science, and the high level of respect with which he is held by all, were key factors in this major accomplishment.”



Dr. Ishwar Aggarwal
Optical Sciences Division

SIGMA XI 1998 APPLIED SCIENCE AWARD

The nomination for this award stated that Dr. Aggarwal has “distinguished himself through the breadth and creativity of his experimental research in infrared materials, optical fibers, and chemical sensors.” Dr. Aggarwal is responsible for directing research in infrared glasses and fibers for various Defense and medical applications and chemical sensors for hazardous and nuclear waste detection.



Dr. Bhatka Rath
*Materials Science and Component
Technology Directorate*

SAMANTA CHANDRA SEKHAR AWARD FOR 1996

The Samanta Chandra Sekhar Award, presented by the Science & Technology Department, Government of Orissa, India, and the Orissa Science Academy, recognizes a scientist working outside the state of Orissa, India. Dr. Rath was recognized for his “valuable contributions in the field of scientific research, which have been considered the most outstanding among all the contributions made by the scientists outside the state of Orissa during the five years preceding 1996.”



Dr. Burton G. Hurdle
Acoustics Division

IEEE OCEANIC ENGINEERING SOCIETY DISTINGUISHED TECHNICAL ACHIEVEMENT AWARD

This award was presented to Dr. Hurdle for his outstanding contribution to understanding the oceanography and acoustics of the Nordic Seas. Dr. Hurdle has been quite active in the formulation of the Acoustic Division’s scientific program by developing new concepts. His recent research has focused on the use of complex ocean interference fields to enhance knowledge of the acoustics of the oceans and the effects of geophysics and gas hydrates on low-frequency propagation. He was the Chief Scientist and Editor of a two-volume reference book on *The Nordic Seas* (1986) and the *Acoustics of the Nordic Seas* (1991) which represent a major contribution to the U.S. Navy and the ocean engineering community.

Internal Awards

LIFETIME ACHIEVEMENT AWARD

Dr. Isabella Karle and Mr. Peter Wilhelm were presented NRL's Lifetime Achievement Award for extraordinary achievements and contributions. This award is the highest local honor that an NRL Commanding Officer can confer on a civilian employee.



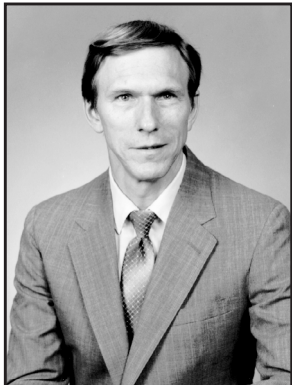
Dr. Isabella Karle
Laboratory for Structure of Matter

Dr. Karle was cited for “effecting major advances in chemistry and the chemical industry by developing an analytical tool that can determine accurately and with dispatch, the three dimensional arrangements of atoms in a very broad range of substances. Such substances include materials of interest to the Department of Defense, the medical community, and the nation as a whole. Dr. Karle has not only applied her methodology in her research program to many substances of importance, but her efforts have been very greatly magnified by the worldwide adaptation and application of her methodology. As a result, many thousands of new structures are determined each year for the valuable purpose of relating structure to function. Throughout her 52 years of exemplary service to the Naval Research Laboratory, the Department of the Navy, the Department of Defense, and the nation, Dr. Karle has been an inspiration to her professional colleagues and to her many students.”



Mr. Peter Wilhelm
Naval Center for Space Technology

Mr. Wilhelm was cited for “exceptional technical expertise, outstanding management, and dedication to excellence in support of Navy and national space programs, including Clementine, the Multiple Satellite Dispenser, the Low-power Atmospheric Compensation Experiment, TIMATION/NAVSTAR GPS, the Living Plume Shield satellites, and the Solar Radiation satellite program...His achievements in high-performance, long-life satellites, multiple satellite launching systems, gravity gradient stabilization systems, low-power/low-weight electronics, station-keeping microthrusters, and solid-state memory systems have been critical to maintaining U.S. superiority in space. His innovative concepts for satellite orbit insertion, transfer, and maneuvering systems have made major national space systems affordable and have permitted their ultimate development and deployment in service to the warfighter. Mr. Wilhelm's extraordinary leadership, superb engineering accomplishments, and inspiring vision have contributed substantially to Navy leadership in space.”



Dr. Robert Lehmberg
Plasma Physics Division

1997 E.O. HULBURT SCIENCE AWARD

The E.O. Hulburt Science Award is the highest civilian honor awarded for scientific achievement by the Naval Research Laboratory. Dr. Lehmberg was cited for his “theoretical development of the optical smoothing technique called induced spatial incoherence (ISI), which led to the development of the Nike KrF laser, with the first laser fusion experiments not dominated by beam nonuniformities, and the revitalization of the direct drive pellet concept with KrF lasers as a serious contender for laser fusion.”



Mr. Brian Solan
Tactical Electronic Warfare Division

NAVY SUPERIOR CIVILIAN SERVICE AWARD

Mr. Solan was cited for “his professional achievement in the performance of his duties while serving at the Naval Special Warfare Development Group from April 1995 to December 1996.” According to the citation, “Mr. Solan performed his duties in an exemplary and highly professional manner. His technical expertise and devotion to duty contributed greatly to the operational readiness of U.S. Special Operations Forces. With ingenuity and innovation, he developed a mission builder program that significantly increased the situational awareness of commanders and their units. He provided expert mission analysis and assistance to the U.S. Special Operations Command planners in five U.S. Special Operations Contingency Planning efforts. In addition, he deployed to an initial staging base on ten major U.S. Special Operations Command Joint Exercises where he assisted planners in threat modeling, analysis, and radar detection predictions for Special Operations Forces assets.”



Ms. Margaret Powell
Space Systems Development
Department

NAVY MERITORIOUS CIVILIAN SERVICE AWARD

According to the award citation, Ms. Powell “accepted the challenge of becoming the DON Year 2000 Coordinator. Her superior leadership and management of this highly complex endeavor have directly benefited the DON.” She worked closely with the DON and Department of Defense officials while managing the daily operations of the DON Year 2000 efforts.



Ms. Harriet Halper
Business Operations Directorate

NAVY MERITORIOUS CIVILIAN SERVICE AWARD

According to the award citation, Ms. Halper “has contributed greatly to the achievement of the organizational goals of NRL by serving on special project assignments from the senior management and by her leadership in the staffing and operation of the Counsel’s Office of NRL.” She is both a practicing attorney and manager of NRL’s Office of Counsel.



Dr. Melvin Kruer
Optical Sciences Division

NAVY MERITORIOUS CIVILIAN SERVICE AWARD

According to the award citation, Dr. Kruer “has made significant contributions to the development of mid-infrared focal plane array detectors. He has guided the work that has placed NRL in the forefront of mid-infrared focal plane array sensor research and development. This includes the development of efficient non-uniformity correction techniques, layered detector arrays, and increased dynamic range mid-infrared arrays.” He has been very active in the technical community through service on Navy, Tri-Service, and professional panels and committees.



CAPT Raymond Leonard, III, USN
Executive Directorate

LEGION OF MERIT

For the President of the United States, the Honorable John Dalton, Secretary of the Navy, cited CAPT Leonard for “exceptionally meritorious conduct in the performance of outstanding service as Chief Staff Officer of the Naval Research Laboratory, Washington, D.C., from July 1994 through June 1998. CAPT Leonard brought to the Laboratory a wealth of technical and operational experience, and displayed exceptional professionalism in multiple roles. As the Chief Staff Officer, he provided invaluable management direction for a world-class industrially funded research activity with an \$800 million annual budget and more than 3,200 personnel at 13 separate sites. As the Command’s Inspector General, CAPT Leonard conducted several highly sensitive and complex investigations with extraordinary tact and impeccable thoroughness, enabling the Laboratory to successfully resolve each issue. ...By his outstanding leadership, uncompromising ethical standards, and inspiring dedication to duty, CAPT Leonard reflected great credit upon himself and upheld the highest traditions of the United States Naval Service.”



Ms. Laurie Stackpole
Technical Information Division

COMMANDING OFFICER'S AWARD FOR ACHIEVEMENT IN THE FIELD OF EQUAL EMPLOYMENT OPPORTUNITY (EEO)

Ms. Stackpole was cited for “continuous, unswerving dedication to the principles of Equal Employment Opportunity through the development and promotion of a diverse, professional staff, and her recognition of the value of each employee contributing to the support of the NRL mission.” She exemplifies the quality of the Laboratory and demonstrates her personal belief in the goals of the Laboratory by actively recruiting from the entire pool of available qualified candidates. She then assures that staff members carry the Laboratory banner with the strengths of preparedness, poise, knowledge, and respect. Ms. Fuller-Mora was cited for her

“long-term and ongoing support of the NRL goal of achieving EEO in the sciences by her mentoring and community outreach activities.” During the 17 years she has worked at NRL, she has been actively involved with issues related to equal employment opportunity for both women and minorities. Dr. Fuller-Mora helped to establish NRL’s mentor program. She has been extremely involved in NRL’s Community Outreach Program, and she has mentored students who visit her laboratory having an interest in a career in science.



Ms. Wendy Fuller-Mora
Materials Science and
Component Technology Division



Ms. Mary Anne Lindsey
Space Science Division

COMMANDING OFFICER'S AWARD FOR EXCELLENCE IN SECRETARIAL SUPPORT

Ms. Lindsey was cited for her “outstanding performance and exceptional support of the Upper Atmospheric Physics Branch. Her exemplary achievements are acknowledged throughout the NRL community and by international organizations as being at the very top of her profession.” She was particularly recognized for her administrative support of the Middle Atmospheric High Resolution Investigation (MAHRSI). She has had major responsibility for coordinating program activities, including delivery and integration, for this international collaboration between NRL, the German Space Agency, and the University of Wuppertal in Germany. As noted in the nomination, “her ability to deal with NRL support services and to expedite the complex arrangements to ensure the scientific success of MAHRSI has been nothing short of remarkable.”

Group Awards



(Left to right) Mr. James Marshall, Ms. Carol Hambric, Ms. Linda Greenway, and Ms. Leona Jackson

1997 CRYSTAL AWARD OF EXCELLENCE

Technical Information Division

The Visual Design/Imaging Center has received a 1997 Crystal Award of Excellence for its CD-ROM entry "Advancing Technology through Naval Research." The Communicator Awards' prestigious Crystal Award of Excellence is presented to those entrants "whose ability to communicate elevates them above the best in the field." Winners of the Communicator Awards come from video production companies, independent producers, directors, writers, videographers, editors and other production professionals, corporate communication departments, government entities, broadcast and cable television operations, advertising and public relations agencies, and other businesses and individuals throughout the country.



BIOSENSORS & BIOELECTRONICS AWARD

Chemistry Division

(Left to right) Mr. Steven Metzger, Dr. Mohan Natesan, Dr. Gil Lee, Dr. Paul Sheehan, Dr. Richard Colton, and Dr. David Baselt

Members of the Surface Chemistry Branch were honored with the Biosensors & Bioelectronics Award for their paper entitled, "A Biosensor Based on Magnetoresistance Technology." The award was given by the Fifth World Congress on Biosensors in Berlin, Germany. The paper was selected as "the most original contribution" from nearly 500 submissions. The paper describes NRL's ongoing development of the Bead Array Counter (BARC) biosensor that will detect viral and bacterial pathogens by measuring, at the level of single molecules, the forces that bind DNA-DNA, antibody-antigen, or ligand-receptor pairs together. The ability of the sensor to directly measure the strength of intermolecular interactions suggests applications in the field of drug discovery, while its projected high sensitivity and small size would be ideal attributes for on-site testing.



Secretary of Defense William Cohen and Dr. Ben Cantrell

VICE PRESIDENT AL GORE'S HAMMER AWARD
Radar Division

Secretary of Defense William S. Cohen honored members of NRL's Radar Division with Vice President Al Gore's Hammer Award for their involvement in the NATO Seasparrow Surface Missile System (NSSMS) Capability Modernization program. The group was cited for their "contribution to building a government that works better and costs less." The NSSMS is the first DoD international cooperative project to receive the award. NRL's contribution to the program was the development of a very low-cost replacement signal data processor for the NSSMS. The NSSMS' reengineering effort resulted in development and production cost savings, a reduction in annual maintenance costs, a reduction in system training requirements, and it provided the fleet with new and enhanced performance capabilities.



NRL'S AWARD FOR EXCELLENCE IN MISSION SUPPORT
Management Information Systems Team

(Left to right) Mr. Michael Carico, Mr. Ben Berliant, Ms. Pam Lowery, Ms. Becky Douglass, CAPT Bruce Buckley, Ms. Barbara Hildreth, Mr. Ken Bell, Ms. Karen Hart, Mr. Bill Barton, and Mr. Bill Gollaher (not shown)

This award was presented to the Management Information Systems Team of the Management Information Systems Staff for providing significant contributions while working in positions that support the Laboratory's scientific and technical community. According to the citation, the team "was instrumental in developing, implementing, and supporting the NRL Procurement Information Processing Systems (PIPS) that significantly improved the efficiency of NRL operations; demonstrated exceptional effectiveness in analyzing and devising solutions to problems; and completed (and continue to complete) an extraordinary amount of work under adverse conditions, such as shortage of staff, heavy workloads, and short deadlines."



THE 1998 NRL REVIEW ARTICLE AWARDS

(Left to right) Dr. Simon Chang, Dr. Albert Bosse, Dr. Peter Vogt,
Dr. Teddy Holt, Dr. Chester Poranski, and Dr. Victor Chen

Awards for *NRL Review* articles recognize authors who submit outstanding research articles for this scientific publication. The articles are judged on the relevance of the work to the Navy and DoD, readability to the college-graduate level, clearness and conciseness of writing, and the effective use of graphics that are interesting and informative. The following awards were presented for articles that appeared in the *1998 NRL Review*.

FEATURED RESEARCH ARTICLE

“*Exploring an Active, Methane-hydrate-infested Mud Volcano on the Ocean Floor*,” Dr. Peter Vogt (Marine Geosciences Division)

DIRECTORATE AWARDS FOR SCIENTIFIC ARTICLES

Systems Directorate: “*Time-Frequency Processing for Radar Imaging*,” Dr. Victor Chen (Radar Division)

Materials Science and Component Technology Directorate: “*X-Ray Backscatter Inspection of Sonar Domes*,” Dr. Chester Poranski, Mr. Edward Greenawald, Mr. Leroy Levenberry, and Dr. Young Ham (Chemistry Division)

Ocean and Atmospheric Science and Technology Directorate: “*A Meteorological Reanalysis for the Study of Gulf War Illness*,” Dr. Teddy Holt, Dr. Douglas Westphal, Dr. Simon Chang, Ms. Nancy Baker, Dr. Timothy Hogan, Mr. Louis Brody, Mr. Robert Godfrey, Dr. James Goerss, Mr. Dennis Laws, and Mr. Charles Hines (Marine Meteorology Division)

Naval Center for Space Technology: “*Attitude Determination Using GPS and Smart Structures*,” Dr. Albert Bosse, Dr. Glenn Creamer, Dr. George Kirby, Mr. Ronald Weber, and Dr. Shalom Fisher (Spacecraft Engineering Department)



**NATIONAL ASSOCIATION OF GOVERNMENT COMMUNICATORS
BLUE PENCIL AWARD**

*Technical Information Division
First Place, 1998 NRL Review*

Four-color Publication for a Technical Audience

(Left to right) first row: Richard Bussey, Jonna Atkinson, Donna Gloystein, Dr. John Bultman;
second row: Leona Sprankel, Gayle Fullerton, Judy Kogok, Rosie Bankert, Paul Sweeney;
third row: Kathy Parrish, James Marshall, Tim Calderwood, Pete Imhof, Maureen Long, David van Keuren.
Missing from photograph: Jan Morrow, Marsha Bray, Michael Savell, Saul Oresky, Suzanne Guilmineau,
Diltricia Montgomery, Barbara Jolliffe, and Patricia Staffieri.

Several members of the Technical Information Division's *NRL Review* team won a first place trophy for their submission of the *1998 NRL Review* in the 1998 National Association of Government Communicators Blue Pencil competition. This *Review* won in the category of "full-color publication for a technical audience." The goal of the NAGC awards is to recognize outstanding government communications projects and their producers. NAGC is the only professional association dedicated exclusively to federal, state, and local government communicators. Entries for the Blue Pencil competition are judged on writing, editorial content, layout and design, achievement of purpose, and cost-effectiveness.



NAVY AWARD OF MERIT FOR GROUP ACHIEVEMENT

Optical Sciences Division

(Left to right) Dr. Edward Stone, Mr. R. Bernard Brown, Dr. Melvin Krueger,
Mr. Dale Linne von Berg, and Dr. John Lee

This award was presented to scientists and engineers in NRL's Optical Sciences Division for their work in conducting a successful demonstration of the TARPS-CD (Tactical Airborne Reconnaissance Pod System-Completely Digital) on a Navy F-14 aircraft for the first time, with the real-time downlinking of imagery to a tactical ground station set-up on the Pentagon grounds. The citation notes, "This demonstration was the first time a high-resolution, large area coverage tactical reconnaissance capability providing imagery to a ground station display had been performed in real-time. The NRL team successfully addressed a diverse and complex set of challenges, demonstrating superior technical insight, excellent engineering judgment, and outstanding organizational and management skills in successfully implementing the complex demonstration."

Alan Berman Research Publication and Edison Patent Awards

The Annual Research Publication Awards Program was established in 1968 to recognize the authors of the best NRL publications each year. These awards not only honor individuals for superior scientific accomplishments in the field of naval research but also seek to promote continued excellence in research and in its documentation. In 1982, the name of this award was changed to the Alan Berman Research Publication Award in honor of its founder.

There were 193 separate publications submitted by the divisions in 1998 to be considered for recognition. Of those considered, 37 were selected. These selected publications represent 161 authors, each of whom received a publication awards certificate, a bronze paperweight, and a booklet listing the publications that were chosen for special recognition. In addition, NRL authors share in their respective division's monetary award.

The winning papers and their respective authors are listed below by their research units. Non-Laboratory coauthors are indicated by an asterisk.

NRL also recognizes patents as part of its annual publication awards program. The NRL Edison Patent Award was established in January 1991 to recognize NRL employees for outstanding patents issued to NRL by the U.S. Patent and Trademark Office during the preceding calendar year. The award recognizes significant NRL contributions to science and engineering as demonstrated by the patent process that are perceived to have the greatest potential benefit to the country. Of the 6 patents considered for 1998, 3 were selected, representing 8 inventors. They are listed under the NRL Edison Patent Awards.

Systems Directorate

Fabrication and Radio Frequency Characterization of High Dielectric Loss Tubule-Based Composites Near Percolation
Scott L. Browning, Jonas Lodge, Ronald R. Price,
John H. Schelleng, Paul E. Schoen, and Daniel Zabetakis

Radar Division

Voltage Controlled Ferroelectric Lens Phased Arrays
Jaganmohan B.L. Rao, Dharmesh P. Patel, and Vladimir Krichevsky

HF-Over-the-Horizon Radar Ship Detection with Short Dwells Using Clutter Cancellation
Benjamin T. Root

Information Technology Division

Using Abstraction and Model Checking to Detect Safety Violations in Requirements Specifications
Constance L. Heitmeyer, James C. Kirby, Jr.,
Bruce G. Labaw, Myla M. Archer, and Ramesh Bharadwaj

Anonymous Connections and Onion Routing
Michael G. Reed, Paul F. Syverson, and David M. Goldschlag

Plasma Physics Division

*Quasi-Neutral Particle Simulation of Magnetized Plasma Discharges:
General Formalism and Application to ECR Discharges*
Martin Lampe, Glenn Joyce, Wallace M. Manheimer, and Steven P. Slinker

K-Shell Radiation Physics in the Ultrahigh Optical Depth Pinches of the Z Generator
John P. Apruzese, Peter E. Pulsifier, Jack Davis, Robert W. Clark, Kenneth G. Whitney,
J. Ward Thornhill, T.W.L. Sanford,* G.A. Chandler,* C. Deeney,* D.L. Fehl,*
T.J. Nash,* R.B. Spielman,* W.A. Stygar,* K.W. Struve,* R.C. Mock,* T.L. Gilliland,* D.O. Jobe,*
J.S. McGurn,* J.F. Seamen,* J.A. Torres,* and M. Vargas*

Electronics Science and Technology Division

AlSb/InAs HEMT's for Low-Voltage, High-Speed Applications
J. Bradley Boos, Walter Kruppa, Brian R. Bennett,
Doewon Park, Steven W. Kirchoefer, Robert Bass, and Harry B. Dietrich

The Principle of Detailed Balance and the Lindblad Dissipative Quantum Dynamics
Attipat K. Rajagopal

Center for Bio/Molecular Science and Engineering

Remote Sensing Using an Airborne Biosensor
Francis S. Ligler, George P. Anderson, Peggy T. Davidson, Richard J. Foch,
David A. Stenger, Jeffrey T. Ives,* Keeley D. King,* Gregory Page,* and James Whelan*

Cooperative Chiral Order in Polysocyanates: New Statistical Problems
Jonathan V. Selinger and Robin L.B. Selinger*

Acoustics Division

Matched-Beam Processing: Application to a Horizontal Line Array in Shallow Water
Tsih C. Yang and Thomas Yates*

Inverse Neumann Obstacle Problem
Luise S. Couchman, Jeremy Warner,* and Dilip N. Ghosh Roy*

Remote Sensing Division

*Increases in Middle Atmospheric Water Vapor as Observed by the Halogen Occultation Experiment
and the Ground-Based Water Vapor Millimeter-Wave Spectrometer from 1991 to 1997*
Gerald E. Nedoluha, Richard M. Bevilacqua, R. Michael Gomez, David E. Siskind,
Brian C. Hicks, James M. Russell III,* and Brian J. Connor*

Subsurface, Surface, and Radar Modeling of a Gulf Stream Current Convergence
Robert W. Jansen, Colin Y. Shen, Scott R. Chubb, Arnold L. Cooper, and Thomas E. Evans

Oceanography Division

Sea Surface Height Variations in the Yellow and East China Seas
Gregg A. Jacobs, William J. Teague,
Shelley K. Riedlinger, Ruth H. Preller, and John P. Blaha*

Marine Geosciences Division

*Migration Process and Consideration for the Object-Oriented
Vector Product Format to ObjectStore Database Management System*
Kevin B. Shaw, Miyi J. Chung, and Maria Cobb

Beach Cusp Formation and Spacings at Duck, USA
K. Todd Holland

Marine Meteorology Division

*Western Pacific Warm Pool Region Sensitivity to Convective Triggering by
Boundary Layer Thermals in the NOGAPS Atmospheric GCM*
James A. Ridout and Carolyn A. Reynolds

*Effects of Degraded Sensor Resolution Upon Passive
Microwave Precipitation Retrievals of Tropical Rainfall*
Francis J. Turk, F.S. Marzano,* and A. Mugnai*

Space Science Division

Gamma-Ray Spectral States of Galactic Black Hole Candidates
J. Eric Grove, W. Neil Johnson, Richard A. Kroeger,
Jeffrey A. Skibo, K. McNaron-Brown,* and B.F. Philips*

*Geomagnetic Storms Caused by Coronal Mass Ejections (CMEs):
March 1996 Through June 1997*
Guenter E. Brueckner, Russell A. Howard, J.-P. Delaboudiniere,* S.E. Paswaters,*
D. Wang,* O.C. St.Cyr,* R. Schwenn,* P. Lamy,* G.M. Simnett,* and B. Thompson*

Space Systems Development Department

LEO Orbit Determination with Differential GPS
Peter J. Melvin

*Modulating Retroreflector Architecture Using Multiple
Quantum Wells for Free Space Optical Communications*
G. Charmaine Gilbreath, William S. Rabinovich, Douglas S. Katzer,
Kiki Ikossi-Anastasiou, H. Charles Merk, Michael J. Vilcheck,
Rita Mahon,* Michael R. Corson,* John F. Kline,* and Joshua Resnick*

Spacecraft Engineering Department

Cost-Benefit Analysis of On-Orbit Satellite Servicing
Nicholas M. Davinic, Scott S. Chappie, Alan J. Arkus,* and Joel Greenberg*

Automatic Rendering of Astrodynamics Expressions for Efficient Evaluation
Liam M. Healy and Jeffrey J. Travisano*

NRL Edison (Patent) Awards

Method and Apparatus for Side Pumping an Optical Fiber
Lew Goldberg

Electronic Devices With InAlAsSb/AlSb Barrier
J. Bradley Boos, Walter Kruppa, Doewon Park, and Brian R. Bennett

Chemical and Biological Sensor Using an Ultra-Sensitive Force Transducer
Gil U. Lee, David A. Kidwell, and Richard J. Colton



***The Development and Mitigation of Backdrafts:
A Full Experimental Study***
Science-as-Art contest – First Place winner
Submitted by: CDR John P. Farley

The use of Class B fuels aboard Naval ships presents unique challenges when leaks and/or fires develop. As opposed to Class A materials, Class B fuels tend to volatilize more quickly, resulting in rapidly growing fires or the buildup of fuel vapors. Buildup of vapors within the space can create dangerous reflashes and explosions, particularly during space reentry. In an effort to improve Naval firefighting procedures, an experimental study was performed to develop safe, reproducible full-scale tests as a basis to study the development and mitigation of Class B backdraft explosions. The study identified that the critical fuel mass fraction, required for the development of diesel fuel backdraft explosions, was 0.16 for fully vitiated conditions. The data also showed that the critical fuel mass fraction was dependent on the oxygen concentration in the compartment, the fuel type, and the fluid dynamics of the mixing fuel and air streams.

The injection of water spray was determined to be an effective mitigating tactic to completely suppress Class B backdraft explosions. Analysis revealed that the backdraft suppression occurred primarily by means of diluting the atmosphere and reducing the fuel mass fraction rather than by a thermal mechanism of cooling.

- 217 Programs for NRL Employees—Graduate Programs; Continuing Education; Technology Transfer; Technology Base; Professional Development; Equal Employment Opportunity (EEO) Programs; and Other Activities
- 221 Programs for Non-NRL Employees—Recent Ph.D., Faculty Member, and College Graduate Programs; Professional Appointments; Student Programs; and High School Programs

Programs for NRL Employees

During 1998, under the auspices of the Employee Development Branch, NRL employees participated in 3786 individual training events. Many of these were presented as either videotaped or on-site instructed courses on diverse technical subjects, management techniques, and enhancement of such personal skills as efficient use of time, speed reading, memory improvement, and interpersonal communications. Courses are also available by means of computer-based training (CBT) and live television, for nationwide monitoring.

One common study procedure is for employees to work full time at the Laboratory while taking job-related scientific courses at universities and schools in the Washington area. The training ranges from a single course to full graduate and postgraduate programs. Tuition for training is paid by NRL. The formal programs offered by NRL are described here.

GRADUATE PROGRAMS

- The **Advanced Graduate Research Program** (formerly the Sabbatical Study Program, which began in 1964) enables selected professional employees to devote full time to research or pursue work in their own or a related field for 1 year at an institution or research facility of their choice without the loss of regular salary, leave, or fringe benefits. NRL pays all educational costs, travel, and moving expenses for the employee and dependents. Criteria for eligibility include professional stature consistent with the applicant's opportunities and experience, a satisfactory program of study, and acceptance by the facility selected by the applicant. The program is open to paraprofessional employees (and above) who have completed 6 years of Federal Service, 4 of which have been at NRL.

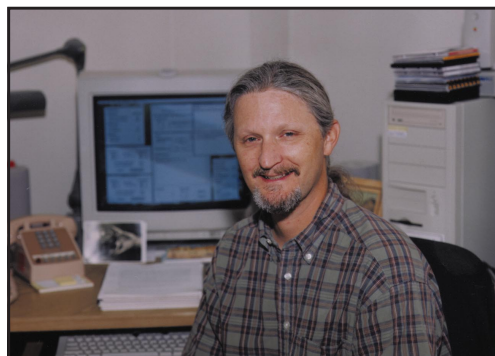
- The **Edison Memorial Graduate Training Program** enables employees to pursue advanced studies in their fields at local universities. Participants in this program work 24 hours each workweek and pursue their studies during the other 16 hours. The criteria for eligibility include a minimum of 1 year of service at NRL, a bachelor's or master's degree in an

appropriate field, and professional standing in keeping with the candidate's opportunities and experience.

- To be eligible for the **Select Graduate Training Program**, employees must have a college degree in an appropriate field and must have demonstrated ability and aptitude for advanced training. Students accepted into this program devote a full academic year to graduate study. While attending school, they receive one-half of their salary, and NRL pays for tuition and laboratory expenses.

- The **Naval Postgraduate School (NPS)**, located in Monterey, California, provides graduate programs to enhance the technical preparation of Naval officers and civilian employees who serve the Navy in the fields of science, engineering, operations analysis, and management. It awards a master of arts degree in national security affairs and a master of science degree in many technical disciplines.

NRL employees desiring to pursue graduate studies at NPS may apply for a maximum of six quarters away from NRL, with thesis work accomplished at NRL. Specific programs are described in the NPS catalog. Participants will continue to receive full pay and benefits during the period of study.



Mr. Derek Brock, of the Information Technology Division, is currently participating in the Edison Memorial Graduate Training Program at George Washington University, Washington, DC.

- In addition to NRL and university offerings, application may be made to a number of noteworthy programs and fellowships. Examples of such opportunities are the **Alfred P. Sloan Fellows Program**, **Brookings Institute Advanced Study Program**, the **Fellowship in Congressional Operations**, and the **Women's Executive Leadership Program**. These and other programs are announced from time to time, as schedules are published.

- Research conducted at NRL may be used as **thesis material for an advanced degree**. This original research is supervised by a qualified employee of NRL who is approved by the graduate school. The candidate should have completed the required course work and should have satisfied the language, residence, and other requirements of the graduate school from which the degree is sought. NRL provides space, research facilities, and supervision but leaves decisions on academic policy to the cooperating schools.

CONTINUING EDUCATION

- Local colleges and universities offer **undergraduate and graduate courses** at NRL for employees interested in improving their skills and keeping abreast of current developments in their fields. These courses are also available at many other DoD installations in the Washington, D.C. area.

- The Employee Development Branch at NRL offers **short courses** to all employees in a number of fields of interest including technical subjects, computer operation, supervisory and management techniques, and clerical/secretarial skills. Laboratory employees may attend these courses at nongovernment facilities as well. Interagency courses in management, personnel, finance, supervisory development, and clerical skills are also available.

For further information on any of the above programs, contact the Employee Development Branch (Code 1840) at (202) 767-2956.

TECHNOLOGY TRANSFER

- The **Office of Research and Technology Applications Program** (ORTA) ensures the full use of the results of the Nation's federal investment in research and development by transferring federally owned or originated technology to state and local governments and the private sector. (Contact Code 1004: Dr. Richard Rein, at (202) 767-7230 or Dr. Catherine Cotell at (202) 404-8411.)



Dr. Bernard Mrstik of the Electronics Technology and Science Division recently completed the Advanced Graduate Research Program at the Katholieke Universiteit, Leuven, Belgium.

TECHNOLOGY BASE

- The **Navy Science Assistance Program** (NSAP) establishes an information loop between the Fleet and the R&D shore establishments to expedite technology transfer to the user. The program addresses operational problems, focuses resources to solve specific technical problems, and develops a nucleus of senior scientific personnel familiar with the impact of current research and system performance on military operations. The program also provides 2-year science advisor positions in the Fleet. NRL is a participant of this ONR program.

- The **Scientist-to-Sea Program** (STSP) provides increased opportunities for Navy R&D laboratory/center personnel to go to sea to gain first-hand insight into operational factors affecting system design, performance, and operations on a variety of ships. NRL is a participant of this NSAP-ONR program.

For further information on these and other Technology Base Programs, contact Dr. Stephen Sacks, Code 5006, at (202) 767-3666.

PROFESSIONAL DEVELOPMENT

NRL has several programs, professional society chapters, and informal clubs that enhance the professional growth of employees. Some of these are listed below.

- The **Counseling Referral Service** (C/RS) helps employees to achieve optimal job performance through counseling and resolution of problems such

as family, stress and anxiety, behavioral, emotional, and alcohol- or drug-related problems that may adversely impact job performance.

C/RS provides confidential assessments and short-term counseling, training workshops, and referrals to additional resources in the community. (Contact Ms. Eileen Long-Farias at (202) 767-6857.)

- A chartered chapter of **Women in Science and Engineering (WISE)** was established at NRL in 1983. In 1997, the NRL WISE Chapter and the NRL Women in Science and Technology Network merged to form the NRL WISE Network. The goals of the organization are to encourage and promote the professional growth of women in science and engineering. Informal luncheons and seminars are scheduled to discuss scientific research areas, career opportunities, and career-building strategies, and to brainstorm solutions to problems encountered by women in science and engineering. WISE also sponsors a colloquium series that features outstanding women scientists. (Contact Dr. Elizabeth A. Dobisz at (202) 767-5159, Dr. Zakya Kafafi at (202) 767-9529, or Dr. Kristl Hathaway at (202) 767-4289.)

- **Sigma Xi**, the scientific research society, encourages and acknowledges original investigation in pure and applied science. As an honor society for research scientists, individuals who have demonstrated the ability to perform original research are elected to membership in local chapters. The NRL Edison Chapter, comprising approximately 600 members, recognizes original research by presenting awards annually in pure and applied science to outstanding NRL staff members. The chapter also sponsors lectures at NRL on a wide range of scientific topics for the entire NRL community. These lectures are delivered by scientists from all over the nation and the world. The highlight of the Sigma Xi lecture series is the Edison Memorial Lecture, traditionally featuring a distinguished scientist. (Contact Dr. David van Keuren at (202) 767-4263 or Dr. Arthur Jordan at (202) 767-1937.)

- The **NRL Mentor Program** was established to provide an innovative approach to professional and career training and an environment for personal and professional growth. It is open to permanent NRL employees in all job series and at all sites. Mentorees are matched with successful, experienced colleagues who can provide them with the knowledge and skills needed to maximize their contribution to the success

of their immediate organization, to NRL, to the Navy, and to their chosen career fields. The ultimate goal of the program is to increase job productivity, creativity, and satisfaction through better communication, understanding, and training. NRL Instruction 12400.1 established the NRL Mentor Program, and it provides the policy and procedures for the program. (Contact Ms. Natalie Gibbs at (202) 767-3034.)

- The Charlotte Moore-Sitterly Chapter of **Federally Employed Women, Inc. (FEW)** was chartered at NRL in 1993. FEW is an international organization of federally employed women and men whose purpose is to eliminate sex discrimination and sexual harassment and enhance career opportunities for women in government. FEW works closely with other Federal agencies and organizations, including the Office of Personnel Management, Equal Employment Opportunity Commission, and Federal Women's Program subcommittees. (Contact Dr. Virginia Degiorgi at (202) 767-9027.)

- Employees interested in developing effective self-expression, listening, thinking, and leadership potential are invited to join either of two NRL chapters of **Toastmasters International**. Members of these clubs, who possess diverse career backgrounds and talents, meet two to four times a month in an effort to learn to communicate not by rules but by practice in an atmosphere of understanding and helpful fellowship. NRL's Commanding Officer and Director of Research endorse Toastmasters as an official training medium at NRL. (Contact Kathleen Parrish at (202) 767-2782 for more information.)

EQUAL EMPLOYMENT OPPORTUNITY (EEO) PROGRAMS

Equal employment opportunity is a fundamental NRL policy for all employees regardless of race, color, national origin, sex, religion, age, or physical/mental handicap. The NRL EEO Office is a service organization whose major functions include counseling employees in an effort to resolve employee/management conflicts, processing formal discrimination complaints, providing EEO training, and recruiting for affirmative employment candidates. The NRL EEO Office is also responsible for sponsoring special-emphasis programs to promote awareness and increase sensitivity and appreciation of the issues or the history relating to: females; individuals with disabilities; Hispanic Americans; African Americans; and individuals of American Indian/Alaskan-Native and Asian-



Warm handshakes, meaningful gestures, confident presentations, and enthusiastic applause marked the graduation ceremony of sixteen 5th and 6th grade students from Patterson Elementary School who completed a 10-week Youth Leadership Program. This program is co-sponsored by NRL's Community Outreach Program and the Thomas Edison Toastmasters Club.

American/Pacific Islander descent. (Contact the NRL Deputy EEO Officer at (202) 767-5264 for additional information on any of our programs or services.)

OTHER ACTIVITIES

• The **Community Outreach Program** traditionally has used its extensive resources to foster programs that provide benefits to students and other community citizens. Volunteer employees assist with and judge science fairs, give lectures, tutor, mentor, coach, and serve as classroom resource teachers. The program also sponsors African American History Month art and essay contests for local schools, student tours of NRL, a student Toastmasters Youth Leadership Program, an annual holiday party for neighborhood children, and other programs that support the local community. Also through this program, NRL has active partnerships with four District of Columbia, three Aberdeen, Maryland, and three Calvert County, Maryland, public schools. (Contact Mr. Dom Panciarelli at (202) 767-2541.)

• Other programs that enhance the development of NRL employees include four computer user groups (**IBM PC**, **Mac**, **NeXT**, and **Sun**) and the **Amateur Radio Club**. The **Recreation Club** encourages the wide interest of sports for employees with its many facilities and programs, such as a heated indoor pool; basketball and volleyball court; weight room; table tennis; hot tub and sauna; five martial arts disciplines; aerobics classes; swimming lessons; water walking and exercise; swing dance sessions; and softball and basketball leagues. Sportswear, NRL paraphernalia, discount tickets to amusement parks, and film-developing services are available at the Rec Club office. The **Showboaters**, a nonprofit drama group that presents live theater for the enjoyment of NRL and the community, performs two major productions each year in addition to occasional performances at Laboratory functions and benefits for local charities. Although based at NRL, membership in Showboaters is not limited to NRL employees.

Programs for Non-NRL Employees

Several programs have been established for non-NRL professionals. These programs encourage and support the participation of visiting scientists and engineers in research of interest to the Laboratory. Some of the programs may serve as stepping-stones to federal careers in science and technology. Their objective is to enhance the quality of the Laboratory's research activities through working associations and interchanges with highly capable scientists and engineers and to provide opportunities for outside scientists and engineers to work in the Navy laboratory environment. Along with enhancing the Laboratory's research, these programs acquaint participants with Navy capabilities and concerns.

RECENT PH.D., FACULTY MEMBER, AND COLLEGE GRADUATE PROGRAMS

- The **National Research Council (NRC) Cooperative Research Associateship Program** selects associates who conduct research at NRL in their chosen fields in collaboration with NRL scientists and engineers. The tenure period is 2 years.

- The **American Society for Engineering Education (ASEE) Postdoctoral Fellowship Program** aims to increase the involvement of highly trained scientists and engineers in disciplines necessary to meet the evolving needs of naval technology. Appointments are for 1 year (renewable for a second and sometimes a third year).

- The **Consortium for Oceanographic Research Education (CORE) Postdoctoral Fellowship Program** is administered in much the same manner as the above two programs. However, this program is focused on selecting associates with advanced degrees in the oceanic and atmospheric environmental sciences. The purpose of this program is to recruit scientists and engineers in these specialized areas.

- The American Society for Engineering Education also administers the **Navy/ASEE Summer Faculty Research and Sabbatical Leave Program** for university faculty members to work for 10 weeks (or longer, for those eligible for sabbatical leave)

with professional peers in participating Navy laboratories on research of mutual interest.

- The **NRL/United States Naval Academy (USNA) Cooperative Program for Scientific Interchange** allows faculty members of the U.S. Naval Academy to participate in NRL research. This collaboration benefits the Academy by providing the opportunity for USNA faculty members to work on research of a more practical or applied nature. In turn, NRL's research program is strengthened by the available scientific and engineering expertise of the USNA faculty.

- The **National Defense Science and Engineering Graduate Fellowship Program** helps U.S. citizens obtain advanced training in disciplines of science and engineering critical to the U.S. Navy. The 3-year program awards fellowships to recent outstanding graduates to support their study and research leading to doctoral degrees in specified disciplines such as electrical engineering, computer sciences, material sciences, applied physics, and ocean engineering. Award recipients are encouraged to continue their study and research in a Navy laboratory during the summer.

For further information about the above six programs, contact Ms. Lesley Renfro at (202) 404-7450.

PROFESSIONAL APPOINTMENTS

- **Faculty Member Appointments** use the special skills and abilities of faculty members for short periods to fill positions of a scientific, engineering, professional, or analytical nature.

- **Consultants and experts** are employed because they are outstanding in their fields of specialization or because they possess ability of a rare nature and could not normally be employed as regular civil servants.

- **Intergovernmental Personnel Act Appointments** temporarily assign personnel from state or local governments or educational institutions to the Federal Government (or vice versa) to improve public services rendered by all levels of government.

STUDENT PROGRAMS

The student programs are tailored to the undergraduate and graduate students to provide employment opportunities and work experience in naval research. These programs are designed to attract applicants for student and full professional employment in fields such as engineering, physics, mathematics, and computer sciences. The student employment programs are designed to help students and educational institutions gain a better understanding of NRL's research, its challenges, and its opportunities. Employment programs for college students include the following:

- An agreement between NRL-SSC and **Mississippi's Alliance for Minority Participation** places students whose background and interests match the Laboratory's field of research with NRL mentors in a 10-week research environment. Together with accomplished senior researchers and faculty advisors, students plan, develop, and conduct a summer research project to include challenging, hands-on experiences with research equipment and principles of modern research. (Contact Ms. Linda Ladner at (601) 688-4754.)

- The **Student Career Experience Program** (formerly known as Cooperative Education Program) employs students in study-related occupations. The program is conducted in accordance with a planned schedule and a working agreement among NRL, the educational institution, and the student. Primary focus is on the pursuit of bachelors degrees in engineering, computer science, or the physical sciences.

- The **Student Temporary Employment Program (STEP)** enables students to earn a salary while continuing their studies and offers them valuable work experience.

- The **Summer Employment Program** employs students for the summer in paraprofessional and technician positions in engineering, physical sciences, computer sciences, and mathematics.

- The **Student Volunteer Program** helps students gain valuable experience by allowing them to voluntarily perform educationally related work at NRL.

For additional information on these undergraduate and graduate college student programs, contact the Staffing Branch, Code 1810 at (202) 767-8318.

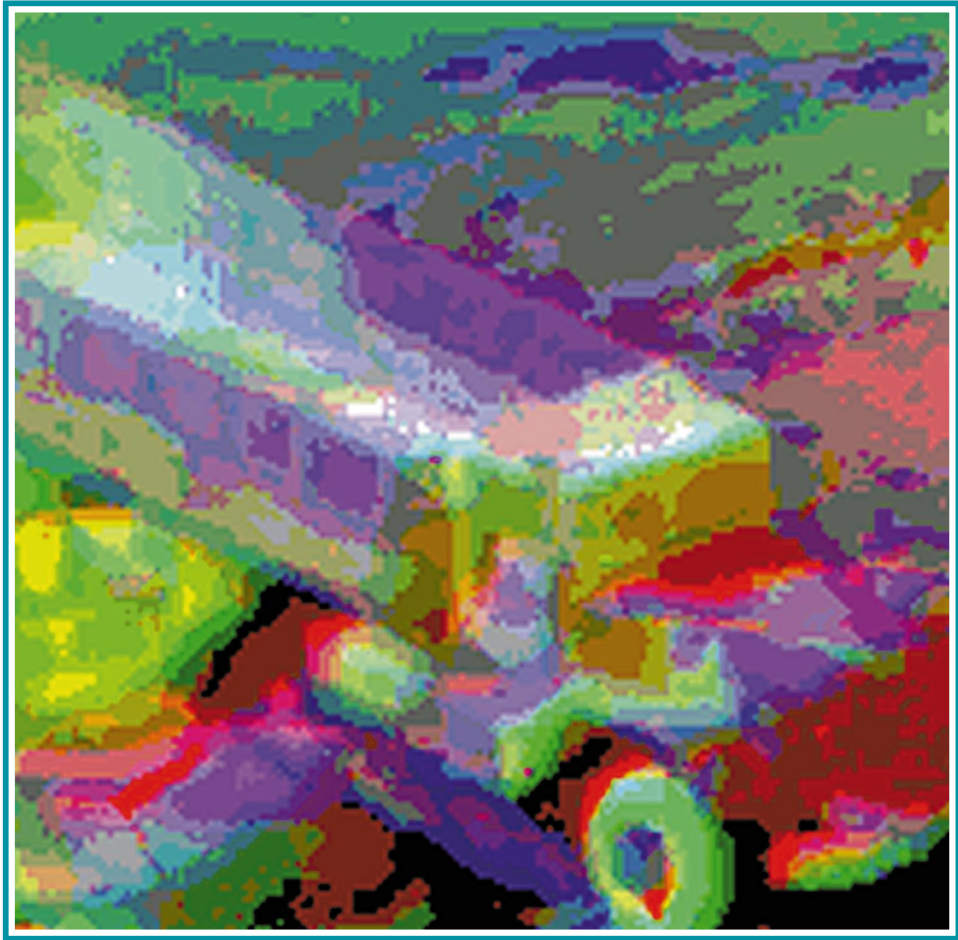
HIGH SCHOOL PROGRAMS

- The **DoD Science & Engineering Apprenticeship Program (SEAP)** employs high school juniors, seniors, and college students to serve for 8 weeks as junior research associates. The college students must have participated in SEAP during high school. Under the direction of a mentor, students gain a better understanding of research, its challenges, and its opportunities through participation in scientific programs. Criteria for eligibility are based on science and mathematics courses completed and grades achieved; scientific motivation, curiosity, and capacity for sustained hard work; a desire for a technical career; teacher recommendations; and achievement test scores. The NRL Program is the lead program and the largest in DoD.

For additional information, contact the Employee Development Branch (Code 1840) at (202) 767-2956.



In the chemistry laboratory, Lala Qadir extracts a sample of the sonicated energetic contaminated wastewater to analyze later using UV-VIS spectroscopy.



Infrared Color Vision: Color Constancy
Science-as-Art contest – Third Place winner
Submitted by: Dean Scribner and Jon Schuler

Infrared color vision is a method being developed to combine data from multiple spectral bands into a single composite color image for display to a human observer. Two major issues when creating intuitively meaningful color images are (1) obtaining good color contrast between objects and backgrounds, and (2) achieving consistent colors regardless of environmental conditions such as illumination and temperature. Multispectral IR imagery was collected with an NRL 12-band MWIR/LWIR sensor. The data were color-processed using several different algorithms. As a baseline, standard statistical processes were applied to achieve maximum color contrast. This is compared to other methods that attempt to replicate image preprocessing techniques that exist in the human color vision system. In the latter case, this processing involved applying color constancy algorithms developed by NRL researchers. The image seen here is one example of many scenes that were recorded at different times of the day and night. It shows a truck viewed in the afternoon using two MWIR bands and one LWIR band.

225	Technical Output
226	Technology Transfer at NRL
227	Key Personnel
228	Employment Opportunities for Entry-Level and Experienced Personnel
229	Location of NRL in the Capital Area
230	Contributions by Divisions, Laboratories, and Departments
233	Subject Index
236	Author Index

Technical Output

The Navy continues to be a pioneer in initiating new developments and a leader in applying these advancements to military requirements. The primary method of informing the scientific and engineering community of the advances made at NRL is through the Laboratory's technical output—reports, articles in scientific journals, contributions to books, papers presented to scientific societies and topical conferences, patents, and inventions.

The figures for calendar year 1998 presented below represent the output of NRL facilities in Washington, D.C.; Bay St. Louis, Mississippi; and Monterey, California.

In addition to the output listed, NRL scientists made more than 1440 oral presentations during 1998.

Type of Contribution	Unclassified	Classified	Total
Articles in periodicals, chapters in books, and papers in published proceedings	1274	0	1274
NRL Formal Reports	26	3	29
NRL Memorandum Reports	96	9	105
Books	3	0	3
Patents granted			78
Statutory Invention Registrations (SIRs)			6

*This is a provisional total based on information available to the Ruth H. Hooker Research Library and Technical Information Center on January 26, 1999. Additional publications carrying a 1998 publication date are anticipated.

Technology Transfer at NRL

There are many ways for private companies to benefit from the technical resources of NRL. Some of these include: (1) entering into Cooperative Research and Development Agreements (CRADAs), (2) obtaining licenses for Navy-owned patents, and (3) consulting with NRL scientists and engineers.

Entering into a CRADA is an excellent way for U.S. companies to gain access to commercially important NRL research and development. Authorized under the Federal Technology Transfer Act of 1986, a CRADA is an agreement between one or more federal laboratories and one or more nonfederal parties, such as private companies. Designed to encourage and facilitate cooperative R&D, CRADAs can involve research in any area that is consistent with NRL's mission.

Additionally, the Federal Government can license its own inventions. NRL has developed many new technologies and processes in areas as diverse as advanced materials, chemistry, biotechnology, optics, ocean and atmospheric sciences, and electronics. NRL currently has over 500 patents available for license in these fields.

As the Navy's corporate laboratory, NRL draws on the powerful resources of an interdisciplinary combination of scientific expertise and modern facilities. NRL's technical staff is recruited from all disciplines of engineering and the physical sciences and is available to work with private companies to help them solve their technical problems. Many of the staff have

received the Award for Excellence in Technology Transfer from the Federal Laboratory Consortium (FLC). This award recognizes employees who have accomplished outstanding work in the process of transferring laboratory-developed technology.

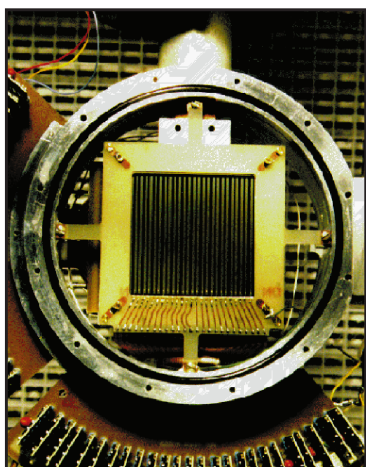
During 1998, the CRADAs signed by NRL have ranged from collaborations to assist companies with the commercialization of technologies they have licensed from NRL to the use of unique NRL capabilities to test, evaluate, or design new products for defense and commercial applications.

For example, NRL's Chemistry Division and Quantum Magnetics, Inc., are working under the scope of a CRADA to incorporate fast recovery time electronics into the NRL Nuclear Quadrupole Resonance (NQR) system for detection of contraband at airport security stations. Quantum Magnetics has licensed NRL's portfolio of patents on NQR.

Additionally, a CRADA with Physical Sciences, Inc., and NRL's Space Sciences Division is developing NRL's germanium strip detector for X-ray and gamma-ray spectrometry and imaging.

Navy users are also benefiting directly from NRL CRADAs. Satellite meteorological application software developed by NRL-Monterey is being incorporated into the TeraScan software package marketed by SeaSpace Corporation. The Navy uses SeaSpace's TeraScan software on the Navy Satellite Display System-Enhanced (NSDS-E) at four regional centers throughout the world. The CRADA is allowing Navy operational forecasters faster and easier access to the NRL-developed meteorological application modules.

For additional information, contact NRL's Technology Transfer Office, 4555 Overlook Ave., S.W., Washington, DC 20375-5320, or call (202) 767-7230; e-mail: techtransfer@nrl.navy.mil; URL: <http://infonext.nrl.navy.mil/~techtran/>.



Photograph of a 25 x 25 strip position-sensitive germanium detector being investigated under the scope of a CRADA with Physical Sciences, Inc., under the direction of Richard Kroeger, Code 7651. The detector operates at a temperature of 80K and measures both the position and energy of low-energy gamma rays. The combination of the two will lead to more detailed imaging and spectroscopy, which, in turn, are required in fields such as astrophysics, medical imaging, nondestructive testing, surveys of radioactive sites, and nuclear treaty verification.

Key Personnel

Area Code (202) unless otherwise listed
 Personnel Locator - 767-3200
 DSN-297 or 754

Code	Office		Phone Number
EXECUTIVE DIRECTORATE			
1000	Commanding Officer	CAPT B.W. Buckley, USN	767-3403
1000.1	Inspector General	CAPT G. Brown, Jr., USN	767-3621
1001	Director of Research	Dr. T. Coffey	767-3301
1001.1	Executive Assistant	Mr. D. DeYoung	767-2445
1002	Chief Staff Officer	CAPT G. Brown, Jr., USN	767-3621
1004	Head, Technology Transfer	Dr. R. Rein	767-7230
1006	Head, Office of Program Administration and Policy Development	Ms. L. McDonald	767-3091
1200	Head, Command Support Division	Mr. J.C. Payne	767-3048
1220	Head, Security	Dr. J.T. Miller	767-0793
1230	Public Affairs Officer	Mr. R. Thompson (Acting)	767-2541
1240	Head, Safety Branch	Mr. K.J. King	767-2232
1400	Head, Military Support Division	CDR A. Leigh, USN	767-2273
1600	Officer-in-Charge, Flight Support Detachment	CDR T.A. McMurry, USN	301-342-3751
1800	Director, Human Resources Office	Ms. B.A. Duffield	767-3421
1803	Deputy EEO Officer	Ms. D. Erwin	767-2486
3204	Deputy for Small Business	Ms. L. Byrne	767-6263
BUSINESS OPERATIONS DIRECTORATE			
3000	Associate Director of Research	Mr. R.E. Doak	767-2371
3008	Office of Counsel	Mr. T.E. McDonnell (Acting)	404-1551
3200	Head, Contracting Division	Mr. J.C. Ely	767-5227
3300	Comptroller, Financial Management Division	Mr. D. Therning	767-3405
3400	Supply Officer	Ms. C. Hartman	767-3446
3500	Director, Research and Development Services Division	Mr. S. Harrison	767-3697
SYSTEMS DIRECTORATE			
5000	Associate Director of Research	Dr. R.A. LeFande	767-3324
5200	Head, Technical Information Division	Mr. T. Calderwood (Acting)	767-2187
5300	Superintendent, Radar Division	Dr. G.V. Trunk	767-2573
5500	Superintendent, Information Technology Division	Dr. R.P. Shumaker	767-2903
5600	Superintendent, Optical Sciences Division	Dr. T.G. Giallorenzi	767-3171
5700	Superintendent, Tactical Electronic Warfare Division	Dr. J.A. Montgomery	767-6278
MATERIALS SCIENCE AND COMPONENT TECHNOLOGY DIRECTORATE			
6000	Associate Director of Research	Dr. B.B. Rath	767-3566
6030	Head, Laboratory for Structure of Matter	Dr. J. Karle	767-2665
6100	Superintendent, Chemistry Division	Dr. J.S. Murday	767-3026
6300	Superintendent, Materials Science & Technology Division	Dr. D.U. Gubser	767-2926
6400	Director, Lab. for Computational Physics and Fluid Dynamics	Dr. J.P. Boris	767-3055
6600	Superintendent, Condensed Matter & Radiation Sciences Division	Dr. D.J. Nagel	767-2931
6700	Superintendent, Plasma Physics Division	Dr. S. Ossakow	767-2723
6800	Superintendent, Electronics Science & Technology Division	Dr. G.M. Borsuk	767-3525
6900	Director, Center for Bio/Molecular Science and Engineering	Dr. J.M. Schnur	404-6000
OCEAN AND ATMOSPHERIC SCIENCE AND TECHNOLOGY DIRECTORATE			
7000	Associate Director of Research	Dr. E.O. Hartwig	404-8690
7100	Superintendent, Acoustics Division	Dr. E.R. Franchi	767-3482
7200	Superintendent, Remote Sensing Division	Dr. P. Schwartz	767-3391
7300	Superintendent, Oceanography Division	Dr. W.B. Moseley	228-688-4670
7400	Superintendent, Marine Geosciences Division	Dr. H.C. Eppert, Jr.	228-688-4650
7500	Superintendent, Marine Meteorology Division	Dr. P.E. Merilees	831-656-4721
7600	Superintendent, Space Science Division	Dr. H. Gursky	767-6343
NAVAL CENTER FOR SPACE TECHNOLOGY			
8000	Director	Mr. P.G. Wilhelm	767-6547
8100	Superintendent, Space Systems Development Department	Mr. R.E. Eisenhauer	767-0410
8200	Superintendent, Spacecraft Engineering Department	Mr. H.E. Senasack, Jr.	767-6411

Employment Opportunities for Entry-Level and Experienced Personnel

The *NRL Review* illustrates some of the exciting science and engineering carried out at the Naval Research Laboratory, as well as the potential for new personnel. In this regard, NRL offers a wide variety of challenging positions that involve the full range of work, from basic and applied research to equipment development. The nature of the research and development conducted at NRL requires professionals with experience. Typically there is a continuing need for electronics, mechanical, aerospace, ceramic and materials engineers, metallurgists, computer scientists, and oceanographers with bachelor's and/or advanced degrees and physical and computer scientists with Ph.D. degrees. Opportunities exist in the areas described below:

Ceramic Engineers and Materials Scientists/Engineers. These employees are recruited to work on materials, microstructure characterization, electronic ceramics, solid-state physics, fiber optics, electro-optics, microelectronics, fracture mechanics, vacuum science, laser physics technology, and radio frequency/microwave/millimeter wave/infrared technology.

Electronics Engineers and Computer Scientists. These employees may work in the areas of communications systems, electromagnetic scattering, electronics instrumentation, electronic warfare systems, radio frequency/microwave/millimeter wave/infrared technology, radar systems, laser physics technology, radio-wave propagation, electron device technology, spacecraft design, artificial intelligence, information processing, signal processing, plasma physics, vacuum science, microelectronics, electro-optics, fiber optics, solid state, software engineering, computer design/architecture, ocean acoustics, stress analysis, and expert systems.

Mechanical Engineers. These employees may be assigned to spacecraft design, remote sensing, pro-

pulsion, experimental fluid mechanics, experimental structural mechanics, solid mechanics, elastic/plastic fracture mechanics, materials, finite-element methods, nondestructive evaluation, characterization of fracture resistance of structural alloys, combustion, and CAD/CAM.

Chemists. Chemists are recruited to work in the areas of combustion, polymer science, bioengineering and molecular engineering, surface science, materials, fiber optics, electro-optics, microelectronics, electron-device technology, and laser physics.

Physicists. Physics graduates may concentrate on such fields as materials, solid-state physics, fiber optics, electro-optics, microelectronics, vacuum science, plasma physics, fluid mechanics, signal processing, ocean acoustics, information processing, artificial intelligence, electron-device technology, radio-wave propagation, laser physics, ultraviolet/X-ray/gamma-ray technology, electronic warfare, electromagnetic interaction, communications systems, radio frequency/microwave/millimeter wave/infrared technology, and computational physics.

Oceanographers, Meteorologists, and Marine Geophysicists. These employees work in the areas of ocean dynamics, air-sea interaction, upper-ocean dynamics, oceanographic bio-optical modeling, oceanic and atmospheric numerical modeling and prediction, artificial intelligence applications for satellite analyses, benthic processes, aerogeophysics, marine sedimentary processes, and advanced mapping techniques. Oceanographers and marine geophysicists are located in Washington, D.C., and the Stennis Space Center, Bay St. Louis, Mississippi. Meteorologists are located in Washington, D.C., and Monterey, California.

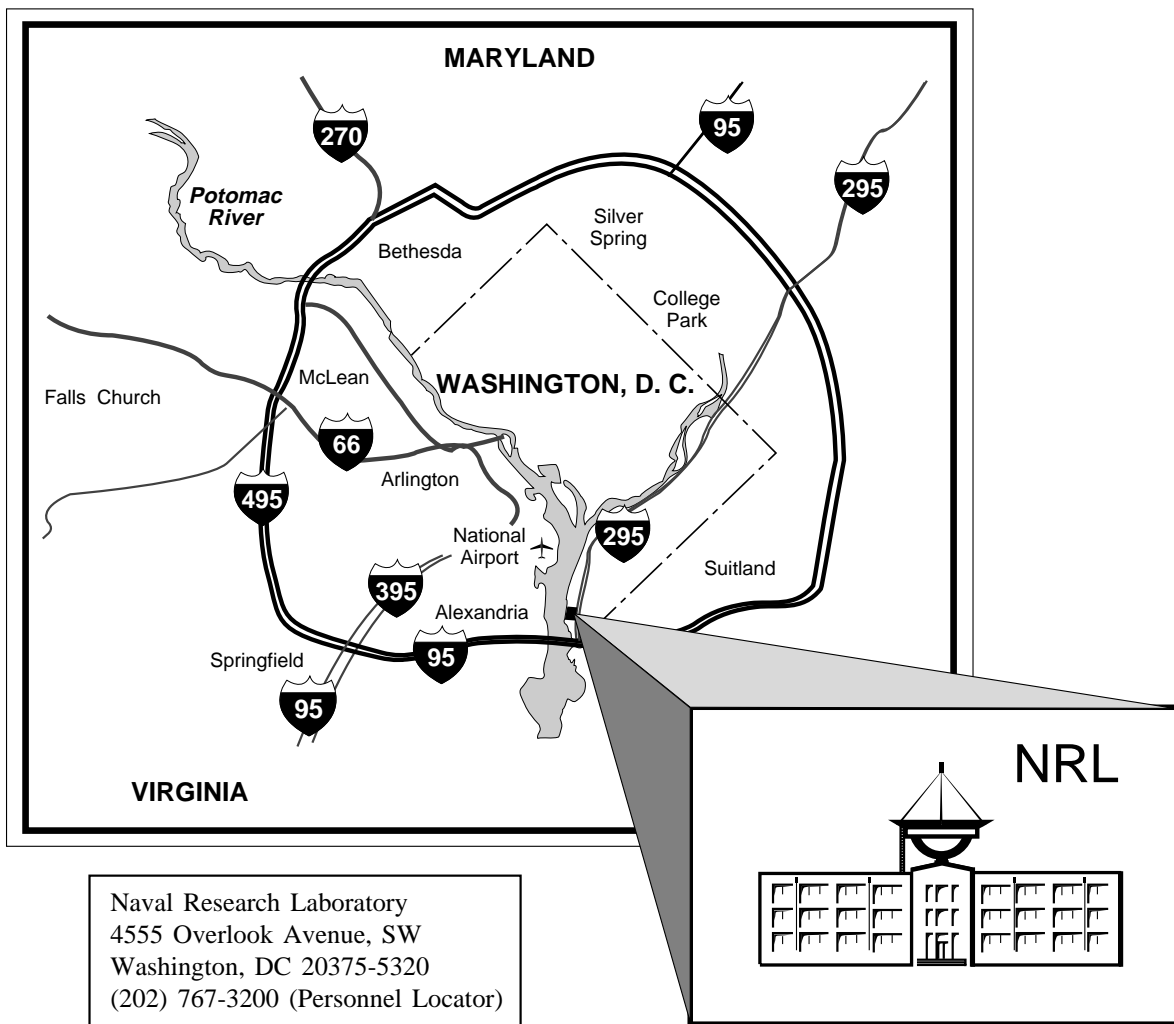
APPLICATION AND INFORMATION

Interested applicants should submit an Application for Federal Employment (SF-171), an Optional Application for Federal Employment (OF-612), or a resume. The OF-612 and SF-171 can be obtained from local Office of Personnel Management and Human Resource Offices of federal agencies.

Direct inquiries to:

Naval Research Laboratory
Human Resources Office, Code 1810 RV
Washington, DC 20375-5324
(202) 767-3030

Location of NRL in the Capital Area



Contributions by Divisions, Laboratories, and Departments

Radar Division

- 93 Automatic Radar Periscope Detection and Discrimination
D.W. Baden, R.S. DeCampo, G. Herman, and D.W. Kerr
- 94 Development Testing of AN/SPQ-9B Radar Preproduction Model
D.J. Cardiel, L.M. Schaus, and L.M. Leibowitz

Information Technology Division

- 120 Automating CIC Communications for Reduced Manning
A. Schmidt-Nielsen, L.B. Achille, and K.G. Schulze
- 117 Gaiter: A Locomotion Control for Distributed Simulation
J.N. Templeman, L.E. Sibert, P.S. Denbrook, R.C. Page, and J.A. McCune
- 119 Triangulation Range—Imaging Using Correlation Codes
F. Pipitone and R. Hartley

Optical Sciences Division

- 155 Optical Detection of Defects Below the Surface of Nontransparent Materials
M. Bashkansky, M.D. Duncan, and J.F. Reintjes
- 159 The NRL Infrared Range Facility
K.A. Snail and R.G. Priest
- 156 Dark HORSE (Hyperspectral Overhead Reconnaissance—Surveillance Experiment)
J.V. Michalowicz and F. Bucholtz
- 127 Novel Aerogel Materials
D.R. Rolison and C.I. Merzbacher

Tactical Electronic Warfare Division

- 107 EX 252 IR Seduction Decoy
W. Humphries and M.A. Snapp
- 96 A Method for Determining the Angle of Arrival (AOA) of Impinging Radio Waves in the Presence of Multipath
J.H. Frankovich and A.Y. Tse
- 169 Ground Truth Reference System
A.C. Hosmer

Laboratory for Structure of Matter

- 125 Protein Crystal Growth Cessation and Reinitiation
M.A. Perozzo and J.H. Konnert

Chemistry Division

- 127 Novel Aerogel Materials
D.R. Rolison and C.I. Merzbacher
- 87 Carbon Nanotubes: Experiments Catch Up with Theory
C.T. White and J.W. Mintmire
- 174 Reduced Manning—Its Impact on Damage Control
P.A. Tatem and F.W. Williams
- 84 Structure/Property Relationships and Applications of Low Dielectric Cyanurate Resins
L.J. Buckley and A.W. Snow

Materials Science and Technology Division

- 55 Thirty Years of NRL Research in Functional Ceramics: From Failure Analysis to Novel Ceramic Devices
D. Lewis III, C. Kim, C.C.M. Wu, T.L. Jessen, M. Kahn, and M.T. Chase

170 Master Stability Functions for Synchronizing Systems
L.M. Pecora and T.L. Carroll

128 A New Way to Measure Spin Polarization
R.J. Soulen, Jr., M.S. Osofsky, B. Nadgorny, and J. Byers

132 Disorder-Induced Colossal Magnetoresistance
R. Stroud, V. Browning, J. Byers, V. Harris, and W. Fuller-Mora

Laboratory for Computational Physics and Fluid Dynamics

175 Transition to Detonation in Turbulent Flames
A.M. Khokhlov and E.S. Oran

Condensed Matter and Radiation Sciences Division

99 The Microelectronics and Photonics Test Bed Experiment
A.B. Campbell, III and S. Buchner

130 Computational Screening of Candidate Thermoelectric Materials
D.J. Singh

132 Disorder-Induced Colossal Magnetoresistance
R. Stroud, V. Browning, J. Byers, V. Harris, and W. Fuller-Mora

141 Nuclear Contamination Studies in the Russian Arctic
D.R. Johnson, S.E. King, M. Krosshavn, and T.A. McClimans

Plasma Physics Division

109 The Path to Record Kilovolt X-Ray Emission
J. Davis, J.P. Apruzese, K.G. Whitney, J.W. Thornhill, and R.W. Clark

112 The Behavior of Deuterium at Extreme Pressures
A.N. Mostovych

183 Ionospheric Forecasting with Dynamic GPS Assimilation
M.J. Keskinen

Electronics Science and Technology Division

100 Fabrication of a Fast Turn-off Transistor by Wafer Bonding
K.D. Hobart, F.J. Kub, G. Dolny, M. Zafrani, and J.M. Neilson

153 Confined Photons in Semiconductor Microcavities
T.L. Reinecke, P.A. Knipp, M. Bayer, and A. Forchel

102 Low-Power, High-Speed InAs-Based High Electron Mobility Transistors
J.B. Boos, B.R. Bennett, W. Kruppa, D. Park, and M.J. Yang

Center for Bio/Molecular Science and Engineering

35 Array-Based Biosensor for Multianalyte Sensing
J.P. Golden, C.A. Rowe, M.J. Feldstein, S.B. Scruggs, L.M. Tender, and F.S. Ligler

86 New Materials for Heavy Metal Removal Applications
M. Pazirandeh and J.M. Mauro

Acoustics Division

72 Sound Propagation Through a Sand-Water Interface
H.J. Simpson and B.H. Houston

71 A Search Algorithm for Resonance Anomalies (SARA)
S.A. Chin-Bing, D.B. King, R.A. Zingarelli, and A. Warn Varnas

75 Estimation of Seabed Properties from Chirp Sonar Data
B. Turgut, S.N. Wolf, and M. Orr

Remote Sensing Division

163 Multifrequency Polarimetric SAR Images of Gulf Stream Features from Space
S.R. Chubb, T.F. Donato, F. Askari, A.L. Cooper, and S.A. Mango

- 137 POAM III Monitors the Polar Stratosphere
*J.S. Hornstein, R.M. Bevilacqua,
R.L. Lucke, E.P. Shettle, M. Daehler,
K.W. Hoppel, G. Nedoluha, D.T.
Chen, D.R. Korwan, M.D. Fromm,
and J.D. Lumpe*

- 186 Far-Infrared Spectroscopy of Colliding
Galaxies
J. Fischer and M. Luhman

Oceanography Division

- 71 A Search Algorithm for Resonance
Anomalies (SARA)
*S.A. Chin-Bing, D.B. King,
R.A. Zingarelli, and A. Warn Varnas*
- 141 Nuclear Contamination Studies in the
Russian Arctic
*D.R. Johnson, S.E. King,
M. Krosshavn, and T.A. McClimans*
- 145 Baroclinic Oscillations on the
Louisiana Continental Shelf during
Hurricane Andrew
T.R. Keen and S.E. Allen

Marine Geosciences Division

- 148 High-Resolution Observations of Foreshore
Morphodynamics
K.T. Holland and J. Puleo
- 164 Autonomous Survey System
B.S. Bourgeois and A.B. Martinez

Marine Meteorology Division

- 43 The North Pacific Experiment
(NORPEX-98)
*R.H. Langland, R. Gelaro,
G.D. Rohaly, and T.E. Rosmond*
- 143 The Dynamics of Unusual Coastal Wave
Clouds
S.D. Burk and T. Haack

Space Science Division

- 188 Modelling Radiation Effects on Spacecraft:
CREME96
A.J. Tylka

Space Systems Development Department

- 177 Atmospheric RF Propagation Effects on
Tracking, Navigation, and Communication
Links
J. Choi and M. Regan
- 81 Flight Test Data from the Sodium Sulfur
Battery Cell Space Experiment
J.C. Garner

Spacecraft Engineering Department

- 190 Interim Control Module (ICM)
A.B. Jacoby
- 192 First U.S. Flight Hall Thruster Electric
Propulsion System
P.R. Lynn, Jr. and M.F. Osborn II

Subject Index

- 3-MeV Tandem Van de Graaff, 13
- Acoustic propagation, 71
- Acoustics, 15, 25
- Actuators, 55
- Administrative Services Branch, 20
- Advanced Graduate Research Program, 217
- Advanced Research and Global Observation Satellite (ARGOS), 18
- Advanced Techniques, 21
- Aerogel, 127
- Airborne Geographical Sensor Suite (AGSS), 21
- Alfred P. Sloan Fellows Program, 218
- American Society for Engineering Education (ASEE) Postdoctoral Fellowship Program, 221
- AN/SPQ-9B radar, 94
- Andreev reflection, 128
- Angle of arrival (AOA), 96
- Antiship missile defense (ASMD), 94
- Array, 35
- Assimilation, 183
- Atomic force microscopy, 125
- Attitude control, 190
- Automatic radar periscope detection and discrimination, 93
- Automation, 174
- Autonomous surveying, 164
- AVID Media Composer 1000, 20
- Ballistic transport, 87
- Beach, 148
- Bergen Data Center, 17, 23
- Bio/Molecular Science and Engineering, 14
- Bioremediation, 86
- Biosensor, 35
- Biosorbent polymeric proteins, 86
- Blue Jets, 5
- Bragg Crystal Spectrometer (BCS), 18
- Brandywine, Maryland, 23
- Brookings Institute Advanced Study Program, 218
- Capacitors, 55
- Carbon nanotubes, 87
- Catalysts, 127
- CCD, 35
- Center for Computational Science (CCS), 9, 20
- Ceramics, 55
- Chaff, 21
- Chaos, 170
- Chemistry, 10, 24
- Chesapeake Bay Detachment (CBD), 9, 21
- Chirp sonar, 75
- Circulation, 141
- Class 10 clean room, 26
- Colossal magnetoresistance, 132
- Combustion theory, 175
- Command Information Center (CIC) communications, 120
- Community Outreach Program, 8, 220
- Compact Antenna Range, 9
- Composites, 55
- Computer-aided Engineering (CAE) Facility, 9
- Condensed Matter and Radiation Sciences, 12
- Continental shelf, 145
- Cooling, 130
- Cooperative Aircraft Identification (CAI) System, 9
- Cooperative Engagement Capability (CEC), 21
- Corporate Facilities Investment Plan (CFIP), 24
- Counseling Referral Service (C/RS), 218
- Countermeasures, 107
- CREME96, 188
- Current front, 163
- Cyanurates, 84
- Damage control, 174
- Decision-making, 120
- Decoy, 107
- Deflagration-to-detonation transition, 175
- Density functional theory, 130
- Detonation, 175
- Deuterium, 112
- Development testing (DT), 94
- Diamond Jubilee, 4
- Digital acquisition buoy systems (DABS), 15
- Digital Processing Facility, 10
- DoD High Performance Computing Centers, 17
- DoD Science & Engineering Apprentice Program (SEAP), 222
- Edison Memorial Graduate Training Program, 217
- Electric propulsion, 192
- Electromagnetic Compatibility (EMC) Facility, 9
- Electronic Attack, 169
- Electronic Warfare, 10
- Electronics Science and Technology, 14, 24, 26
- Elves, 5
- Emission Measurements Facility, 10
- Employee Development Branch, 217
- Environmental Quality Sciences Section, 11
- EPICENTER, 14, 25, 26
- Equation-of-state (EOS), 112
- Exhibits Program, 20
- Extreme Ultraviolet Imaging Telescope (EIT), 18
- ex-USS *Shadwell* (LSD-15), 11, 23
- Faculty Member Appointments, 221
- Federal Executive and Professional Association, 8
- Federally Employed Women, Inc. (FEW), 8, 219
- Fellowship in Congressional Operations, 218
- Fire I, 11
- Fleet Numerical Meteorology and Oceanography Center (FNMOC), 17, 22
- Flight Support Detachment (NRL FSD), 8, 21, 26
- Fluorescence, 35
- Fluoropolymers, 84
- Fly's Eye, 21
- Focal-Plane Evaluation Facility, 10
- Forecasting, 183
- Free-Surface Hydrodynamics Laboratory, 25
- Galactic Radiation and Background (GRAB) satellite, 4
- Galaxies, 186
- GAMBLE II, 13
- Gateway, 19
- Geostationary Satellite Processing Facility, 23
- Global Imaging of the Ionosphere (GIMI), 18
- Global Positioning System (GPS), 169, 183
- GROTTO, 21
- Ground Truth Reference System, 169
- Gulf Stream, 163

Hall thruster, 192
 Heavy metals, 86
 HEMTs, 102
 High Performance Computing Modernization Program (HPCMP), 20, 24
 High pressure, 112
 High-frequency devices, 102
 High-Power Microwave (HPM) Facility, 12
 High-Resolution Airglow and Auroral Spectroscopy (HIRAAS), 18
 High-surface-area electrodes, 127
 High-temperature superconducting electromagnet, 5
 Hurricanes, 145
 Hydrates, 5
 Hyperspectral Imaging, 5
 Hyperspectral, 156
 Immersive Room, 9
 Immersive training, 117
 InAs, 102
 Individual combatant simulation, 117
 Inertial Navigation System (INS), 169
 Information Security Engineering Laboratory, 9
 Information Technology Division, (ITD), 9, 24, 26
 InfoWeb Information System, 19
 Infrared, 107, 159
 Infrared Range Facility, 5
 Infrared spectroscopy, 186
 Infrared Test Chamber, 10
 Integrated Electronic Warfare System (IEWS), 21
 Intergovernmental Personnel Act Appointments, 221
 Interim Control Module (ICM), 190
 Internal waves, 71, 145
 International Space Station (ISS), 190
 Inverse synthetic aperture radar (ISAR), 8
 Ion Implantation Facility, 13
 Ionosphere, 183
 IR Missile-Seeker Evaluation Facility, 10
 IR Range, 10
 ISI "Web of Science" Science Citation Index Expanded, 19
 JEM-3010 scanning and transmission electron microscope (STEM), 17
 John B. Hovermale Visualization Laboratory, 17, 23
 Joint Laboratory, 25
 Kara Sea, 141
 Laboratory for Advanced Material Synthesis (LAMS), 14, 25
 Laboratory for Advanced Materials Processing, 26
 Laboratory for Computational Physics and Fluid Dynamics, 11
 Laboratory for Proximal Probe Nanofabrication, 26
 Laboratory for the Structure of Matter, 10
 Large Area Plasma Processing System (LAPPS) facility, 13, 24
 Large-Angle Spectrometric Coronagraph (LASCO), 18, 26
 Large-Optic, High-Precision Tracker system, 10
 Laser Facilities, 12
 Littoral, 71
 Low dielectric resins, 84
 Low observables, 159
 Lysozyme, 125
 Magnetic Observatory, 17, 22
 Map Data Formatting Facility, 22
 Marine boundary layer, 143
 Marine Corrosion Test Facility, 22
 Marine Geosciences, 16, 25
 Marine Meteorology Division (NRL-MRY), 17, 22
 Master Environmental Laboratory, 23
 Materials Science and Technology, 11, 26
 Materials, 130
 Maverick Missile IR group, 21
 Mesoporous, 127
 Methane seepage, 5
 Microcavity, 153
 Midway Research Center, 23
 MIRS, 5
 Mississippi's Alliance for Minority Participation, 222
 Molecular electronic devices, 87
 Moving-Map Composer Facility, 17
 Multimedia Center, 20
 Multipath, 96
 Multiresident Andrew File System (MRAFS), 20
 Multispectral, 156
 Nanoelectronics Processing Facility (NPF), 14, 24
 Nanoscale, 127
 Nanoscale composites, 127
 Nanostructures, 87
 National Defense Science and Engineering Graduate Fellowship Program, 221
 National Research Council (NRC) Cooperative Research Associateship Program, 221
 Naval Center for Space Technology (NCST), 18
 Naval Meteorology and Oceanography Command, 22
 Naval Oceanographic Office, 22
 Naval Postgraduate School (NPS), 217
 Naval Postgraduate School (NPS) Annex, 22
 Navy and Joint Typhoon Warning Center, 18
 Navy Earth Map Observer (NEMO), 4
 Navy Prototype Optical Interferometer (NPOI), 16
 Navy Science Assistance Program (NSAP), 218
 Navy Technology Center for Safety and Survivability, 22
 Navy/ASEE Summer Faculty Research and Sabbatical Leave Program, 221
 NEWAVE facility, 10
 NICE.net, 9, 21
 NOAA National Weather Service Forecast Office (NWSFO), 22
 Nonacoustic Antisubmarine Warfare (NAASW), 21
 Nondestructive evaluation, 155
 NRL Federal Credit Union (NRL FCU), 8
 NRL Mentor Program, 219
 NRL-Monterey (NRL-MRY), 17
 NSDS-E (Navy Satellite Display System-Enhanced), 18
 Numerical simulations, 175
 Ocean Research Laboratory, 25
 Oceanographic Surveillance (OS), 21
 Oceanography, 16
 OCLC First Search, 19
 Office of Research and Technology Applications Program (ORTA), 218
 One-dimensional inverse problem, 75
 Optical coherence tomography (OCT), 155
 Optical Sciences, 10
 Oriented Scintillation Spectrometer Experiment (OSSE), 18
 Oscillators, 170
 Oxide electronics, 132
 Ozone hole, 137
 Ozone layer, 137
 P-3 Orion turboprop aircraft, 23
 Parallel High Performance Computer/Graphics Facility, 11
 Pattern Analysis Laboratory, 22
 Penthouse Processing Facility (PPF), 14, 24
 Pharos III, 13
 Piezoelectric, 55
 Plasma Physics, 13, 24, 26
 Polar Ozone and Aerosol Monitor III (POAM III) instrument, 4
 Pomonkey, Maryland, 23
 Power switching device, 100

Preambulation, 117
 Predictability, 43
 Photon, 153
 Protein crystal growth, 125
 Publication services, 19
 Quantum wells, 102
 Radar Imaging Facility, 8
 Radar Signature Calculation Facility, 9
 Radar Test Bed Facility, 9
 Radar, 8
 Radiation, 99
 Radio frequency (RF), 96
 Radio waves, 96
 Radionuclides, 141
 Radomes, 84
 Range scanner, 119
 Range, 119
 Ray-bending, 177
 Real aperture radar (RAR), 21
 Reconnaissance, 156
 Recreation Club, 8, 220
 Red Sprites, 5
 Reduced manning, 120, 174
 Remote Sensing, 16, 25
 Remote Ultra-Low Light Imager (RULLI), 21
 Responsive Workbench, 9
 Robotics Laboratory, 9
 Ruth H. Hooker Research Library, 19
 S.S. *Keldysh*, 5
 Salt Water Tank Facility, 25
 Satellite technology, 188
 Satellite-Linked Vertical Line Array (SLVA) system, 15
 Science-as-Art, 4
 Science Innovation Awards, 4
 Scientific Visualization Laboratory (Viz Lab), 9, 20
 Scientist-to-Sea Program (STSP), 218
 Sea WiFS data, 16
 Search and rescue (SAR) refractivity, 177
 Sea-skimming missiles, 94
 Sediment acoustics, 75
 Sediment transport, 148
 Select Graduate Training Program, 217
 Semiconductor lasers, 5
 Sensors, 127
 Ship-motion simulator (SMS), 21
 Shock, 112
 Showboaters, 8, 220
 Siderostats, 16
 Sigma Xi, 8, 219
 Signal loss, 71
 Single-event effects, 99, 188
 Singular vectors, 43
 Small-angle scattering, 127
 Sodium sulfur battery cells, 81
 Solar Coronagraph Optical Test Chamber (SCOTCH), 26
 Solar Heliospheric Observatory satellite, 18
 Solar Ultraviolet Spectral Irradiance Monitor (SUSIM) experiment, 18
 Sol-gel, 127
 Solitons, 71
 Sound propagation in sandy bottoms, 72
 Space, 99
 Space radiation, 188
 Space Science, 18
 Space Shuttle, 81, 163
 Space Technology, 18
 Spacecraft propulsion, 192
 Space-time adaptive processing (STAP) array, 8
 Spin polarization, 128
 Stennis Space Center (NRL-SSC), 22
 Stereo, 148
 STILAS Web-based catalog, 19
 Stratospheric aerosol layer, 137
 Student Career Experience Program, 8, 222
 Student Temporary Employment Program (STEP), 222
 Student Volunteer Program, 222
 Submarine canyon, 145
 Summer Employment Program, 222
 Superconductivity, 128
 Surveillance, 156
 Swash, 148
 Swath bathymetry, 164
 Synchronization, 170
 Synchrotron Radiation Facility, 13
 Synthetic aperture radar (SAR), 163
 Systems/Photographic Branch, 20
 Table-Top Terawatt (T³), 13, 26
 Tactical Atmospheric Modeling System/Real-Time (TAMS/RT), 23
 Tactical Electronic Warfare (TEW) Division, 10
 Tactical Environmental Support System (TESS), 23
 Tactical Oceanography Simulation Laboratory (TOSL), 15
 Targeted observations, 43
 Technology Transfer, 5
 The Consortium for Oceanographic Research Education (CORE) Postdoctoral Fellowship Program, 221
 The NRL/United States Naval Academy (USNA) Cooperative Program for Scientific Interchange, 221
 Theater Air Defense programs, 26
 Thermoelectric materials, 127
 Thermoelectrics, 130
 Thin films, 132
 Thin-Film Preparation Facilities, 12
 Toastmasters International, 8, 219
 Toastmasters Youth Leadership Program, 8
 TORPEDO Ultra, 19
 Trace Element Accelerator Mass Spectrometry (TEAMS) - 3 MV Tandem Pelletron Accelerator Facility, 12
 Transducers, 55
 Transient astrophysical sources, 5
 Triangulation, 119
 Troposphere Tracking Navigation Communication Links, 177
 Turbulent flame, 175
 Ultralow-loss, Fiber-Optic Waveguide Facility, 10
 Unconventional Stellar Aspect (USA), 18
 Upper Atmosphere Research Satellite (UARS), 18
 Vacuum Ultraviolet Space Instrument Test Facility, 26
 Vanguard I satellite, 4
 Video services, 20
 Video, 148
 Virtual locomotion, 117
 Virtual Reality (VR) Laboratory, 9
 Visual Design/Imaging Center, 20
 Wafer bonding, 100
 Waveclouds, 143
 Women in Science and Engineering (WISE), 8, 219
 Women's Executive Leadership Program, 218
 X rays, 109
 X-ray Facility, 12
 Z-Pinch, 109

Author Index

- Achille, L.B., 120
Allen, S.E., 145
Apruzese, J.P., 109
Askari, F., 163
Baden, D.W., 93
Bashkansky, M., 155
Bayer, M., 153
Bennett, B.R., 102
Bevilacqua, R.M., 137
Boos, J.B., 102
Bourgeois, B.S., 164
Browning, V., 132
Buchner, S., 99
Bucholtz, F., 156
Buckley, L.J., 84
Burk, S.D., 143
Byers, J., 128
Byers, J., 132
Campbell, III, A.B., 99
Cardiel, D.J., 94
Carroll, T.L., 170
Chase, M.T., 55
Chen, D.T., 137
Chin-Bing, S.A., 71
Choi, J., 177
Chubb, S.R., 163
Clark, R.W., 109
Cooper, A.L., 163
Daehler, M., 137
Davis, J., 109
DeCampo, R.S., 93
Denbrook, P.S., 117
Dolny, G., 100
Donato, T.F., 163
Duncan, M.D., 155
Feldstein, M.J., 35
Fischer, J., 186
Forchel, A., 153
Frankovich, J.H., 96
Fromm, M.D., 137
Fuller-Mora, W., 132
Garner, J.C., 81
Gelaro, R., 43
Golden, J.P., 35
Haack, T., 143
Harris, V., 132
Hartley, R., 119
Herman, G., 93
Hobart, K.D., 100
Holland, K.T., 148
Hoppel, K.W., 137
Hornstein, J.S., 137
Hosmer, A.C., 169
Houston, B.H., 72
Humphries, W., 107
Jacoby, A.B., 190
Jessen, T.L., 55
Johnson, D.R., 141
Kahn, M., 55
Keen, T.R., 145
Kerr, D.W., 93
Keskinen, M.J., 183
Khokhlov, A.M., 175
Kim, C., 55
King, D.B., 71
King, S.E., 141
Knipp, P.A., 153
Konnert, J.H., 125
Korwan, D.R., 137
Krosshavn, M., 141
Kruppa, W., 102
Kub, F.J., 100
Langland, R.H., 43
Leibowitz, L.M., 94
Lewis III, D., 55
Ligler, F.S., 34
Lucke, R.L., 137
Luhman, M.L., 186
Lumpe, J.D., 137
Lynn, Jr., P.R., 192
Mango, S.A., 163
Martinez, A.B., 164
Mauro, J.M., 86
McClimans, T.A., 141
McCune, J.A., 117
Merzbacher, C.I., 127
Michalowicz, J.V., 156
Mintmire, J.W., 87
Mostovych, A.N., 112
Nadgorny, B., 128
Nedoluha, G., 137
Neilson, J.M., 100
Oran, E.S., 175
Orr, M., 75
Osborn II, M.F., 192
Osofsky, M.S., 128
Page, R.C., 117
Park, D., 102
Pazirandeh, M., 86
Pecora, L.M., 170
Perozzo, M.A., 125
Pipitone, F., 119
Priest, R.G., 159
Puleo, J., 148
Regan, M., 177
Reinecke, T.L., 153
Reintjes, J.F., 155
Rohaly, G.D., 43
Rolison, D.R., 127
Rosmond, T.E., 43
Rowe, C.A., 35
Schaus, L.M., 94
Schmidt-Nielsen, A., 120
Schulze, K.G., 120
Scruggs, S.B., 35
Shettle, E.P., 137
Sibert, L.E., 117
Simpson, H.J., 72
Singh, D.J., 130
Snail, K.A., 159
Snapp, M.A., 107
Snow, A.W., 84
Soulen, Jr., R.J., 128
Stroud, R., 132
Tatem, P.A., 174
Templeman, J.N., 117
Tender, L.M., 35
Thornhill, J.W., 109
Tse, A.Y., 96
Turgut, A., 75
Tylka, A.J., 188
Varnas, A.W., 71
White, C.T., 87
Whitney, K.G., 109
Williams, F.W., 174
Wolf, S.N., 75
Wu, C.C.M., 55
Yang, M.J., 102
Zafrani, M., 100
Zingarelli, R.A., 71

NRL Review Staff

SENIOR SCIENCE EDITOR

Dr. John D. Bultman

TID COORDINATOR

Jonna Atkinson

TID CONSULTANT

Kathleen Parrish

ACTING HEAD, TID

Timothy Calderwood

COMPUTERIZED COMPOSITION AND DESIGN

Jonna Atkinson and Donna Gloystein

EDITORIAL ASSISTANCE

Marsha Bray, Maureen Long, and Saul Oresky

GRAPHIC SUPPORT

Jonna Atkinson, Donna Gloystein, and Suzanne Guilmineau

HISTORICAL UPDATE

Dr. David van Keuren

PHOTOGRAPHIC PRODUCTION

Gayle Fullerton and Michael Savell

PRODUCTION ASSISTANCE

Rosie Bankert, Diltricia Montgomery, Leona Sprankel, and Paul Sweeney

DISTRIBUTION

Rosie Bankert

REVIEWED AND APPROVED

NRL/PU/5230--99-373

April 1999



Bruce W. Buckley
Captain, USN
Commanding Officer



Naval Research Laboratory
4555 Overlook Ave., SW
Washington, DC 20375-5320
Public Affairs Office, Code 1230
(202) 767-2541

<http://www.nrl.navy.mil>